UNIVERSITÉ PARIS XIII - SORBONNE PARIS NORD

École Doctorale Sciences, Technologies, Santé Galilée

Modélisation mathématique des maladies inflammatoires chroniques de l'intestin

Mathematical modelling of chronic inflammatory bowel diseases

THÈSE DE DOCTORAT
présentée par

Safaa AL ALI

Laboratoire Analyse, Géométrie et Applications (LAGA)

pour l'obtention du grade de
DOCTEUR EN MATHÉMATIQUES APPLIQUÉES

soutenue le 20 Juillet 2022 devant le jury d'examen composé de :

HISTACE Aymeric, ENSAE, Paris Cergy Université . . . . Rapporteur
POIGNARD Clair, INRIA, Bordeaux . . . . Rapporteur
LE GUYADER Carole, INSA, Rouen . . . . Examinatrice
OGIER-DENIS Éric, INSERM, Paris . . . . Membre du jury
TRETON Xavier, MD, Université de Paris . . . . Membre du jury
ZAAG Hatem, LAGA, USPN . . . . Co-directeur de thèse
LI-THIAO-TÉ Sébastien, LAGA, USPN . . . . Co-directeur de thèse
CHAUSSARD John, LAGA, USPN . . . . Co-encadrant de thèse

Abstract

Ulcerative colitis (or "UC") is a chronic inflammatory bowel disease. It is incurable and can lead to the removal of part of the large intestine and/or colorectal cancer. It affects the intestinal wall with lesions such as bleeding, ulcers and blurring at vascular pattern visibility. By inserting a camera into the colon (colonoscopy), the gastroenterologist can visualize the intestinal wall and thus assess the severity of the disease. Current severity scores are based on the gastroenterologist's interpretation and only consider the most severe lesions. They ignore the spatial extent and local distribution of the lesions along with the colon segments.

The goal of this thesis is to provide an objective evaluation of the ulcerative colitis severity. Our works are based on the analysis of endoscopic videos and mathematical modelling techniques.

First of all, we propose an algorithm to automatically detect bleeding and ulcers. We use endoscopic videos containing rectangular annotations and subsequently, many mislabelled pixels are present. We, therefore, compute the performance of the detectors at the annotations level instead of the pixels level. We also propose a models sampling method that speed-up the algorithm. We show good agreement with doctors' annotations.

Then, a diagram of visualization of the lesions throughout the colon was proposed. The obtained results show the lesions' spatial distribution in the whole colon. In addition, they allow a finer distinction between patients with the same severity score and thus better evaluation of the disease severity.

The next work is the modelling of the severity taking into account the spatial distribution of the lesions on the segments of the colon. The results show a correlation with current severity scores.

Next, we study the bias in the distribution of lesions close to the rectum. We also bring proof to some medical statements related to the disease severity.

Finally, a reaction-diffusion equation was introduced to model the distribution of lesions in the colon. The objective is to study the spatial dynamics of the lesions as they propagate in the colon. In application to UC patients, we compute the speed of propagation of lesions in the colon as well as the time for which the

whole colon will be inflamed. The results suggest dissimilar behaviour between patients with the same severity score.

All these works are carried out in close collaboration with biologists from Labex-Inflamex as well as gastroenterologists from Bichat and Beaujon hospitals.

Résumé

La rectocolite hémorragique ("RCH") est une maladie inflammatoire chronique de l'intestin. Elle est incurable et peut conduire à l'ablation d'une partie du gros intestin et/ou à un cancer colorectal. Elle affecte la paroi intestinale avec des lésions telles que des saignements, des ulcères et un brouillage au niveau de la visibilité de la trame vasculaire. En insérant une caméra dans le côlon (coloscopie), le gastro-entérologue peut visualiser la paroi intestinale et ainsi évaluer la gravité de la maladie. Les scores de gravité actuels sont basés sur l'interprétation du gastro-entérologue et ne prennent en compte que les lésions les plus graves. Ils ignorent l'étendue spatiale et la distribution locale des lésions sur les segments du côlon.

L'objectif de cette thèse est de fournir une évaluation objective de la sévérité de la rectocolite hémorragique. Nos travaux sont basés sur l'analyse de vidéos endoscopiques et sur des techniques de modélisation mathématique.

Tout d'abord, nous proposons un algorithme pour détecter automatiquement les saignements et les ulcères. Nous utilisons des vidéos endoscopiques contenant des annotations rectangulaires et par conséquent, de nombreux pixels mal étiquetés sont présents. Nous calculons donc la performance des détecteurs au niveau des annotations plutôt qu'au niveau des pixels. Nous proposons également une méthode d'échantillonnage de modèles qui accélère l'algorithme. Nous montrons un bon accord avec les annotations des médecins.

Ensuite, un schéma de visualisation des lésions à travers le côlon a été proposé. Les résultats obtenus montrent la distribution spatiale des lésions dans l'ensemble du côlon. De plus, ils permettent une distinction plus fine entre les patients ayant le même score de gravité et donc une meilleure évaluation de la sévérité de la maladie.

Le travail suivant est la modélisation de la sévérité en tenant compte de la distribution spatiale des lésions sur les segments du côlon. Les résultats montrent une corrélation avec les scores de sévérité actuels.

Ensuite, nous étudions le biais de la distribution des lésions à proximité du rectum. Nous apportons également des preuves à certaines hypothèses médicales liées à la gravité de la maladie.

Enfin, une équation de réaction-diffusion est introduite pour modéliser la distribution des lésions dans le colon. L'objectif est d'étudier la dynamique spatiale des lésions lorsqu'elles se propagent dans le côlon. En application aux patients atteints de la RCH, nous calculons la vitesse de propagation des lésions dans le côlon ainsi que le temps pendant lequel le côlon entier sera enflammé. Les résultats suggèrent un comportement différent entre les patients ayant le même score de sévérité.

Tous ces travaux sont menés en collaboration étroite vec les biologistes du Labex-Inflamex ainsi que les gastro-entérologues des hôpitaux Bichat et Beaujon.

Mots clé – Rectocolite hémorragique, saignement, ulcère, score de sévérité, détection automatique, équation de réaction-diffusion.

Remerciements

Quoique j'aille écrire, je ne remercierai jamais assez les gens sans qui la réalisation de cette thèse ne serait pas ce qu'elle est (on ne se rend compte de la chance qu'on a eu qu'une fois les années écoulées...). Cette thèse était une très bonne opportunité pour moi pour rencontrer et discuter avec des chercheurs de différentes spécialités au carrefour des mathématiques, de la biologie et de la médecine.

Ce travail n'aurait pu être mené à bien sans le financement apporté par la Fondation Sciences Maths de Paris (FSMP), via le programme MathInnov. Je remercie les responsables surtout pour le suivi accordé lors de la période de covid pour mener mes travaux de thèse dans les meilleures conditions possibles.

Je tiens tout d'abord à remercier mes co-directeurs de thèse, M. Hatem Zaag et M. Sébastien Li-Thiao-Té pour m'avoir fait confiance à mener ce projet de thèse assez pluridisciplinaire que nouveau. M. Zaag, je vous remercie pour le support apporté dès notre premier échange mail pour mon stage de M2. Je vous remercie également pour le support moral, administratif et la patience tout au long de ces années de thèse, qui étaient parfois dures et compliquées.

M. Li-Thiao-Té, je vous suis également reconnaissante pour le temps conséquent que vous m'avez accordé, les qualités pédagogiques et scientifiques de nos longues réunions et discussions, et plus particulièrement l'effort pour m'aider à comprendre les enjeux médicaux de ma thèse. J'ai beaucoup appris à vos côtés et je vous adresse toute ma gratitude pour tout cela.

J'adresse de chaleureux remerciements à mon co-encadrant de thèse, John Chaussard pour les encouragements continus dès la première réunion. Son énergie et sa confiance ont été des éléments moteurs pour moi en stage de M2 mené sous sa co-direction ainsi que mes débuts de thèse. J'ai pris un grand plaisir à travailler avec lui, surtout en m'aidant à débloquer les problèmes de programmation.

enseignant avec toi. J'adresse également un chaleureux remerciement à mes étudiants que je pense être chanceuse de les avoir lors de mes cours. J'espère qu'un jour vous allez lire ces mots et ce travail. Je vous souhaite une très bonne continuation dans vos études. Je pense « Enseigner » ne pourra pas être si riche et amusant sans vos efforts menés avec moi. Vos retours positifs m'ont trop affecté!

L'amitié est la plus belle des histoires que l'on peut avoir dans la vie. Je n'oublie pas de remercier du fond du cœur mes amis en dehors du laboratoire, avec qui j'ai eu une vie sociale très active et sans qui je n'aurais jamais pu dépasser les moments de stress et de pression vécus durant la thèse. En particulier mes plus proches copines au Liban, Hind que j'ai connue depuis le collège et Mayssa que j'ai rencontré lors de mon premier M2 à l'Université Libanaise, avec qui un chemin d'étude à commencer et une véritable relation a continué. Merci également à mes cousines adorables Farida, Rima et Rouba pour les jolis moments passés lors de mes vacances passées au Liban. En France, j'ai eu la chance de partager des journées avec mes cousins-es Razane, Ahmed, Houda, Hani, Ziad, Chifaa et Fatima. Chifaa ma petite-cousine, tu as tellement grandi que tu m'entoures maintenant avec toute ta tendresse. Tu m'as consacré tellement du temps pour écouter, déstresser et calmer quand les choses ne marchaient pas comme je le voulaient. I love you to the moon and back !

Lors de mon deuxième M2 effectué à Sorbonne Université, j'ai rencontré la personne que dire aimer reste insuffisant d'exprimer mes sentiments envers elle : "Hadjar". Je ne trouve pas les mots convenables pour exprimer ma chance et ma gratitude de t'avoir mon amie. Je ne peux pas te remercier suffisamment pour le support continu, la motivation et l'encouragement que tu m'as offerts durant ces années passées. Je t'aime beaucoup ! Je te souhaite un avenir aussi brillant que ton sourire et ton coeur!

Je ne trouverai jamais les mots pour exprimer ma profonde et sincère reconnaissance à mes chers parents qui m'ont encouragé dès mon jeune âge à exceller dans mes études et qui m'ont offert les meilleures conditions possibles afin d'avancer aisément dans mon cursus:

***Papa**, mon amour, qui m'a quitté très tôt, en t'écrivant ces mots mes larmes ne se calment et la douleur ne s'efface jamais. Ta perte était et continue à être la plus grande tragédie rencontrée dans ma vie. Ce changement brutal et radical dans ma vie est terrible à l'accepter. Quand j'avais appris la date de soutenance, tu étais la première personne à qui j'avais pensé. Tu m'as tellement demandé cette date mais j'étais toujours incapable de te l'annoncer. Aujourd'hui, huit mois passés depuis ton décès, je peux te l'annoncer mais malheureusement tu n'es plus là pour partager cette journée avec moi. Je tiens à te remercier d'être en premier lieu mon papa, ensuite pour tous les sacrifices et l'amour que tu nous as donnés, mon frère et moi. Merci également pour nos longues discussions et tes encouragements. Devenir docteure en mathématiques était ton rêve, et là ça se réalise! Papa, tes regards, ta voix et ta tendresse manquent beaucoup à ma vie.*

***Maman**, non uniquement tu as joué le rôle de parent mais aussi de support et d'amitié. Je te remercie infiniment pour les années de vie, les sacrifices et le support que tu m'as donné. Je te dis comme toujours je suis la fille la plus chanceuse pour t'avoir maman. Je te remercie pour tout, la joie, l'effort, le suivi et surtout la patience durant le chemin de mes études, qui n'était pas toujours facile. Je te remercie de m'avoir écouté pendant des heures parler de mon sujet de thèse, qui ne te motivait pas forcément... Je t'aime très fort! et je souhaite t'avoir pour de longues années dans ma vie!*

À l'âme de mon cher Papa,
À ma chère Maman,
je dédie ce manuscrit!

Contents

14

16

List of Abbreviations

AUROC	Area Under the Receiver Operating Curve
BBPS	Boston Bowel Preparation Scale
CD	Crohn Disease
CFL	Courant Friedrichs Levy condition
CML	Chronic Myelogenous Leukemia
CRC	Colon Carcinoma (also called colorectal cancer)
CRP	C-reactive Protein
CT	Computed Tomography
CMYK	Cyan Magenta Yellow Black
DAI	Disease Activity Index
EAI	Endoscopic Activity Index
fps	frames per second
FTCS	Forward in Time and Centered in Space
FKPP	Fisher Kolmogorov Petrovski Puskinov
FN	False Negative
FP	False Positive
GIT	Gastrointestinal Tract
GLCM	Grey Level Co-occurence Matrix
HSI	Hue Saturation Intensity
HSV	Hue Saturation Value
IBDs	Inflammatory Bowel Diseases
IC	Indeterminate Colitis
KNN	K-Nearest Neighbors
LED	Light Emitting Diode
LM	Leung Malik filters
MCC	Matthews Coefficient Correlation
MRI	Magnetic Resonance Imaging
MSB	Most Significant Bit
MSE	Mean Square Error
PCA	Principal Component Analysis
RGB	Red Green Blue
ROC	Receiver Operating Curve

ROI	**R**egion **o**f **I**nterest
RT	**R**andom **T**ree
SVM	**S**upport **V**ector **M**achines
TP	**T**rue **P**ositive
TN	**T**rue **N**egative
TW	**T**ravelling **W**ave
UC	**U**lcerative **C**olitis
UCCIS	**U**lcerative **C**olitis **C**olonoscopic **I**ndex of **S**everity
UCDAI	**U**lcerative **C**olitis **D**isease **A**ctivity **I**ndex
UCEIS	**U**lcerative **C**olitis **E**ndoscopic **I**ndex **S**core
WCE	**W**ireless **C**apsule **E**ndoscopy
YCbCr	**Y**(Luma) **C**hrominance-**b**lue **C**hrominance-**r**ed
YIQ	**Y**(Luma) **I**n-phase **Q**uadrature

Chapter 1

General introduction

1.1 General context

Inflammatory bowel diseases are chronic and life-long illnesses characterized by inflammation of the gastrointestinal tract. They encompass two main entities: Crohn disease (CD) and Ulcerative colitis (UC). CD affects the gastrointestinal tract with discontinuous lesions. Conversely, UC only affects the colon and is characterized by continuous inflammation of the superficial mucosa starting from the rectum, see Figure 1.1.
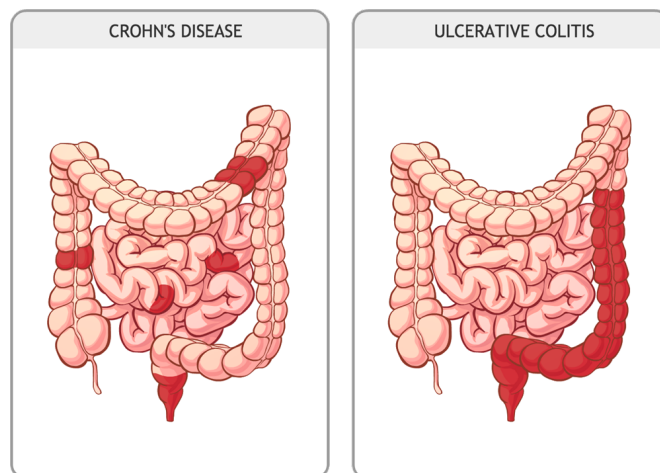
Figure 1.1: Crohn's and Ulcerative Colitis diseases extent in the gastrointestinal tract. CD affects the GIT by a discontinuous patchy pattern of lesions while the UC affects continuously the rectum and the colon.

IBDs show a strong increase in prevalence all over the world [Sum+17b]. They significantly impact the lives of patients who have to face many challenges related to the disease and its complications. The patients are always feeling tired

and need more rest compared to healthy people. The disease also affects their psychological well-being due to their reduced ability to meet their individual needs for function and productivity [MJ+17]. Therefore, IBDs patients develop stress, anxiety or depression which impacts their social relationships. As IBDs are incurable, patients need lifetime follow-up and treatments which lead to a cost burden for them.

The visualisation of the gut's interior is crucial for the diagnosis, treatment and follow-up of inflammatory bowel diseases. Doctors usually employ two techniques: wireless capsule endoscopy which is more suitable for the diagnosis of Crohn's disease [Idd+00] and colonoscopy which is convenient for ulcerative colitis disease [Pro+18]. The colonoscopy procedure consists in using a thin flexible tube with a mini video camera to screen the colon and rectum interior and is performed by an experienced clinician (cf Figure 1.2). The colonoscopy video is used to assess disease activity using a numerical score also called severity score. Current severity scores like Mayo [Rut+05] and UCEIS [Tra+12] only consider the most severe lesions of type bleeding, ulcers and main visibility of the vascular pattern. This disease severity evaluation depends on the gastroenterologist's interpretation and discards the spatial extent as well as the local distribution of lesions into the colon.
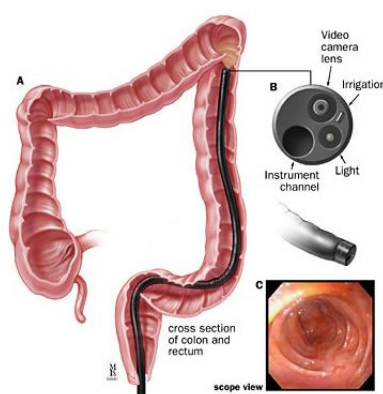
Figure 1.2: Colonoscope is inserted by the rectum to visualize the interior of the colon.

This thesis aims to provide an objective assessment of the ulcerative colitis disease severity. Towards this direction, we decide to combine colonoscopy video analysis and mathematical modelling techniques. We also decide to take into account the spatial distribution of lesions into the colon.

1.2 Collaboration with the doctors

This thesis is the result of interactions between biologists, gastroenterologists and mathematicians. The INFLAMEX center of excellence in France (ANR-10-LABX-17) brings together research teams from all disciplines around inflammatory diseases. In particular, an ongoing collaboration has been established between the gastroenterology group of the Bichat and Beaujon hospitals (with doctors Yoram Bouhnik, Xavier Treton and Eric Ogier-Denis) and the Math, Bio and Images team (MBI) from the mathematic lab LAGA (Laboratoire Analyse, Géométrie et Applications).

Due to our collaboration with doctors, we have obtained a database called Vatic that includes 49 colonoscopy videos recorded at Bichat and Beaujon hospitals for a set of UC patients and healthy individuals.

1.3 Thesis contributions

This thesis includes five works based on colonoscopy video analysis and mathematical modelling techniques.

- In the first work, we propose an automatic algorithm to detect bleeding and ulcer lesions found in a colonoscopy video. The lesions are annotated by rectangles which results in many errors in the ground truth, especially for corner pixels. In order to cope with this, we propose to modify the sensitivity criteria in order to take into account the detected annotations rather than detected pixels. Furthermore, we propose an efficient sampling scheme to explore the set of linear detectors. The obtained results show good agreement with the ground truth.

- Second, we propose to visualize the spatial distribution of the UC lesions along the colon. We assume that the colon withdrawal speed during the colonoscopy is constant, and subsequently the frames are linearly distributed in the video. The obtained results lead to more information about the colon inflammation status in comparison with current severity scores and a fine distinction between patients with the same endoscopic scores.

- In the third work, we model the disease severity by taking into consideration the lesion's spatial distribution in the colon. We, therefore, study several decompositions of the colon segments and we show high agreement with current severity scores.

- Next, we bring some proofs to a set of medical hypotheses. We introduce the notion of compatible models that perform less than the best model with some predefined error threshold. We show that the lesions are more abundant near the rectum, the UC severity increases with the number of

lesions found in the colonoscopy video, and there is a large variability between doctors during the severity assessment of both, bleeding and ulcers lesions.

- Finally, we model the spatial distribution of UC lesions with the Fisher Kolmogorov- Petrovski-Puskinov (FKPP) equation. Using the colonoscopy of the patient, we estimate the speed of lesions propagation. We also compute the time at which all the colon will be affected by the disease. The results show similar velocities of lesions propagation for patients having the same endoscopic scores. However, all the colon segments will be affected at a very dissimilar times. Furthermore, the bleeding appears to invade the colon faster than ulcers.

1.4   Outline of the thesis

The rest of the manuscript is organized as follows: the first four chapters are devoted to exploring the medical content of the thesis while the following five chapters are dedicated to the research works established during this thesis.

- In chapter 2, we present a review of some known medical aspects of ulcerative colitis disease.

- Then, in chapter 3, we study the endoscopy methods employed to screen the interior of the gastrointestinal tract in the case of inflammatory bowel diseases.

- In chapter 4, we explore some severity ranking scores mainly used to assess the ulcerative colitis activity. We will highlight their principal drawbacks. This chapter is crucial since it presents the main motivation for the research conducted in this manuscript.

- In chapter 5, we study the dataset "Vatic" containing endoscopic videos and that consists the core of application of the proposed methods presented in the following chapters.

We structured the works of the thesis as follows:

- In chapter 6, we present the automatic detection method of ulcerative colitis lesions. The results are supported by tests on the Vatic database.

- In chapter 7, we show the spatial distribution of the UC lesions along the colon and we compare the results for patients having equal severity scores. Many hypotheses were made, and we will discuss them also.

- In chapter 8, we propose the mathematical model of the disease severity by taking into account the spatial distribution of the lesions along with the colon.

- In chapter 9, we bring some answers and proofs to a set of medical hypotheses concerning the abundance of the lesions in the colon and the

variability of the severity scoring among the doctors. In this chapter, we present a new notion about the modelling process by proposing the use of compatible models.

- Finally, in chapter 10, we use the reaction-diffusion equations to model the spatial distribution of the lesions. More precisely, we show that we can compute relevant information about the disease activity such as the speed at which the lesions will affect the healthy parts of the colon.

In the appendices, we show the results for the visualisation of the lesions on the colon for all the patients of the Vatic database as well as recall some basic notions about the numerical simulations used to discretize the partial differential equations.

1.5 Publications

Some of the works explained in this manuscript have been presented to the following conferences and workshops:

- Detection of endoscopic lesions from limited quality annotations in colonoscopy videos, European Crohn's and Colitis Organisation Congress (ECCO), Vienna, February 2022 (Remotely), [Ala+22].

- Automatic bleeding and ulcer detection from limited quality annotations in ulcerative colitis, Crohn's & Colitis Congress, Las Vegas, January 2022 (Remotely), [AA+22].

- Automatic detection of ulcerative colitis disease in colonoscopy videos, Research School Mathematics, Signal Processing and Learning, CIRM, Marseille, France, 2021 (Remotely).

- Mathematical modelling of the spatial distribution of lesions in inflammatory bowel disease, Workshop on Mathematics of Complex Systems in Biology and Medicine, CIRM, Marseille, France, 2020.

In addition, some manuscripts are in progress to be published:

- Automatic detection of ulcerative colitis lesions from colonoscopy videos that is illustrated in chapter 6.

- Geometrical ulcerative colitis lesions' maps: towards a fine classification of patients and better disease severity evaluation (cf chapter 7).

- Reaction-diffusion equations to model the spatial distribution of UC lesions that is presented in chapter 10.

Chapter 2

Ulcerative Colitis disease

Abstract

This chapter is devoted to the presentation of ulcerative colitis which concerns all chapters of the thesis.

First, we discuss some known medical aspects of the disease such as its pathogenesis. Second, we present its epidemiology such as its worldwide incidence and possible risk factors. Third, we present some symptoms that characterize the disease. Next, we explore the medical tests used for diagnosis. Finally, we discuss some of the techniques that can be applied to control the disease, such as diet, medication and surgery.

The cellular actions due to UC inflammation suggest reduction in the intestinal barrier and thus promote diffusion of the inflammation to healthy parts of the mucosa. Therefore, we will consider this phenomenon to model the spatial distribution of the inflammation into the colon.

In addition, the spatial extent and local inflammation at colon segments are not yet reported in the actual medical procedures for the diagnosis of the disease. Therefore, in this thesis, we will provide algorithms and mathematical models that can help calculate the spatial extent of lesions to visualize lesion severity throughout the colon, model disease severity, and estimate the long-term progression of lesions in the colon.

2.1 Introduction

The first report that described the ulcerative colitis disease dates to 1850 [DF11].
Ulcerative Colitis disease (UC) is a lifelong disease with a relapse remitting
course. It affects the innermost lining of the large intestine (also called the colon)
by inflammations and ulcers. In comparison with the normal colon, irritated
colon presents sores and bleeding (cf Figure 2.1).
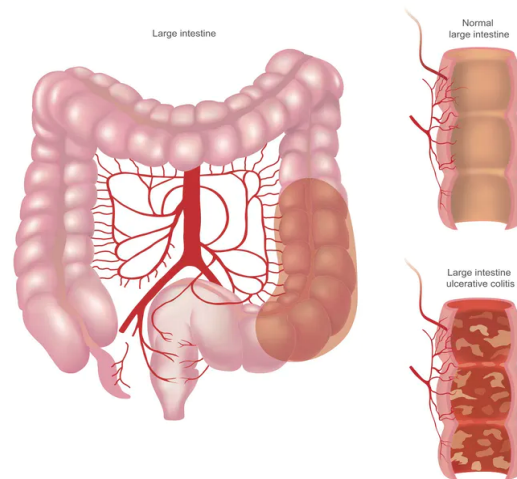
Figure 2.1: Normal colon and UC irritated colon (Source Getty Images).

The rectum is always affected by the disease which can extend proximally along
a variable length of the colon. Depending on the affected colon parts, we distin-
guish five common forms of UC (cf Figure 2.2):

(a) **Ulcerative proctitis** when the inflammation is limited to the rectum. Rectal
bleeding may be the only sign of the disease.

(b) **Proctosigmoiditis** when inflammation involves the rectum and the sig-
moid colon corresponding to the lower end part of the colon. Signs and
symptoms include bloody diarrhea, abdominal cramps and pain.

(c) **Left-sided colitis** also recognized as distal colitis corresponding to the
case of inflammation extending continuously from the rectum to the de-
scending colon. Signs and symptoms include bloody diarrhea, abdominal
cramping and pain on the left side, and urgency to defecate.

(d) **Extensive ulcerative colitis** when inflammation affects the colon begin-
ning from the rectum to the transverse colon.

(e) **Pancolitis** when the entire colon is damaged. Symptoms include bloody
diarrhea that may be severe, abdominal cramps and pain, fatigue, and
significant weight loss.
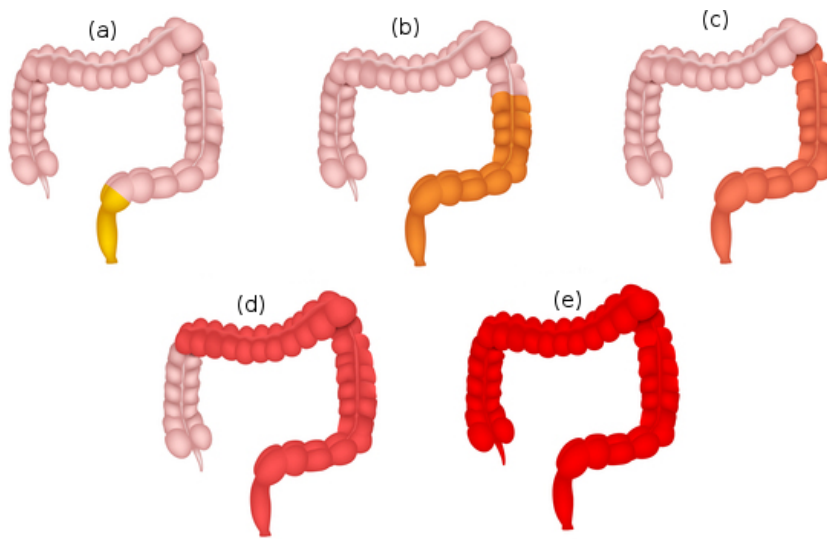
Figure 2.2: Main types of Ulcerative Colitis: (a) ulcerative proctitis, (b) proctosigmoiditis, (c) left-sided colitis, (d) extensive ulcerative colitis, (e) pancolitis.

In the last decades, high efforts were made to understand the pathogenesis of ulcerative colitis. Several types of cells were identified that suggest UC inflammation. We will discuss this in section 2.2. The origins of UC are not yet identified, however many factors can trigger inflammation. In section 2.3 we will present some possible factors that increase the risk of having the disease. Inflammation of UC almost causes diarrhoea leading to stomach discomfort and rapid emptying of the colon. Several other symptoms can occur during the flare-up of the disease. We will explore them in section 2.4. The diagnosis of the disease is generally associated with various clinical, biological and endoscopic examinations that we will summarize in section 2.5. Depending on the stage of the disease and the declaration of the patient, a therapeutic strategy is launched. In section 2.6 we will study some of the currently applied disease management procedures. We end the chapter by presenting some gaps among proposed diagnosis techniques in section 2.7.

2.2 Pathophysiology

Although the UC pathogenesis is not fully understood, it is known that deregulated immune action play crucial role, more particularly the excessive immune response to the environemental factors. Consequently, several deregulated actions are observed such as modification of luminal microbial diversity, alteration of the epithelial and mucosal barrier [Yes+20] as presented in Figure 2.3.
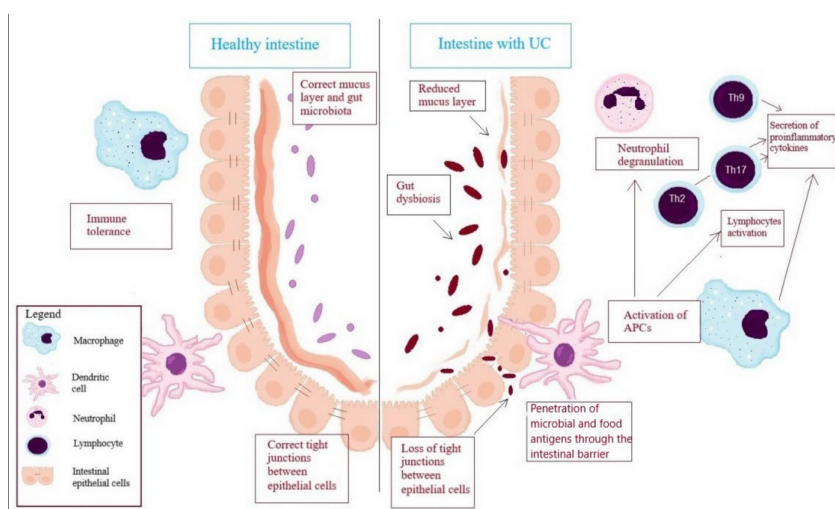
Figure 2.3:   Molecular mechanisms during inflammation caused by UC
[KOKV22]. The mucosal and submucosal layers are damaged because of in-
flammation.

The mucous layer and the intestinal epithelium are the first physical and chem-
ical barriers against intestinal bacteria, pathogens and food antigens. Integrity
of the intestinal barrier is provided by junctions between epithelial cells and
the immune cells present some immune tolerance. In the case of UC, a layer of
mucus is reduced and the gut microbiota is abnormal. The loss of tight junc-
tions allows bacteria and dietary antigens to pass through the intestinal barrier.
As result, many reactions occur such as the activation of T lymphocytes, the
increased presence of B lymphocytes and the production of antibodies as well
as pro-inflammatory mediators. In particular, macrophages and dendritic cells
enhance neutrophil migration and degranulation, as well as activating lympho-
cytes Th2, Th17, Th9. Activation of immune cells results in the secretion of
pro-inflammatory cytokines, i.e., $TNF-\alpha$, $IFN-\gamma$, and IL-13, which increases
the permeability of the intestinal barrier and thus promotes inflammation in the
intestinal mucosa [KOKV22].

2.3   Epidemiology

2.3.1   Geography

In the last decades, ulcerative colitis disease has shown increased prevalence
around the world. In Figure 2.4, we present the incidence of UC around the
world. Industrialised countries like North America, Western Europe, Southern
Asia and Australia have the highest rates of UC growth. On the other hand, ac-
cording to GlobalData the estimated diagnosed prevalent cases of ulcerative col-
itis in eight countries (US, France, Germany, Italy, Spain, UK, Japan and Canada)
will increase from 1.7 million cases in 2019 to 2 million cases in 2029, with an an-
nual growth rate of 1.36%.
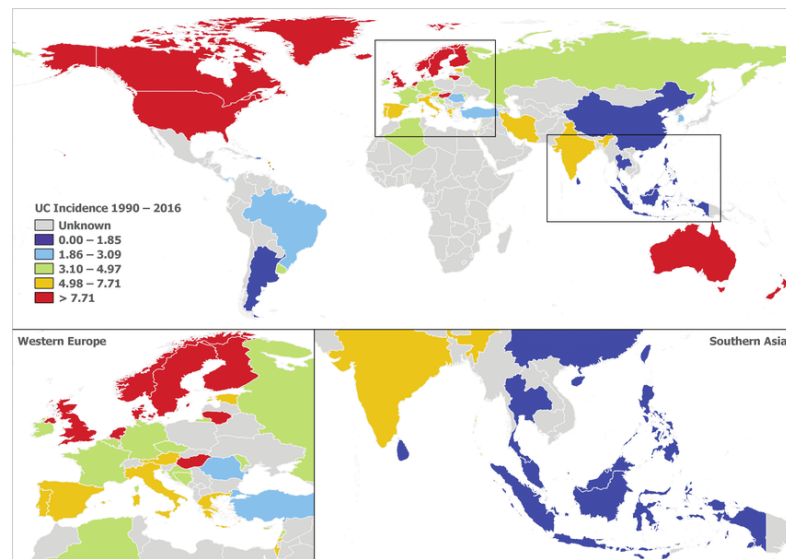
Figure 2.4: Worldwide map of the regional growth rates of UC disease. Countries in dark red represent the highest incidence of UC, while the gray ones indicate absence of data (Source University of Calgary).

2.3.2 Risk factors

Even though the exact origins of the disease is unknown, a combination of some genetic and environmental factors may increase the risk of having the disease in life. These factors include:

- **Age.** There are peaks of UC diagnosed cases at the ages 15 to 30 and then again for the range 50 to 80 [Lan+07].

- **Ethnicity.** Ashkenazi Jews have a rate of ulcerative colitis that is three to five times higher than that of other ethnic groups [Ord+12].

- **Family history.** Reports have shown that up to 20% of UC patients have a family member or relative experienced with UC or IBD. The risk of UC is particularly high in first-degree relatives. More particularly, between 5.7% and 15.5% of UC patients have a first-degree relative with the same disease [Mon+87; FMM80].

- **Genetic.** UC may affect genetically susceptible people in response to environmental triggers resulting in epithelial barrier integrity, autophagy, handling of bacteria, chemokines.

- **Intake of drugs.** Drugs including aspirin and ibuprofen can irritate the colon wall.

- **Environmental factors.** Microorganisms and infections may increase the UC risk.

- **Nutrition and lifestyle.** We can mention preprocessed foods, smoking, stress, anxiety.

2.4   Symptoms

Patients suffering from UC usually exhibit multiple hallmark symptoms such as fever, abdominal pain and cramping, irregular heartbeats, intermittent bloody diarrhea, rectal bleeding, weight loss and general disconfort. Extra-intestinal manifestations such as arthritis and skin lesions may be present.

The most UC patients experience come-and-go phases of active symptoms. However, if the disease have affected the rectum and the colon, then the patient may often suffer from severe reccurring symptoms with remission times.

2.5   Diagnosis

There is currently no standard test for diagnosing ulcerative colitis [STI87]. At present, the diagnosis of UC involves a combination of clinical, biological and endoscopic measures.

2.5.1   Clinical examination

Doctors usually start with a physical exam. Patients will be asked several questions about general health, diet, family history, home environment, and daily activities. During the clinical examination, the doctor can check blood pressure, heart rate. He can use a stethoscope to listen to the sounds in the patient's abdomen. He may press on the abdomen to feel tenderness or masses. Depending on the situation, the doctor may then recommend a series of diagnostic tests.

In the following, we will present a brief review of possible medical tests required upon the diagnosis of ulcerative colitis.

2.5.2   Laboratory tests

- **Blood tests** are carried out to screen anemia and/or inflammations (cf Figure 2.5). Albumin tests are sometimes required to assess the patient nutritional status. In addition, the doctor may look for electrolyte abnormalities and liver issues.

- **Stool samples** to detect some markers of inflammation such as the calprotectin and C-reactive protein (CRP). The calprotectin is a small protein, mainly secreted by polymorphonuclear cells in the lumen of the digestive tract and is excreted in the stool.
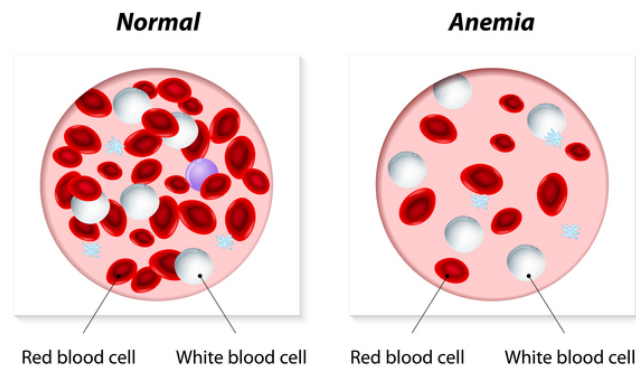
Figure 2.5: Anemia signs shown during a blood test (Credit Designua/Shutterstock.com).

2.5.3 Imaging tests

Medical imaging can reveal the status of the body and tissues. In the case of UC, the doctor requests a set of imaging tests of type (see Figure 2.6):

- Computed tomography (CT) scan,
- Abdominal X-ray,
- Magnetic resonance imaging (MRI),
- Radiography.

(a) X-ray.

(b) CT scan.

(c) MRI.

Figure 2.6: Examples of medical imaging used for the UC diagnosis. (a) X-ray images permit the visualization of the contours of the bowel, (b) CT-scan produces digital images of the colonic wall, (c) MRI can show the wall thickening variation due to UC inflammation.

2.5.4 Colonoscopy

Colonoscopy is a medical procedure that consists of visualizing the intestinal mucosa. We will explore it in chapter 3.

- **Sigmoidoscopy** used to look at the rectum and the lower parts of the colon.

- **Complete colonoscopy** applied to investigate the whole colon mucosa. It produces video that countains images showing signs of inflammations characterized by lesions such as bleeding and ulcers (cf Figure 2.7).
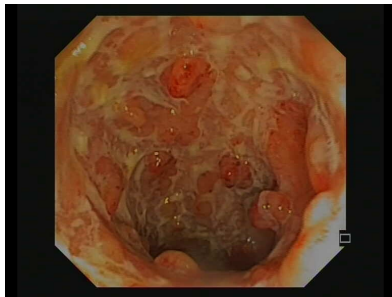
(a) Ulceration.

(b) Bleeding.

Figure 2.7: Endoscopic abnormalities that are signs of UC disease found during a colonoscopy video.

2.5.5 Histological tests

During the colonoscopy examination of the colon, the doctor can take some tissue samples, i.e. biopsies to guide his diagnosis. Indeed, as we discussed in section 2.2, the epithelial barrier is always damaged due to UC disease. Typical histological findings include continued mucosal inflammation expansion. At moderate levels of the disease, there is acute cryptitis progressing to crypt abscesses. In Figure 2.8, the crypt shows dilation and is filled with neutrophils and debris. In the severe stage of the disease, mucous ulcers occur. In cases that last for several years, the mucosa may develop dysplasia leading to an increased risk of developing colorectal cancer.
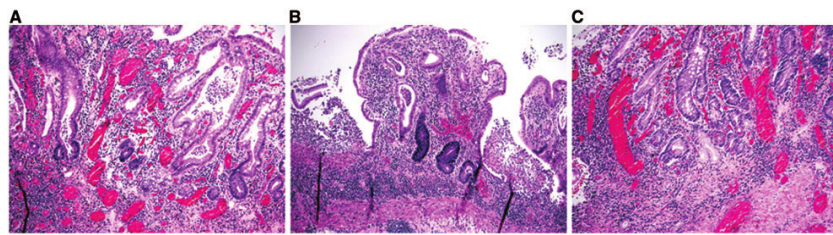
Figure 2.8: Histological damage caused by UC inflammation. (A) and (B) architectural distortion, including crypt shortening, variation in crypts size and shape, (C) paneth cell metaplasia and pyloric gland metaplasia in the left colon [DXL14].

2.6 Treatment and prognosis

Curative medical treatments are not yet available for UC disease. The currently available drug treatments are designed to control pain as well as reduce the frequency and duration of relapses. Depending on the disease severity and patient clinical status, several treatment procedures may be applied like specific diet plans, anti-inflammatory drugs or surgical intervention in the case of failure with previous techniques.

2.6.1 Changes in diet and lifestyle

Although food is not the direct cause of UC, it can set off the disease flares. Maintaining a high-calorie diet or a lactose-free diet can improve symptoms. Therefore some dietary advice can be useful to control the symptoms such as: eating small meals, drinking more water, avoid caffeine and alcohol. In Table 2.1, we present foods recommendation to control the disease symptoms. Foods that are hard to digest may trigger the symptoms. There is no perfect or single diet for all UC patients.

Food to avoid	Food to eat
fruits with seeds and skins	low fiber and cooked fruits
dairy products	cooked, non-cruciferous vegetables
spicy foods	refined grains
nuts	omega-3 fatty acids

Table 2.1: Some of recommended foods diet to control UC symptoms.

Exercising regularly and managing the stress levels can help in reducing the disease symptoms activity.

2.6.2 Anti-inflammatory therapy

Several drugs are used in medical practice to control the UC disease: aminosalicylate derivatives, corticosteroids, immunosuppressants, antidiarrhoeals, antispasmodics, anti-TNFs, integrin $\alpha 4$-$\beta 7$. Several drugs have shown effectiveness in clinical trials like infliximab, adalimumab, vedolizumab, and many others [Tho+15].

Nevertheless, the proposed drugs cannot control all the patients similarly. Also, no drug has been fully shown to be the best one. The treatment of the UC depends of its severity i.e amount of inflammation and extent in addition to the patient's nature, then it is not unique.

2.6.3 Surgery

For some UC patients, the different methods of disease management fail, then surgery, called colectomy is required to remove the affected parts of the large intestine. More particularly, the surgery is prescribed to cases like:

- Avoidance of the side effects of drugs.

- Control or stop of the symptoms that are difficult to manage.

- Prevention from the colon carcinoma (CRC).

- Elimination of bleeding.

We distinguish several types of colectomy (cf Figure 2.9):

- **Total colectomy** when the entire colon is removed.

- **Partial colectomy** (also known as subtotal colectomy) in the case of removing of the majority parts of the colon. The sigmoid colon is only left and it is connected to the small intestine.

- **Hemicolectomy** which depends on the part of colon that will be removed is known as:

  - **Left hemicolectomy** in the case of amputation of the left colon segment

  - **Right hemicolectomy** in the case of amputation of the right colon segment

  - **Transverse hemicolectomy** in the case of amputation of the transverse colon segment

- **Sigmoid colectomy** in the case of resection of the sigmoid colon

- **Proctocolectomy** when the colon and the rectum are totally removed.
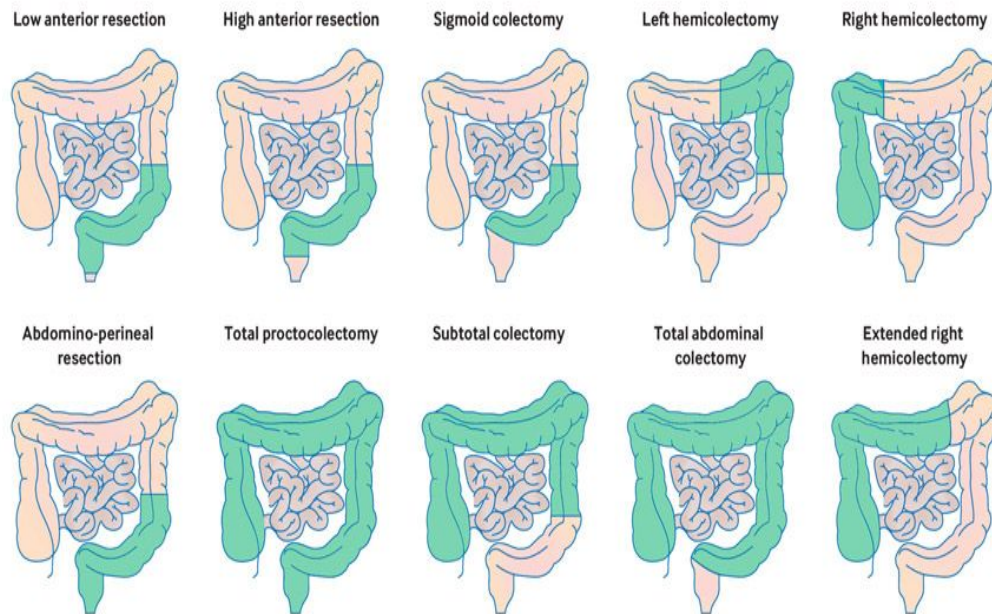
Figure 2.9: Types of colectomy surgery operations. Removed parts are indicated in green color whereas the remained colon parts are in light pink color (Source `https://drdavidford.com/procedures/colectomy-colon-removal-by-dr-david-w-ford`).

2.7 Discussion

Pathogenesis of the disease. The imbalance into the micribiota cells and their activation lead to destruction of the epithelial membrane and damage in the mucosa. The cells will thus continue to affect un-inflammed parts of the mucosa resulting in inflammation diffusion into the colon. Therefore in chapter 10, we consider this phenomena to model the spatial distribution of the inflammation into the colon.

Stopping point of the inflammation. Figure 2.2 shows different progression breakpoints of inflammatory phenomena caused by UC. This is the limit of the colored parts (yellow for case (a), orange for cases (b,c) and red for cases (d,e)). The point in the colon where the spread of the disease ceases to progress is so far unexplainable, and cannot be effectively identified by the video obtained after a colonoscopy. Further studies are needed to identify the inflammation endpoint.

Evaluation of the disease severity. After colonoscopy exploration of the digestive tract, the doctor aims to find the principal lesions of the UC like bleeding, ulcers and vascular pattern visibility. Then, he gives a numerical score, also called endoscopic score, to evaluate the disease activity in order to begin the

management of the disease by drugs or surgery. In chapter 4, we explore several endoscopic scores for UC. We will discuss also some of their drawbacks.

Objective biomarkers. The calprotectin is recognized as a reliable and non-invasive marker of the inflammation of the digestive tract. It plays a crucial role in different situations such as:

- Diagnosis assistance to differentiate between functional or irritable bowel syndrome (IBS) pain and those of origin IBDs. An increased dosage value of calprotectin can be a sign of various diseases such as IBDs, infectious and parasitic enteritis, colorectal cancer, an overdose of nonsteroidal anti-inflammatory drugs.

- Following-up IBDs like the measure of the response for some treatments.

- Postoperative.

On the other hand, the CRP is generally secreted by the liver after stimulation with interleukin 6 (IL-6). In the case of UC, the increased growth in CRP value indicates a severe form. However, it is less specific than the faecal calprotectin to indicate inflammation of the intestinal tract [CMH15].

Further studies are requested to include these objective biomarkers during the evaluation of the severity of the disease as well as after proceeding with a treatment strategy to study its efficacy.

Spatial extent of the inflammation. The spatial extent and localization of the inflammation are crucial for an appropriate diagnosis of the disease and consequently better follow-up. During the disease evolution, the proximal extent of inflammation progresses, and after 20 years about 50% of patients have cumulative pancolitis i.e. the whole colon is affected [Cos+11]. The UC may generate some complications for the colon such as perforation or abnormal dilation (megacolon). Furthermore, UC patients present an elevated risk to develop colon cancer and are estimated to be 2% after 10 years, 8% after 20 years and 18% after 30 years of the disease [LL08]. However, proposed imaging tests, which are two-dimensional sections of the body, cannot reveal a complete view of the inflammation severity according to the colon segments. Colonoscopy video as well is not treated to show the spatial extent of the lesions along with colon. These drawbacks have motivated us to propose an algorithm able to show the spatial extent and local lesions severity for all the colon segments (cf chapter 7).

Surgery. There are about 30% of UC patients undergoing surgery during their life. It has been shown also that around 10% to 15% of patients diagnosed with UC follows a surgery operation within the first 10 years of disease progression. However, surgical intervention can lead to some complications. Consequently, to proceed with a colectomy operation, the doctor needs to know the affected

parts of the colon to be able to decide the necessity or not and the type of special medications and surgical intervention as well as the speed at which the inflammation is progressing. We decide in chapter 10 to propose a mathematical model able to provide the long-term inflammation progressing into the colon.

2.8 Conclusion

This chapter describes the ulcerative colitis disease for which the works of the thesis is dedicated.

Although the exact pathogenesis that evolved during the UC is not completely recognized, some types of cells are recently identified like activation of T lymphocytes, macrophages and pro-inflammatory cytokines. The intestinal barrier is damaged leading to inflammation propagation. This mmotivated us to model to diffusion of the lesions in the colon by a reaction-diffusion equation (cf chapter 10).

When drugs show no efficacy, the doctor suggests surgery to remove affected parts of the large intestine. However, the diagnosis methods present a lack of important information about the disease extent and local inflammation severity measure on colon segments. We will highlight this along with the thesis chapters and we will introduce methods able to provide such information. Moreover, we will use it to localize the lesions into the colon (chapter 7), to model the severity scores (chapter 8), study the lesions' repartition bias (chapter 9) and compute the time for which all the colon will be affected (chapter 10).

Chapter 3

Exploration of the digestive tract: wireless capsule endoscopy and colonoscopy

Abstract

The investigation of the gut's interior is crucial for the diagnosis, treatment and follow-up of inflammatory bowel diseases. The doctors usually use two main techniques for IBD: wireless capsule endoscopy (WCE) or colonoscopy.

Due to its ability to screen the upper part of the gastrointestinal tract, the wireless capsule endoscopy is more suitable for the diagnosis of Crohn's disease while colonoscopy is convenient for ulcerative colitis disease.

The obtained videos contain images presenting the lesions that characterize the digestive tract inflammatory diseases like bleeding, ulcers and the vascular pattern visibility. These videos will be later used to assess the disease severity through the endoscopic scores that will be presented later in chapter 4.

3.1   Endoscopy

Endoscopy is a medical operation that consists in inserting a camera into the openings of the body like the mouth, anus, or any small incisions in the knee or abdomen for example. The word "endoscope" is made of two Greek roots: "endo" which means "inside", and "skopos", which means "to target or watch". In other words, endoscope means looking inside the body. There are several types of endoscopy depending on the part of the body or the organ that the doctor wishes to explore (see Table 3.1).

Area/tract	Organ	Type of endoscopy
Ear	Ear	Otoscopy
Respiratory	Nose	Rhinoscopy
	Lower Respiratory tract	bronchoscopy
Larynx	Larynx	Laryngoscopy
Gastrointestinal	Esophagus, stomach, and duodenum	Esophagogastroduodenoscopy
	Small intestine	Enteroscopy
	Colon	Colonoscopy
	Rectum and the lower part of the colon (i.e. the sigmoid colon)	Sigmoidoscopy
	Bile duct, rectum	Rectoscopy
	Anus	Anoscopy
Through small incisions	Abdominal or pelvic cavity	Laparoscopy
	Interior of a joint	Arthroscopy
	Organs of the chest	Thoracoscopy and mediastinoscopy

Table 3.1: Some types of endoscopy.

Endoscopic examination often involves surgical procedures such as collecting tissue samples or removing suspicious polyps and tumours. Endoscopy can be also useful for treatment purposes such as cauterization of a bleeding vessel or removal of the appendix during laparoscopic surgery (appendectomies). Other applications can be found in the references [Met96; Buc+18; Che+21; Dav+21].

In this thesis, we are interested in the diagnosis of inflammatory bowel diseases, therefore we will focus on the exploration of the gastrointestinal digestive tract. i.e. the oesophagus, the stomach, the small intestine and the colon (or the large intestine) presented in Figure 3.1, [Bas+12]. In that sense, the doctors use Wireless Capsule Endoscopy (cf Figure 3.2a) or colonoscopy (cf Figure 3.2b). In the next sections, we will explore the two procedures, the medical tools, the procedures steps and some side effects of each one.
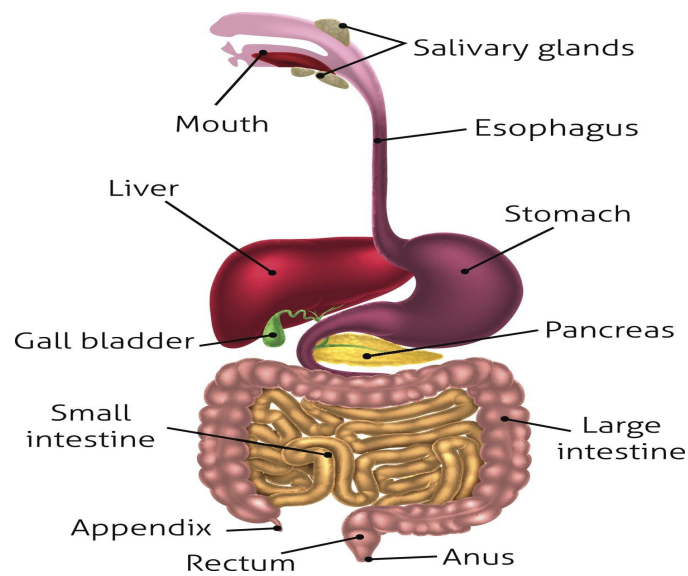
Figure 3.1: Diagram of the digestive tract
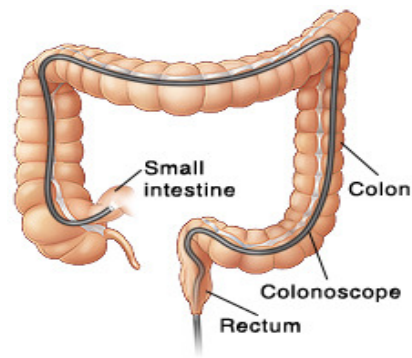
(a) Wireless Capsule Endoscopy device.   (b) Colonoscope.

Figure 3.2: Medical devices used during the exploration of the digestive tract.

3.2 Wireless Capsule Endoscopy (WCE)

3.2.1 Medical device

The first WCE tool was developed by the Given Imaging compagny and got the approval of the Food and Drug Administration (FDA) in 2001. In general, WCE is a tiny medical device of approximately 26×11 millimetre size as presented in Figure 3.3, with eight principal components:

1. Optical Dome,

2. Lens holder,

3. Lens,

4. Light-Emitting Diode (LED) responsible for the light illumination,

5. Sensor with 140-degree angle of view and high-quality images,

6. Battery,

7. Transmitter,

8. Antenna.
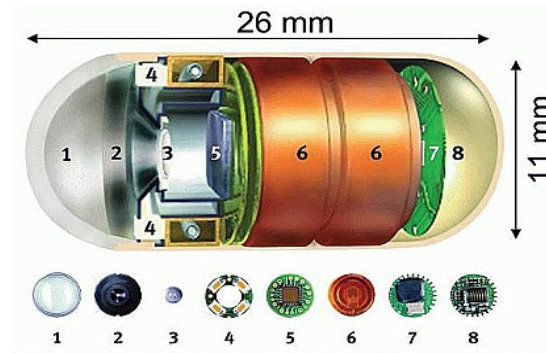
Figure 3.3: The architecture of the WCE [OEI18].

Figure 3.4 shows the complete system used during a WCE examination. The characteristics of some commercial systems are listed in Figure 3.5.

Figure 3.4: The complete system used during a WCE examination. It consists of the capsule device, the sensing system with sensing pads and the data recorder, the battery pack, and the personnal computer workstation.

Capsule Endoscopy
Devices used to perform endoscopy operations

|	PillCam	OLYMPUS	MiroCam	OMOM
Capsule	PillCam® SB 3 Given Imaging	EndoCapsule® Olympus America	MiroCam® IntroMedic Company	OMOM® Jinshan Science and Technology
Size	Length: 26.2 mm Diameter: 11.4 mm	Length: 26 mm Diameter: 11mm	Length: 24.5 mm Diameter: 10.8 mm	Length: 27.9 mm Diameter: 13 mm
Weight	3.00g	3.50g	3.25-4.70g	6.00g
Battery life	8 hours or longer	8 hours or longer	11 hours or longer	6-8 hours or longer
Resolution	340x340	512x512	320x320	640x480
Frames per second	2 fps or 2-6 fps	2 fps	3 fps	2 fps
Field of view	156°	145°	170°	140°
Communication	Radio frequency communication	Radio frequency communication	Human body communication	Radio frequency communication
FDA approval	Yes	Yes	Yes	No
Price per capsule	$500	$500	$500	$250

Figure 3.5: Features characterizing some available WCE devices.

In particular, we are interested in three parameters: the camera resolution, the battery life and the transmitter capacity:

- The first parameter concerns the camera resolution which varies between 320×320 pixels and 640×480 pixels. The camera quality is also central to the visibility of the mucosa abnormalities like the vascular pattern and other lesions.

- The second parameter is the battery life. The WCE devices currently applied for medical practice can last for around 8 hours. This leads to videos containing about 50 to 60 thousand images to be analyzed to assess the condition of the mucosa. Generally done by the specialist, the video review is a very time-consuming task with an elevated probability of lesions missing.

- The third parameter is the transmitter capacity. Current devices in Figure 3.5 have approximately the same rate of frames per second (fps) which is around 2 to 3 fps.

3.2.2 Medical procedure

To get a better visualization of the gastrointestinal tract, the patient must undergo some procedures to avoid the obscuration of some parts of the intestinal wall caused by persisting residuals. The patient must fast (food and drink) for at least 12 hours before the examination. If it is not sufficient, the doctor can propose some laxatives.

On the day of the examination, the recorder is attached to the patient abdomen (cf Figure 3.4). The recorder is firstly connected, then the patient swallows the capsule with a cup of water. The capsule takes images for about 8 hours. It will be ejected naturally between eight to seventy-two hours later.

After two hours of the capsule ejection, the patient can take clear liquids (such as water). After another two hours, he can take a light lunch.

If within two weeks, the capsule was not ejected, the patient contacts the doctor who orders an X-ray image to detect the localisation of the capsule and then remove it from his body.

3.2.3   Difficulties

The use of WCE can evolve some difficulties that can be summarized as follows:

- The procedure of reviewing and analyzing a WCE video is a very time-consuming task. There are a large number of images (50000 to 60000) to analyze.

- The abnormalities are difficult to see. The colored images present an almost similar aspect for certain cases which makes their detection quite difficult.

- During the movement of the capsule throughout the digestive system, it is difficult to detect its location regarding the digestive tract.

- Image appearance is the same in all parts of the digestive tract, so image characteristics cannot be used to localise the capsule.

- the speed at which the capsule moves is not constant. It is difficult to compute the capsule speed from the video.

- The last part of the colon is not recorded depending on battery life.

3.3   Colonoscopy

Colonoscopy is a medical examination for screening abnormalities of the colon mucosa such as bleeding, ulcerations, vascular pattern appearance. It is also employed for detecting adenomas or polyps which may turn into cancer in the case of colorectal cancer.

To have an efficient colon examination using colonoscopy, we need the combination of three elements [ARG15]:

1. Equipment structure namely the colonoscope (Figure 3.6) in particular the camera resolution which impacts the quality of obtained images and

videos, and the medical tools used for polyp removal and/or biopsies extraction. We will discuss this in subsection 3.3.1.

2. Patient preparation i.e. the cleansing of the colon, to eliminate all possible solid matter residue (stool) which can obscure the visibility of the status of the colonic lining during the examination. This will be explored in subsection 3.3.2.

3. Physician experience which is involved both in manipulating the instrument and in the review of the video.

3.3.1 Medical instruments

The endoscope device, also called colonoscope, used during a colonoscopy examination is a cylindrical, long thin flexible tube (cf Figure 3.6).
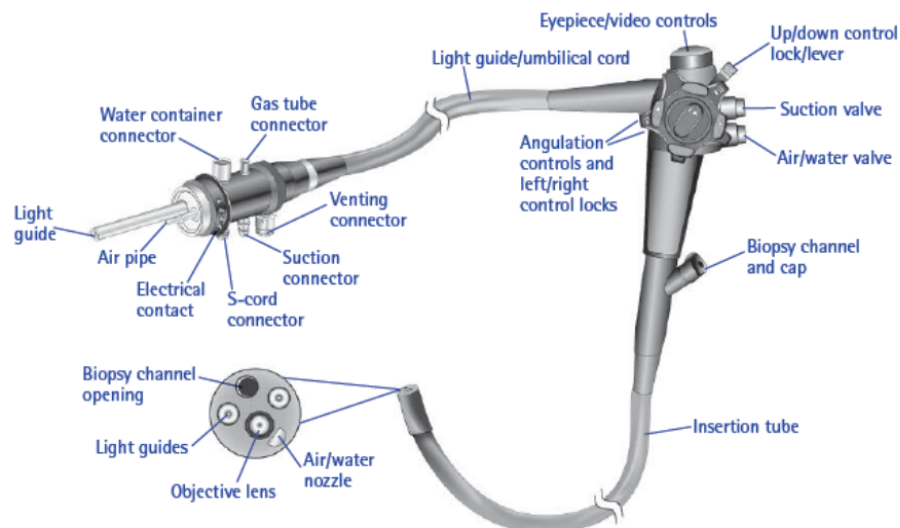
Figure 3.6: Flexible endoscope instrument used to explore the interior of the colon.

The length and diameter of adult endoscopes vary between 160 cm and 180 cm, and between 1 cm and 1.2 cm respectively [SP21]. Whereas, endoscopes for children have lengths varying between 1330 mm and 1700 mm, with diameters equal 9.8 mm to 11.8 mm. More details can be found in [Bar+12].

The colonoscope can be handled by a single individual: the gastroenterologist or the specialist realizing the examination. It consists of a proximal housing connected by an umbilical cord to a light source [SP21]. The colonoscope has a tiny camera on the end of it, which is connected to a monitor as presented in Figure 3.7.

Figure 3.7: Monitor machine to which the endoscope in Figure 3.6 is related in order to trasmit the images of the colon.

In the handle part of the scope (Figure 3.8), it exists a dial to increase or decrease its rigidity. If the scope rigidity is high, this may lead to pain and perforation of the gut wall. The eyepiece, control bottom for angulation and suction are designed to be in the proximal housing usually handled by the left-right of the doctor while the right hand manages the advancement and withdrawal of the endoscope during the procedure. The multiple angulation movements of the scope permit wider visualization of the interior of the colon. The control ackward is also adapted to manipulate the images obtained during the colonoscopy such as recording, taking screenshots, zooming.
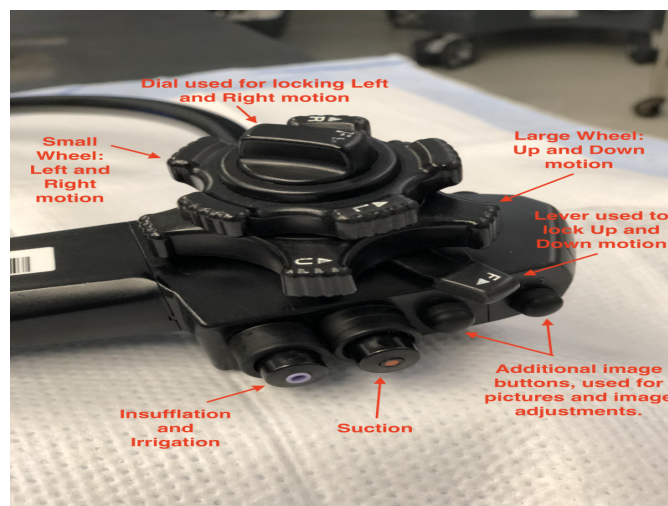

Figure 3.8: Zoom on the endoscope part that will be handled by the doctor and related to the external monitor machine (cf [SP21]).

The doctor may use biopsy forceps to collect tissue samples (Figure 3.9), or snare forceps to remove polyps (Figure 3.10). Needles and clip appliers can be used to stop bleeding in a vessel or cauterize bleeding tissue. Water and air can be inserted during the colonoscopy to clean the colon. This will be detailed in subsection 3.3.2.
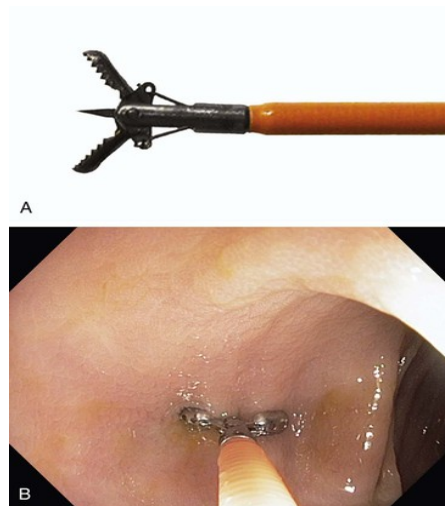
Figure 3.9: (A). Biopsy forceps, (B). Application of the forceps to collect biopsies during the colonoscopy.

Figure 3.10: Snare forceps (left) and it is application during the colonoscopy (right) for polyp removal.

3.3.2 Medical procedure

To perform a successful colonoscopy, we must clean out the colon from any possible solid residual. Therefore, the doctor may indicate to the patient to have a special diet a day or several days before the examination. In most cases, the patient should follow a low fibre regime. This consists of stopping the consumption of solid food, gelatin (Jell-O) and dairy products. This type of food is hard to digest and may cause constipation and interfere with the camera and consequently obscure the visibility of the colon lining. Moreover, the patient must avoid red or purple color liquids such as prune and orange juice. These drinks can discolor the liquid at the colon lining level which will appear like blood and

thus lead to incorrect bleeding lesions retrieval for example. The visibility of the vascular pattern will also not be assessed effectively.

On the other hand, the patient will be asked to increase the consumption of clear beverages including plain or carbonated water, tea or coffee without cream/milk, clear sports fluids, lemonade. If this diet was not sufficient to empty the colon, some laxatives can be proposed by the doctor in order to improve the elimination of possible residues.

The colon preparation is evaluated using Boston Bowel Preparation Scale (BBPS) created by the Boston University in 2009 [Lai+09]. The BBPS scores the three principal segments of the colon each one from 0 to 3 using the Table 3.2. The three parts composing the colon are the right segment evolving the cecum and the ascending colon; the transverse segment, including the hepatic and the splenic flexures; and the descending segment, counting for the descending colon, sigmoid and rectum.

Description	Scoring
Unprepared colon segment with mucosa not seen due to solid stool that cannot be cleared	0
Portion of mucosa of the colon segment seen, other areas of the colon segment not well seen due to staining, residual stool and/or opaque liquid	1
Minor amount of residual staining, small fragments of stool and/or opaque liquid, mucosa of colon segment seen well	2
Entire mucosa of colon segment seen well with no residual staining, small fragments of stool or opaque liquid. The wording of the scale was finalized after incorporating feedback from three colleagues experienced in colonoscopy	3

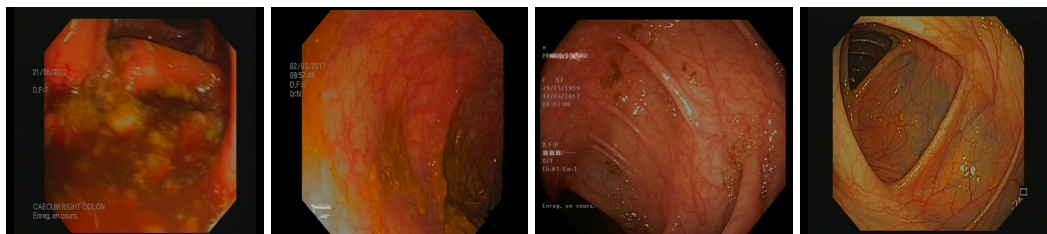Table 3.2: Computation of the BBPS index per segment [Lai+09].

Figure 3.11: Examples of the use of BBPS score to evaluate bowel preparation on a given segment of the colon. From left to right, the classification of bowel preparation is respectively unsatisfactory or poor (BBPS=0), fair (BBPS=1), good (BBPS=2) and excellent bowel preparation (BBPS = 3).

An ideal preparation corresponds to a score = 9. It is suggested to repeat the colonoscopy examination if the total BBPS score is less than or equal to 3 or one of the three considered segments is rated 1. In this case, a new colonoscopy examination should be rescheduled, and new preparation indications to be adapted, which is very complicated for the patient in terms of health and finance.

Colonoscopy is an examination that is carried out in the majority of cases under general anesthesia, this step is also called sedation. Some pain reliever and an intravenous sedative (i.e. introduced by the vein) will be given to the patient just a few times before the colonoscopy.

The colonoscopy procedure will begin with the patient lying flat on a padded examination table. He will be positioned on the left side while his knees are drawn up towards his chest to get a better angle to the colon. The colonoscope is slowly advanced from the end of the rectum under direct vision and is moved around the various bends of the colon.

For thorough colon examination, the colon should be expanded to let the endoscope move easily. Therefore, the doctor may apply some pressure to let the endoscope move ahead of the entire colon. And sometimes, the patient will be asked to change position to have a better examination process in the case of conscious sedation.

Additionally, in some cases air (carbon dioxide) and/or water are inflated to unfold tissues. Depending on the visibility option during the colonoscopy, the "underwater" technique (Figure 3.13) can replace air inflation or be combined with it. However, this technique involves sudden movements of the endoscope, due to the forced motions caused by the water introduction. Consequently, many blurred images are generated (see for example the images of Figure 3.13). These images artefacts can affect the assessment of UC activity as some parts of the mucosa are even blurred or completely obscured.

During the colonoscopy, the doctor may use biospy forceps to collect tissue samples from the intestinal mucosa (Figure 3.9) or snare forceps to remove malignant polyps (Figure 3.10). Biopsy samples should be taken from normal and abnormal tissue and compared to histological findings. These instruments are of variable size depending on what the doctor sees in the colonoscopy like the size of the polyp for example. For more details about these instruments, we refer the reader to papers [Ura+14; Pig+15; Chi+18].

Once the physician has reached the relation point between the colon and the small intestine, i.e. the cecum, he begins the slow removal of the endoscope.
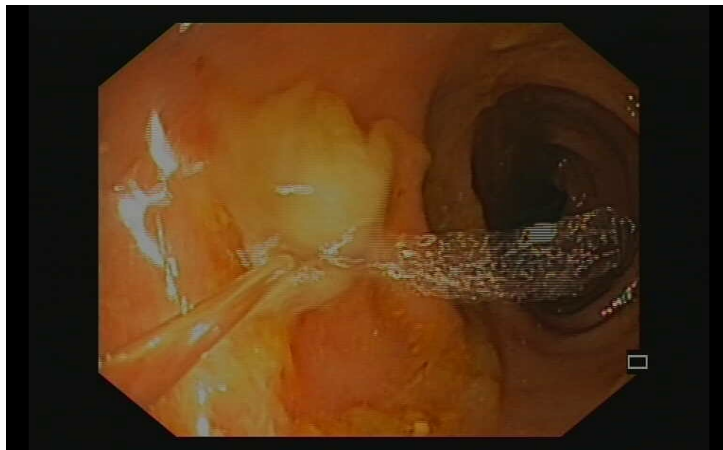
Figure 3.12: Introducing water by the endoscope during the colonoscopy.
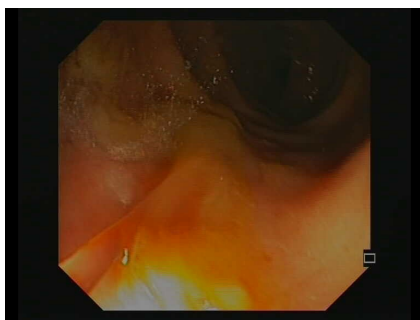
(a) Some parts of the colon are obliterated.
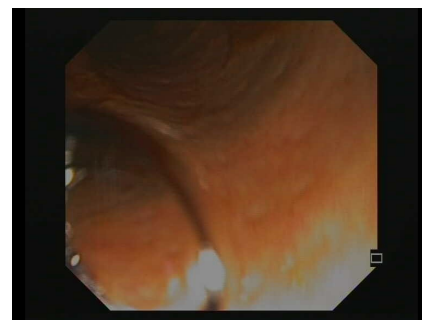
(b) The scope line is visualized.
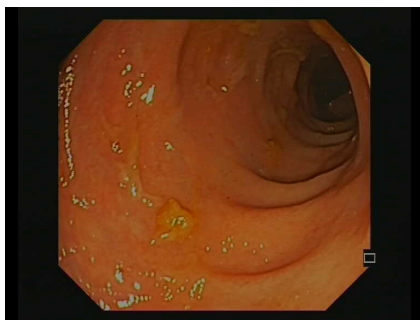
(c) Some white spots on the mucosa.
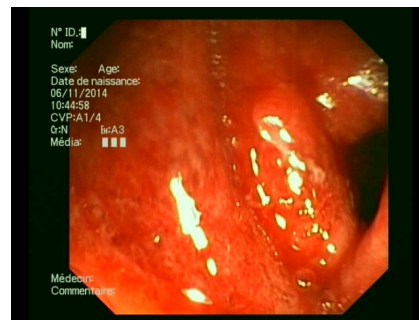
(d) Large spots totally hide the mucosa.

Figure 3.13: Illustration of various images containing artifacts resulting of the use of water during the colonoscopy.

The length of the colon is about five to six feet, which demands about 12 minutes to the colonoscope insertion into the whole colon and additive 12 minutes to remove it. If biopsies removal and/or polys extraction are performed, then colonoscopy procedure varies between 30 minutes to one hour to be completely terminated.

After finishing the colonoscopy, the patient is invited to wait in a recovery room until he completely wakes up if he submitted to general anaesthesia or until the pain medications wore off if he had conscious anaesthesia.

3.3.3 Complications related to the physician competence

The physician's expertise is important for the success of the examination:

- During the colonoscopy, the physician needs to control the speed of the endoscope to have clear images of the mucosa. Some reports show perforation of the colon due to the unsuitable or incorrect movement of the endoscope.

- He must also ensure the withdrawal of the whole colon.

- He must know the use of the medical instruments such as forceps and snares.

- Some problems with colonoscopy can be dangerous such as infections due to the non-cleanliness of the endoscope and the employed instruments used during the procedure.

- The obtained colonoscopy video will be generally reviewed by the physician performing the examination. Like WCE, the video contains a huge amount of images which is a tremendous task. Additionally, to provide a numerical assessment of disease activity, some expertise is required for the physician.

In the following section, we will review the different mucosal abnormalities that doctors may find in the endoscopy videos after WCE and colonoscopy examinations.

3.4 Endoscopic lesions

Endoscopy allows direct visual inspection of the intestinal mucosa and, therefore, helps to assess the severity of inflammation and estimate other possibilities of disease during a flare-up that can mimic an IBD.

In Table 3.3, we present some advantages and disadvantages of the wireless capsule endoscopy and colonoscopy examinations presented in this chapter. In contrary to WCE, colonoscopy procedure [Pro+18] is adapted to check the entire colon and rectum. Therefore, for the diagnosis of UC disease, the gastroenterologists rather use the colonoscopy which allows the colon to be visualized.

Despite differences in the affected mucosal layers, Crohn's and ulcerative colitis diseases share many overlapping lesions visualized during an endoscopic

Parameters	WCE	Colonoscopy
Safety	safe	possible colon perforation
Utility	non-reusable	reusable
Facility	non-invasive	invasive
Controlability	non-controllable	controllable
Device progress	easy movement	moderate due to colon form
Biospsies extraction	impossible	possible
Battery life	limited life	no problem
Detection of the oesophagus and small intestine conditions	possible	impossible
Visibility of the colon and the rectum	useless	useful

Table 3.3: Some pros and cons for wireless capsule endoscopy and colonoscopy examinations.

exploration of the digestive tract. In Table 3.4, we summarise the initial mucosal appearance that characterizes UC and CD. The intestinal lesions include bleeding, ulceration, erythema, mucosa's granularity and damage of the vascular pattern visibility. The most commonly recognized lesions for CD and UC are bleeding and ulcers (cf Figure 3.14).

Features	UC	CD
Bleeding	Always	Almost always
Erythema	Always	Almost always
Loss of vascular pattern	Always	Rare
Granularity of the mucosa	Always	Rare
Cobblestone appearance	No	Yes
Pseudo polyps	Always	Always
Aphtous ulcers	Rare	Always
Deep ulcers	No	Always
Patchy inflammation	Infrequent	Always
Ileal ulcers	No	Always
Rectal involvement	Almost always	Frequent
Fistula	No	Frequent
Perianal lesions	No	Frequent
Stricture	Rare	Frequent

Table 3.4: Aspect of mucosal lesions found during an endoscopy for UC and CD (cf [RA12; LL16]).
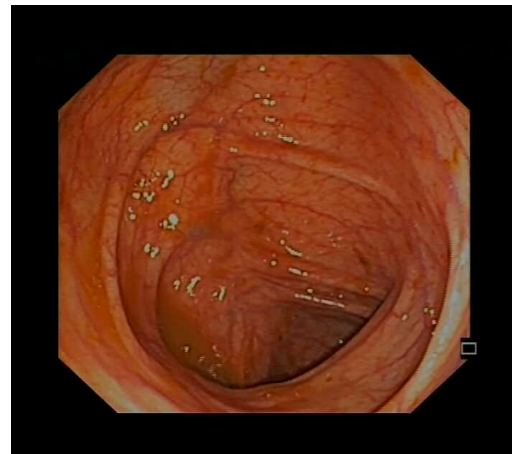
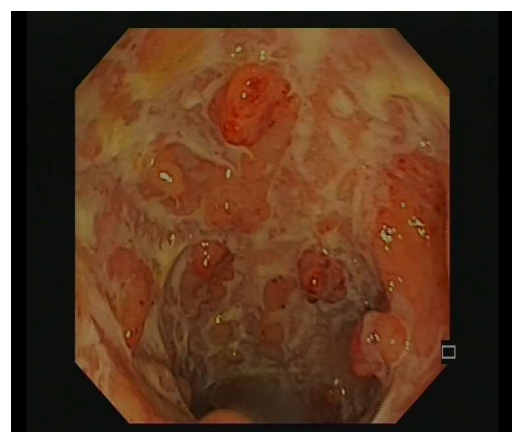Figure 3.14: Endoscopic findings in WCE and colonoscopy for CD (left column) and UC (right column) respectively. First row: healthy mucosa. Principal common lesions: Second row: bleeding lesions. Third row: ulceration lesions.

Several lesions characterize CD and other UC disease. In the case of CD (Figure 3.15), the ulcers lesions tend to be linear and deeper in comparison with UC's ulcers. They are usually associated with the cobblestone appearance of the ileum and strictures in the colon or ileum. Stenoses as well as open internal or perianal fistulas suggest CD disorder and are rarely found for UC patients [RA12]. Furthermore, the damage of the mucosa layer is usually measured with extra lesions during the diagnosis. In the case of suspicious CD, these lesions include the existence of frank erythema, frankly swollen mucosa, ulcerated and non-ulcerated stenosis (cf Table 3.4).

(a)

(b)

(c)

(d)
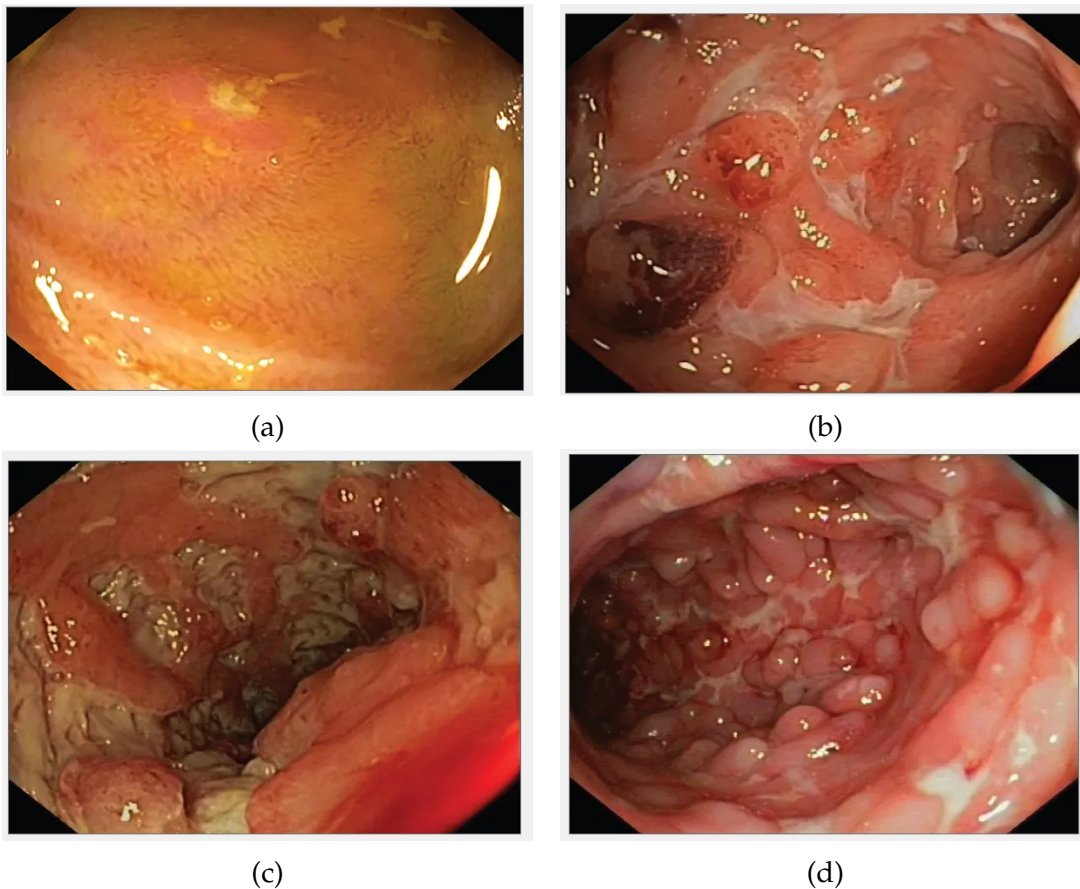
Figure 3.15: Illustration of some sensitive endoscopic lesions that suggest Crohn's disease. (a) Aphthous ulceration. (b) Deep ulceration associated with hemorragic mucosa. (c) Deep ulceration associated with granular mucosa. (d) Cobblestone-like mucosa corresponding to mucosal pattern with raised nodules, resembling the paving of a "Roman" road (copyright Photos).

In the case of UC (Figure 3.16), the mucosa is granular and brittle. When the disease becomes severe, erosions lesions corresponding to superficial mucosal damage appear. Due to oedema, the visibility of the blood vessels can be degraded.

(a) (b)

Figure 3.16: Some endoscopic lesions in the case of UC disease. (a) Granular colonic mucosa with a faded vascular pattern, mild friability, and erythema. (b) Large ulcerations and spontaneous bleeding (copyright Photos).

The severity of the lesions is usually used as a key parameter for the evaluation of the disease activity. However, an index is required to characterize the mucosa status and t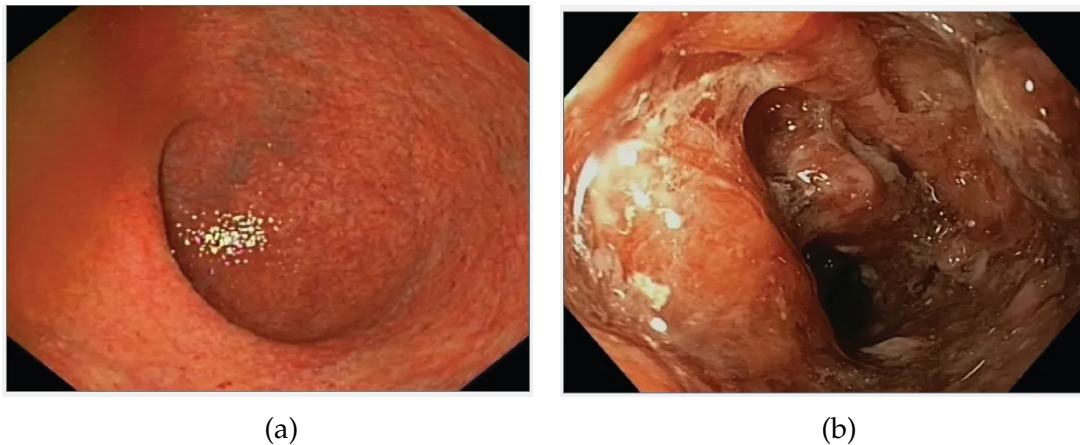hen guide to a convenient treatment. At present, in medical practice and clinical trials, the doctors use the endoscopy videos to provide a numerical evaluation about the severity of the principal descriptors of the disease. This evaluation is called endoscopic score which plays a crucial role in determining the effectiveness of proposed treatments and disease follow-up. In chapter 4, we will describe the numerical assessment of the UC severity used in the medical routine practice. In addition, we will emphasize the endoscopic scores emerged nowadays for disease management and following up as well as treatment efficacy.

3.5 Conclusion

The visualization of the intestinal mucosa state is crucial to the estimation of the disease activity and the evaluation of the treatment efficacy and surveillance. In this chapter, we presented the endoscopy procedures used to investigate the digestive tract in the case of inflammatory bowel diseases. We distinguish two main methods: wireless capsule endoscopy (WCE) and colonoscopy.

In the case of WCE presented in section 3.2, the patient swallows a pill-sized capsule including a camera and light connected via radio frequency system to a recorder. Despite its ease of utilisation and fewer preparation steps required compared to the colonoscopy, the WCE is quite difficult to control once used and the localisation of the lesions is not precisely reported.

In the case of colonoscopy discussed in section 3.3, a camera is used to visualize the interior of the colon and the rectum. Unlike the WCE procedure, some medical interventions can be made during a colonoscopy such as removal of malignant polyps, extraction of biopsies and stopping mucosa's bleeding when it is possible. Contrary to WCE, colonoscopy is an invasive procedure that may cause mucosal perforations or infections.

For detecting small intestine abnormalities and/or suspicious conditions such as Crohn's disease, the gastroenterologist prefers WCE because of its ability to take pictures of the whole digestive tract which cannot be reached by the colonoscope. On the other hand, for the examination of the large intestine like the case of ulcerative colitis disease, he uses the colonoscopy to visualize the colon and rectum.

These techniques both produce an endoscopic video containing images of the gut mucosa (see section 3.4), which the doctor assesses in the form of a numerical score. In the following chapter, we will discuss the grading procedures used for evaluating the UC activity.

Chapter 4

Endoscopic scores

Abstract

Endoscopy is the key tool for the evaluation of the status of the mucosa. To standardize the estimation of disease activity among physicians, an endoscopic scoring system has been established. It is based on the mucosal appearance of features such as the vascular pattern, mucosal erythema, friability, granularity, bleeding, and ulcers. Many ranking scores have been developed for UC and CD.

This thesis focuses on the severity of UC, therefore we will highlight the most commonly used scores to measure UC activity in medical practice.

Although incompletely validated, the endoscopic MAYO and Ulcerative Colitis Endoscopic Index of Severity (UCEIS) scores are preferred in medical practice. Nevertheless, these scores do not take into account the spatial extent of lesions, their number and their surface area throughout the colon.

4.1 Introduction

At present, several endoscopic scoring indices have been introduced for clinical trials and medical practice for IBD diagnosis and treatment follow-up as well. For UC disease, Truelove and Witts [TW55] were the first to propose an endoscopic scoring system. Since then, many researchers have developed endoscopic scores.

The endoscopic scores involve clinical symptoms, biological signs and mucosal appearance during endoscopy examinations as well as physician personal evaluation of disease activity in some cases. As clinical symptoms, we found daily bowel frequency, rectal bleeding, abdominal pain, activity practices and work abilities and extracolonic signs as well. Some scores take into consideration biological parameters such as bloody stool, haemoglobin and heart rates, fever and abdominal tenderness. The main mucosal abnormalities appearance reported for different scores are friability, granularity, oedema, exudation, vascular pattern (Figure 4.2), bleeding (Figure 4.3), erosions and ulcers (Figure 4.4).

The type and number of inspected features are generally not the same for all the scores. While some scores combine clinical, biological and endoscopic parameters, other scores only rate some of the mucosal abnormalities. Some of these scores make a different evaluation for the same type of mucosal abnormality. For instance, spontaneous, middle and deep bleeding are not graded equally. The visibility of the blood vessels also differs when it is partially degraded or completely invisible.

However, it is important to note that all the available scores only grade the most severe lesion of each type regardless of their amount, surface and distribution in the colon.

For all scores, the final score is computed through a linear combination of each feature's sub-score. As per reported scores, the final score range is a numerical value less or equal to 12 depending on the number of the studied features and their scores as well.

A score is requested to be valid, namely it measures accurately the different parameters. Nevertheless, the computation of some scores is complicated due to the high number or type of considered parameters, more particularly, the absence of a precise definition of some parameters is a weakness. Therefore, all the proposed scores are not fully validated for clinical trials and medical practice.

4.2   Truelove and Witts score

The first proposed endoscopic score of the UC disease is the Truelove and Witts Endoscopy Index in 1955 [TW55]. It considers the status of six clinical and biological elements which are stool number per day, nature of blood in stool, temperature, pulse, haemoglobin rate and erythrocyte sedimentation rate (ESR) [1]. The UC disease is then classified into three-level: mild, moderate and severe. The appropriate details are given in Table 4.1. The Truelove ad Witts Index does not present a numerical assessment of the disease which make its use impractical in clinical routine and not obvious between doctors.

Element	Description		
Number of bloody stools per day	< 4	4-6	> 6
Frequency of the blood in stool	Rarely	Intermediate	Often
Fever (°C)	Normal	Intermediate	> 37.5
Hemoglobin (gram/deciLiter, g/dL)	Normal	Intermediate	< 10.5
Heart rate pulse (beats per minute, bpm)	< 90	$\leq$ 90	> 90
ESR (millimeter/Liter, mm/L)	< 20	20-30	>30
Disease classification	Mild	Moderate	Severe

Table 4.1: Computation of the Truelove and Witts endoscopic score [Gaw+17].

4.3   Baron index

Developped in 1964 [BCLJ64a], the Baron index is developed considers descriptors such as bleeding, vascular pattern, friability. The detailed computation of the Baron score is given in Table 4.2. Despite its easy operation, and advantages of presenting a numerical scoring system compared to the Truelove and Witts endoscopic score, the Baron index is still imprecise and not sufficiently correlated to histological abnormalities.

---

[1]ESR is a blood test to detect inflammation which can be generated by a condition such as arthritis, vasculitis, or IBD. This test can be also adapted to monitor an existing disease

Description	Score	Disease classification
Pale mucosa, Normal vascular pattern clearly visible throughout, No spontaneous bleeding and no bleeding to light touch	0	Normal
Glistening mucosa, erythema and oedema, vascular pattern little obliteration	1	Mild
Granularity, bleeding to light touch, no spontaneous bleeding seen ahead of instrument on initial inspection	2	Moderate
Bleeding seen ahead of instrument on initial inspection and on light touching, mucopurulent exudate, occasional mucosal ulceration	3	Severe

Table 4.2: Computation of the Baron Index [Mar06].

4.4 Modified Baron

Feagen et al. in 2005 proposed a modified version of this score, called Modified Baron Index ranging from zero to four and taking into consideration the granularity of the mucosa, bleeding and ulcers [Fea+05]. The score is 0 if the mucosa is normal without the presence of granularity. This evaluation corresponds to endoscopic remission. When the mucosa represents some granularity with damage in vascular pattern, the disease severity score is 1. In the case of friable mucosa, the score is 2. The score of 3 corresponds to tiny ulcerations with spontaneous bleeding, and it is 4 in the case of gross ulcerations. The modified Baron index gives the same score to the superficial and deep ulcerations.

4.5 Powell-Tuck Index

Later in 1982, Powell-Tuck et al. proposed to combine sigmoidoscopy findings and physical signs such as the body temperature, the abdominal sensitivity to evaluate the UC disease activity (see Table 4.3). Although its effectiveness is to differentiate between the possible nature of mucosa bleeding, the Powell-Tuck Index does not include the evaluation of the appearance of ulcerations and the mucosal healing.

Type	Element	Description	Score
Symptoms	Bowel frequency	3-6	1
		>6	2
	Stool consistency	Formed	0
		Semi-formed	1
		Liquid	2
	Abdominal pain	Before/after bowel movements	1
		Prolonged	2
	Anorexia		1
	Nausea/vomiting		1
	General health	Normal	0
		Slightly impaired	1
		Activities restricted	2
		Unable to work	3
	Extracolonic manifestations	One/mild	1
		More than one/severe	2
Signs	Abdominal tenderness	Mild	1
		Marked	2
		Rebound	3
	Fever	< 37.1	0
		37.1 - 38	1
		>38	2
	Blood in stool	Trace	1
		More than trace	2
	Sigmoidoscopy	Non-hemorrhagic	0
		Friable	1
		Spontaneous bleed	2

Table 4.3: Computation of the Powell-Tuck Index [Wal+98].

4.6 Sutherland index

In the work of Sutherland et al. [Sut+87] in 1987, the assessment of the mucosal healing is included leading to a score of four levels ranging from 0 to 3 for each considered element (cf Table 4.4). The authors classified the mucosal status into normal, slight or moderate friability, exudation. The final score is the sum of each element's score. According to the computation of the Sutherland Index, the disease activity is then classified as follow:

- inactive (Index ≤ 2),

- mild (3 < Index < 5),

- moderate (6 < Index < 10),

- severe (11 < Index < 12).

Element	Description			
Diarreha frequency per day	Normal	1-2	3-4	>5
Rectal bleeding	None	Streaks	Obvious	Often
Mucosal appearance	Normal	Slight	Moderate	Exudation or spontaneous bleeding
Physician's global disease evaluation	Normal	Mild	Moderate	Severe
Score	0	1	2	3

Table 4.4: Computation of the Sutherland endoscopic Index [Sut+87].

The Sutherland index is subjective due to consideration of the physician global rating.

4.7 Rachmilewitz index

Later proposed, the index of Rachmilewitz [Rac89] is established during the colonoscopy examination and is more precise than the Baron index. It counts more elements such as the granite appearance and the fragility of the mucosa, vascular pattern, ulcerations and erosions. Like the Sutherland index, it varies between 0 and 12 (see Table 4.5), but it is not validated prospectively. The Rachmilewitz index is also subjective and quite difficult to be used in clinical practice.

Element	Description	Score
Mucosal granularity	Absent	0
	Present	2
Vascular pattern	Normal	0
	Degraded	1
	Invisible	2
Fragility of the mucosa	None	0
	Bleeding on contact	1
	Spontaneous bleeding	4
Erosions and ulcerations	None	0
	No confluent Erosions	2
	Confluent erosions or deep ulcerations	4

Table 4.5: Computation of the Rachmilewitz Index [Mar06].

4.8 Endoscopic Activity Index (EAI)

In 2010 [Nag+10], Naganuma developed a new endoscopic score called Endoscopic Activity Index (EAI) for evaluating six elements: size and depth of ulceration, redness, bleeding, mucosal oedema and mucous exudate (cf Table 4.6).

The EAI score is useful in the case of acute ulcerative colitis patients, and it is correlated to clinical activity [Nag+10].

Feature	Description	Score
Size of ulcers	None	0
	Erosion/small ulcer	1
	Intermediate	2
	Wide-ranged mucosal defects	3
Depth of ulcers	None	0
	Shallow	1
	Intermediate	2
	Deep	3
Redness	None	0
	Mild	1
	Marked	2
Bleeding	None	0
	Contact bleeding	1
	Spontaneous	2
	Massive	3
Edema	None	0
	Mild	1
	Moderate	2
	Severe	3
Mucous exudate	None	0
	Mild	1
	Marked	2

Table 4.6: Computation of the EAI score [Nag+10].

4.9   UC Colonoscopic Index of Severity (UCCIS)

A new UC Colonoscopic Index of Severity, denoted by UCCIS, was introduced by Samuel et al. in 2013 [Sam+13]. It counts five mucosal abnormalities: the vascular pattern, bleeding, ulcers, mucosal friability and granularity. The authors assess the presence and severity of each lesion on the five colon principal segments (rectum, sigmoid, descending, transverse, and cecum/ ascending).

As supplement disease evaluation, they decide to add evaluation of two elements: the segmental assessment of endoscopic severity denoted by SAES, and the global assessment of endoscopic severity denoted by GAES for the considered colon segments in addition to a 10 cm visual analogue scale (from normal to severe).

The grade zero of the parameters SAES and GAES corresponds to a normal vascular pattern with the absence of bleeding and ulcers. Grade one ties in the case of the presence of erythema and patch/total obliteration of the vascular pattern. Grade two is given for the presence of friability with bleeding, granularity and erosions. The highest level four corresponds to spontaneous bleeding and/or

gross ulcerations.

The authors reported a high-level inter-observer agreement. However, the final numerical score is not clearly defined which make its utilization difficult for medical issues.

4.10 Current endoscopic scores

In current medical practice and clinical trials, the doctors use two endoscopic scores: MAYO or the so-called Ulcerative Colitis Disease Activity Index (UC-DAI, [Rut+05]) and Ulcerative Colitis Endoscopic Index Score (UCEIS, [Tra+12]).

In this thesis, we used these scores for comparison of lesions profiles between patients (chapter 7) or with proposed modelling results (chapter 8) or for validation of some proposed hypotheses (chapter 9).

4.10.1 MAYO score

The MAYO score or the so-called Ulcerative Colitis Disease Activity Index (UC-DAI, [Rut+05]) mixes evaluation of clinical and endoscopic variables. It is composed of 4 categories of measurement (stool frequency, bleeding, endoscopic appearance and overall physician assessment) each one rated from 0 to 3. The final score varies between 0 and 12 (cf Table 4.7). In particular, the MAYO score integrates elements from the clinical status of the patient and the results of the endoscopic exam. The final UC disease severity assessment via the MAYO score will be:

- inactive disease (Score $\leq$ 2 points)

- mild disease (3 points $\leq$ Score $\leq$ 5 points)

- moderate disease (6 points $\leq$ Score $\leq$ 10 points)

- severe disease (11 points $\leq$ Score $\leq$ 12 points)

Despite its simple use, the MAYO score (cf Table 4.7) presents many defects. There are difficulties in distinguishing between mild UC lesions and moderate UC lesions, more precisely the absence of distinction between superficial and deep ulceration, which causes opposite therapeutic consequences. Therefore, sometimes doctors prefer to use its simplified version, called the MAYO subscore (or Disease Activity Index, DAI) composed of four levels of measurement mainly depending on the presence/absence of bleeding, ulcers, erosions and the status of the vascular pattern (cf Table 4.8).

Descriptor	Description	Scoring
Stool frequency	Normal	0
	1-2 stools/day more than normal	1
	3-4 stools/day more than normal	2
	> 4 stools/day more than normal	3
Rectal Bleeding	None	0
	Visible blood with stool less than half the time	1
	Visible blood with stool less than half the time or more	2
	Passing blood alone	3
Mucosal appearance at endoscopy	Normal or inactive disease	0
	Mild disease (erythema, decreased vascular pattern, mild friability)	1
	Moderate disease (marked erythema, absent vascular pattern, friability, erosions)	2
	Severe disease (spontaneous bleeding, ulceration)	3
Physician's rating of disease activity	Normal	0
	Mild	1
	Moderate	2
	Severe	3
Total		$0 - 12$

Table 4.7: Computation of the MAYO score [Lew+08].

Disease activity	Endoscopic features	Scoring
Normal or inactive disease	None	0
Mild	Erythema, decreased vascular pattern, mild friability	1
Moderate	Marked erythema, absent vascular pattern, friability, erosions	2
Severe	Spontaneous bleeding, ulceration	3

Table 4.8: Computation of the MAYO sub-score.
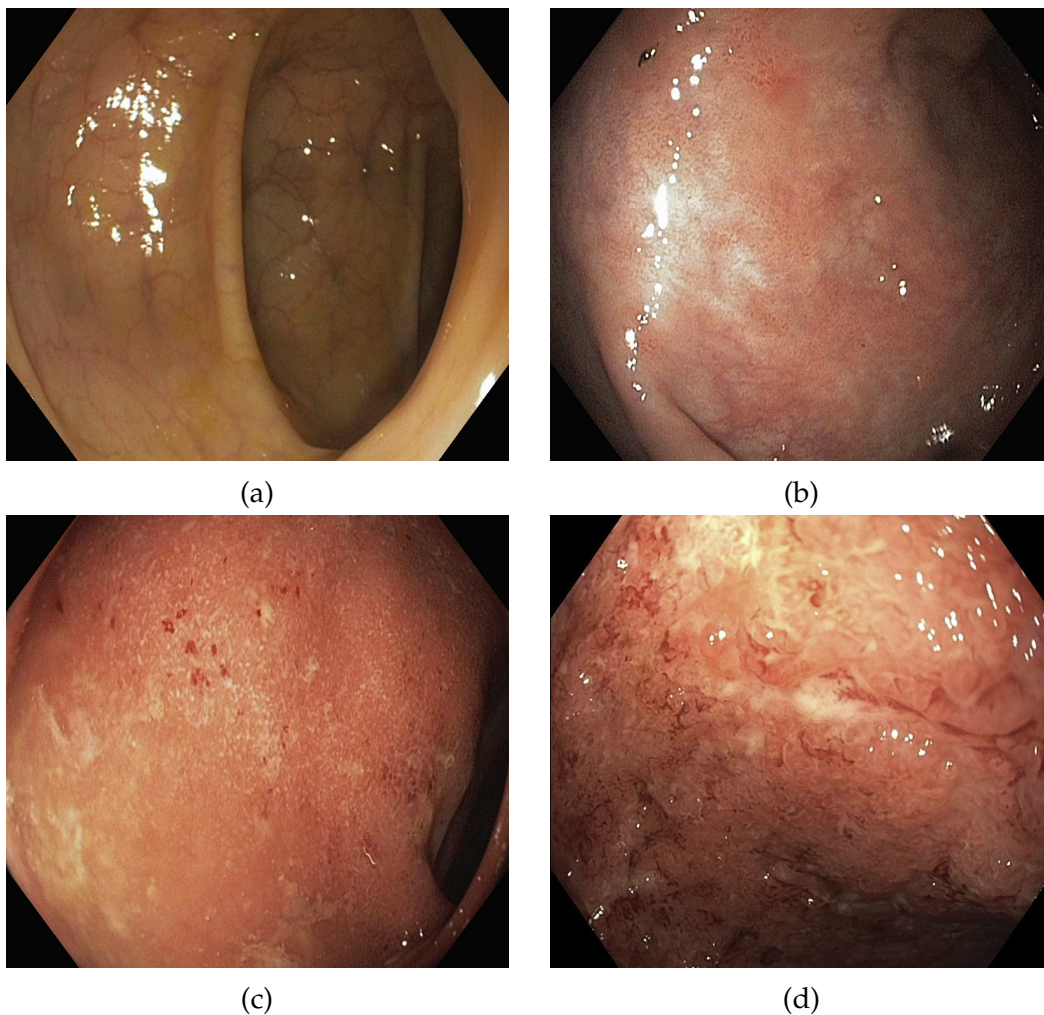
Figure 4.1: MAYO subscore evaluation. (a) Score 0, normal mucosa appearance with absence of abnormalities. (b) Score 1, the mucosa presents erythema and friability. (c) Score 2, presence of erosions. (d) Score 3, the mucosa is bleeding and ulcerated [LPF20].

4.10.2   Ulcerative Colitis Endoscopic Index Score (UCEIS)

In 2012 [Tra+12], Travis et al. proposed a simple and reliable endoscopic severity score UCEIS. Their study was performed by 30 investigators of different nationalities into two phases. They used a total of 680 sigmoidoscopy videos containing five videos for healthy individuals, and five videos for severe UC hospitalized patients. For the first stage of the study, 10 investigators have evaluated 16 to 24 randomly selected videos according to their experience to attempt the presence and absence of 10 principal UC endoscopic descriptors presented in previous studies [BCLJ64b; Gom+86; Per+87; Orl+98; DLLA04]. The ten principal descriptors are listed in the first column of Table 4.9.

Descriptor from litterature	ponderated kappa intra-observer	ponderated kappa inter-observer
Erosions and ulcers	0.65	0.45
Vascular pattern	0.61	0.42
Bleeding	0.6	0.37
Extent of erosions or ulcers	0.60	0.42
Spontaneous friability	0.49	0.40
Mucopus	0.47	0.40
Mucosal granularity	0.45	0.34
Mucosal oedema	0.43	0.31
Mucosal erythema	0.43	0.35
Contact friability	0.33	0.34

Table 4.9: Intra and inter observers variations to define the 3 descriptors of the UC disease to generate the UCEIS score [Tra+12].

For the second stage, the 30 investigators assess the overall UC activity in 25 different videos on a 0 to 100 visual analogue scale (VAS). Table 4.9 illustrates the numerical agreement between investigators for the selected descriptors based on the ponderated Cohen's kappa coefficient (k) [2].

The final UCEIS score rates the most severe lesion of the three principal descriptors type vascular pattern, bleeding and erosions/ulcerations chosen according to the maximum values of the ponderated Cohen's kappa coefficient (k).

In Table 4.10, we present the computation of the final score, UCEIS. Bleeding, erosions and ulcers lesions are ranked between 0 and 3, while the vascular pattern is ranked between 0 and 2. The sum of all sub-rates is the final score (0-8).

---

[2]kappa is a statistical variable that measures the agreement between two raters. $k = 1$ means complete agreement between investigators

Descriptor	Description	Definition	Scoring
Vascular pattern	Normal	Normal vascular pattern with arborisation of capillaries clearly defined or with blurring or patchy loss of capillary margins	0
	Patchy obliteration	Patchy obliteration of vascular pattern	1
	Obliterated	Complete obliteration of vascular pattern	2
Bleeding	None	No visible blood	0
	Mucosal	Some spots of coagulated blood on the surface of the mucosa ahead of the scope that can be washed away	1
	Luminal mild	Some free liquid blood in the lumen	2
	Luminal moderate or severe	Frank blood in the lumen ahead of the endoscope or visible oozing from the mucosa after washing intraluminal blood, or visible oozing from a hemorrhagic mucosa	3
Erosions and ulcers	None	No visible erosions or ulcers	0
	Erosions	Tiny defects ($\leq$ 5 mm) in the mucosa of a white or yellow color with a flat edge	1
	Superficial ulcer	Larger defects ($>$ 5 mm) in the mucosa, which are discrete fibrin-coverted ulcers when compared with erosions but remain superficial	2
	Deep ulcer	Deeper excavated defects in the mucosa with a slightly raised edge	3
Total			$0-8$

Table 4.10: Computation of the UCEIS score [Tra+13].

(a)   (b)   (c)
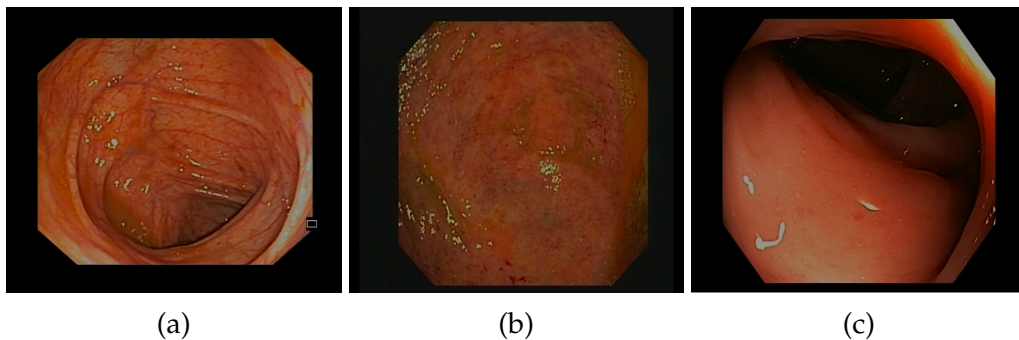
Figure 4.2: UCEIS sub-score for the descriptor vascular pattern (from left to right): Score = 0, Score = 1, and Score =3.

(a)   (b)   (c)
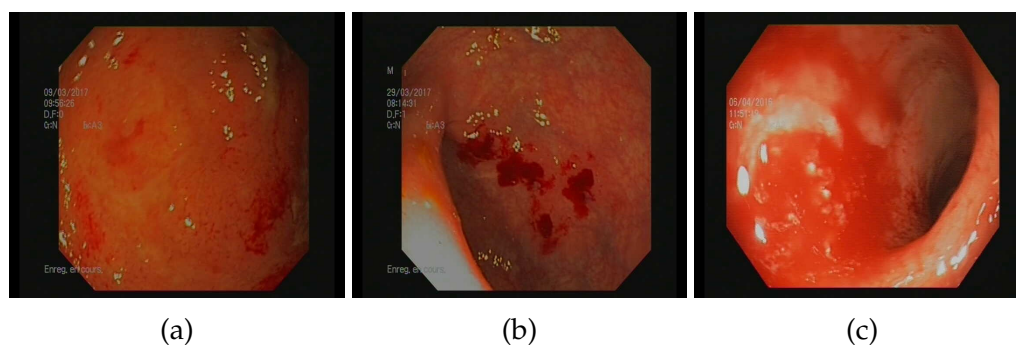
Figure 4.3: Some bleeding lesions findings in a colonoscopy video. (a) Spontaneous bleeding scored 1, (b) Moderate bleeding patchs scored 2 and (c) Severe bleeding scored 3.

(a)   (b)   (c)
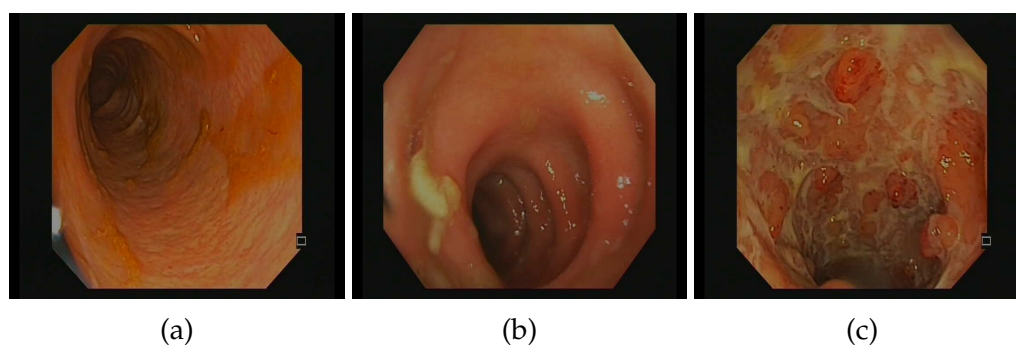
Figure 4.4: Examples of ulcerations and erosions lesions in a colonoscopy video. (a) Erosions corresponding to superficial mucosal damaging are generally scored 1 (b) Ulcers caracterized by a necrosis at the level of the mucosa thickness are scored 2, (c) Deep erosions and ulcers affecting the whole colon lining are scored 3.

Although the UCEIS score does not consider mucosal healing, it is a simple and convenient method to measure the severity of the UC disease. As for the previous scores, UCEIS rates the most severe lesion of type bleed, ulcer, and vascular pattern and does not take into consideration the spatial extent of the lesions in the colon. In comparison to the UCEIS score, it can be relevant to only focus on the endoscopic sub-score instead of the complete MAYO score which only considers mucosal abnormalities.

4.11   Discussion

In Table 4.11, we summarise the most common endoscopic variables of the mucosa's abnormalities reported in the endoscopic scores. They involve bleeding, ulcerations as well as mucosal friability, granularity and blood vessel visibility.

Score	Bleeding	Erosion/Ulcer	Exudation	Friability	Granularity	Edema	Vascular pattern
Truelove & Witts					✓		
Baron index	✓	✓	✓		✓	✓	✓
Modified Baron	✓	✓		✓	✓		✓
Powell-Tuck	✓						
Sutherland	✓		✓	✓			
Mayo	✓	✓		✓			✓
Rachmilewitz		✓		✓			✓
EAI	✓	✓	✓			✓	
UCEIS	✓	✓					✓
UCCIS	✓	✓		✓	✓		✓

Table 4.11: Common descriptors of the UC used for the computation of the endoscopic scores.

As we mentioned at the beginning of this chapter, the scores include different types of features: clinical, biological and endoscopic. A combination of the three types of parameters is employed in the Powell-Tuck score (section 4.5). The Truelove and Witts index considers a set of clinical and biological parameters (section 4.2). In addition to clinical features and mucosal abnormalities, the overall physician interpretation is considered in Sutherland (section 4.6) and Mayo score (subsection 4.10.1). The majority of the other scores, i.e. Baron index (section 4.3), Rachmilewitz score (section 4.7), EAI (section 4.8), UCCIS (section 4.9), Mayo sub-score and UCEIS (subsection 4.10.2), include only mucosal abnormalities.

The number of endoscopic variables, meaning the mucosal abnormalities, used for severity scoring computation is also variable among UC endoscopic scores. The Baron index counts six elements, the Mayo sub-score and UCCIS include five parameters, EAI takes into consideration only four mucosal abnormalities. The Rachmilewitz and UCEIS scores count three parameters.

One major drawback of all the reported endoscopic scores is that they miss the evaluation of the mucosa healing. Mucosal healing is defined as the cure of all presented ulcerations in the colon and histological inflammation [LKM19]. Specifically, for ulcerative colitis disease, the remission of the mucosa involves the absence of friability, bleeding, erosions and ulcerations [AN17]. Even with UCEIS, which gives a zero score in the case of absence of lesions, mucosal remission is not evaluated precisely. This is a problem because the goal of the therapies currently proposed for the management of IBDs is to maintain the healing of the mucosa from existing lesions. Indeed, mucosal healing is correlated with decreased rates of surgeries, required hospitalizations, and corticosteroid-associated morbidity. Additionally, the target of therapy is to maintain remission with the prevention of long-term complications such as colorectal cancer, irreversible colon damage, and colectomy.

Most of the scores cited in the chapter evaluate the status of the mucosa without reporting the colonic segment concerned and the number of lesions. The UCCIS is the single score taking into account all colonic segments. However, the definition of the local score for each segment is not clearly stated. The presented scores miss the assessment of the spatial extent of the lesions along the colon, their amount as well as the relapse and remitting course of the disease. Later, the lack of such type of information may lead to an incomplete evaluation of the disease severity, and consequently the monitoring of the disease course. The extent of disease is relevant to disease classification and prognosis because of the correlation between extensive ulcerative colitis and the high risk of complications such as colorectal cancer and colectomy.

Furthermore, an endoscopic score must be validated, i.e. it accurately measures the result that it is intended to assess. Although the Mayo sub-score, UCEIS and UCCIS have been widely validated in comparison to other scores, none of these scores has been fully validated [Vas+18a].

Finally, the scoring systems generally rely on the gastroenterologist's interpretation when reviewing the colonoscopy video and target the evaluation of the most severe lesions. Reliability estimates for some scores for the same doctor and with other colleagues was studied in [Vas+18a]. Among the severity scoring presented previously, in only five scores the intra and inter reliability was reported. Generally, the parameter kappa statistics is used for a numerical evaluation of the assessment of the raters scoring reliability. According to [Vas+18a], in the case of the Mayo sub-score k inter-rater is between 0.45 and 0.75 and the intra-rater reliability is 0.75. For EAI, the inter-rater reliability estimates are better, with $k = 0.97$. For Baron score, the inter-rater and intra-rater reliability are $k = 0.61$ and $k = 0.47$ respectively. As the UCCIS takes into account colonic segments, the reported inter-rater variability values in literature were considered on each segment, and it is between 0.56 and 0.88. A comparative conclusion between these scores cannot be informative since, the number of raters, videos and variables considered in each score is not the same in the reported studies.

To reduce this variability, colonoscopy videos are usually graded by third-party experts in a procedure called central reading. A central reading system is often used to mean that the interpretation of imaging findings is not, or not only, done by local endoscopists of the hospital but instead is supervised, amended or adjudicated by at least one off-site/external reader who is neither aware of nor influenced by knowledge of the patient characteristics or treatment arm assignment. This helps to ensure having a more accurate and unbiased grading of disease activity [Pan+16].

4.12   Conclusion

In this chapter, we review some of the available endoscopic scores used to evaluate the severity of ulcerative colitis disease. They take into consideration several features of type clinical, biological and endoscopic.

In general, endoscopic scores are computed as the sum of the grades of individual feature. Only the most severe lesion is considered, regardless of the overall spatial distribution and amount of lesions along the colon. Scoring also relies on the gastroenterologist's personal interpretation, and blind contral-reading procedures have been proposed to reduce this varaibility.

Currently, the doctors use the Mayo endoscopic subscore and the UCEIS score in clinical trials and medical practice (cf section 4.10). They only consider mucosal abnormalities. The Mayo sub-score ranks the presence and absence of five lesions which are erythema, friability, bleeding, ulcers and vascular pattern visibility. Whereas, the UCEIS ranks three mucosal abnormalities: bleeding, ulcers and vascular pattern. The final Mayo endoscopic sub-score varies between 0 and 3 while the final UCEIS value is between 0 and 8.

In our work, we attempt to take into account the spatial extent of lesions as well as their amount or surface to visualize their spatial distribution in chapter 7, to mathematically model the UC severity in chapter 8, to study some medical questions in chapter 9 and estimate the inflammation invasion time in chapter 10.

Chapter 5

Vatic database

Abstract

This chapter is dedicated to the presentation of the dataset of 49 colonoscopy videos that will be used in the thesis.

First, we describe the colonoscopy videos obtained during the collaboration with the Bichat and Beaujon hospitals. Secondly, we explain the annotation process of UC lesions provided by gastroenterologists. Thirdly, we present some examples of utilisation of the available data, mainly how we compute the number and surface of the annotations.

These annotations will be used along with the thesis works like the visualisation of the spatial distribution of lesions in chapter 7, the severity scores modelling in chapter 8, and the computation of the lesions propagation speed in chapter 10.

5.1 Presentation of the Vatic database

Since our goal is to provide an objective assessment of the severity of the disease, we need colonoscopy videos where the doctor marks the frames showing visible lesions. During the collaboration with the gastroenterology group of the Bichat-Beaujon hospitals, we obtained 49 colonoscopy videos. The database, that we called "Vatic", involves patients affected by UC disease in different stages and forms, for both genders, women and men. In a total of 37 videos, the doctors have marked the lesions such as bleeding and ulcers. The remaining twelve videos are for healthy persons.

In Figure 5.1, we show images extracted from Vatic database videos. The colon presents ulcerations and bleeding contrary to a healthy colon given by Figure 5.2.
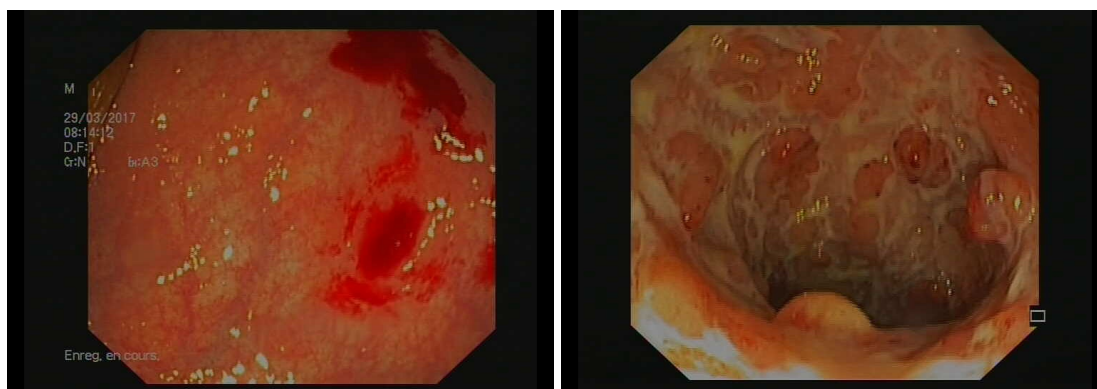
Figure 5.1: Example of endoscopic images found in Vatic database videos for UC patients. Bleeding lesions (on left) and ulcers lesions (on right).
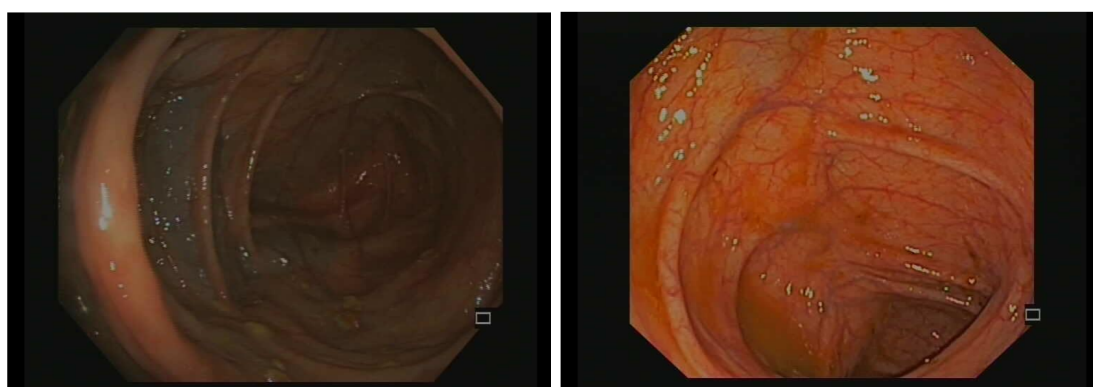
Figure 5.2: Example of endoscopic images found in Vatic database videos for healthy people. There are no mucosal abnormalities such as bleeding and erosions or ulcerations. The blood vessels are visible, the colon is in a good status.

The videos' length is not the same for all the patients since some of the videos correspond to uncompleted colonoscopy. The number of frames for available

videos ranges between 379 and 6073. The total number of images in Vatic is 101473, for which 86168 images refer to UC patients. The image resolution is 768×576 pixels, except for two videos where the image size is 640×480 pixels.

On the other hand, the Vatic database includes the disease severity assessment for 13 patients. In particular, three gastroenterologists evaluated the endoscopic scores: Mayo sub-score and UCEIS as given in Table 5.1.

	UCEIS			MAYO		
Video number	XT	CS	YB	XT	CS	YB
1	8	8	7	3	3	3
2	7	6	8	3	3	3
3	2	2	3	1	1	2
5	1	1	1	1	1	1
6	3	2	1	1	1	1
7	1	4	0	1	2	0
9	5	5	4	3	3	3
10	5	5	5	3	3	2
13	5	6	3	3	3	2
15	5	3	2	3	1	1
16	7	6	3	3	3	2
17	5	4	3	3	3	2
21	7	7	4	3	3	2

Table 5.1: Endoscopic scores (UCEIS and MAYO sub-score) for 13 patients from Vatic database evaluated by Drs XT, CS and YB.

5.2 Videos annotation

The Vatic software [VPR13] enables tracking objects paths along a given video using linear interpolation between consecutive movements of the targeted objects which consequently makes it possible to follow the movements of objects while reducing human work.

The principle of the Vatic annotation process is that the user plays the video, draws bounding boxes around objects of interest (see Figure 5.3), and follows each object throughout its appearance in the video. Each object can have multiple attributes that further describe its actions.

In our situation, the objects of interest are lesions, more precisely bleeding and ulcer lesions found in colonoscopy videos. During the video annotation process, the doctor can adjust the reading speed, search throughout the timeline, and mark lesions occluded or off-screen. Since scenes quickly become cluttered,

the doctor making the annotations can lock the lesions to prevent accidental changes to their paths.

In Figure 5.3, we show an example of the Vatic interface. We see two features whose paths are to be tracked in the video: bleeding and ulcer. When he detects a new lesion on the screen, the doctor clicks on the button "New object" on the top right, then draws a box at the desired area of the figure and adjusts the size of the box later to meet all the localised lesions. The list of marked lesions appears on the right.
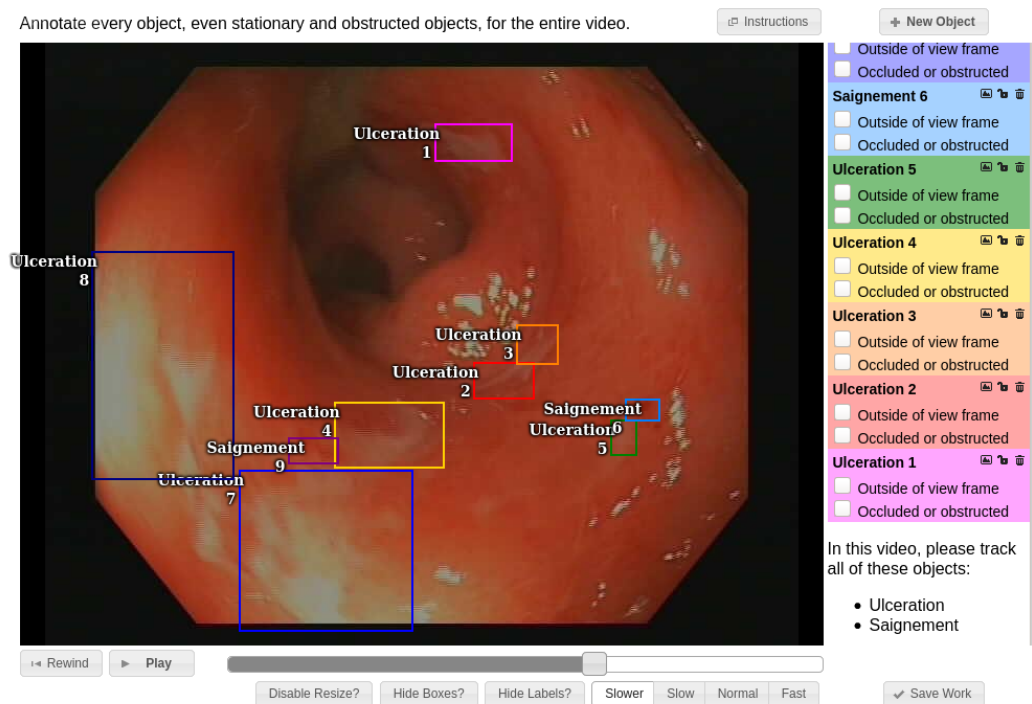
Figure 5.3: A screenshot for a colonoscopy image annotated using Vatic software [VPR13].

The annotation of lesions using Vatic software comprises some advantages and disadvantages:

- The main advantage of this software is the reduction of time review and annotation procedure. The doctor annotates all the lesions in the first frame of the colonoscopy video, then he advances to the next frame, updates all of the annotations, and repeats this process for the entire video. Consequently, the doctor watches the video only once since when a frame is labelled, he will never need to return to it. Moreover, Vatic can be used to obtain a considerable annotated database.

- The disadvantage of Vatic is the many errors generated during the annotation of the ground truth. The lesions are in general of arbitrary shapes

which makes their delimitation with boxes imprecise, as done in our work. Many normal pixels are labelled "abnormal", i.e. with lesions, once they are inside a given box (see Figure 5.3). This mislabelling problem will later affect the performance of the model to automatically detect ulcerative colitis lesions (cf chapter 6). As a solution, we propose to count detected annotations instead of detected pixels.

5.3 How to use the annotations ?

The doctors' annotations can be exported to CSV format. We launch the following command lines in a Linux terminal to save the text format of a given annotated video:

Code chunk 1: shell

```
ssh comptepersonnel@laga-vatic
Mot de passe: ***
cd vatic
cd vatic
turkic dump video.avi -o video.txt
exit
scp comptepersonnel@laga-vatic:vatic/vatic/video.txt ./
Mot de passe: ***
```

Herein an example of the first ten lines of the text document corresponding to video 1 of the database.

Code chunk 2: shell (part 2)

```
head "video1.txt"
```

Interpret with `shell`

```
0 475 129 598 406 0 0 0 0 "Ulceration"
0 487 148 592 364 1 0 0 1 "Ulceration"
0 500 167 586 323 2 0 0 1 "Ulceration"
0 513 187 581 282 3 0 0 0 "Ulceration"
0 502 171 593 328 4 0 0 1 "Ulceration"
0 491 155 605 374 5 0 0 1 "Ulceration"
0 481 139 618 421 6 0 0 0 "Ulceration"
0 478 140 615 427 7 0 0 1 "Ulceration"
0 475 142 613 433 8 0 0 1 "Ulceration"
0 473 144 611 439 9 0 0 0 "Ulceration"
```

With the following signification of each column [VPR13]:

- Column 1: Track lesion identity

- Column 2: xmin the top left x-coordinate of the annotation box

- Column 3: ymin the top left y-coordinate of the annotation box

- Column 4: xmax the bottom right x-coordinate of the annotation box

- Column 5: ymax the bottom right y-coordinate of the annotation box

- Column 6: frame number of the presented annotation

- Column 7: lost. If 1, the annotation is outside of the view screen

- Column 8: occluded. If 1, the annotation is occluded.

- Column 9: invisibility of lesion

- Column 10: lesion label (bleeding or ulceration) enclosed in quotation marks

In Figure 5.3, we have many rectangular annotations for each feature (bleeding and ulcerations). They correspond to a newly added annotation on the frame. However, it does not mean that we have a new type of lesion corresponding to mucosa abnormalities like erosions, vascular pattern visibility nor type of the specific descriptor (bleeding of type luminal, mucosal, superficial/ ulcerations of type superficial or deep). Therefore, to facilitate the reading and analysis process of the annotations, we decide to mark all bleeding annotations by red rectangles and ulcer annotations by yellow rectangles (see Figure 5.4).

| (a) | (b) |
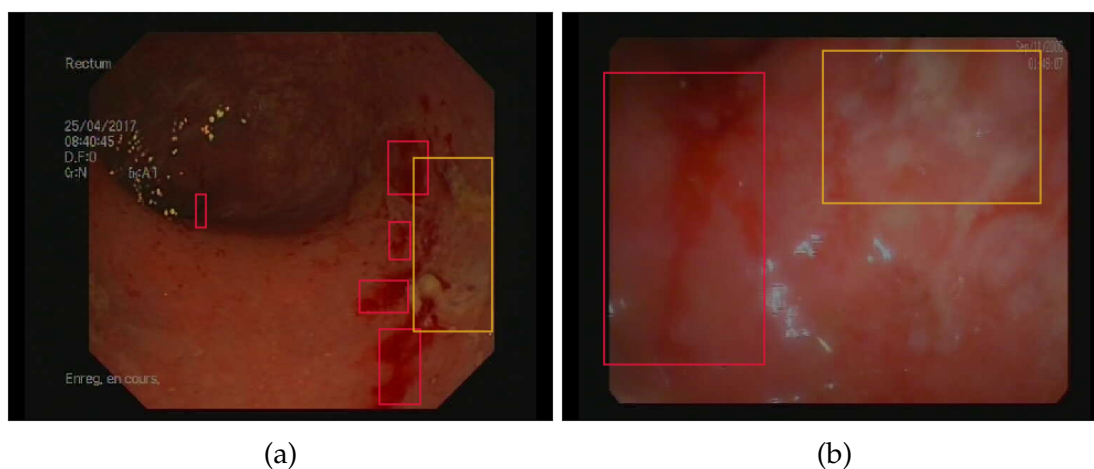
Figure 5.4: Annotated frames extracted from Vatic database. Red rectangles indicate bleeding lesions while orange rectangles indicate ulcers lesions.

The current endoscopic scores miss the count and spatial distribution of the lesions along the colon (cf chapter 4). Because of taking into consideration such information to measure the disease severity in this manuscript, we will present to the reader some of the python codes launched along the thesis chapters to extract annotation information starting from appropriate functions to some application examples on patients of the Vatic database. First of all, we import the requested python librairies:

Code chunk 3: Data-code.py

```python
# python librairies
import matplotlib as mpl
mpl.use('PDF')
import matplotlib.pyplot as plt
import numpy as np
import cv2, io, string
from math import sqrt,exp
import pickle
```

Then we extract the set of images for all the videos. The variables that will be used along the chapters are `num_video` and `fichier_image_video`. The `num_video` designs the video number while `fichier_image_video` indicates folder containing images of each video.

Code chunk 4: Data-code.py (part 2)

```python
# Data base informations
num_video= list of video number in Vatic database
fichier_image_video= list of folders containing images of each video
```

We use the following python function to count the annotations in given video:

Code chunk 5: Data-code.py (part 3)

```python
def Count_Lesions(num_video):
    fichier_txt="Folder of videos in format text/video%d.txt"%(num_video)
    fichier = io.open(fichier_txt, 'r')
    Lignes = fichier.readlines()
    Maxannot = Lignes[len(Lignes) - 1]
    lMaxannot = Maxannot.split()
    Nfmax = int(lMaxannot[5])
    NannotS_frame,NannotU_frame=np.zeros(Nfmax), np.zeros(Nfmax)
    for frame in range(0, Nfmax):
        for ligne in Lignes:
            l = ligne.split()
            if (int(l[7]) + int(l[6])) == 0 and int(l[5]) == frame:
                if '"Saignement"' in l:
                    NannotS_frame[frame]+=1
                elif '"Ulceration"' in l:
                    NannotU_frame[frame]+=1

    return NannotS_frame,NannotU_frame
```

We run the code to all the Vatic videos and save the results for bleeding into vector `Data_Count_b` and for ulcers into `Data_Count_u`.

Code chunk 6: Data-code.py (part 4)

```python
# application to Vatic database
y_b_count, y_u_count=[[]]*len(num_video),[[]]*len(num_video)
for index in range(len(num_video)):
    y_b_c,y_u_c= Count_Lesions(num_video[index])
    y_b_count[index].append(y_b_c)
    y_u_count[index].append(y_u_c)

# Saving results
with open('Folder-DataVatic-Count.pickle','wb') as f:
        pickle.dump([y_b_count,y_u_count],f)

# Using saved data
with open('Folder-DataVatic-Count.pickle','rb') as f:
        y_b_count,y_u_count=pickle.load(f)

# bleeding
Data_Count_b = [ [individualArray] for individualArray in y_b_count ]
Data_Count_b=Data_Count_b[0][0]
# ulcer
Data_Count_u = [ [individualArray] for individualArray in y_u_count]
Data_Count_u=Data_Count_u[0][0]
```

Figure 5.4a contains five bleeding annotations and one ulcer annotation. Whereas, in Figure 5.4b, the doctor have annotated one lesion for each type, i.e. bleeding and ulcers.

Code chunk 7: Data-code.py (part 5)

```python
print Data_Count_b[8][850],Data_Count_u[8][850]
print Data_Count_b[22][364],Data_Count_u[22][364]
```

Interpret with `python2`

```
5.0 1.0
1.0 1.0
```

Moreover, we look into the computation of the annotations areas by the function `Data_perc_annotations` and then we save the obtained results into vector `Data_Perc_b` for bleeding and `Data_Perc_u` for ulcers.

Code chunk 8: Data-code.py (part 6)

```python
# FIV: fichier_image_video
# computation of percent of abnormal pixels per frame
def Data_perc_annotations(num_video,FIV):
    fichier_video="Folder of images of video/%s"%(FIV)
    fichier_txt="Folder of videos in format text/video%d.txt"%(num_video)
    fichier = io.open(fichier_txt, 'r')
    Lignes = fichier.readlines()
    Maxannot = Lignes[len(Lignes) - 1]
    lMaxannot = Maxannot.split()
    Nfmax = int(lMaxannot[5])
    Masque = "%s/Test-Fig-Masque.png" % (fichier_video)
    M = cv2.imread(Masque)
    M = cv2.erode(M[:, :, 1], 255 * np.ones((5, 5), np.uint8))
    M1 = cv2.imread(Masque)
    M1 = cv2.erode(M1[:, :, 1], 255 * np.ones((5, 5), np.uint8))
    n_masque = np.sum(M == 255)
    per_bleed, per_ulcer=np.zeros(Nfmax),np.zeros(Nfmax)
    for frame in range(0, Nfmax):
        for ligne in Lignes:
            l = ligne.split()
            if (int(l[7]) + int(l[6])) == 0 and int(l[5]) == frame:
                if '"Saignement"' in l:
                    M[int(l[2]):int(l[4]) + 1, int(l[1]):int(l[3]) + 1] = 100
                elif '"Ulceration"' in l:
                    M[int(l[2]):int(l[4]) + 1, int(l[1]):int(l[3]) + 1] = 200

        M[M1 == 0] = 0
        per_bleed[frame]=float(np.sum(M==100))/n_masque
        per_ulcer[frame]=float(np.sum(M==200))/n_masque

    return per_bleed,per_ulcer, Nfmax
```

Code chunk 9: Data-code.py (part 7)

```python
# application to Vatic database
y_b_percent, y_u_percent=[[]]*len(num_video),[[]]*len(num_video)
for index in range(len(num_video)):
    y_b_p,y_u_p= Data_perc_annotations(num_video[index],fichier_image_video)
    y_b_percent[index].append(y_b_p)
    y_u_percent[index].append(y_u_p)

# Saving results
with open('Folder-DataVatic-Percent.pickle','wb') as f:
        pickle.dump([y_b_percent,y_u_percent],f)

# Use of saved results
with open('Folder-DataVatic-Percent.pickle','rb') as f:
        [y_b_percent,y_u_percent]= pickle.load(f)

# bleeding
Data_Perc_b = [ [individualArray] for individualArray in y_b_percent]
Data_Perc_b=Data_Perc_b[0][0]
# ulcer
Data_Perc_u = [ [individualArray] for individualArray in y_u_percent]
Data_Perc_u=Data_Perc_u[0][0]
```

As applied to Figure 5.4, about 73% of pixels are labelled bleeding while 10% are labelled ulcers in Figure 5.4a. In the case of Figure 5.4b, relative to the total image size, the bleeding annotation area is 41% and the ulcer area is 21%.

Code chunk 10: Data-code.py (part 8)

```python
print round(Data_Perc_b[8][850],3),round(Data_Perc_u[8][850],3)
print round(Data_Perc_b[22][364],3),round(Data_Perc_u[22][364],3)
```

Interpret with `python2`

```
0.73 0.103
0.412 0.212
```

We conclude that the different types of extracted data (count of annotations, area of annotations) can promote different information about the inflammation of the colon. In some cases, the size or area of lesions may yield complement information to their count. For instance, in Figure 5.4, although the two figures include only one ulcer annotation, the area of ulcers in Figure 5.4b is greater than the ulcers area of Figure 5.4a (21% versus 10%).

5.4 Conclusion

This chapter describes the dataset of colonoscopy videos called Vatic, that will be employed in all the thesis.

It includes 49 videos for patients affected by UC and healthy people. The endoscopic images are of high-resolution, mainly 768×576 pixels for most of the videos.

The bleeding and ulcer lesions were annotated based on the Vatic [VPR13] software. It consists in delineating the lesions by boxes and tracking them in the video using linear interpolation between the consecutive frames. The doctor only needs to annotate a given lesion a limited number of times. The annotation process leads to a huge amount of annotated images. However, due to the rectangular shapes of annotations and complex shapes of lesions, many mislabeled pixels occur.

Finally, we show how we use this data to compute the surface and number of annotations in a given image. This information will be employed for all the following chapters.

Chapter 6

Automatic detection of ulcerative colitis lesions in colonoscopy videos

Abstract

The severity grading using the UCEIS and MAYO-sub scores is based on the subjective interpretation of the doctor and does not take into account the size of the lesions, their number and their distribution. Automatic lesion detection methods can enable a more precise assessment of lesion severity but it depends on the training set quality. In this chapter, we propose an algorithm to automatically detect ulcerative colitis lesions from colonoscopy videos of the Vatic database.

During the procedure, the doctors use only rectangles to delineate bleeding and ulcers. This annotation process leads to many errors due to many mislabeled pixels, especially in the corners of the rectangles. This affects later the evaluation of the models' performance and the ability to find correct models. As a solution, we propose to evaluate the model sensitivity on the annotation level considering that a model correctly identifies a lesion if it agrees with the expert on a subset of the annotation, and count the detected annotations weighted by their area or their count. Moreover, we propose an efficient sampling scheme to explore the set of linear classifiers in suitable color spaces.

On a data set of 5 colonoscopy videos, we find that all sampled models have a non-zero true negative rate. Despite the limited quality of the annotations, we correctly identify the lesions (93% specificity / 89% for bleeding and 57% specificity / 83% sensitivity for ulcers). Tested on 10 videos, the performance of the detectors was computed reliably. We evaluate sensitivity and specificity on 20 random subsets containing 10% of the images and obtain similar performance for the same patient for all models.

However, the inter-patient performance is variable and the best models fail on some patients (sensitivity below 20% in some cases). This suggests that the variability in the appearance of the lesions between patients should be considered before conducting an automatic detection algorithm.

6.1   Problem statement and motivation

The severity assessment is generally based on the evaluation of the state of the mucosa to detect abnormalities and damage. In this way, the gastroenterologist has to review the video obtained after the investigation of the digestive tract using the WCE or the colonoscopy procedure (cf chapter 3).

The wireless capsule camera takes 50000 to 60000 pictures with the rate of 2 to 4 frames per second (fps). On the other hand, it has been recommended that the time that an endoscopist takes to withdraw the endoscope should be in an average of at least six to ten minutes in normal colons, in the absence of biopsies and polypectomies [Rex07]. The obtained video may then contain 10800 to 180000 frames.

Therefore, for the two types of medical examination/endoscopy, the doctor has to review a huge amount of images to detect lesions and evaluate their severity. In general, the endoscopic abnormalities are present in only a few images [KFR18]. The lesion detection is therefore a tedious task that requires a lot of time and a high level of concentration of the doctor to detect by naked eye the mucosal abnormalities.

In addition, the severity assessment of the ulcerative colitis disease using the endoscopic scores such as UCEIS and MAYO sub-score (see chapter 4) is subjective because it relies on the gastroenterologist's personal interpretation. A given lesion in an endoscopic image may be evaluated differently between doctors [KG15]. Thereby, the disease severity grading is not reproducible neither inter-doctor nor intra-doctors.

Consequently, automatic lesion detection techniques can bring significant benefits by improving the reproducibility of severity assessment while decreasing the physician burden. Although the lesions' appearance is similar between UC and CD, we anticipate that the currently available methods are biased to their training set, i.e. to well-delineated video-capsule images [GFW18; HH15; Liu+16; Naw+14; Vas+18b] as opposed to complete colonoscopy videos obtained on the local instruments. In this chapter, we propose to automatically detect bleeding and ulcers found in colonoscopy videos extracted from the Vatic database.

In section 6.2, we recall the annotation process for the Vatic database. Many automatic methods were proposed in the context of endoscopic abnormalities detection, especially bleeding and ulcers. We will present some of these methods in section 6.3. In section 6.4, we discuss our proposed method that takes into account the annotations errors. In addition, we propose a sampling strategy

that rejects trivial classifiers and speed up the computation time. The obtained results are discussed in section 6.5.

6.2 Lesions annotation process

In general, an automatic detection technique requires a phase of abnormalities annotation. Manual and precise delimitation of the lesions in the colonoscopy videos is a laborious mission involving considerable effort and time from doctors because of the large number of images and the complicated forms of the lesions.

To minimise the burden of the annotation process, we suggest to doctors delineate the bleeding and ulcers lesions of the colonoscopy videos using rectangles instead of precise boundaries delineation. Indeed, during the colonoscopy procedure, the doctor aims to visualize the colonic mucosa and control the endoscope directions, which may lead to viewing a given lesion on successive frames. In order to help the doctors for annotating the lesion only on its first appearance, we proposed to use an interface inspired by the Vatic software [VPR13] discussed in chapter 5.

In Figure 6.1, we present examples of annotated lesions extracted from the Vatic database. The bleeding and ulcers lesions are of variable and complex geometric shapes. Therefore, their delimitation by rectangles is quite imprecise. In Figure 6.1a, the doctor has used small rectangles to localise almost all of the bleeding lesions. However, he didn't cover all of them and he missed some of the lesions at the bottom right of the frame. The pixels surrounding bleeding in Figure 6.1b were included in the rectangles although they are healthy pixels. Similar problems occur in the case of ulcers annotations (cf Figure 6.1c and Figure 6.1d). Consequently, many normal pixels have been labelled as abnormal since they are inside a given box.

Therefore, the performance of the detector to correctly identify lesion pixels will not be computed accurately. To deal with this problem, we propose to take these pixels into account when calculating the detector's capacity to correctly identify lesion pixels.

Let us first recall some automatic methods proposed to detect bleeding and ulcers visualized during the endoscopy exploration of the digestive tract.

(a)   (b)

(c)   (d)
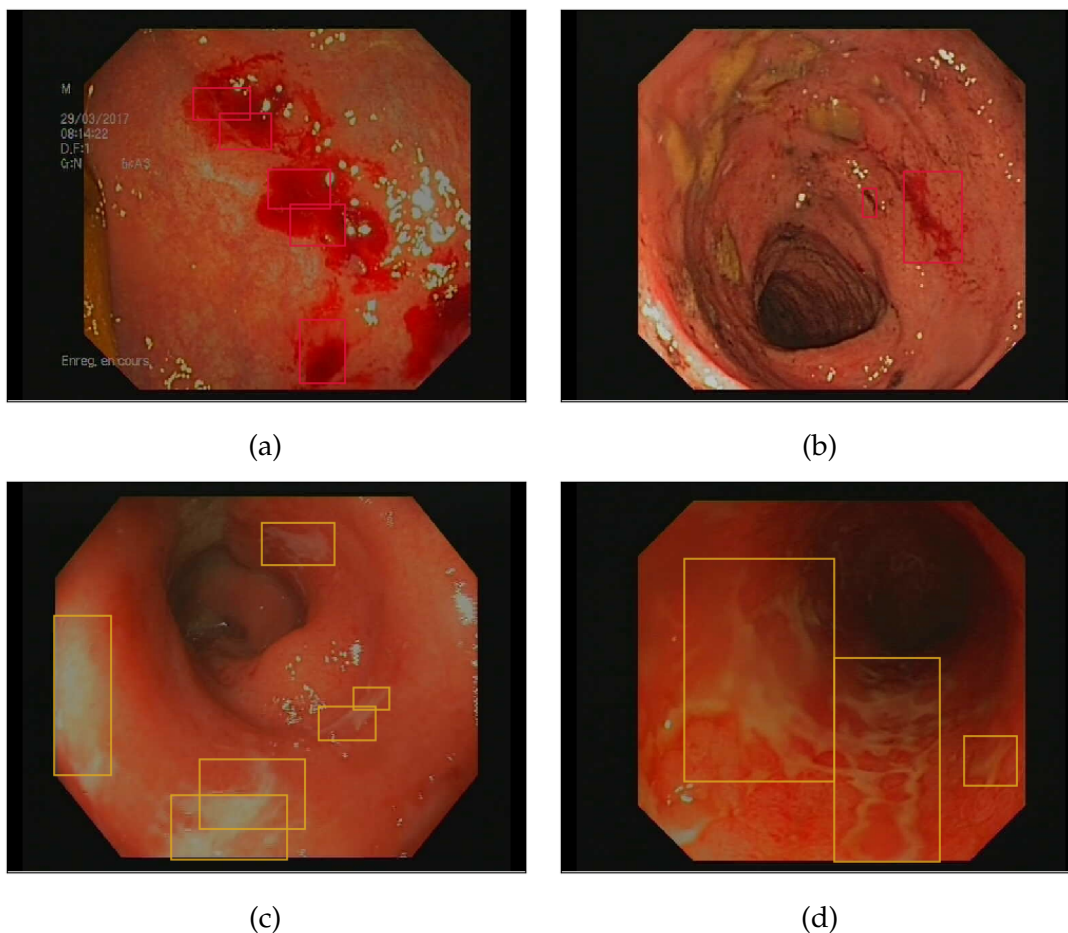
Figure 6.1: Example of endoscopic images annotated using Vatic software [VPR13]. The bleeding lesions are delineated by red rectangles (first row) while ulcer lesions are indicated by yellow rectangles (second row).

6.3   State of the art of endoscopic lesions detection methods

The methods of automatic detection of endoscopic lesions were emerged many years ago and begin challenging with machine learning evolution in medical applications. For the detection of the endoscopic abnormalities in wireless capsule endoscopy or colonoscopy videos, computer analysis techniques try to solve two kinds of problems. First, given a set of pixels, a region of interest (ROI) or a complete frame, binary classification algorithms are used to select a label between "lesion" (also called abnormal) or "not lesion" (also called normal). Second, segmentation algorithms are used to find regions with the same label such as bleeding or ulcers regions. Many of automatic detection methods used color features to train their models, while others combine it to the texture information to enhance the performance detection. In the following, we will discuss some of these methods.

6.3.1 Automatic detection methods of bleeding

Color information is the primary indicator used by specialists to distinguish between mucosal lesions and the surrounding normal mucosa. In particular, bleeding lesions usually show dark red areas with diverse shapes and sizes. Most classification methods attempt to select a suitable color space, with maximum contrast between bleeding and non-bleeding regions.

6.3.1.1 Color features in RGB space and its sub-spaces

As bleeding pixels are red, it is natural to consider detection and classification in the RGB color space, or direct transformations of RGB ([FMG11; Fu+14; Gho+14a; Gho+18a; KFR18; Gho+14b; SBW14]).

In 2011, Fu et al. [FMG11] propose to work on the ratios (R/G,R/B,R/G+B+R) for each pixel. They train a 3-layer perceptron with 2 nonlinear outputs and 20 neurons in the hidden layers on 1000 bleeding pixels and 1000 non-bleeding pixels. The pixels in each video frame are labelled by the perceptron, then morphological erosion is applied to regularize the region. The authors report a sensitivity and accuracy of 94%, while the specificity was up to 95% for the classification of frames presenting bleeding regions.

Later in 2014 [Fu+14], the authors extend their approach by working with superpixel regions, and a support vector machines (SVM) classifier trained on 60,000 pixels. To construct superpixel regions, the authors use the algorithm in [Ach+12a], with color similarity calculated by the Euclidean distance in the CIElab space, and spatial distance between pixels. For final decision/classification, from each region, three-color ratios (R/G,R/B,R/R+G+B, the same ratios of their previous work) are fed into an SVM classifier. The proposed method provides 99% sensitivity, 94% specificity and 95% of accuracy.

In the same year, Ghosh et al [Gho+14a] proposed to use the R/G histogram, which is less dependent on illumination, then apply k-Nearest Neighbors (KNN). They extracted several statistical parameters like mean, mode, variance, kurtosis, maxima, minima, skewness, then tested the performance of several combinations of the computed parameters with the KNN classifier using 200 WCE images extracted from a publicly available database [Pub]. The authors report that the combination of only three parameters, i.e. {median, variance, kurtosis} is sufficient to identify bleeding frames with an accuracy of 98.5%.

In [Gho+18a], Ghosh et al. extend their work on the R/G color histogram. First, every image is decomposed into 7×7 pixels blocks and 6 statistical parameters are extracted (mean, median, max, min, the value of the central pixel and its deviation from the mean of the block) from each block. The blocks are then

separated into two classes with a KNN algorithm. Each image is summarised by three numbers: the averages of the components of each centroid, and the difference between the two averages. To detect bleeding in colonoscopy video frames, an SVM classifier is trained on a set of 2350 WCE 3-number summaries with 10 cross-validations. The authors report an overall area under the curve (AUC) value up to 0.989, while the specificity and accuracy were upper than 98%.

6.3.1.2   Color histogram parameters

Some bleeding detection algorithms work on the histogram bin levels instead of the pixel intensity values [Gho+14a; KFR18].

Kundu et al. [KFR18] first compute ROIs defined by the color ratios $R/B > m$ and $R/G > n$. The parameters $m = 2.8$ and $n = 2$ are chosen according to the maximal accuracy of pixel detection compared to ground truth provided for 65 images, with pixel-level mean accuracy (88.54%) and the lowest standard deviation (3.64%). The ROIs are then classified with a KNN classifier using the 64 histogram bins in the green channel. The method performance was 97.86% for accuracy, 95.20% for sensitivity and 98.32% for specificity.

Other methods work on color histograms in the original RGB space, with more complex classification methods ([Gho+14b; SBW14; GFW18]).

In [Gho+14b], the authors propose to combine the RGB values into a single number with bit concatenation and work on the resulting histogram. Every pixel is represented by 3L bits where L is the number of bits beginning from the Most Significant Bit plane (MSB). SVM classification on the 128 bins of the resulting histogram provides an accuracy of 94.5%, the sensitivity of 93% and specificity of 94.88% for bleeding detection.

In [SBW14], the authors propose to classify regions into bleeding or non-bleeding based on 5 statistical features (mean, standard deviation, entropy, skew and energy) computed on each of the three RGB color channels. When applied to a WCE image, the frame is first segmented into large regions by reducing the color palette, then a trained two-layer neural network provides the classification label for each region. All 2^{15} combinations of features were evaluated, and the authors obtain 93% of accuracy, 96% for sensitivity and specificity 90% for the best combination, i.e. mean, energy and entropy in the red channel, mean in the green channel, and energy in the blue channel. The authors also propose a semi-automatic annotation algorithm based on region growing from manual seeds to obtain a large training data set.

In [GFW18], the authors propose to classify bleeding images with KNN applied to specific histogram bins of the RGB color space. After decomposing images into blocks such as in [Gho+18a], they compute a vector of features such as mean, median, maximum and minimum. To compute the classifier inputs, they use the color histogram of 2^{3L} bins for each block, where L is the number of bits chosen for the color space. Due to the fact that the blue color value superior to 128 is negligible in WCE images, they only consider the blue color range (0 to 127). After, they apply the principal component analysis (PCA). On the other hand, to localise the bleeding zone, they add to features the intensity of the central pixel for each block. The pixel is then labelled bleed/non-bleed according to the block to which it belongs. After, they apply morphological dilation followed by erosion to delineate the suspected bleeding zones. According to reported results, with 16 color histogram bins in RGB, they classify correctly bleeding frames with an overall performance of 99.15%, 99.47% and 97.85% in terms of accuracy, specificity, and sensitivity respectively. They localise bleeding zones with a precision of 95.33% in 70 tested images.

More recently, researchers of the approach called CHOBS presented in [GFW18] proposed to extract statistical parameters from a block of pixels in the RGB color histogram and then classify the images with the KNN algorithm. They segment each image into pixel blocks of 7×7 pixels to extract local statistical features. Bin frequencies of the color histogram are used to be the global feature. They proceed to reduce the size of the features by first taking only bin probability that contains a specified range of blue color (chosen to be 0-127), resulting in 50% dimension reduction without missing relevant bleeding area's information and then to applying the PCA. The final block feature for frame detection contains a list of the block's mean in all the color planes. On the other hand, to localise the bleeding zone, they construct a five-dimensional feature containing mean, median, min, max and the block pixel intensity value. The pixel is then labelled bleed/non-bleed according to the block to which it belongs. After, they apply morphological dilation followed by erosion to delineate the suspected bleeding zones. The authors reported that with 14% overlapping authorisation between two successive blocks and 16 color histogram bins, they classify correctly bleeding frames with an overall performance of 99.15%, 99.47% and 97.85% in terms of accuracy, specificity, and sensitivity respectively.

6.3.1.3 Color features in other spaces than RGB

As the RGB space may not be suited to bleeding classification, some methods have considered other color spaces such as YIQ ,HSV and HSI [Gho+15; Dee+18; Pan+11].

In the work of [Gho+15], the authors use the SVM classifier with statistical features computed from extracted ROIs in a projection of the Luma In-phase

Quadrature (YIQ) color space. The ROI was chosen according to a threshold value Q = 0. In the composite coordinate plane (Y.I)/Q, they compute (mean, median, skewness, minima) from each pixel of the supposed ROI. In comparison to 50 original WCE bleeding images labelling, their algorithm provides an overlap of 96.89%. And, testing the proposed approach on a set of 1000 images, the authors report an accuracy of 93.9% and sensitivity of 93.5% outperforming the method presented in [Gho+14a].

Deeba et al. [Dee+18] merge two SVM classifiers built respectively from features extracted from RGB and HSV color histograms. Due to the fact that acute bleeding occurs in several consecutive frames, they construct supposed bleeding areas using region growing proposed by [SBW14] with automatic seed selection during the training phase. From each ROI, they compute five statistical features (mean, standard deviation, entropy, skew, energy). Each SVM is trained by alternating between SVM parameter optimization, five-fold cross-validation and feature selection. The RGB SVM classifier obtains (accuracy=49.5%, specificity=32.4% and precision=33.4%), while the HSV classifier provides (accuracy =93.9%, specificity=94.9% and precision=85.7%). For each ROI, the largest distance from the SVM decision boundary is used to select the most reliable classifier. This combination of two color spaces improves sensitivity to 92% and specificity to 95%. Also, the method presents better accuracy (94.5%) but slightly higher computation complexity (0.2 seconds per frame) compared to the method of Sainju et al. [SBW14] (0.11 seconds per frame and 71.4% accuracy).

In [Pan+11], the authors used RGB and Hue-saturation-intensity (HSI) pixel intensities to construct a six-dimensional feature vector. They train a three-layered probabilistic neural network on a total of 768 530 pixels and report a sensitivity of 93.1% and specificity of 85.8%.

6.3.1.4   Color and texture descriptors

Recently, Pogorelov et al. [Pog+19] proposed to consider image texture besides color. They used RGB color features (R/G, R/B, R/R+G+B ...) and 22 texture parameters (entropy, contrast, dissimilarity, ...) extracted from the grey-level co-occurrence matrix (GLCM) used for input for pixel-wise classification. Among the variety of machine-learning approaches tested (Random Forest (RT), Random Tree (RT), ZeroR ...), the output result for pixels detection was the highest for the SVM classifier with specificity (95.55%), accuracy (97.77%), sensitivity (97.76%), F1 score (97.80%) and ROC (99.7%). Images with more than 280 bleeding pixels are classified as bleeding frames like [Sum+17a]. The proposed method outperforms that presented in [Fu+14] in terms of accuracy (97.6% against 95%). According to their results, the color ratio coefficient Red over Green (R/G) showed the highest capability of detecting bleeding with a Matthews Coefficient Correlation (MCC) of 0.832.

6.3.2 Automatic detection methods of ulcers

Ulcerative lesions show as white spots distributed on the gut wall, which explains why most methods focus on detecting bright pixels in various color spaces [Sum+15; Sum+17b; GDS16; Yua+15; KG15; YWT+14; Fan+18].

6.3.2.1 Color features

Multiple color spaces (RGB, YCbCr, CMYK or HSV) and their sub-spaces have shown successful gastrointestinal ulcer detection ability. Instead of using only the canals of a unique color space, some algorithms of ulcer detection include the use of combined color channels in order to improve their performance.

In [Sum+15], the authors use statistical analysis of ulcer pixel values against foreground pixel values in RGB and CIElab (Lab) spaces. For each color band, they compute the distribution of ulcer and non-ulcer pixels and determine the overlapping rate. Next, they train SVM on a set of 110 images (50 ulcerated/60 normal) of 576×576 pixel resolution and test a variety of combination bands information. They conclude that the feature set of dimension three, (L, a and G) gives the best detection performance (sensitivity = 88.09% and specificity = 90.88%).

Later, in the paper [Sum+17b], Suman et al. propose to extend their work of [Sum+15] by introducing multiple color spaces (RGB, HSV, YCbCr, CMYK, YUV, CIElab, XYZ). In order to find the best color canal for lesions detection, they tested the 22 canals and find that Cr (red chrominance) and labA give the minimum overlapping rate between ulcerated and normal pixels. Training the SVM algorithm on 8000 endoscopic images (divided into 5000 ulcer/3000 normal), the best canals combination was of dimension three counting for the bands Cr from YCbCr, Y from CMYK and B from RGB reporting high-performance ability (accuracy=97.89%, sensitivity=96% and specificity=95%) exceeding the use of HSV space alone like [KG15].

6.3.2.2 Color histogram features in RGB

As mentioned above, ulcer pixels exhibit shadows of white or yellowish colors that are difficult to distinguish due to illumination variation during colonoscopy. In [GDS16], the authors propose a KNN classifier based on RGB histogram bins. They use a data set of 220 endoscopic images (110 ulcers/110 normal) to compute the optimal number of bins in the range [8, 256]. With 32 bins for each color plane, their method exhibits an accuracy of 87.27%, a sensitivity of 88.64% and specificity of 85.75%.

6.3.2.3   Texture features

Ulcers are characterised by rough surfaces compared to the surrounding mucosa which makes which is why texture features may be suited for ulcer detection. Some studies [Yua+15; KG15; YWT+14] propose texture descriptors in order to localise ulcers.

In [Yua+15], the authors propose to combine color and texture features extracted from super-pixel regions with an SVM classifier. They compute the superpixels by SLIC algorithm ([Ach+12b]). They use the color channels S from HSV and M from CMYK due to their ability to highlight the ulcerative regions. They also use texture features obtained from Leung-Malik (LM) filters [LM01]. On a data set of 340 images extracted from 20 WCE videos, the authors report an accuracy of 92.65%, a sensitivity of 94.12% and specificity of 91.18%.

In [KG15], the authors use textural features as input to an SVM classifier. They propose to extract texture information from color spaces RGB, HSV and YCbCr and compute statistical moments (mean, standard deviation, skewness) of the Contourlet transform and Log Gabor filter. With a data set of 137 images, they show that the HSV and YCbCr color spaces provide the highest accuracy (96.16%) and specificity (95.83%) respectively.

Yeh et al. [YWT+14] explore different choices of features, feature reduction methods, classification methods to obtain the best overall classifier. Regions containing abnormal pixels are identified as connex regions via a color coherence threshold in RGB and HSV spaces, and textural parameters are obtained from the Grey Level Co-occurrence Matrix. Different combinations of saturation value, coherence threshold, number of features, feature selection algorithm and classification algorithm are compared. The authors report that the different choices of classification method and coherence threshold lead to similar performance. The best classification is obtained with decision trees. The best sensitivity (93.6%) for bleeding detection was obtained with the combination of saturation value 65, coherence threshold 5, 20 features and feature selection method ReliefF. For ulcers, the best combination was of saturation value 70, coherence threshold 10, number of parameters 40 and feature selection method ReliefF.

6.4   Proposed method

In this section, we will present our proposed method to deal with annotation errors in the Vatic database. It involves several steps as given in Figure 6.2. First of all, we remove all black pixels surrounding the informative pixels. Then we compute the color histograms of healthy pixels. We propose then an effective sampling method to explore the linear models. Also, we propose to modify the

computation of the sensitivity criteria to encounter mislabeled pixels. Finally, we optimise the performance of the detectors using the Youden index.

```
┌─────────┐   ┌──────────────────┐   ┌──────────────────┐
│  Input  │──▶│  Pre-processing  │──▶│ Compute (R,G) &  │
│ videos  │   │(removal of black │   │     (Cr,Y)       │
│         │   │     pixels)      │   │Histograms of     │
└─────────┘   └──────────────────┘   │ normal pixels    │
                                      └──────────────────┘

  ┌──────────────────┐   ┌──────────────────┐   ┌──────────────────┐
  │Sample only models│──▶│   Optimise S     │──▶│   Best lesion    │
  │crossing the      │   │    using         │   │ detection models │
  │contour           │   │ Youden index     │   │                  │
  │(see Figure 6.6)  │   │given by Equation │   │                  │
  └──────────────────┘   │     (6.9)        │   └──────────────────┘
                         └──────────────────┘
```
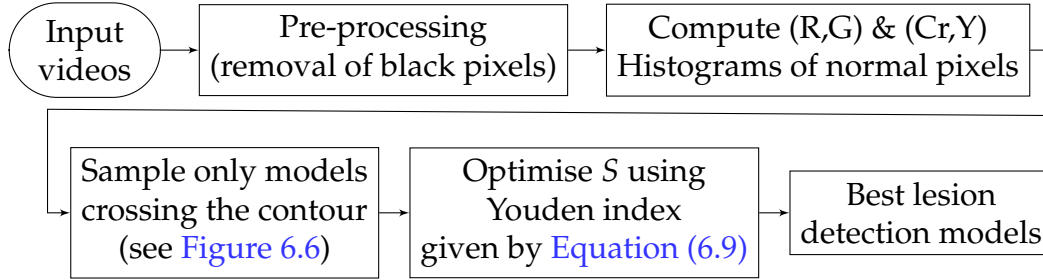
Figure 6.2: Flowchart of the computation of the bleeding and ulcers detectors in (R,G) and (Cr,Y) spaces respectively. According to the desired data, i.e. area or number of detected annotations, S designs Sensitivity^A (Equation (6.7)) or Sensitivity^N (Equation (6.8)) respectively.

6.4.1 Learning dataset

For the learning stage, we decide to use a database of 5 colonoscopy videos as detailed in Table 6.1. The database contains both bleeding (1629 frames) and ulcer (1760 frames) annotations, for a total of 4349 frames.

Video	Bleeding frames	Ulcer frames	Total frames number
video 1	671	554	812
video 2	224	378	378
video 3	254	86	1116
video 4	140	204	910
video 5	340	538	1133
Total	1629	1760	4349

Table 6.1: Dataset used in the proposed approach during the training stage. Number of frames used for training: total number in the video, number of frames with bleeding annotations, number of frames with ulcer annotations.

6.4.2 Pre-processing

Due to the camera's field of view, only an octagonal portion of the image is actually recorded in the endoscopic video, and the outer portions are set to black (see Figure 6.3a). Additionally, some textual information is embedded in the video frames and should be removed prior to bleeding or ulcer detection. Both correspond to pixels with similar colors throughout the video. Consequently, we detect them as pixels with small grey-level variance and grow the detected region with morphological erosion to obtain a mask for each video as shown in Figure 6.3b.

Morphological erosion operation is used to remove the noisy spots of the image (or to discard isolated regions (very small)). Suppose A is the image after pixel classification and B is a structuring element. The erosion of A by B, denoted $A \ominus B$, is defined as follows:

$$A \ominus B = \{z | (B)_z \subseteq A\} \tag{6.1}$$

The erosion of A by B is the set of all points z such that B, translated by z, is contained in A. In our work, we use a $B = 5 \times 5$ structuring element with full of values 255.

As the lighting shines on wet spots on the gut wall, some patches appear very bright but do not correspond to ulcers (see Figure 6.1c and Figure 6.1d). We remove them before ulcer detection the Y component, i.e. $\mathbb{1}_{\{Y > c\}}$. As these were not annotated, we chose the value $c = 150$ by visual inspection.

(a)   (b)
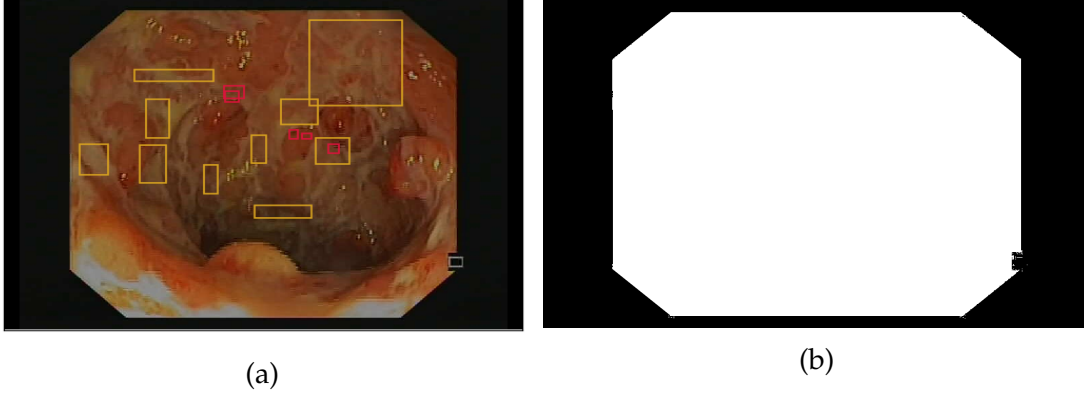
Figure 6.3: Endoscopic frames (left) and corresponding mask (right) used to remove pixels that do not correspond to the colonic wall.

6.4.3   Definition of the detectors

In the videos, the bleeding shows as red patches compared to the surrounding regions, whereas ulceration regions show as pinkish white color area spreading on the gut wall (cf Figure 6.1).

Following [Gho+14a; GFW18; Gho+18a], we consider the problem of labeling pixels into bleeding/non-bleeding based on the pixel value in RGB color space. As the previous authors have shown that the R/G ratio is relevant (it leads to 11% overlap between normal /abnormal pixels in [Gho+18a]), we consider the set of linear classifiers in the (R,G) subspace, i.e. $\{aR + b > G \text{ for } (a, b) \in \mathbb{R}^2\}$.

The color space YCbCr shows effectiveness for delimiting the ulcer lesions as it is shown on the example of endoscopy images in Figure 6.4. The Y canal (second column) shows the contours of the spatial distribution of ulcers whereas the canal Cr (third column) exhibits high-intensity values on the normal pixels

and dark color shadow on ulcers patches, which approves the idea of looking for a linear relationship between these two color bands to localise the ulcer lesions.

As consequence, following the works of [Sum+17b; KG15], we consider the set of linear classifiers in the (Y, Cr) subspace of the YCbCr color space i.e. $\{aCr + b < Y \text{ for } (a, b) \in \mathbb{R}^2\}$.

As the videos are encoded in RGB, we apply the following transformation [Kum+] for ulcer detection:

$$\begin{bmatrix} Y \\ C_b \\ C_r \end{bmatrix} = \begin{bmatrix} 16 \\ 128 \\ 128 \end{bmatrix} + \begin{bmatrix} 0.279 & 0.504 & 0.098 \\ -0.148 & -0.291 & 0.439 \\ 0.439 & -0.368 & -0.071 \end{bmatrix} \times \begin{bmatrix} R \\ G \\ B \end{bmatrix} \quad (6.2)$$
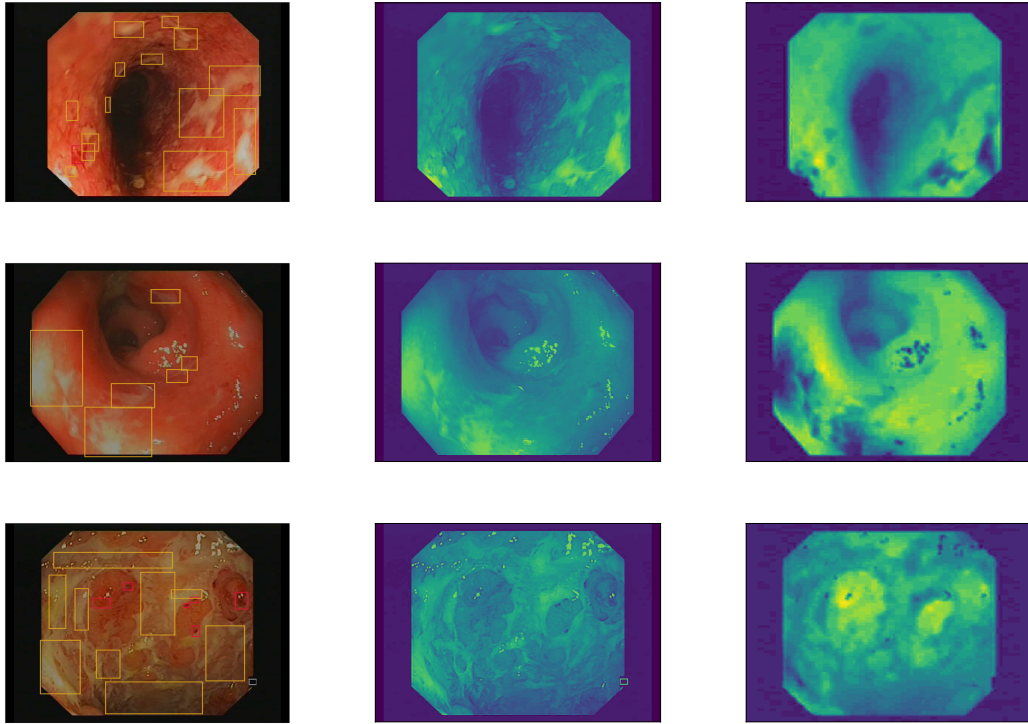
Figure 6.4: Examples of endoscopy images in our data base, From the left: original images, transformation in the Y and Cr respectively using Equation (6.2).

6.4.4 Random sampling of the detectors

The first step for model search is to explore all the color spaces (R,G) for bleeding and (Cr,Y) for ulcers. To count all the linear models in the space $[0 : 255] \times [0 : 255]$ requires a lot of time to run, then we decide to sample only one hundred

models for each type of lesion as one can see in Figure 6.5. It can be noticable that if a line does not cross the histogram than any of normal pixel will be identified by the detector and consequently the true negative rate of this detector will be zero.
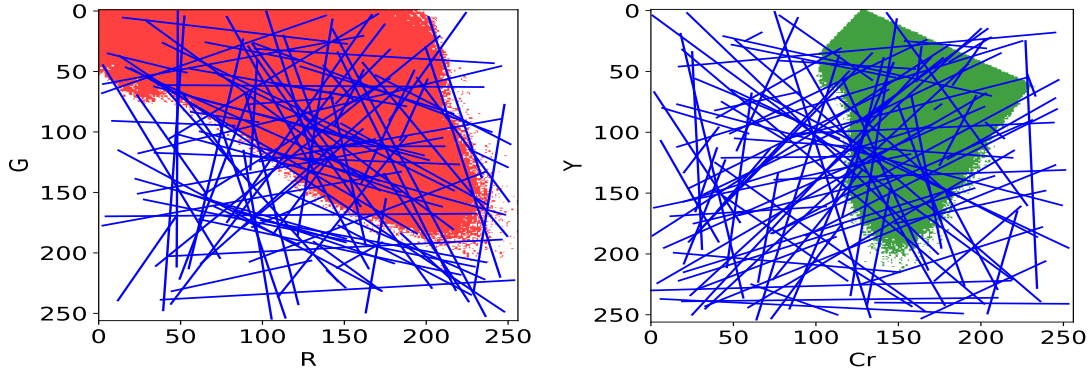
Figure 6.5: Random sampling of 100 linear models (blue lines) without histogram restriction to detect bleeding and ulcer lesions. Histograms of normal pixels in the (R,G) on the left and (Cr,Y) on the right.

Moreover, the overlap between the color distributions of the lesions class and non-lesions class is unavoidable and some amount of compromise is necessary. Consequently, we should restrict the optimization space to the set of linear classifiers that go through the interior of the histogram.

On the other hand, if a line goes through the interior, it must cross the boundary of the set. We can avoid sampling redundant linear classifiers and speed up the computation time by focusing on the contour of the histogram instead of its interior. To sample the set of lines, we will thus draw two points in the contour of the (R,G) and (Cr,Y) histograms (represented in Figure 6.6) and consider the line that goes through these two points as the associated linear classifier.
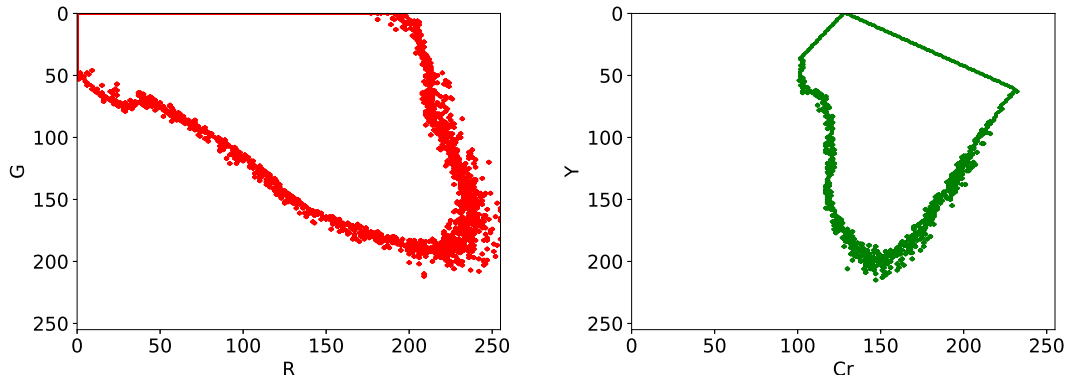
Figure 6.6: Contour of the (R,G) histogram of normal pixels (left) and (Cr,Y) histogram (right).

6.4.5 Performance evaluation: a modified sensitivity

The detector performance is evaluated depending on its capacity to correctly identify the pixels lables: normal and abnormal. Several performance criteria are proposed. Let first recall the currently used performance criteria to evaluate a detector ability to correctly identify abnormal and normal pixels.

During the application of our algorithm, there are four distinct cases of abnormality detection outcomes that may occur [SW11] (see Figure 6.7):

- True Positives (TP), i.e. the number of abnormal pixels correctly identified as abnormal
- True Negatives (TN), i.e. the number of normal pixels correctly identified as normal
- False Positives (FP), i.e. the number of normal pixels identified as abnormal
- False Negatives (FN), i.e. the number of abnormal pixels identified as normal

In Figure 6.7, the positive rate, denoted by "P", indicates the count of positive pixels i.e. those labelled as lesion, whereas the negative rate, denoted by "N", is the count of pixels labelled as normal, namely they are the pixels out of the annotations in our case for example.

Figure 6.7: Confusion matrix to compute the lesions classification probabilities. True class designs the labels by the doctors whereas predicted class is related to the detector classification on the pixels level.

In the textbook statistics, many classification performance criteria can be extracted from the confusion matrix such as:

- Specificity, also called the true negative rate, measures the proportion of normal pixels correctly identified with the detector and it is computed by the formula:

$$\text{Specificity} = \frac{TN}{TN + FP} \tag{6.3}$$

- Sensitivity, also called the true positive rate, measures the correctness of abnormal pixels detection and it is given by the following formula:

$$\text{Sensitivity} = \frac{TP}{TP + FN} \qquad (6.4)$$

- Precision, the positive predicted value given by

$$\text{Precision} = \frac{TP}{TP + FP} \qquad (6.5)$$

- Accuracy

$$\text{Accuracy} = \frac{(TP + TN)}{P + N} \qquad (6.6)$$

Due to the annotations errors in our database as discussed before, we expect over-inflated levels of FP and FN based on the database annotations. This will hide the correct classifier, and decrease the confidence in our results. Hence, evaluating specificity and sensitivity rely on our ability to correctly identify classification errors, that is to say on reliable pixel annotations by gastroenterologists.

To counter these problems, we propose to modify the definition of sensitivity in order to take the labeling issues into account. More precisely, we want pixels that were annotated by the gastroenterologist but not detected to count as true positives when they are near pixels detected by our algorithm.

Consequently we will count as true positives all pixels belonging to a gastroenterologist annotation as soon as one pixel is detected inside the annotation. Due to the fact that all pixels inside an annotation are either true positives or false negatives, this scheme corresponds to counting "detected annotations" instead of "detected pixels" in the definition of sensitivity. More precisely, an annotation is considered as detected if at least one pixel inside is detected. Alternatively, we can count "detected annotations" weighted by their surface or count.
Thus, we can denote two notions of sensitivity on annotation level:

$$\text{Sensitivity}^A \quad = \quad \frac{\text{Area of detected annotations}}{\text{Total area of annotations}} \qquad (6.7)$$

$$\text{Sensitivity}^N \quad = \quad \frac{\text{Number of detected annotations}}{\text{Total number of annotations}} \qquad (6.8)$$

The specificity criteria (Equation (6.3)) was not modified, namely it is computed on pixels level, because we expect missing annotations to represent a small number of pixels relative to the number of non-annotated pixels $\sum TN + \sum FP$.

In the next section, we will present the optimization procedure applied to find the best linear detectors.

6.4.6 Optimization to find the best detector

Detector performance can be graphically represented with the aid of sensitivity vs (1-specificity) plot. As we are only interested in single detectors, each detector's performance is represented as a point in the Receiver Operating Characteristic (ROC) space, as opposed to a curve, which represents a family of detectors indexed by a threshold parameter. As we have proposed two forms of the modified sensitivity, we will present two figures, one with the criteria "Sensitivity^A", and one with the criteria "Sensitivity^N".

The ideal classifier corresponds to the upper left corner or coordinate (0,1), with no false negatives (100% for sensitivity) and no false positives (100% specificity). Other good models are a compromise between sensitivity and specificity and are close to (0,1).

In this manuscript, we choose to select the classifier that is farthest from the line of no-discrimination, i.e. which has the largest euclidean distance from the diagonal in ROC space. Consequently, our algorithm searches the optimal model $\hat{m}$ such that maximises the Youden index [You50] denoted by J and given by the following formula:

$$
\begin{aligned}
\hat{m} &= \underset{m}{\operatorname{argmax}} \, d_{\text{ROC}}(\{y = x\}, m) \\
&= \underset{m}{\operatorname{argmax}} \, J(m) \\
&= \underset{m}{\operatorname{argmax}} \, (S(m) + \text{Specificity}(m) - 1) \quad\quad (6.9)
\end{aligned}
$$

where $S(m)$ denotes the sensitivity of classifier m (Sensitivity^A or Sensitivity^N). As we detect the bleeding and ulcers separately, the optimization process of Equation (6.9) will be performed twice, for bleeding and ulcers.

6.5 Results of lesions's detection

We train our algorithm discussed in section 6.4 on the videos of the learning database (cf Table 6.1). The detectors performance will be represented by classical criteria: Specificity and Sensitivity computed on pixels levels as well as by the proposed sensitivity criteria computed on annotation level: Sensitivity^A and Sensitivity^N.

6.5.1 Best bleeding detectors

We made random search for possible optimal linear models crossing the contours of the (R,G) histogram of normal pixels (Figure 6.6) by choosing a sample of size 100 as explained previously (see Figure 6.8).
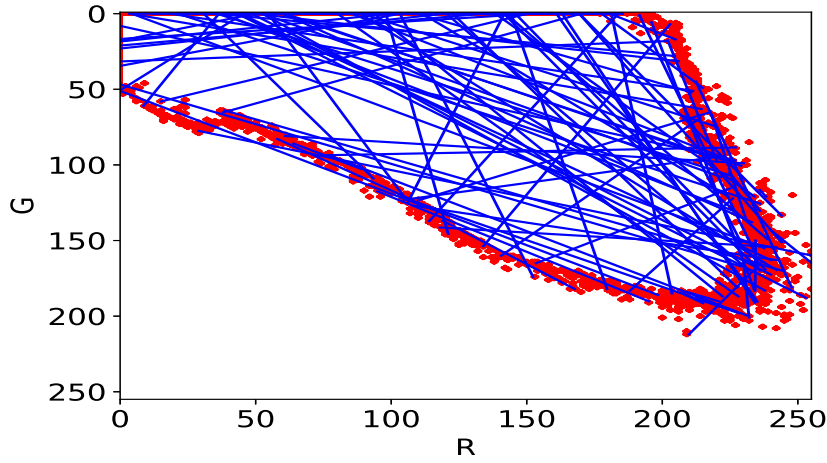
Figure 6.8: 100 linear classifiers are sampled by drawing two points from the contour of the (R,G) histogram of normal pixels.

In the ROC space, we plot the S vs (1-specificity). In Figure 6.9, on the left S is Sensitivity^A while on the right S is Sensitivity^N, plots to visualize the performance of the detectors. The three best models that maximise the Youden index are represented by black dots.
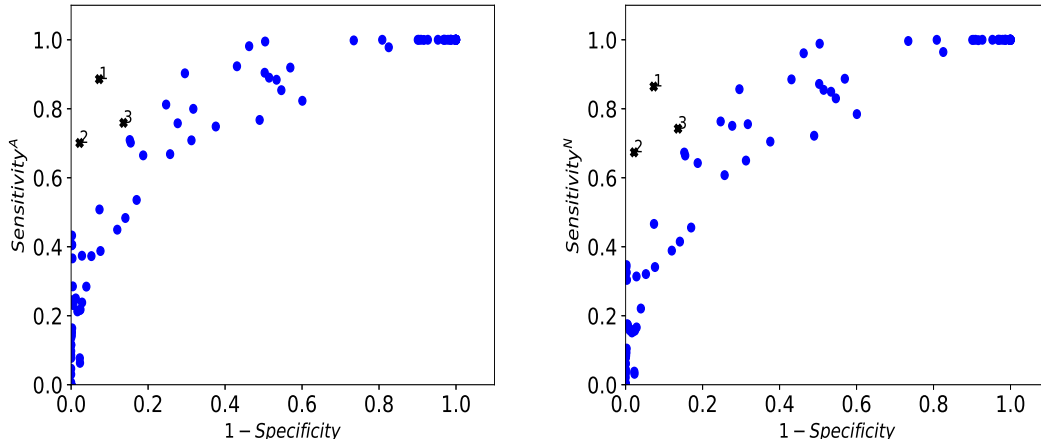
Figure 6.9: ROC space for bleeding by Sensitivity^A (on the left) Sensitivity^N (on the right).

In Figure 6.10, we compare the result of the best detector, i.e. model $G < 0.298R - 1.03$, to the ground truth provided by the gastroenterologist. The pixels classified as bleeding are in red whereas the normal pixels are in green.

Despite the difference in exposure to light, there is a good agreement between the detected areas and the annotated pixels for all four samples. In addition,

the detector bleeding regions are precisely delineated in contradiction to the rectangular annotations. The detection of the normal pixels is accurate, i.e. green regions are correctly identified as normal tissues/pixels. The bleeding lesions of the frame at the third row were precisely selected by the best model despite being missed by the expert. The frames in the last row, some dark red normal pixels corresponding to the colon interior edge at a turning angle, were classified as abnormal with the detector. We therefore can conclude that the best linear model can exhibit the relevant areas and select ROIs that were not annotated.

Table 6.2 reports the performance of the best linear bleeding models in terms Specificity, Sensitivity^A, Sensitivity^N and standard sensitivity.

Best models for bleeding	Specificity	Sensitivity^A	Sensitivity^N	Sensitivity
$G < 0.298R - 1.03$	92.71%	88.58%	86.44%	9.56%
$G < 0.264R - 4.837$	97.79%	70.08%	67.37%	4.16%
$G < -0.066R + 31.58$	86.39%	75.92%	74.23%	13.79%

Table 6.2: Performance of the best linear models for bleeding detection. Good performance is obtained based on Sensitivity^A or Sensitivity^N, but standard sensitivity is low due to annotation errors.

As expected, the detected areas do not overlap with rectangular annotations which generates low standard sensitivity estimates. From Table 6.2, based on the three best models, we estimate that around 90% of bleeding annotations are incorrect or imprecise.

As we said previousely, the detection of bleeding and ulcer was done separately. The next section entails the results of ulcer detection using the (Cr,Y) color histogram.
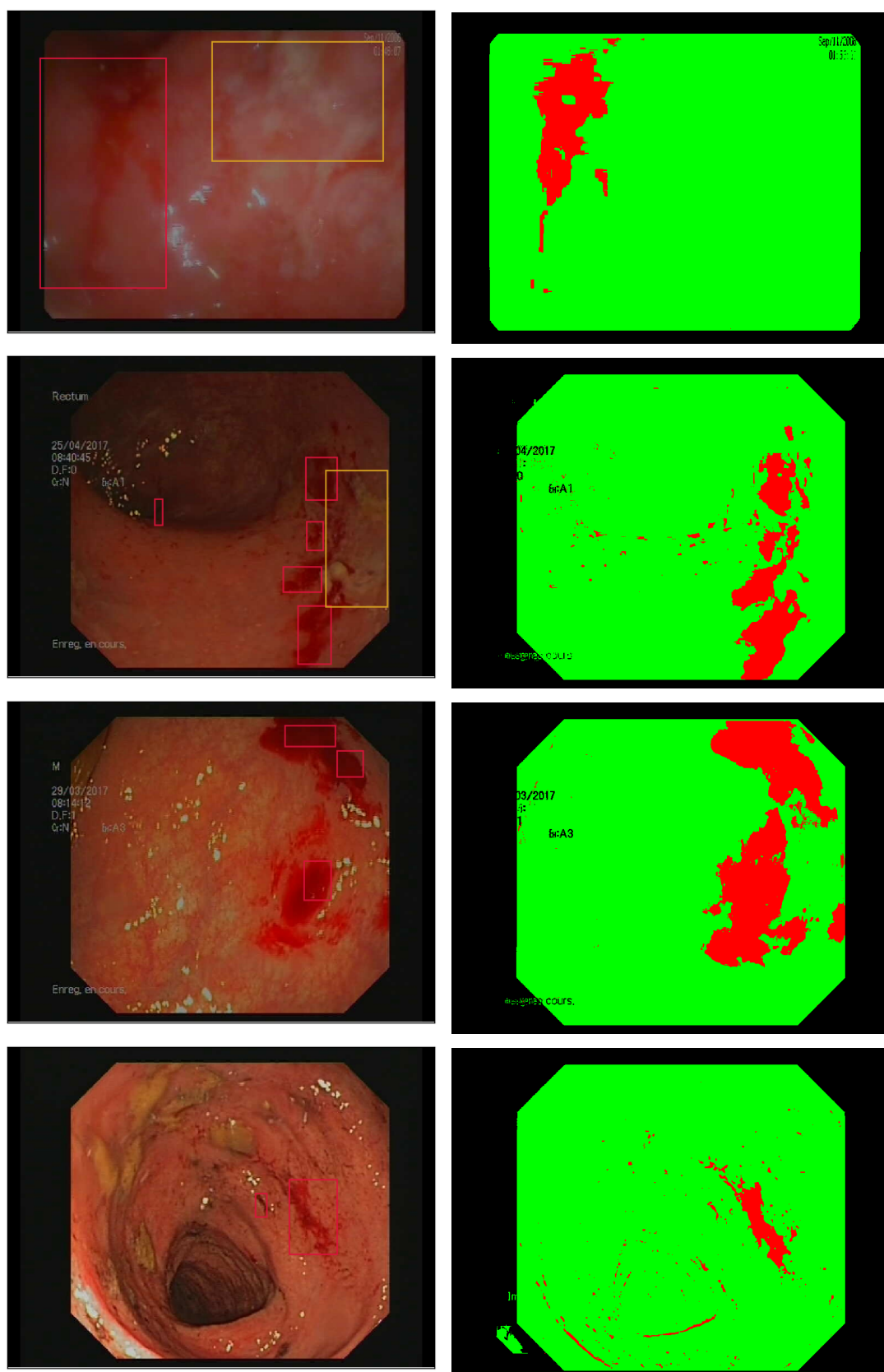
Figure 6.10: Annotated frame (left) and corresponding bleeding detection with the best linear models of Table 6.2 (right).

6.5.2 Best ulcer detectors

Similarly to the work done for bleeding, we decide to perform the ulcer detection with respect to the steps presented in Figure 6.2 using the (Cr,Y) color histogram instead of the (R,G) color space.
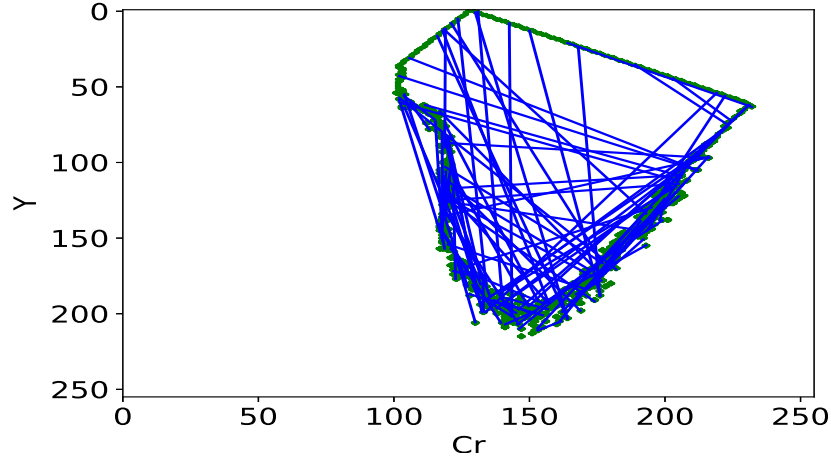
Figure 6.11: 100 linear classifiers are sampled by drawing two points from the contour of the (Cr,Y) histogram of normal pixels.

In the ROC space (cf Figure 6.12), we plot the S vs (1-specificity), S can be Sensitivity^A or Sensitivity^N, plots to visualize the performance of the detectors. The performance of the three best linear models according to the Sensitivity^A are given in Table 6.3.
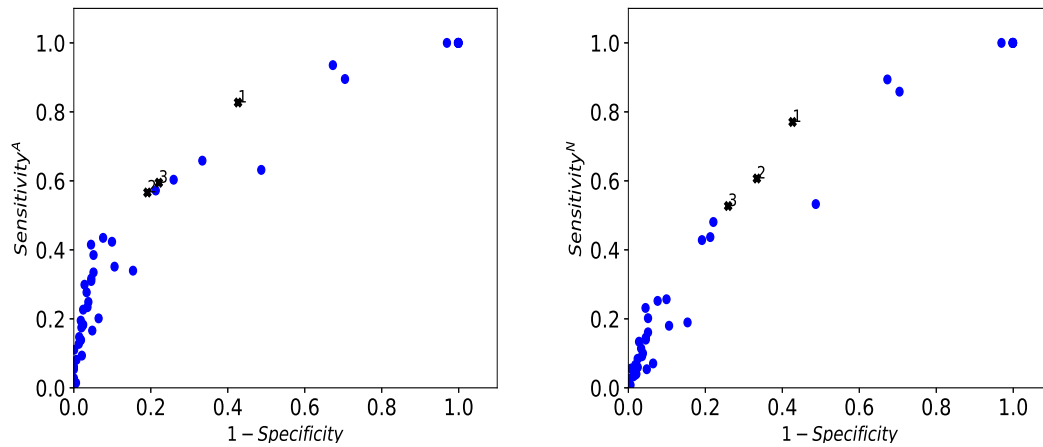
Figure 6.12: ROC space for ulcers by Sensitivity^A (on the left) Sensitivity^N (on the right). The best three models are denoted by black dots.

We compare the detected ulcers with the ground truth provided by the doctors in Figure 6.13.
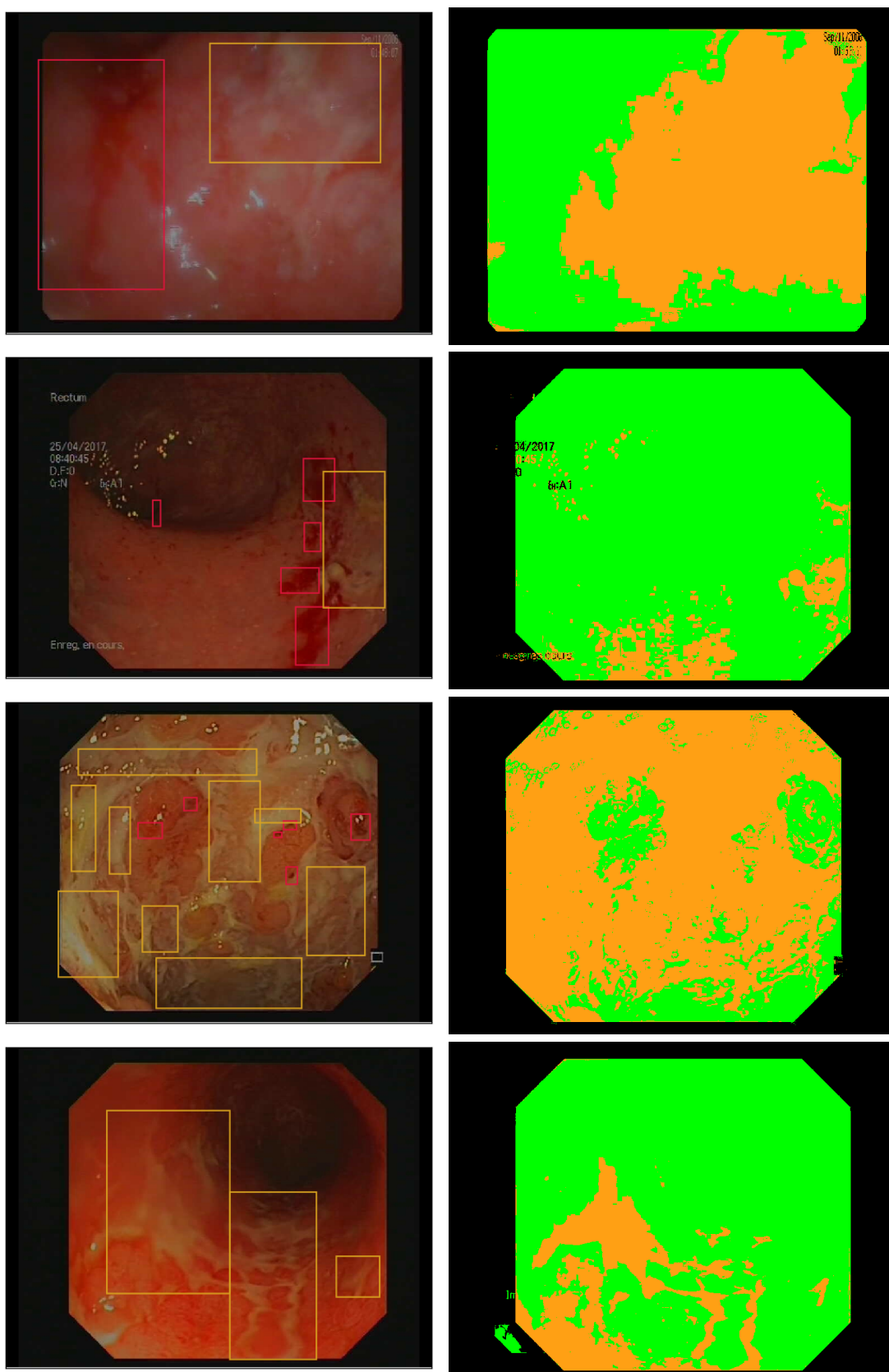
Figure 6.13: Annotated frame (left) and corresponding ulcer detection with the best linear models of Table 6.3 (right).

As in the case of bleeding detection, there is a good agreement between the detected areas (in orange) and the annotated areas (delimited by yellow rectangles). The geometry of the ulcers is correctly identified by our model, especially at the edge, which is not possible by the rectangular annotations.

On the other hand, the ulcers show as white or yellowish color on the mucosa, consequently, they may conduct to confuse with specular reflection. This increase later the probability of miss classification and performance decrease. In the samples of Figure 6.13, the first and third frames contain many luminar reflection which are classified as ulcers by the best linear model.

From Table 6.2 and Table 6.3, we conclude that training the detection algorithm with standard sensitivity would provide nonsensical models, whereas we cab achieve good performance level with our proposed criteria $Sensitivity^A$.

Best models for ulcers	Specificity	$Sensitivity^A$	$Sensitivity^N$	Sensitivity
$Y > 0.698Cr - 42.799$	57.33%	82.71%	77.06%	38.85%
$Y > 0.505Cr + 8.816$	80.88%	56.62%	42.83%	14.27%
$Y > 0.499Cr + 6.318$	77.91%	59.46%	48.08%	17.17%

Table 6.3: Performance of the best linear models for ulcer detection. Good performance is obtained based on $Sensitivity^A$, but standard sensitivity is low due to annotation errors.

6.6 Discussion

As discussed in section 6.3, the RGB color space, and especially the Red and Green channels, has previously been used successfully for bleeding detection, while the YCbCr color space was used for ulcer detection. The information present in the pixel color is not altered by a change of color space, but a suitable color space presents this information in a more straightforward way, and dimension reduction methods such as PCA can automatically perform this. In this manuscript, choosing the right colorspace based on the previous literature (see [Gho+14b; Dee+18; HH15; Pog+19] for bleeding and [Sum+17b; Yua+15; KG15] for ulcers) enables us to work with 2D linear models instead of 3D models.

The use of rectangular annotation in our database (see Figure 6.10 and Figure 6.13) or circular regions selection entails a considerable quantity of ground truth errors because annotations do not match the arbitrary and complicated shapes of the lesions. This is a major difficulty in our context, regardless of the type of model or machine-learning approach.

To ease the annotation burden, semi-automatic region selection algorithms have been proposed. In the work of Sainju et al. [SBW14], the growing region algorithm in [TC92] creates homogeneous bleeding regions from consecutive capsule endoscopy frames. A seed is manually selected by the user then enlarged by adding 8-connected neighbors, and the new centroid is taken as the seed for the following frame. This method extracts only one region per lesion, which can unbalance the normal and bleeding regions in the training database. In addition, it does not perform well in the absence of lesions due to forward and backward camera's movements or in patients with mild forms of UC.

In [Dee+18], the authors use a similar method to extract the bleeding regions but keep only a single frame rather than the complete sequence. In this paper, we propose to adjust the performance criterion of lesion detection rather than automatically annotate the data set.

We chose to work with linear models instead of more sophisticated approaches in order to provide results that are easy to interpret and use in clinical practice. Also, the good performance obtained in this and previous studies ([Dee+18; Gho+14a; Gho+18b; KG15; Sum+17b; Yua+15]) suggests that clinical validation of the approach is the critical step, as opposed to more sophisticated approaches such as SVM or neural networks.

To evaluate the validity of our results, we did not perform cross validation, but show the results of computing specificity and Sensitivity^A on a random subset of frames in each video in Figure 6.14. Cross validation selects random subsets and finds the best model for each subset. Consequently, it selects different models at each run, and evaluates the performance of the optimization algorithm. For clinical practice, we are interested in the performance of specific models, their reliability and generalization to new patients.

In Figure 6.14 we show the performance of the 3 best models for the patients in the training database (left) and 5 new patients (right). For each patient, we estimated specificity and Sensitivity^A on 20 random subsets of a video, each containing 10% of the frames. Only three points are drawn, but the size of the ellipses are computed from the standard deviations of the 20 subsets. Figure 6.14 shows that specificity and Sensitivity^A are estimated precisely, even on a fraction of the frames. This suggests that computational time can be reduced by using only a small subset of the video. However, the performance varies a lot between patients, even inside the training set. This means that the selected models are not universal and that specific models should be trained for each patient. This observation was not reported in previous works because the data-sets used contain frames that are not organized "by patient". Consequently, methodological advances are necessary to make colonoscopy videos comparable, in order to apply trained models to new patients.
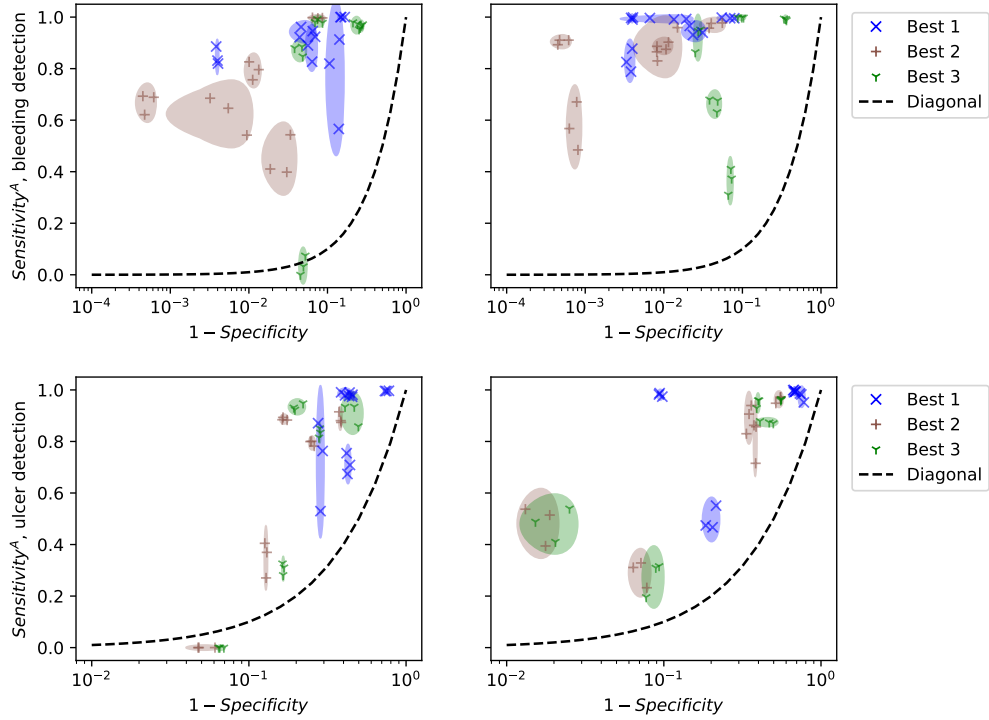
Figure 6.14: Performance of the 3 best linear models depending on patient, 5 training videos (left) and 5 test patients (right).

6.7 Conclusion

In this chapter, we present a technique to automatically detect the bleeding and ulcer lesions found in colonoscopy videos based on the annotations discussed in chapter 5.

The rectangular annotations generated by the Vatic software give rise to many mislabeled pixels due to the complicated shape of a given annotation, not corresponding to rectangles in almost all of the cases. Accordingly, the detector's ability to correctly classify the pixels will not be computed precisely. Therefore, we decide to modify the standard sensitivity performance by a sensitivity that measures the detector's performance according to its ability to correctly detect the lesions instead of the pixels. We thus define two forms of sensitivity, the first one, Sensitivity^N counts the detected lesions weighted by their number, the second one, Sensitivity^A counts the detected lesions weighted by their area (see subsection 6.4.5).

According to the state of the art of automatic detection methods presented in section 6.3, the color parameter is effective to detect bleeding and ulcers lesions. We proposed an efficient sampling scheme to explore the set of linear classifiers in (R,G) and (Cr,Y) for bleeding and ulcer detection respectively.

The bleeding lesions were detected with 93% specificity, 86% Sensitivity^N and 89% Sensitivity^A whereas the performance for ulcer detection was 57% for specificity, 77% for Sensitivity^N and 83% for Sensitivity^A.

We tested the variability of the performance of the best models on 10 colonoscopy videos in section 6.6 by using 20 subsets each containing 10% of the total frames. The performance is computed precisely for all the models and patients.

On the other hand, we show that the best models may fail on some patients (with sensitivity below 20% in some cases). This suggests that the models depend on the characteristics of the patient (mucosa type/appearance) and the medical equipment (type of endoscope, light quality). Therefore, for clinical applications, the normalization of the appearance in the videos is suggested.

Chapter 7

Geometrical map of Ulcerative Colitis lesions

Abstract

The standard endoscopic scores such as UCEIS and MAYO subscore do not take into consideration the spatial extent of the lesions in the colon.

This chapter is devoted to the localisation of the lesions regarding the colon. Therefore, we will use a colon's scheme to represent the bleeding and ulcer lesions found in a colonoscopy video.

In this work, we decide to represent the colon by its curvilinear abscissa. Assuming that the withdrawal speed of the colonoscope is constant, the frames are linearly distributed in the video. The inflammation is taken either from the annotations of the doctor or the results of the detectors computed in chapter 6.

We find that the proposed lesion scheme allows doctors to clearly see the distribution of lesions along the colon. It leads to a fine distinction between patients with the same score.

The proposed method is the first attempt at figuring all the colon lesions found in a colonoscopy video and differentiating between patients of the same class of disease. However, it needs several clinical validation and evaluation steps for the reproducibility.

7.1 Motivation

We have stated in previous chapters that Ulcerative Colitis disease manifests by inflammation beginning by the rectum and spreading continuously into the entire colon. Based on the affected segments of the colon, UC is classified into five classes ranging from proctitis, when the rectum is the only organ affected by inflammation, to pancolitis, when the entire colon is inflamed.

The evaluation of the disease status using endoscopic scores such as UCEIS score and MAYO subscore (cf chapter 4) does not take into account the size of the lesions, their number and spatial distribution in the colon. Indeed, these scores only take into account the most severe lesion, regardless of the overall spatial extension of all the lesions on the mucosa. However, it has been recognized that the disease extension has a significant implication for the prognosis due to the association between the extensive UC and colectomy (cf chapter 2) and colorectal cancer [D'h+07]. The risk of colon cancer is higher than normal if UC disease affects only one part of the colon, and much higher for pancolitis patients.

Moreover, as already mentioned in chapter 2, when a patient fails the proposed treatment, a colectomy is requested. Therefore, it is necessary for the doctor to correctly identify the affected parts of the colon.

In this chapter, we are interested in localising the inflammation of the colon, using colonoscopy videos. We can then provide to the doctors the global status of the lesions in the colon based on their spatial distribution.

In section 7.2, we introduce our proposed method to represent the localisation of the lesions in the colon. First of all, we discuss the colon parametrization considered in this work (cf subsection 7.2.1). Second, we explain how to link the frame to the colon scheme. In section 7.3, we compare the obtained maps between patients having equal endoscopic scores (UCEIS and MAYO subscore). Also, we compare the maps for the annotations of the doctors (cf subsection 7.3.1) to the detection of the automatic models (cf subsection 7.3.2). We finish the chapter with a discussion of some considered hypotheses as well as some problems related to the proposed maps.

7.2 Methodology

7.2.1 Colon parametrization

Figure 7.1 shows the blank colon image used in our work. The cecum is represented by point A with curvilinear abscissa zero (beginning of the colon), the point G corresponds to the curvilinear abscissa 1 representing the end of the rectum (also the end of the colon). The remaining points (B to F) are chosen

to locate angles of the large intestine.
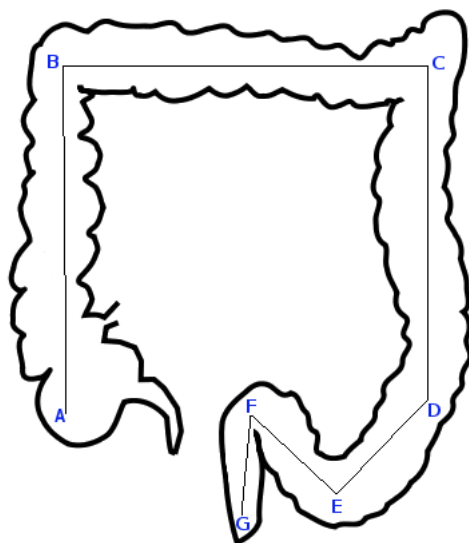
Figure 7.1: Colon curvilinear abscissa. The point A represents the cecum, the points B, C and E represent the turning angles of the colon, while G is placed at the endpoint of the colon (end of the rectum).

The coordinates of the points A to G according to the curvilinear abscissa are given by the following chunk:

```
The coordinates of the points A to G on the curvilinear abscissa are:

absc_A= 0
absc_B= 0.249
absc_C= 0.512
absc_D= 0.752
absc_E= 0.845
absc_F= 0.929
absc_G= 1
```

During this work, the endoscope is inserted first. Video recording starts when it is withdrawn, and we assume that withdrawing happens at a constant speed so that the curvilinear abscissa is linearly related to the frame number.

7.2.2 Generation of the lesions' maps

To generate the map of the lesions, the first step to be ordered is to find the position of the frame according to Figure 7.1. We will use the function `coord_frame` which takes as inputs the frame number and the total video frames number. The output is the frame coordinates represented by the point P that will be placed on Figure 7.1.

Code chunk 11: Localisation-lesions.py (part 4)

```python
# Computation of the frame coordinates
def coord_frame(num_frame, nframe):
    absc_frame = float(num_frame) / nframe
    if absc_frame >= absc_A and absc_frame <= absc_B:
        P = (A[0] + AB[0] * (absc_frame - absc_A) / (absc_B - absc_A),
             A[1] + AB[1] * (absc_frame - absc_A) / (absc_B - absc_A))
    if absc_frame >= absc_B and absc_frame <= absc_C:
        P = (B[0] + BC[0] * (absc_frame - absc_B) / (absc_C - absc_B),
             B[1] + BC[1] * (absc_frame - absc_B) / (absc_C - absc_B))
    if absc_frame >= absc_C and absc_frame <= absc_D:
        P = (C[0] + CD[0] * (absc_frame - absc_C) / (absc_D - absc_C),
             C[1] + CD[1] * (absc_frame - absc_C) / (absc_D - absc_C))
    if absc_frame >= absc_D and absc_frame <= absc_E:
        P = (D[0] + DE[0] * (absc_frame - absc_D) / (absc_E - absc_D),
             D[1] + DE[1] * (absc_frame - absc_D) / (absc_E - absc_D))
    if absc_frame >= absc_E and absc_frame <= absc_F:
        P = (E[0] + EF[0] * (absc_frame - absc_E) / (absc_F - absc_E),
             E[1] + EF[1] * (absc_frame - absc_E) / (absc_F - absc_E))
    if absc_frame >= absc_F and absc_frame <= absc_G:
        P = (F[0] + FG[0] * (absc_frame - absc_F) / (absc_G - absc_F),
             F[1] + FG[1] * (absc_frame - absc_F) / (absc_G - absc_F))
    return P
```

Interpret with `python2`

Let us take examples:

Code chunk 12: Localisation-lesions.py (part 5)

```python
coord_frame(45,200)
coord_frame(100,200)
```

Interpret with `python2`

```
(49.69631915564096, 72.11167427554193)
(310.47065517169597, 46.50440635341696)
```

The second step is to represent annotations on the colon scheme. For each frame, we show the total surface of annotations of the same type as a fraction of the image size and we draw an orthogonal line to the colon curvilinear abscissa (cf function `vect_orthogonal`). Bleeding and ulcers are treated separately. The bleeding lesions are shown in red color (cf function `Fct_local_bleeding`) while the ulcer lesions are represented in green color (cf function `Fct_local_ulcer`).

Code chunk 13: Localisation-lesions.py (part 6)

```python
def vect_orthogonal(M,N):
  if N[0]!=M[0]:
    m=( (N[1])-(M[1]) )/( (N[0]) - (M[0]) )
    xo,yo=-m,1
  else:
    xo,yo=1,0

  n=sqrt(xo**2+yo**2)
  xo,yo=xo/n,1/n
  return xo,yo
```

Code chunk 14: Localisation-lesions.py (part 7)

```python
def Fct_local_bleeding(img, abs_curv_P, P,rP):
    RR=(0, 0, 255)
    if rP!=0.0:# there is annotation in the frame
        rP=rP*100.0 # to the clear the visibility on the scheme
        if abs_curv_P >= absc_A and abs_curv_P <= absc_B:
            xo, yo = vect_orthogonal(A, B)
            cv2.line(img,(int(P[0]),int(P[1])),(int(P[0]-xo*rP),\
                            int(P[1]-yo*rP)),RR)
        if abs_curv_P >= absc_B and abs_curv_P <= absc_C:
            xo, yo = vect_orthogonal(B, C)
            cv2.line(img,(int(P[0]),int(P[1])),(int(P[0]+xo*rP),\
                            int(P[1]+yo*rP)),RR)
        if abs_curv_P >= absc_C and abs_curv_P <= absc_D:
            xo, yo = vect_orthogonal(C, D)
            cv2.line(img,(int(P[0]),int(P[1])),(int(P[0]-xo*rP),\
                            int(P[1]-yo*rP/100)),RR)
        if abs_curv_P >= absc_D and abs_curv_P <= absc_E:
            xo, yo = vect_orthogonal(D, E)
            cv2.line(img,(int(P[0]), int(P[1])),(int(P[0]-xo*rP),\
                            int(P[1]-yo*rP)),RR)
        if abs_curv_P >= absc_E and abs_curv_P <= absc_F:
            xo, yo = vect_orthogonal(E, F)
            cv2.line(img,(int(P[0]),int(P[1])),(int(P[0]-xo*rP),\
                            int(P[1]-yo*rP)), RR)
        if abs_curv_P >= absc_F and abs_curv_P <= absc_G:
            xo, yo = vect_orthogonal(F, G)
            cv2.line(img,(int(P[0]),int(P[1])),(int(P[0]-xo*rP),\
                            int(P[1]-yo*rP)),RR)
```

Code chunk 15: Localisation-lesions.py (part 8)

```python
def Fct_local_ulcer(img, abs_curv_P, P,rP):
    GG=(39, 204, 6)# color green
    if rP!=0.0:
        rP=rP*100.0
        if abs_curv_P >= absc_A and abs_curv_P <= absc_B:
            xo, yo = vect_orthogonal(A, B)
            cv2.line(img,(int(P[0]),int(P[1])),(int(P[0]+xo*rP),\
                            int(P[1]+yo*rP)),GG)
        if abs_curv_P >= absc_B and abs_curv_P <= absc_C:
            xo, yo = vect_orthogonal(B, C)
            cv2.line(img,(int(P[0]),int(P[1])),(int(P[0]-xo*rP),\
                            int(P[1]-yo*rP)),GG)
        if abs_curv_P >= absc_C and abs_curv_P <= absc_D:
            xo, yo = vect_orthogonal(C, D)
            cv2.line(img,(int(P[0]),int(P[1])),(int(P[0]+xo*rP),\
                            int(P[1]+yo*rP/10)),GG)
        if abs_curv_P >= absc_D and abs_curv_P <= absc_E:
            xo, yo = vect_orthogonal(D, E)
            cv2.line(img,(int(P[0]),int(P[1])),(int(P[0]+xo*rP),\
                            int(P[1]+yo*rP)),GG)
        if abs_curv_P >= absc_E and abs_curv_P <= absc_F:
            xo, yo = vect_orthogonal(E, F)
            cv2.line(img,(int(P[0]),int(P[1])),(int(P[0]+xo*rP),\
                            int(P[1]+yo*rP)),GG)
        if abs_curv_P >= absc_F and abs_curv_P <= absc_G:
            xo, yo = vect_orthogonal(F, G)
            cv2.line(img,(int(P[0]),int(P[1])),(int(P[0]+xo*rP),\
                            int(P[1]+yo*rP)),GG)
```

We also use the automatic detections obtained in chapter 5 about the surface of annotated lesions in every frame of the video:

Code chunk 16: Localisation-lesions.py (part 9)

```python
# Use of saved results
with open('Folder-DataVatic-Percent.pickle','rb') as f:
        [y_b_percent,y_u_percent]= pickle.load(f)

# bleeding
Data_Perc_b = [ [individualArray] for individualArray in y_b_percent]
Data_Perc_b=Data_Perc_b[0][0]
# ulcer
Data_Perc_u = [ [individualArray] for individualArray in y_u_percent]
Data_Perc_u=Data_Perc_u[0][0]
```

To generate the lesions' map for a given video using saved data, we launch the following code lines:

Code chunk 17: Localisation-lesions.py (part 10)

```python
def Marque_Local_annotation_savdata(num_video, fichier_image_video, img_save,\
        Db,Du):
    img = cv2.imread('/users/alali/Images-colon/Imagecolonbase.png')
    Nfmax = len(Db)
    for frame in range(0, Nfmax):
        P = coord_frame(float(frame), Nfmax)
        abs_curv_P = float(frame) / Nfmax
        Fct_local_ulcer(img, abs_curv_P, P, Du[frame])
        Fct_local_bleeding(img, abs_curv_P, P, Db[frame])

    cv2.imwrite(img_save, img)
```

Code chunk 18: Localisation-lesions.py (part 11)

```python
# num_video = list of video numbers
for v in range(len(num_video)):
    img_save="/Folder-MapsDataVatic-Perc/DrAnnotation-Perc-vid-%s.png" \
                %(num_video[v])
    Marque_Local_annotation_savdata(num_video[v],fichier_image_video[v],\
                img_save,Data_Perc_b[v],Data_Perc_u[v])
```

In the following section, we will discuss the resulting lesions' maps for patients affected by UC disease.

7.3   Results

In order to keep fluent the reading of this thesis, we give the lesions' profiles generated for all the 37 UC patients of the Vatic database, derived from the doctor's annotations as well as the automatic detectors of chapter 6, in the appendix A page 196.

For this section, we rather focus on two main ideas:

1. Our proposed lesions' map can bring finer information about the disease severity in comparison with the current endoscopic scores: Mayo subscore and UCEIS score. Also, it permits a more precise classification between patients having the same score. In subsection 7.3.1, we will state the obtained results for the 13 patients of the Vatic database for which we have the severity scores (cf chapter 5).

2. The models computed in chapter 6 are good to detect bleeding and ulcers in colonoscopy videos. We, therefore, compare for some patients the maps of the detected lesions to those obtained through the doctor's annotations in subsection 7.3.2.

7.3.1 Proposed maps bring more information than endoscopic scores

In general, the UC severity according to the Mayo subscore and the UCEIS score can be roughly classified as follows [Ike+16]:

- Mayo subscore = 0 or UCEIS = 0 $\implies$ remission.
- Mayo subscore = 1 or UCEIS $\in [2,4]$ $\implies$ mild.
- Mayo subscore = 2 or UCEIS $\in [5,6]$ $\implies$ moderate.
- Mayo subscore = 3 or UCEIS $\in [7,8]$ $\implies$ severe.

In Figure 7.2 and Figure 7.3 we show the generated maps for patients having the UCEIS score equal 2 and 4 respectively. The four patients are classified similarly based on the severity scores, i.e. the disease is in a mild stage. However, the maps reveal different states of the disease: the affected colon segments and the severity of the lesions are not necessarily the same. Although the patients of Figure 7.2 have approximately the same affected parts, beginning from the end of the ascending colon segment to the rectum, they do not have the same type of lesions. In Figure 7.2a, the colon presents bleeding and ulcers lesions, whereas, in Figure 7.2b, the colon only presents bleeding lesions. Moreover, in this case, the rectum is bleeding more than the other colon segments.

(a)   (b)
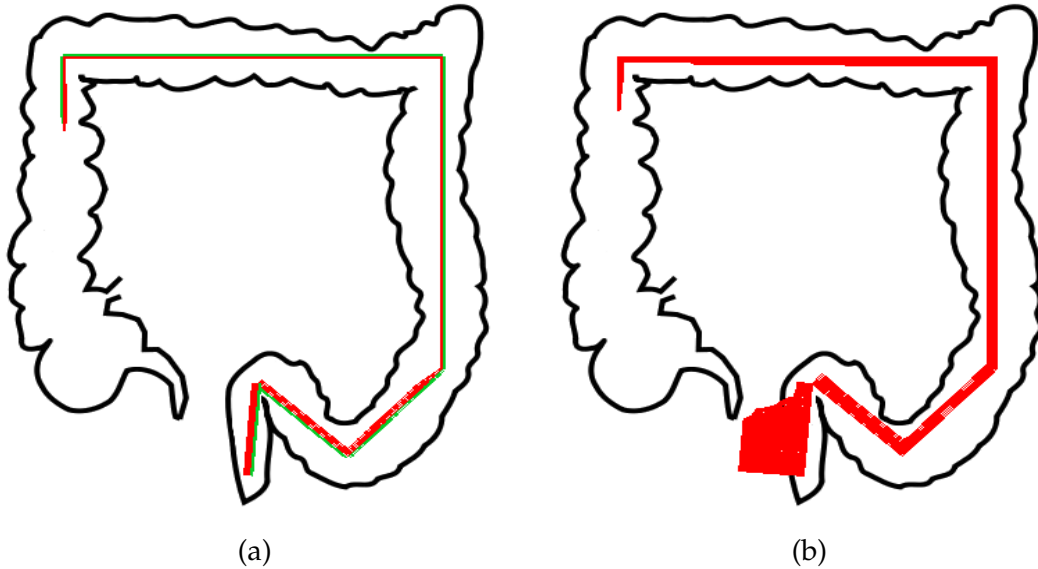
Figure 7.2: Distribution of the bleeding (in red) and ulcer (in green) lesions for patients with UCEIS = 2. (a) The colon is affected by bleeding and ulcer lesions whereas in (b) the colon only present bleeding.

The patients of Figure 7.3 are also classified into mild disease status. The lesions affect all the colon segments which is not the same case of Figure 7.2. In Figure 7.3a, the colon mucosa is very damaged due to the bleeding and ulcers . In Figure 7.3b, the ulcers are more abundant at the descending colon to the end

of the colon. These lesions' maps show that grading the most severe lesion like endoscopic scores is not sufficient to evaluate the mucosa status.

(a)   (b)
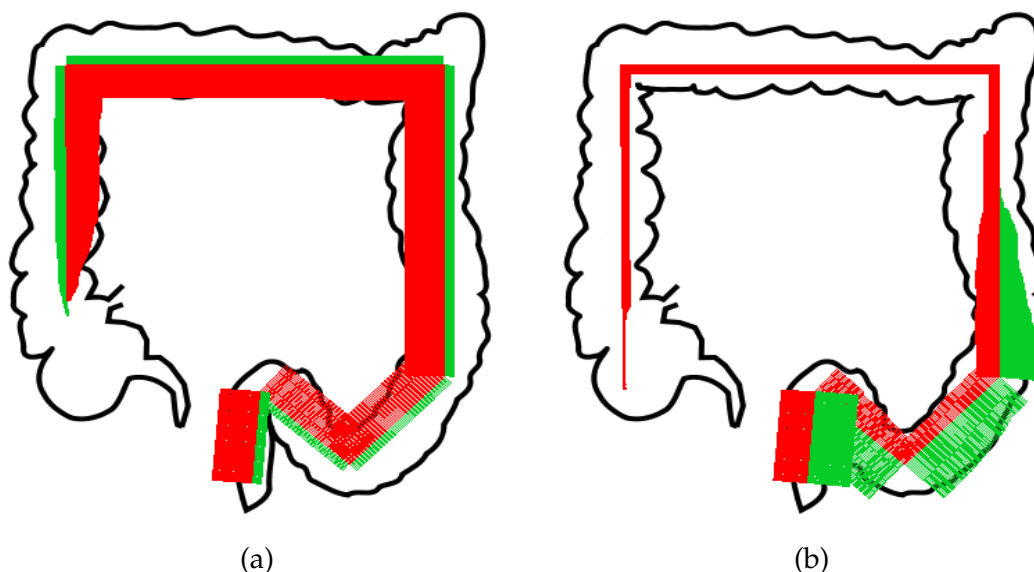
Figure 7.3: Distribution of the bleeding (in red) and ulcer (in green) lesions for patients with UCEIS = 4. The mucosa is affected by bleeding and ulcers. (a) all the colon segments are concerned by ulcers while in (b) the ulcers are affecting only the descending colon to the rectum.

Figure 7.4 and Figure 7.5 show the lesions' maps for patients for which the UC is classified into a moderate stage. In Figure 7.4a, the patient has an ulcerated mucosa rather than bleeding in contrary to the patient of Figure 7.4b where the mucosa bleeds a lot and only some ulcer lesions are present on the descending colon to the rectum. In comparison with Figure 7.5, the patients have the same class of disease, i.e. moderate, but the maps are very dissimilar. All the colon is affected by the lesions, and the area is very remarkable. However, for the patient of Figure 7.5a, the ulcer lesions invade the colon in contrary to the bleeding lesions in the case of Figure 7.5b.
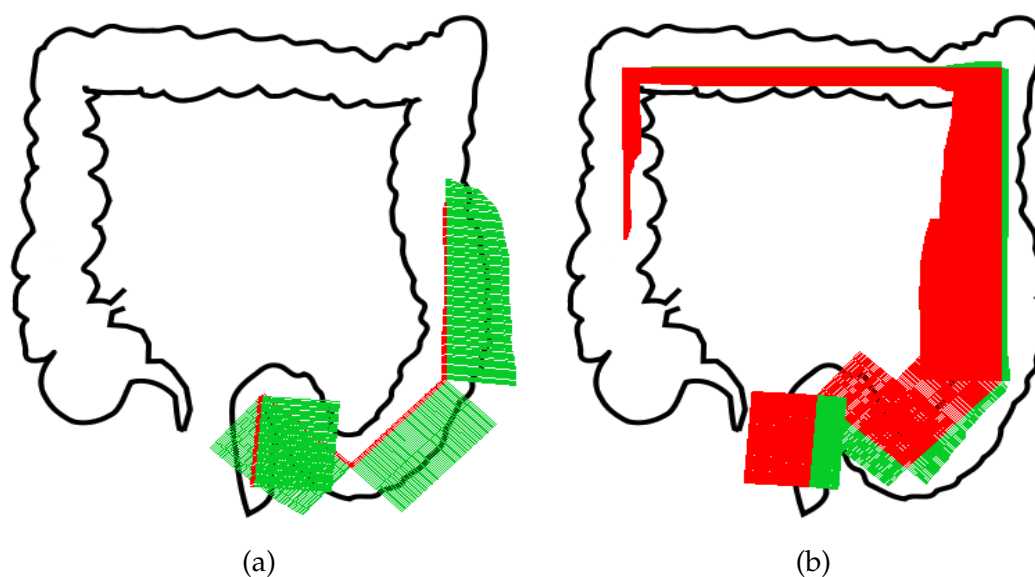
Figure 7.4: Distribution of the bleeding (in red) and ulcer (in green) lesions for patients with UCEIS = 5. In (a) the colon presents a lot of ulcers from the rectum to the middle of the ascending colon, while (b) the colon presents bleeding lesions in almost all the colon to the middle of the descending colon, the ulcerations are mostly concentrated at the sigmoid colon and the rectum.
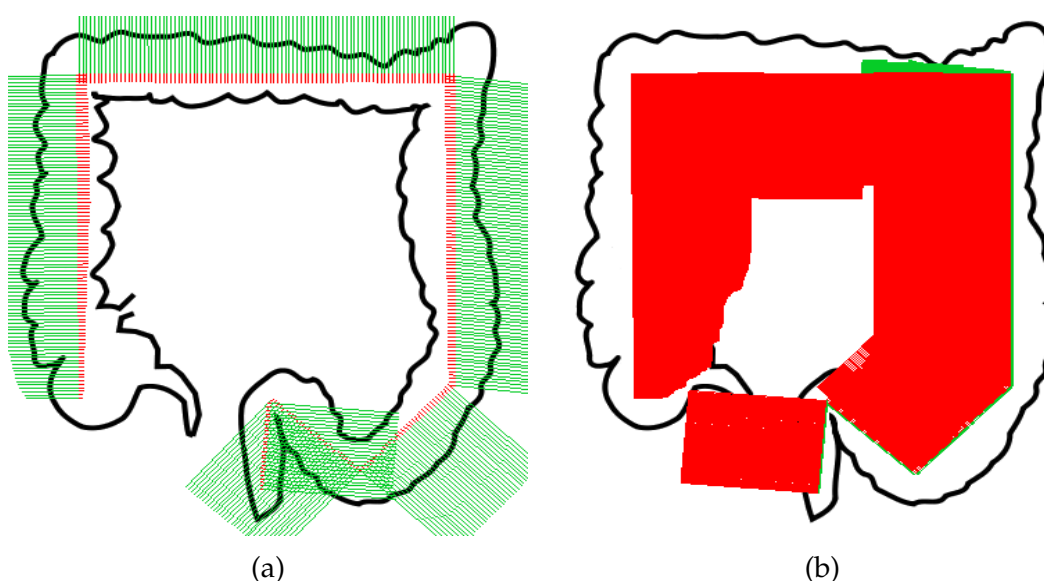
Figure 7.5: Distribution of the bleeding (in red) and ulcer (in green) lesions for patients with UCEIS = 6. In (a), the patient has ulcerated intestinal mucosa while in (b), the patient has a lot of bleeding in the whole colon.

We observe the same dissimilarities in lesions profiles for patients having the same MAYO subscore (Figure 7.6,Figure 7.7,Figure 7.8). In Figure 7.6, the severity of the same type of lesions is very different for patients in a mild stage of the disease. In Figure 7.6a, the bleeding lesions affect severely the mucosa in

comparison with Figure 7.6b where some ulcer and bleeding lesions affect the transverse colon to the end of the rectum. According to the computation of the MAYO subscore (cf chapter 4), score 1 indicates a partial loss of the vascular pattern visibility and friability. The bleeding and ulcers status was not reported. Despite that we did not consider the vascular pattern in the map presented here, we remark that the Mayo subscore is not sufficient to evaluate the condition of the mucosa. Same remarks can be seen in Figure 7.7. Although patients of Figure 7.8 have similarly affected colon segments, the patient of Figure 7.8a have ulcers and bleeding lesions whereas the patient of Figure 7.8b only have the colon is bleeding.

(a)   (b)
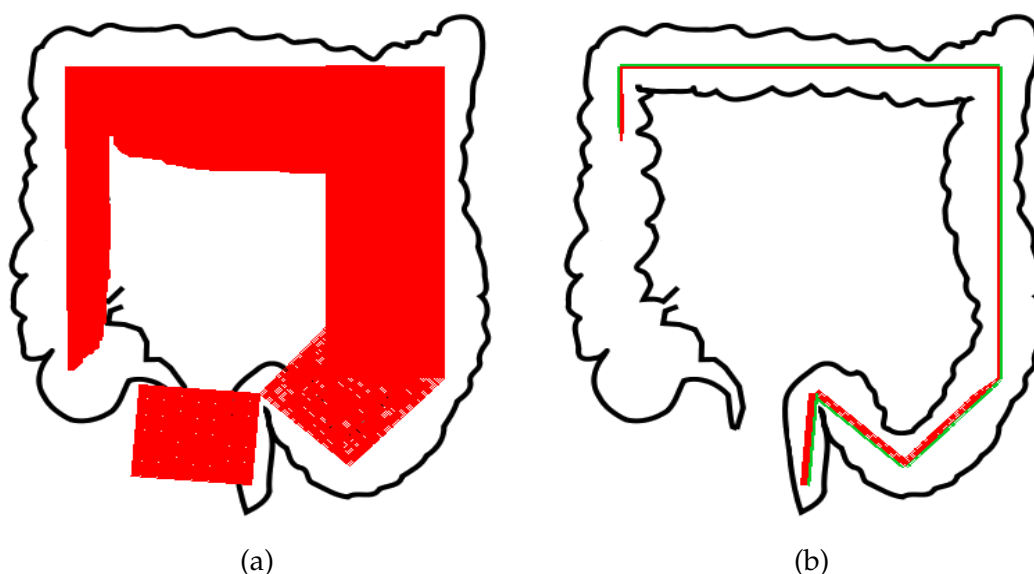
Figure 7.6: Distribution of the bleeding (in red) and ulcer (in green) lesions for patients with MAYO subscore = 1. The colon in (a) bleeds more than in (b).
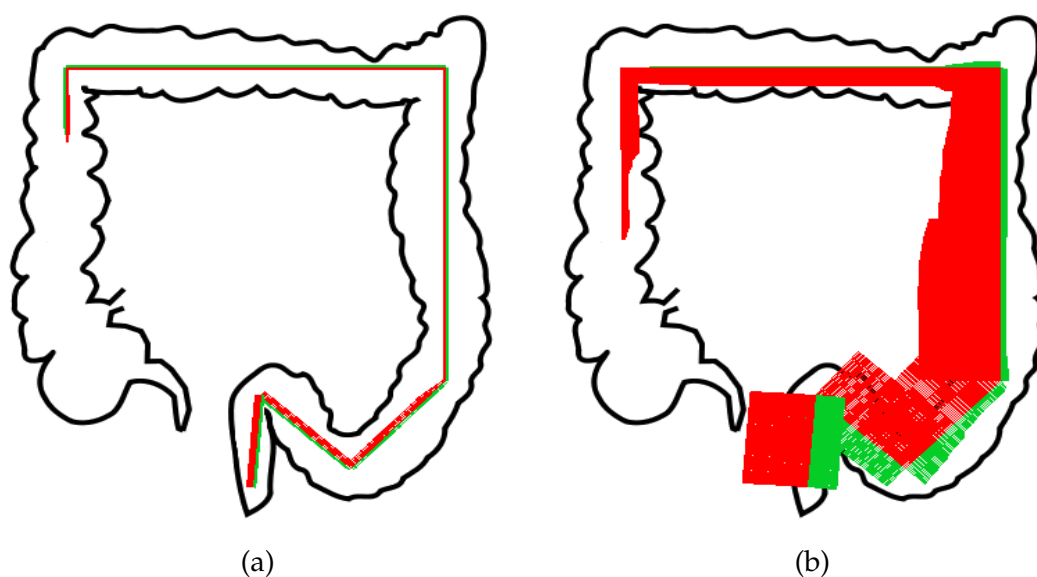
Figure 7.7: Distribution of the bleeding (in red) and ulcer (in green) lesions for patients with MAYO subscore = 2. Although, the patients have similar affected segments, the severity of the lesions in the case of the patient (b) is higher than in the case of the patient (a).
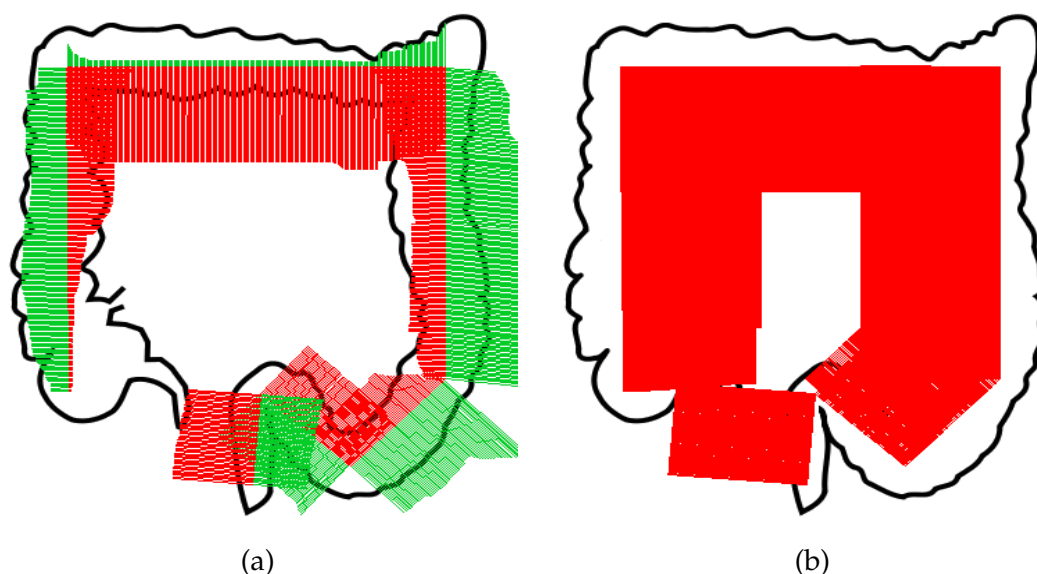
Figure 7.8: Distribution of the bleeding (in red) and ulcer (in green) lesions for patients with MAYO subscore = 3. In (a), the patient presents both bleeding and ulcer lesions while in (b), the patient, only bleeding lesions are found.

We can conclude that the disease does not affect similarly all the patients classified into the same class or having the same scores. These inflammation appearances suggest different treatment strategies and different medications and hence different surgical interventions when needed. These observations lead to the proposition of stratification of patients in a given class of score, and

the necessity of the integration of the spatial information to the UC diagnosis procedure.

7.3.2   Linear models are good to detect UC lesions

In this section, we compare the maps of the detected lesions to the maps of the annotated lesions for the same patient.

We use the optimal linear models computed in chapter 6 for bleeding ($\hat{m}_b$) and ulcer ($\hat{m}_u$) detection subject to the maximum of the criteria Sensitivity^A (cf Equation (6.7)). We recall the parameters of the models:

- $\hat{m}_b : G < 0.298R - 1.03$,
- $\hat{m}_u : Y > 0.698Cr - 42.799$.

For each frame, we compute the count of the classified pixels (into bleeding/ulcers) regarding the total size of the frame. These pixels represent the detected abnormal areas using the models $\hat{m}_b$ and $\hat{m}_u$ for bleeding and ulcer respectively.

Figure 7.9 and Figure 7.10 show the lesions profiles based on the doctor's annotations and automatic detectors for two different patients. In Figure 7.9, the two maps look the same: bleeding and ulcers affect all the colon segments, the most severe damaged parts are the same. We can conclude that the proposed algorithm and criteria Sensitivity^A in chapter 6 are almost effective to locate the abnormal pixels in a given colonoscopy video. However, this is not the case for patient of Figure 7.10, where there is difference in affected segments, here the ascending colon. Indeed, the models performance values reported for ulcer detection confirms that some normal pixels will be incorrectly classified as ulcers. These errors correspond to camera light reflection on the mucosa.
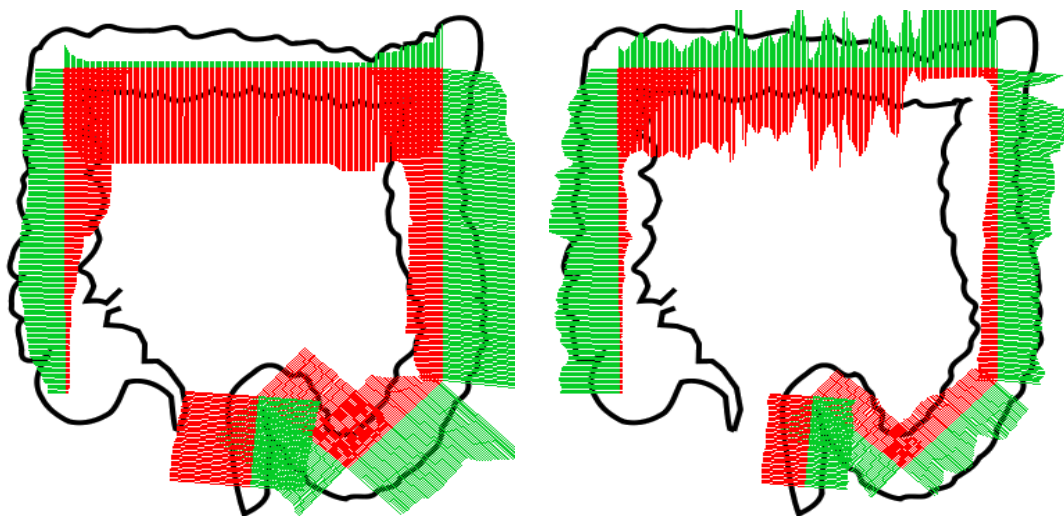
Figure 7.9: Distribution of the UC lesions for the same patient. Medical annotations on the left, and automatic detection on the right. The affected colon segments are the same and the lesions severities are also similar.
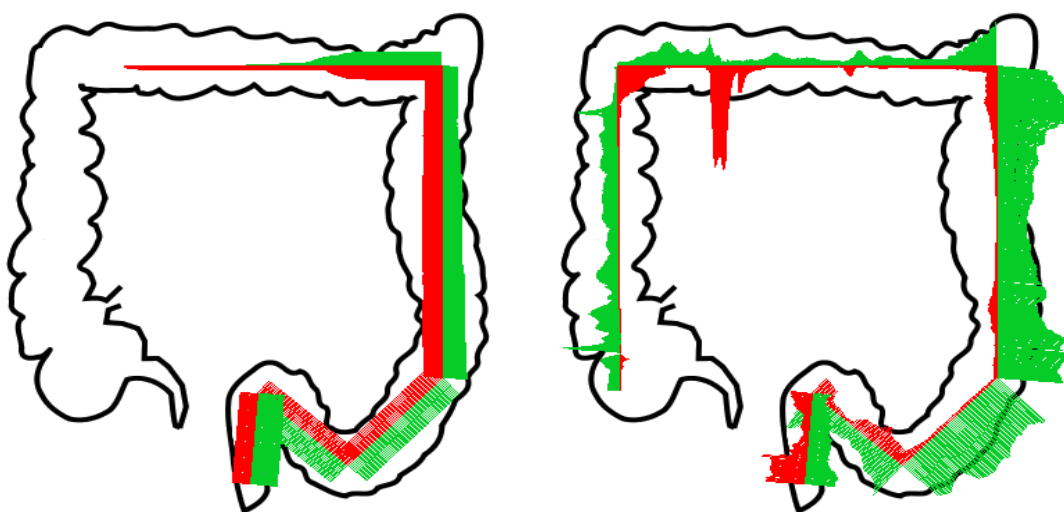
Figure 7.10: Distribution of the UC lesions for the same patient. Medical annotations on the left, and automatic detection on the right. According to the doctor's annotations, the ascending colon is not affected by lesions, however, this is not the case using the automatic models.

7.4 Discussion

7.4.1 Assumed hypotheses

In this work, we made three hypotheses:

1. The colon is a one-dimensional organ .

2. The speed of the endoscope removal during the colonoscopy exam is constant .
3. The considered colon scheme represents the real anatomy of the colon .

Hypothesis 1. The colon is generally a three-dimensional tube for which the length and the diameter differ between humans. However, its length is considered for about five feet and its diameter is three inches. Therefore, in this thesis, we decide to neglect the diameter of the colon. On the other hand, during the colonoscopy the camera angle or orientation is unknown, the lesions' positions according to the colon (tube) are thus unknown. We also neglect this coordinate and consider the colon a one-dimensional object represented by its curvilinear abscissa.

Hypothesis 2. The hypothesis 2 does not reflect exactly how the medical exam is conducted. It is difficult for the gastroenterologist to retain a constant speed while operating the endoscope. During the colonoscopy examination, he needs to watch the monitor to visualize the colon mucosa. However, sometimes he will stop moving the endoscope to take specific pictures of suspicious abnormalities. Furthermore, to confirm his diagnosis, he can take a biopsy sample. This leads to some break-times or brutal movements in the video. Hence, there are a lot of artefacts or errors in the video. These images do not correspond to new locations or spots of the colon, but they correspond to the colon parts that were previously shown in the video. Therefore, when we have considered that the frames are linearly distributed according to the video's time, we have indirectly neglected these artefacts and errors.

Hypothesis 3. The total length of the colon varies depending on a variety of parameters such as gender, height age. Many reports have been published, but no one has yet explained the difference in length. We will pick a paper published in 2019 to extract the information about the colon parts' length. According to the publication of Gaur et al. [Gau+19], the large intestine measures about 123 cm to 152 cm ($\approx$ 5 feet) in length and it is divided into the following parts:
  - the Cecum for about 6 to 9 cm
  - the ascending colon measuring 20 cm to 25 cm long
  - the transverse colon measuring 40 cm to 46 cm long
  - the descending colon of 10 cm to 15 cm long
  - the "S" shaped sigmoid colon which is approximately 35 cm to 45 cm long
  - the rectum of 12 cm.

We compare the measurements provided by [Gau+19] to the colon dimensions considered in this work. According to Gaur [Gau+19], the cecum and the ascending colon represent approximately 21% or 22% of the colon length. According to our work (cf Figure 7.1), the cecum and the ascending colon represented by the segment AB correspond to $\approx$ 25% of the total colon length. The same problem occurs in the transverse colon, which counts for 30 to 33%

of the colon [Gau+19]. In our work, the transverse colon is represented by the segment *BC* which only measures 26% of the colon length. The descending segment measures 0.06% to 0.08% of the colon in real life, but it counts for 24% of the colon length in our work. The sigmoid colon, measuring about 28% or 29% of the colon as indicated in the paper [Gau+19], represents only 18% of the colon in Figure 7.1, corresponding to the segment *DF*.

Consequently, Figure 7.1 used to parameterize the colon does not represent the exact colon anatomy.

7.4.2   Negligence of the turning angles

There are three main angles in the anatomy of the colon, called turning angles: hepatic, splenic and sigmoid. The hepatic angle is located where the colon runs under the liver from the transverse colon. The splenic angle (as it is next to the spleen) is the tight bend between the transverse colon and the descending colon. The sigmoid angle connects the descending colon to the sigmoid colon. The turning angles are generally identified by the gastroenterologist during the colonoscopy examination but they are difficult to detect with a computer algorithm.

To counter this problem, we have proposed to our collaborators' gastroenterologists to locate the position of points B, C and E shown in Figure 7.1 by making a shot during the colonoscopy exam. Unfortunately, the obtained figures for the angles are either very blurred to the rapid movements of the gastroenterologist during the colonoscopy or very similar. We show in Figure 7.11, the images of the three splenic angles of the colon as captured by the gastroenterologist during the colonoscopy. The images are very difficult to be distinguished using image processing algorithms. Therefore, we neglected the locations of the turning angles in our proposed method.
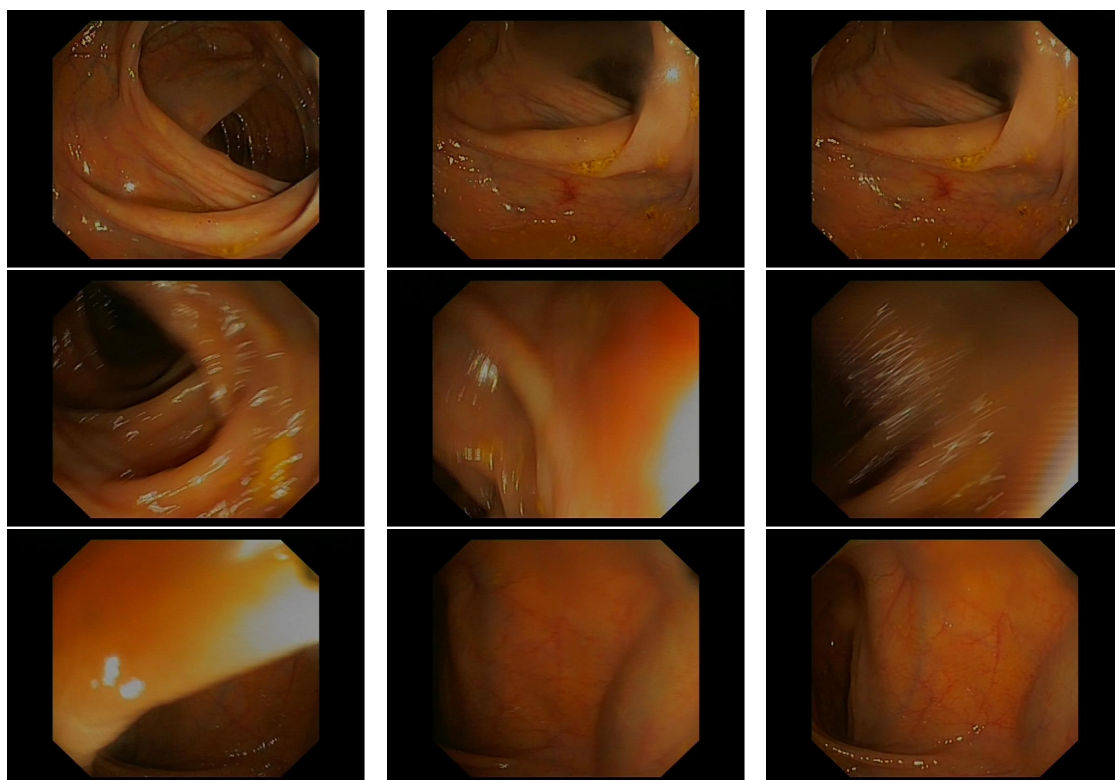
Figure 7.11: Some shots of the colon turning angles made by our collaborators.

7.4.3   Visibility of a lesion in successive frames

Another limitation of the proposed method is that the doctor's annotations were not cleaned. As discussed in chapter 5, the annotations contain many mislabeling errors. We can remark that due to the appearance of a given lesion on a succession of frames, sometimes the length of the representative lines (red and green) in the generated maps was the same for some parts of the colon as we can see for example in Figure 7.12a for bleeding lesions and in Figure 7.12b for ulcerations lesions.

This suggests the need for a video processing step before calculating the map in order to avoid counting the same lesion several times. A possible solution might be to consider the lesion just in the frame where it first appears. Another video processing solution is to study the images taken several times in the video as in the cases where the doctor has some difficulty in moving the endoscope during the colonoscopy. This may lead to correctly identifying the position of the turning angles.
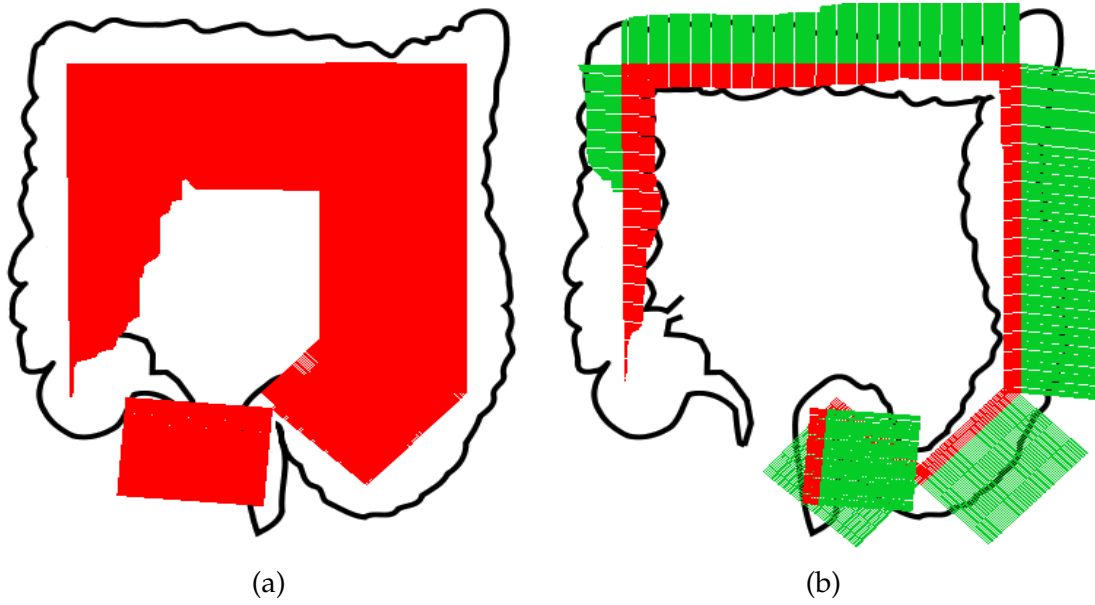
Figure 7.12: Distribution of the annotated bleeding (in red) and ulcer (in green) lesions for patients affected by UC disease. The colon parts from the descending colon to the rectum are affected identically by bleeding (on the left) and ulcer (on the right).

7.4.4 Representation problems at the turning angles

The use of orthogonal lines in the proposed maps can hide the visibility of the lesions in some cases. More precisely, the severity of the lesions is not clearly reported at the turning angles, represented by the points B, C, D in Figure 7.1. For instance, in Figure 7.13, the orthogonal lines are crossing together implying an unclear view of the degree of the lesion at the locations of the turning angles. We cannot decide if the end of the ascending colon is very bleeding or the beginning of the transverse colon.
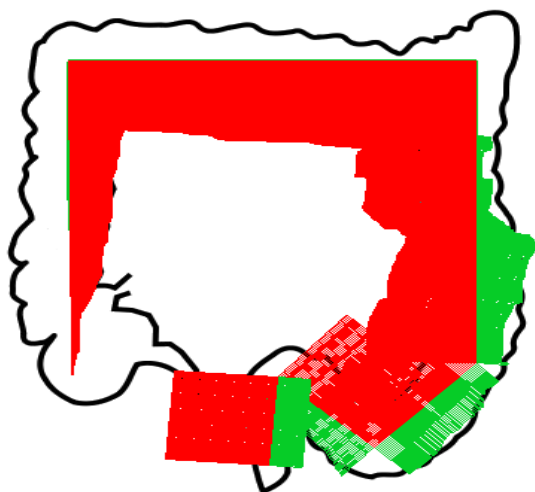
Figure 7.13: At the turning angle of curvilinear abscissa D, there is an overlapping between the red lines representing the bleeding at the surrounded parts leading to ambigous view of the status of the colon at this location.

The same remark holds for the set of points E to G. In Figure 7.14, the problem of overlapping lines occur at the points E, F and G. The bleeding and ulcer surface is not represented in a good manner making their visibility quite difficult and imprecise.
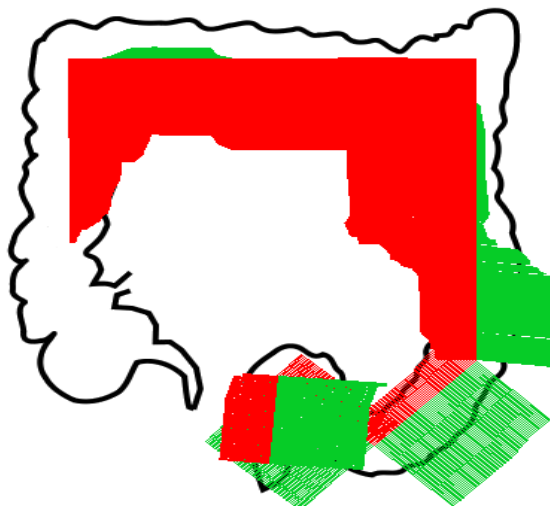
Figure 7.14: At the sigmoid colon, the lesions are not represented clearly. The bleeding on the segment connecting E to F are hidden by ulcers of the segment F to G.

7.4.5   Reproducibility

This work also requires some clinical validation to be applied to new cases of UC patients. We must study its reproducibility for the same patient. The doctors have been asked to do the colonoscopy exam for the patient twice but it is not

done yet because it is quite unpleasant for the patient. Another procedure has been proposed consists of viewing the rectum in double time (at the end of the colonoscopy), but the videos are not yet made.

7.4.6 Need of comparison criteria

To evaluate the capacity of the proposed method, we need to use some distance measurements or performance criteria in order to finely compare the spatial extent of the annotated lesions to the extent of the detected lesions. We did not succeed into finding convenient criteria, we only used visual appearance for comparison.

In the end, we shall be precise that as said in chapter 5, the length of the videos is not the same and some of the videos do not correspond to complete colonoscopy. However, due to a lack of information, for this work, we assumed that all the videos represent the whole colon.

7.5 Conclusion

In this chapter, the objective is to represent the lesions found in the colonoscopy video according to their location in the colon, i.e. the spatial distribution of bleeding and ulcers (cf Figure 7.1).

We parameterize the colon by its curvilinear abscissa (cf subsection 7.2.1). As the frames were supposed linearly distributed in the video (cf subsection 7.4.1), we link the frame number with the curvilinear abscissa by using the linear interpolation.

We generate the map corresponding to the annotations provided by the doctors (cf subsection 7.3.1) and for the detections obtained from our detection method described in subsection 7.3.2.

The obtained results demonstrate a new and more complete representation of the disease status that cannot be provided by the endoscopic scores. It offers a clear representation of the spatial extent of the lesions and provides a fine distinction between patients with the same endoscopic severity score.

The colon parametrization presented in this chapter will be used in the following chapters to establish a severity score taking into consideration the spatial distribution of the lesions (chapter 8), study the lesion distribution near the rectum (chapter 9), and the speed of lesions propagation (chapter 10).

Chapter 8

Modelling the severity of the Ulcerative Colitis disease

Abstract

Severity scores such as UCEIS and MAYO subscore take into consideration only the most severe lesion in a colonoscopy video regardless of its spatial extension in the colon (chapter 4). The representation of the lesions generated in chapter 7 suggests the necessity of their grading during the severity assessment to improve the disease severity estimation and the long-term follow-up. In this chapter, we propose to model the severity of UC considering the spatial distribution of the lesions.

For a first attempt, we investigated a linear model of the severity scores based on the spatial distribution of the lesions regarding their positions in the colon. To do that, we decide to investigate the set {Functions: patient $\implies$ $\mathbb{R}$}. The patient is represented by the count (or area) of annotations found in the colonoscopy video. The colon is parametrized similarly to chapter 7. For each segment of the colon, we inspected the lesion's count (and area) locally. The final score accounts for all the segments.

On a set of 13 patients, we obtain good agreement between the proposed model and the scores provided by the gastroenterologists using the L_2 distance. In addition, we tested different colon configurations i.e. colon segments decomposition. For UCEIS, considering the colon by 6 segments is optimal, whereas the MAYO subscore is better estimated considering the colon into only 4 segments.

Although the modelling procedure was helpful to estimate the UCEIS and MAYO (sub) scores using the localization of the lesions in the colon, it depends on the gastroenterologist scores. Moreover, the proposed scores model does not involve objective biomarkers of the severity such as albumin and C-reactive protein.

8.1   Introduction

In chapter 4, we presented several endoscopic scores used to numerically assess the UC severity after undergoing a colonoscopy examination. The representation of the disease severity is limited to a "small" set of parameters of type clinical, endoscopic and biological and sometimes the personal interpretation of the doctor as well.

The scores currently used in clinical practice, MAYO subscore and UCEIS score are based on the evaluation of five and three parameters respectively depending on the most relevant lesions of the UC disease (cf chapter 4). They take into account bleeding, erosions/ulcerations, vascular pattern and mucosal erythema and friability. Like almost all the endoscopic indices, they don't consider other relevant information such as the spatial localization and the distribution of the lesions along the colon wall.

As a consequence, there is an imprecise evaluation of the disease severity when ignoring information about the lesions' spatial extent and their abundance.Therefore, the endoscopic scores are always incomplete to measure the status of the intestinal mucosa, and they need to consider the spatial localization of the lesions in the colon as well as their local amount or surface.

For this reason, we propose to model the severity of the UC disease by taking into consideration the local severity of the lesions (count or surface) regarding their position on the colon based on the parametrization expanded in chapter 7.

The rest of the chapter is organized as follows. In section 8.2, we give the setups used in this chapter: the endoscopic scores, the colon segments and the proposed model. In section 8.3, we compare the obtained results to the scores provided by three gastroenterologists. In **??**, we discuss some assumptions considered in this work.

8.2   Modelling setups

We will explore the linear models of the set: {Functions: patient $\implies$ Severity}. For this process, we will use a set of 13 patients of Vatic database for whom we have the severity scores (see chapter 5).

8.2.1   Representation of the patient

Using the bleeding and ulcers in colonoscopy video, the patient can be then considered as a point in $\mathbb{R}^2$. We use the total number or surface of the lesions.

```
Bleeding annotations total count for 13 patients is:
[1946, 1101, 67, 2728, 1026, 674, 157, 673, 1081, 202, 8294, 766, 1574]
```

```
Ulcers annotations total count for 13 patients is:
[2332, 3888, 20, 0, 0, 92, 956, 905, 904, 0, 50, 1292, 0]

Bleeding annotations area for 13 patients is:
[0.43, 0.05, 0.02, 0.7, 0.08, 0.24, 0.01, 0.29, 0.08, 0.08, 0.92, 0.11, 0.99]
Ulcers annotations area for 13 patients is:
[0.37, 0.81, 0.02, 0.0, 0.0, 0.07, 0.2, 0.06, 0.09, 0.0, 0.02, 0.11, 0.0]
```

The main objective of this work is to propose a severity score that considers the spatial distribution of UC lesions such as bleeding and ulcers in our case. The segments of the colon are therefore essential to localise the distribution of the lesions. Consequently, the patient will be considered in $\mathbb{R}^{2k}$, where k value is chosen to cover the principal segments of the colon of Figure 7.1. Herein, we consider the maximum number of colon segments is $k = 6$ as one can see in Figure 8.1.
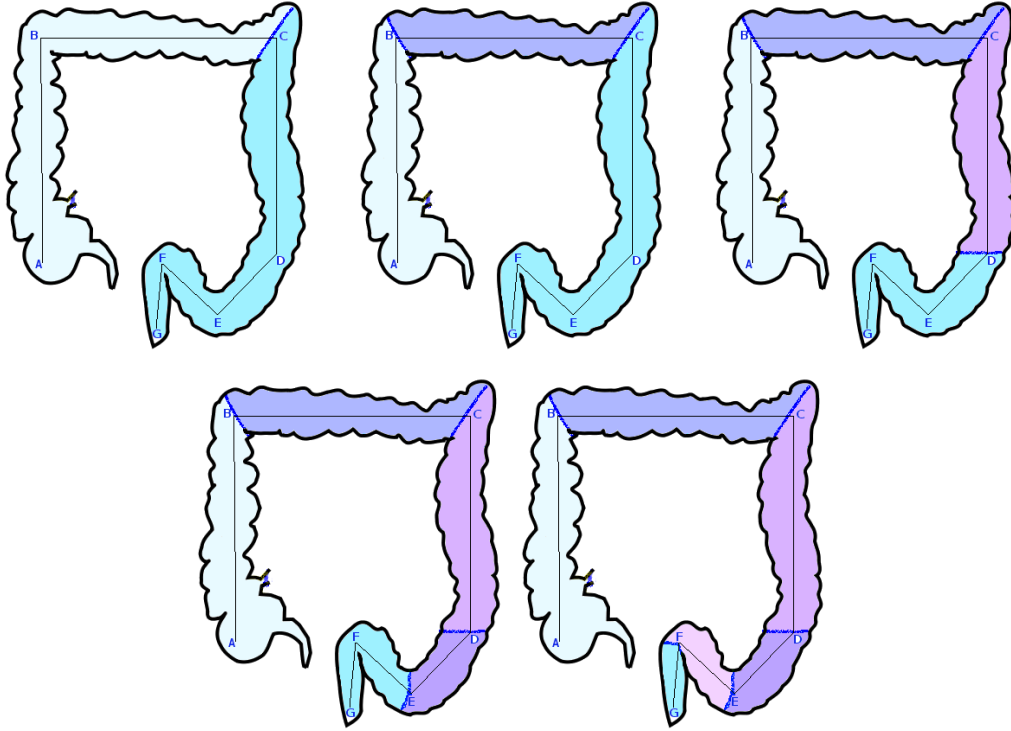
Figure 8.1: Decomposition of the colon into k segments. First line, the colon is decomposed into $k = 2$, $k = 3$, $k = 4$ segments respectively. Second line, the colon is decomposed into $k = 5$ and $k = 6$ segments.

In Figure 8.1, we show the colon decompositions treated in this chapter. We assign a specific color for every segment to facilitate the differentiation between the decompositions. For instance, when the colon is considered as two segments ($k = 2$), we considered the ascending and transverse colon as one segment (denoted by a light blue color), and the other colon parts as one segment (designed by a medium blue color). In the case of the decomposition

into three segments ($k = 3$), we considered the ascending colon, also called the right colon, the transverse colon as two segments, and the other colon parts as the third segment. For $k = 4$, we take into consideration the principal colon segments associated with the anatomy of the colon: ascending, transverse, descending and sigmoid-rectum part. For the upper values of colon segments, namely for the cases of $k = 5$ and $k = 6$, we consider sub-parts of the sigmoid-rectum colon confined between points D and G.

In the following, we present an example for the computation of the local number and surface measure of the lesions for a patient from the Vatic database. He has all the colon affected by bleeding and ulcers as one can see in Figure 8.2:

Figure 8.2: Distribution of bleeding (in red) and ulcers (in green) according to annotations provided by a gastroenterologist.

To compute the number of lesions on a segment "MN" for example, we will consider the number of annotations for all frames having the curvilinear abscissa included into the abscissa M and the abscissa N.

For the patient of Figure 8.2, the count of the lesions for the different colon decompositions are, by taking V_b the bleeding vector and V_u the ulcers vector:

```
Patient is represented by the vector V=[Vb,Vu] where for:
k=1,Vb=[1946.0] & Vu=[2332.0]
k=2,Vb=[ 555. 1391.] & Vu=[ 275. 2057.]
k=3,Vb=[ 385.  180. 1381.] & Vu=[ 219.   79. 2034.]
k=4,Vb=[385. 180. 527. 854.] & Vu=[ 219.   79. 1159.  875.]
k=5,Vb=[385. 180. 527. 294. 560.] & Vu=[ 219.   79. 1159.  424.  451.]
k=6,Vb=[385. 180. 527. 294. 328. 232.]
    & Vu=[ 219.   79. 1159.  424.  272.  179.]
```

When considering the area of lesions for each colon decomposition, we will compute the amount of the annotations surface for all the frames included in this colon segment divided by the length of the considered segment. For the patient that we took as an example, we get the following values for the lesion surface for each considered segment, for all the proposed decompositions:

```
Patient is represented by the vector V=[Vb,Vu] where for:
k=1,Vb=0.427132227741 & Vu=0.369273124895
k=2,Vb=['0.476', '0.378'] & Vu=['0.171', '0.567']
k=3,Vb=['0.195', '0.750', '0.372'] & Vu=['0.274', '0.076', '0.575']
k=4,Vb=['0.195', '0.750', '0.290', '0.451']
    & Vu=['0.274', '0.076', '0.641', '0.511']
k=5,Vb=['0.195', '0.750', '0.290', '0.333', '0.522']
    & Vu=['0.274', '0.076', '0.641', '0.621', '0.445']
k=6,Vb=['0.195', '0.750', '0.290', '0.333', '0.493', '0.556']
    & Vu=['0.274', '0.076', '0.641', '0.621', '0.471', '0.414']
```

Next, we will recall the available endoscopic scores for some patients of the Vatic database.

8.2.2 Representation of the disease severity

The severity of the disease is evaluated using the endoscopic scores i.e. it is considered as an element $\in \mathbb{R}$. During our collaboration with gastroenterologists (XT, CS and YB), we obtained the scores UCEIS and MAYO sub-score for 13 UC patients from the Vatic database that we give in the code chunk:

Code chunk 19: Severity-modelling.py (part 21)

```python
# UCEIS score
UCEIS_XT=[8,7,2,1,3,1,5,5,5,5,7,5,7]
UCEIS_CS=[8,6,2,1,2,4,5,5,6,3,6,4,7]
UCEIS_YB=[7,8,3,1,1,0,4,5,3,2,3,3,4]

# MAYO sub-score
MAYO_XT=[3,3,1,1,1,1,3,3,3,3,3,3,3]
MAYO_CS=[3,3,1,1,1,2,3,3,3,1,3,3,3]
MAYO_YB=[3,3,2,1,1,0,3,2,2,1,2,2,2]
```

In Vatic database, the annotations are anonymous, namely, we don't have the annotations of each gastroenterologist. Thereby, the data extracted from the spatial distribution of lesions used to compute the model of a score is the same for all the experts. The difference is in the value of the scores that every expert associates with a patient. In this work, these scores are not combined in a six-dimensional score.

8.2.3   The model

We decide to model the severity by the linear functions defined as follows:

$$
\begin{aligned}
\mathbb{R}^{2k} &\rightarrow \mathbb{R} \\
(D^b, D^u) &\rightarrow \text{Severity}
\end{aligned}
$$

where $k \in \mathbb{N}^*$ is the index of the colon segment, D^l is the number or surface of lesions, and $l = b$ for bleeding while $l = u$ for ulcers.

The model's parameters are computed through the mean square error minimization (MSE):

$$
\hat{\beta} = \underset{\beta \in \mathbb{R}^{2k+1}}{\mathrm{argmin}} \sum_{i=1}^{i=N_p} (Y_i - X.\beta)^2 \underset{MSE}{\Longrightarrow} \boxed{\hat{\beta} = (X^t.X)^{-1}.X^t.Y}
$$

where $X \in \mathcal{M}(N_p, (2k+1)N_p)$ is the data matrix, N_p is the number f patients (herein 13), and Y is the UCEIS score or the MAYO subscore.

8.3   Results

In this section, we will compute the severity scores using the colon decompositions and the linear model discussed in section 8.2. It encounters two parts:
- In subsection 8.3.1, we compare the estimated scores to those provided by the gastroenterologists.
- Then in subsection 8.3.2, we compute the optimal colon decomposition according to the L_2-distance.

8.3.1   Correlation with the endoscopic scores

A numerical score will be computed for each gastroenterologist. The $x-$axis represents the patient index and the $y-$axis accounts for Mayo subscore and UCEIS score. Gastroenterologist scores will be drawn by a solid line while estimated score will be drawn by a dashed line. The estimated score based on local count of lesions will be designed by Model_Count, whereas it will be designed by Model_Perc in the case of local lesions surface.

In Figure 8.3, we present the obtained score for all the gastroenterologists when $k = 1$. The count and the area of lesions bring almost similar results for the estimation of UCEIS and Mayo subscore. For UCEIS given by Dr. XT, there is a difference of 2 points with the real score for four patients. The Mayo subscore is likely to be better estimated using the count of lesions in the colon than their surface. In contradiction, for Dr. CS, the area of lesions seems to be more suitable to estimate the Mayo subscore. For Dr. YB, the scores are better estimated with the surface of lesions. There is a difference of a maximum of one

point between the given score UCEIS and the estimated score for almost all the patients (9 over 13 patients equivalent to 69% of the patients). Using the lesions count, the results are less better with coincidence for only 54% of the patients. For the Mayo subscore, the results are less good.
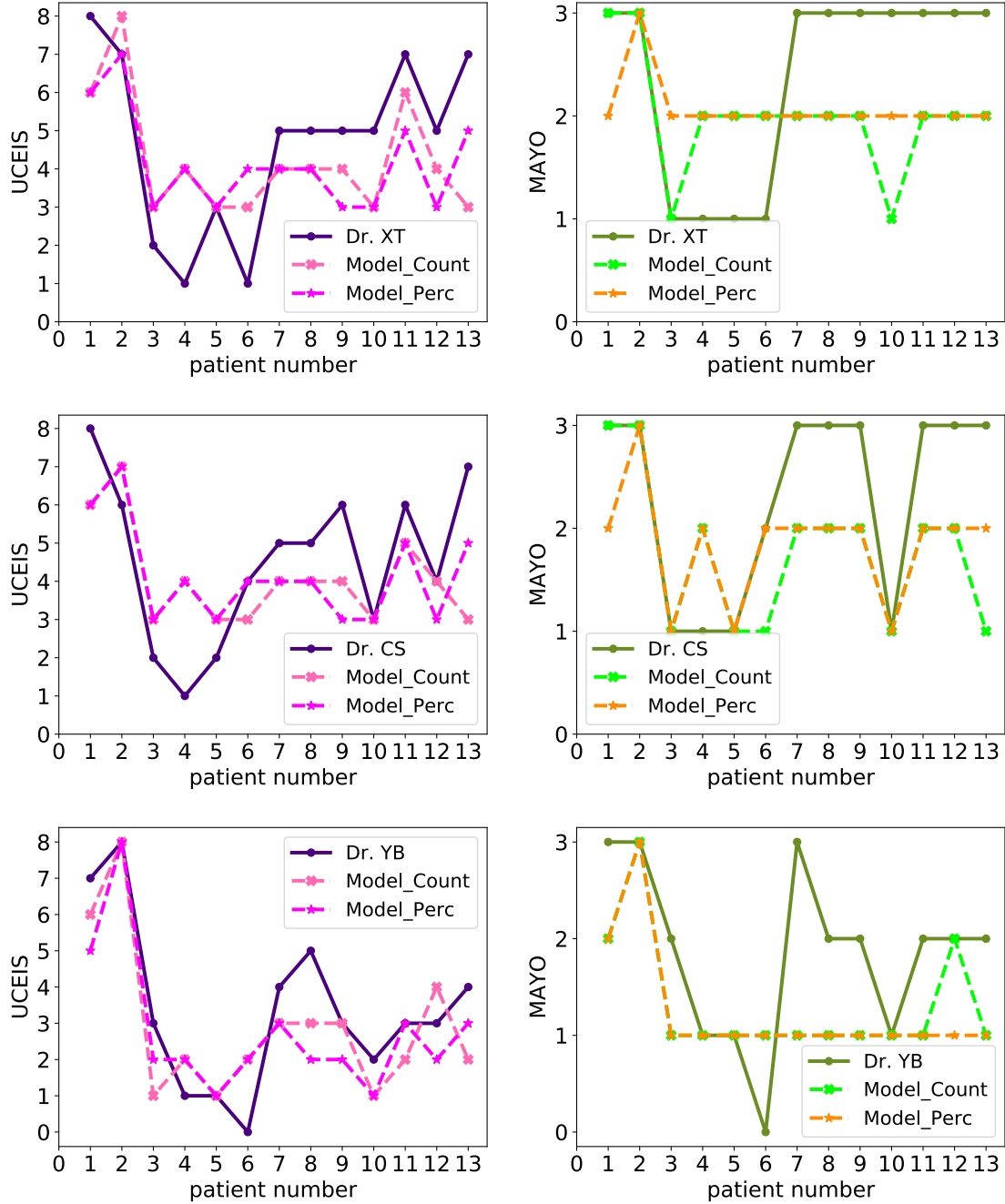
Figure 8.3: Estimated UCEIS at the left and estimated MAYO at the right for the gastroenterologist XT (first row), CS (second row) and YB (third row) in the case where $k = 1$.

In the case where $k = 2$ given in Figure 8.4, the curves of estimated UCEIS are near the real one for approximately all the patients. Same remark to Mayo subscore and all the doctors. There is no relevant differnce with results obatined in the case $k = 3$, see Figure 8.5.
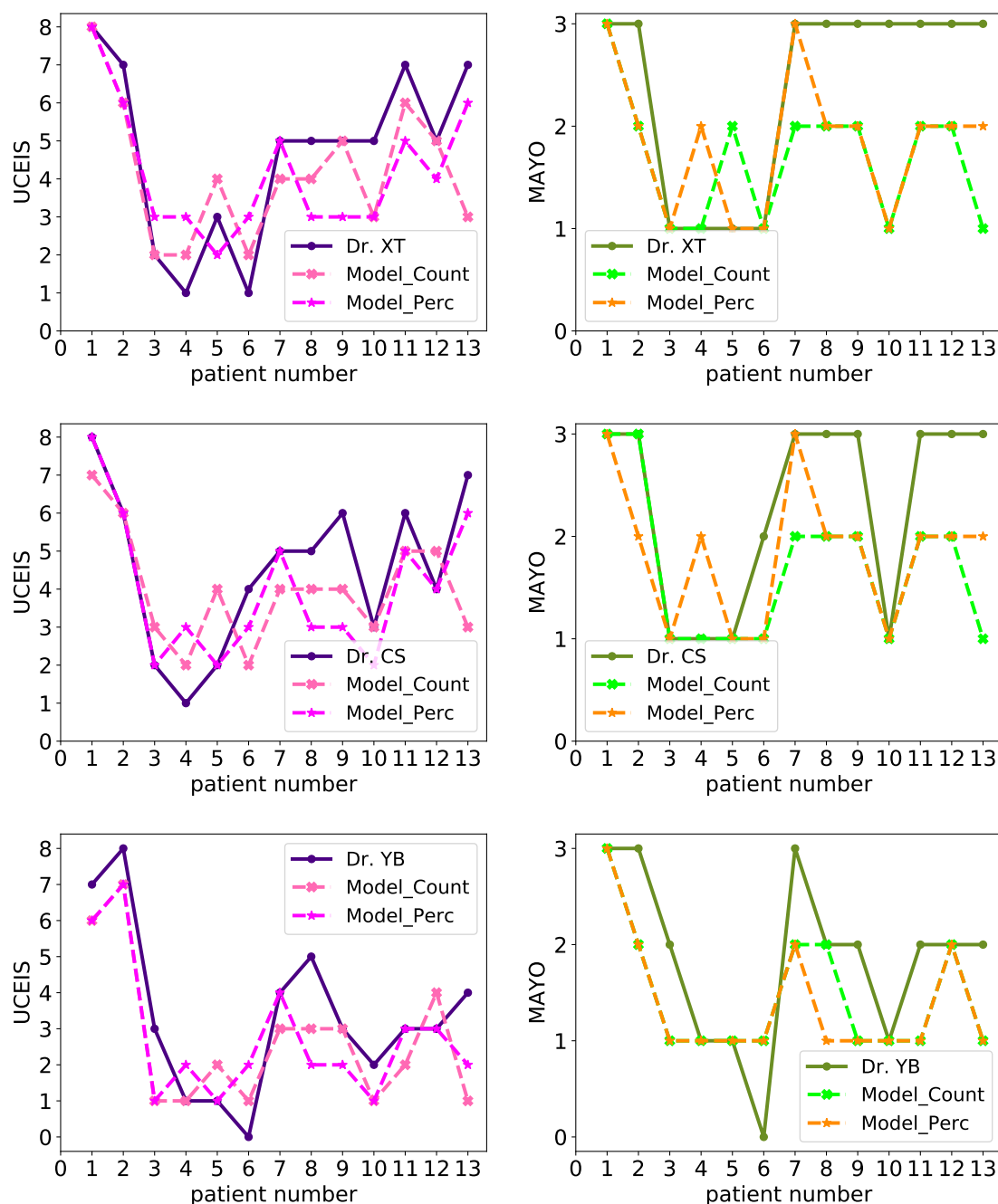
Figure 8.4: Estimated UCEIS at the left and estimated MAYO at the right for the gastroenterologist XT (first row), CS (second row) and YB (third row) in the case where $k = 2$.
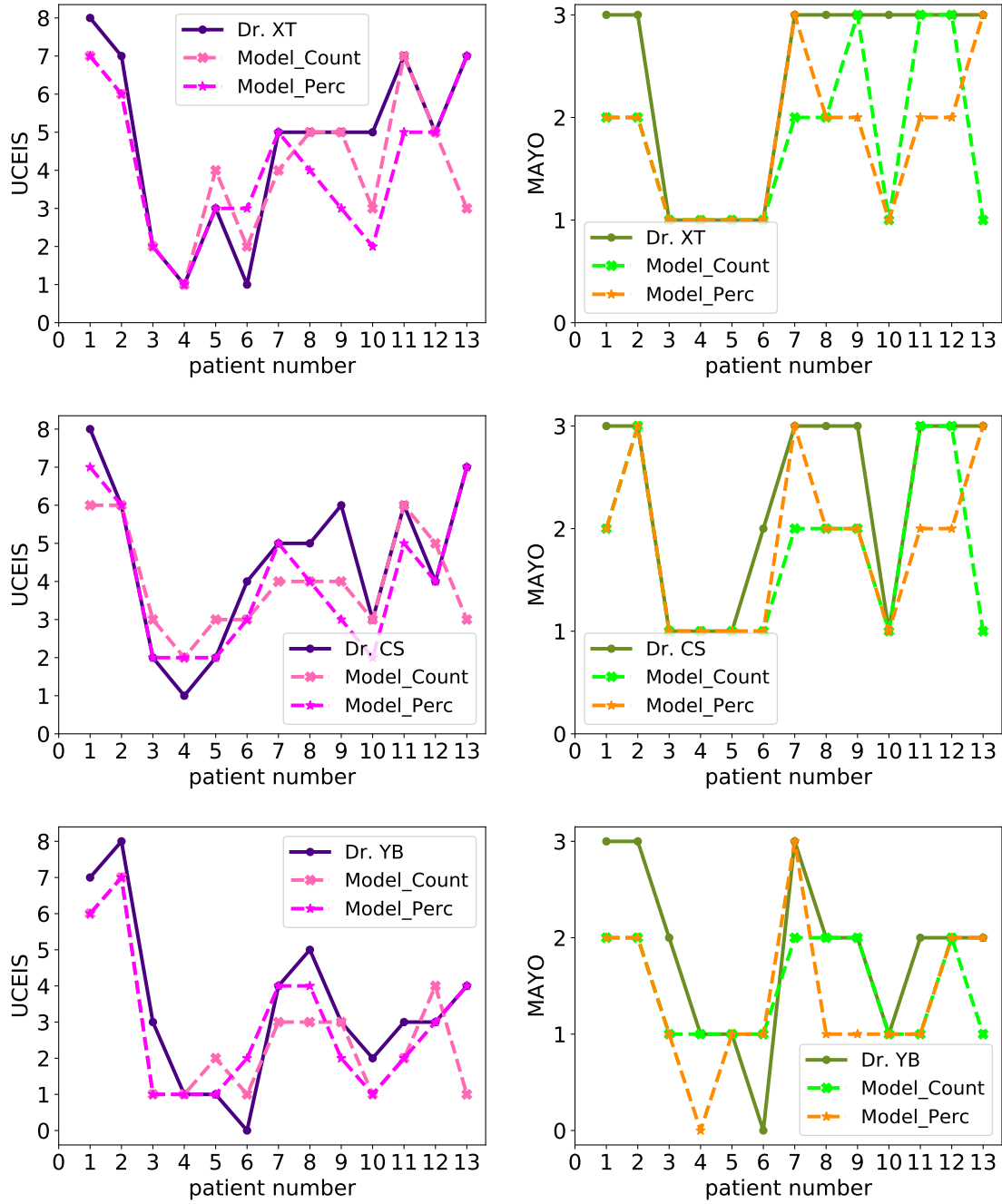
Figure 8.5: Estimated UCEIS at the left and estimated MAYO at the right for the gastroenterologist XT (first row), CS (second row) and YB (third row) in the case where $k = 3$.

Figure 8.6 to Figure 8.8 show the results for $k \geq 4$. One might see that the highest the number of considered colon segments, the better we approximate the severity scores, especially in the case of the UCEIS score.
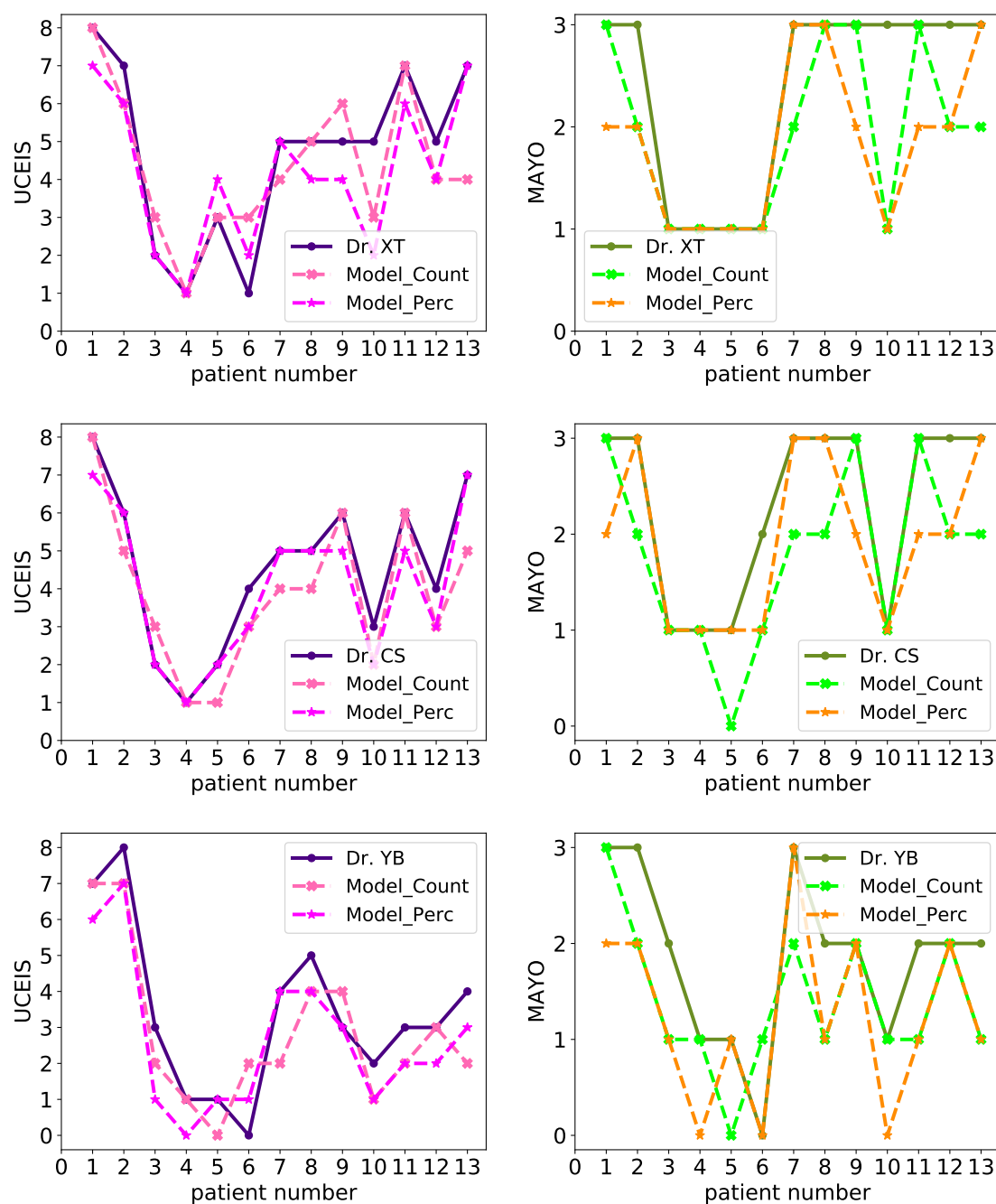
Figure 8.6: Estimated UCEIS at the left and estimated MAYO at the right for the gastroenterologist XT (first row), CS (second row) and YB (third row) in the case where $k = 4$.
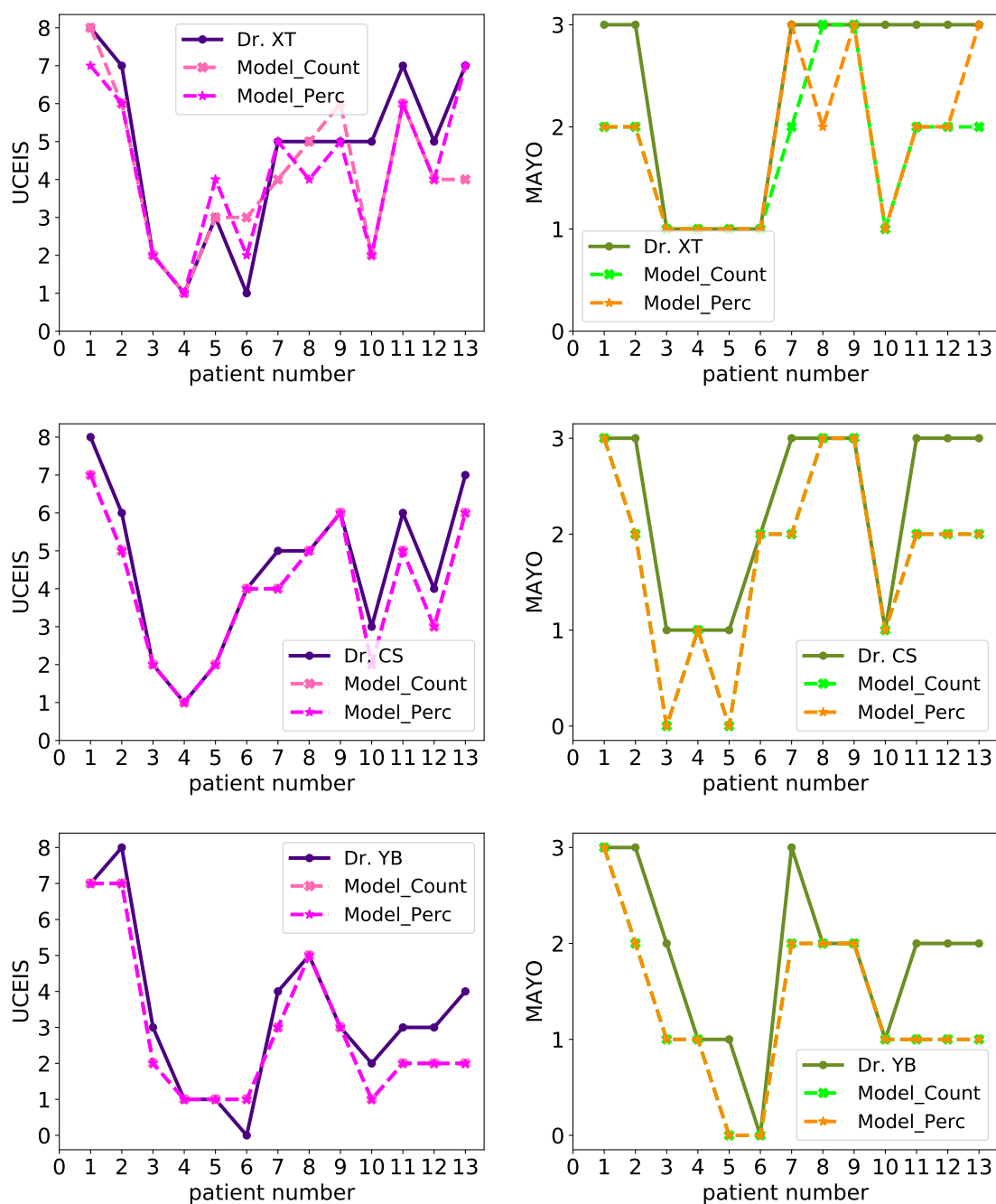
Figure 8.7: Estimated UCEIS at the left and estimated MAYO at the right for the gastroenterologist XT (first row), CS (second row) and YB (third row) in the case where $k = 5$.
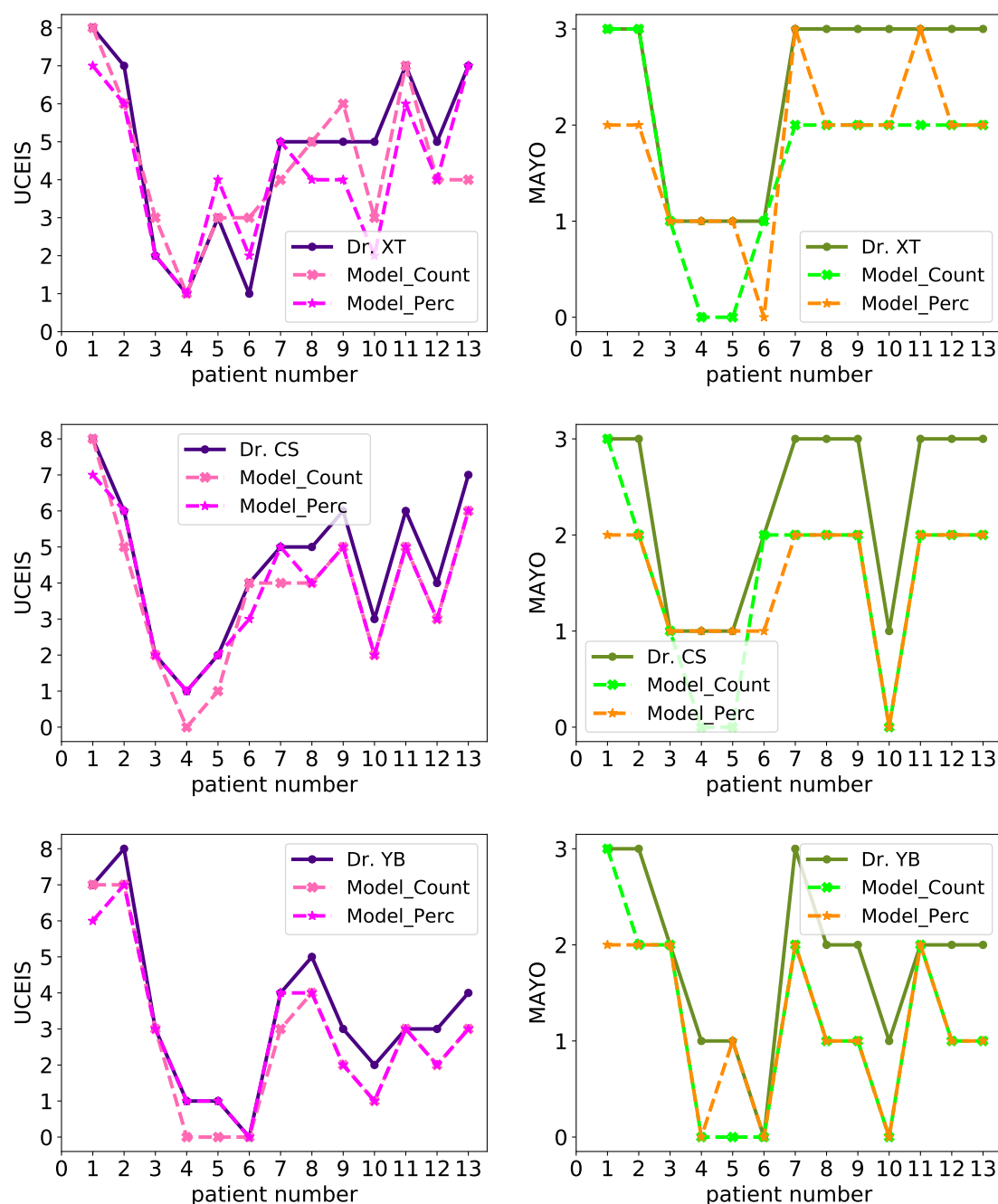
Figure 8.8: Estimated UCEIS at the left and estimated MAYO at the right for the gastroenterologist XT (first row), CS (second row) and YB (third row) in the case where $k = 6$.

Comparing the results for $k = 1$ in Figure 8.3 with the result in the case where $k = 6$ in Figure 8.8, the estimated score UCEIS overlaps with the real one for most of the patients. This phenomenon is less visible to the MAYO sub-score, maybe to the limited values of the scores (0 to 3) compared to the UCEIS, which makes the difference between the gastroenterologist score and the estimated

score more striking.

In the next section, we will seek the optimal colon decomposition for each gastroenterologist and then for all the gastroenterologists.

8.3.2 Best colon decomposition to estimate disease severity

From the previous section, we have noticed that when the number of considered colon segments increases, the error between the estimated score and the standard score is decreasing. To visualize the errors of all the decompositions, we used the bar representation for the two types of data (count and surface).

8.3.2.1 For one gastroenterologist

In this section, we compute the L_2 errors between the severity scores provided by the gastroenterologists and the estimated scores based on the count (or area) of the annotations.

In Figure 8.9, we show the L_2-errors for UCEIS using the count of lesions.. The best colon decomposition corresponds for $k = 6$ for Drs. XT and YB and $k = 5$ for Dr. CS. The optimal number of segments is not the same for all the doctors.
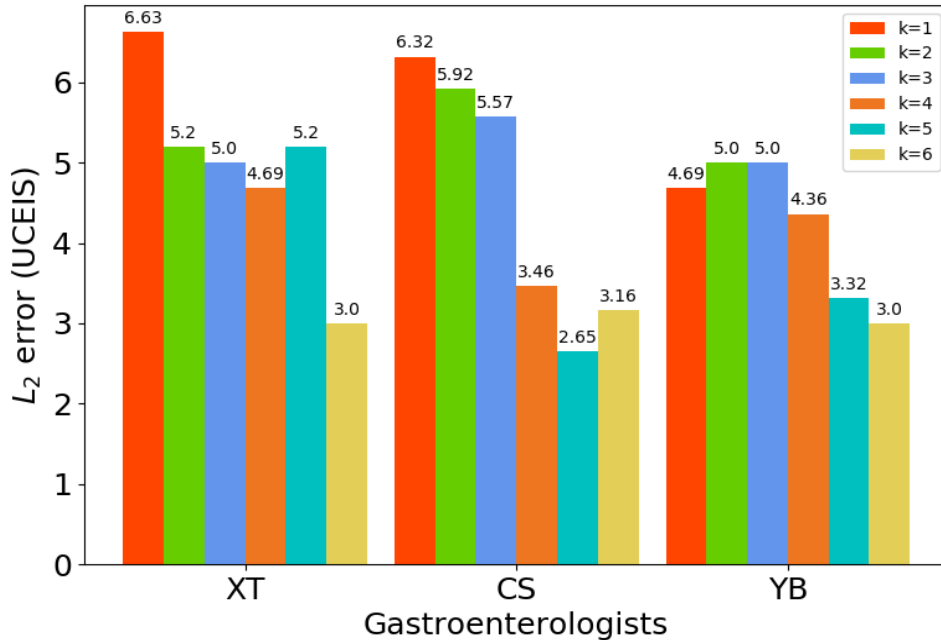
Figure 8.9: L_2 errors between the standard UCEIS score and the estimated score using the count of lesions.

By denoting the model $S(B, U) = a_i C_i^b + b_i C_i^u$, for $1 \leq i \leq k$ the index of the considered colon segment, we can extract the best models of the UC severity for the three gastroenterologists based on UCEIS score:

```
For Dr. XT, the best model with the amount of lesions is for k=6:
a_i= [-0.016, 0.0048, 0.0244, -0.0437, 0.0499, -0.0012]
b_i= [0.0878, -0.0345, -0.0073, -0.0132, 0.0444, -0.1103]
intercept= 2.3411
```

```
For Dr. CS, the best model with the amount of lesions is for k=5:
a_i= [-0.0036, -0.0001, 0.0114, -0.0188, 0.0016]
b_i= [0.0331, -0.0196, 0.0007, 0.0007, -0.003]
intercept= 2.6791
```

```
For Dr. YB, the best model with the amount of lesions is for k=6:
a_i= [-0.0116, 0.0011, 0.0156, 0.0196, 0.0165, -0.0016]
b_i= [0.0496, -0.0066, -0.0073, -0.0172, 0.0609, -0.1146]
intercept= 1.629
```

In Figure 8.10 we show the L_2-errors for Mayo subscore using the count of lesions. The best estimation of the MAYO subscore corresponds to the decomposition $k = 4$ for Dr. XT, for $k = 4$ and $k = 5$ for Dr. CS, whereas the values $k = 2, 3, 5$ segments lead to the optimal model for Dr. YB.
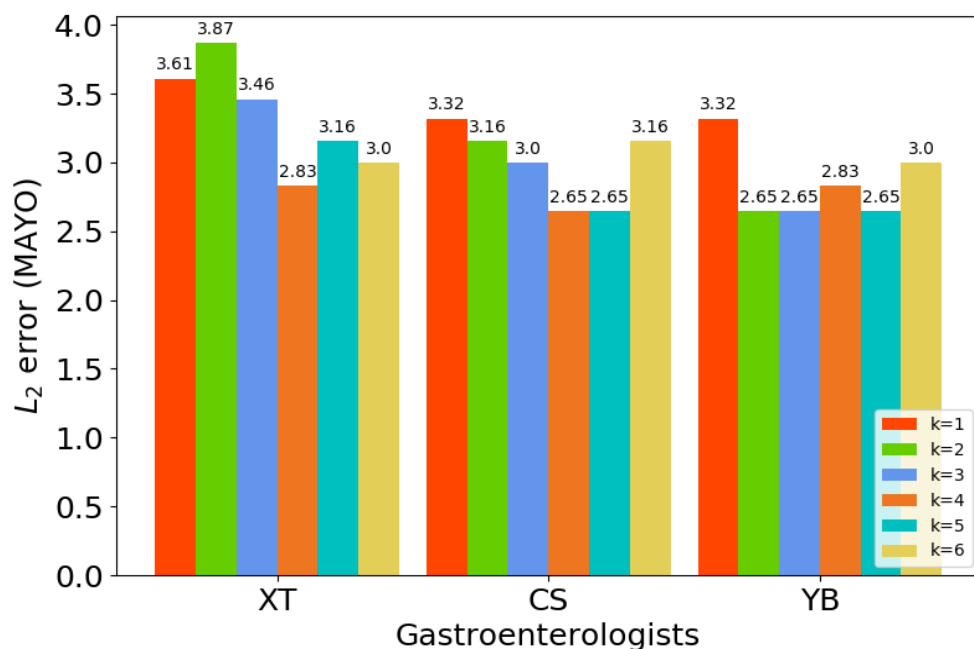
Figure 8.10: L_2 errors between the standard MAYO subscore and the estimated score using the count of lesions.

The parameters of the best models by calibration with the MAYO sub-score are:

```
For Dr. XT, the best model with the amount of lesions is for k=4:
a_i= [-0.0002, -0.0006, 0.0015, -0.0008]
b_i= [-0.0009, 0.0007, 0.0007, 0.0005]
intercept= 1.9309
```
```
For Dr. CS, the best model with the amount of lesions is for k=4:
a_i= [-0.0003, -0.0005, 0.002, -0.0012]
b_i= [0.0021, -0.0014, 0.0008, 0.0004]
intercept= 1.7635
```
```
For Dr. YB, the best model with the amount of lesions is for k=2:
a_i= [1e-06, 0.000201]
b_i= [1.6e-05, 0.000865]
intercept= 1.189278
```

The same work is done for the estimated scores based on the surface of lesions on each segment of the colon. In Figure 8.11 we show the results for the UCEIS score and in Figure 8.12 we show the results for the Mayo subscore. From Figure 8.11, we can notice that the estimation of the UCEIS taking into consideration the surface of the lesions is better in the case where $k = 6$ for Drs. XT and YB. The best parameter is $k = 4$ for Dr. CS. In parallel, the error of the estimation of the MAYO score is minimal for $k = 6$ in the case of Dr XT and $k = 4$ for Dr. CS scoring, while the minimum error is obtained for $k = 5$ for Dr. YB (cf Figure 8.12).
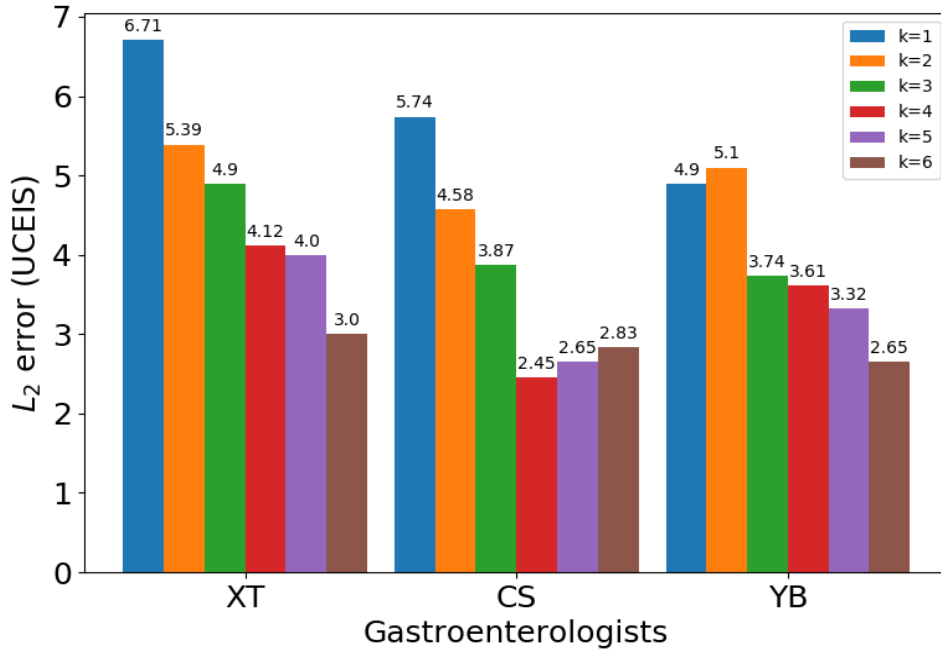
Figure 8.11: L_2 errors between the standard UCEIS score and the estimated score using the surface of lesions.
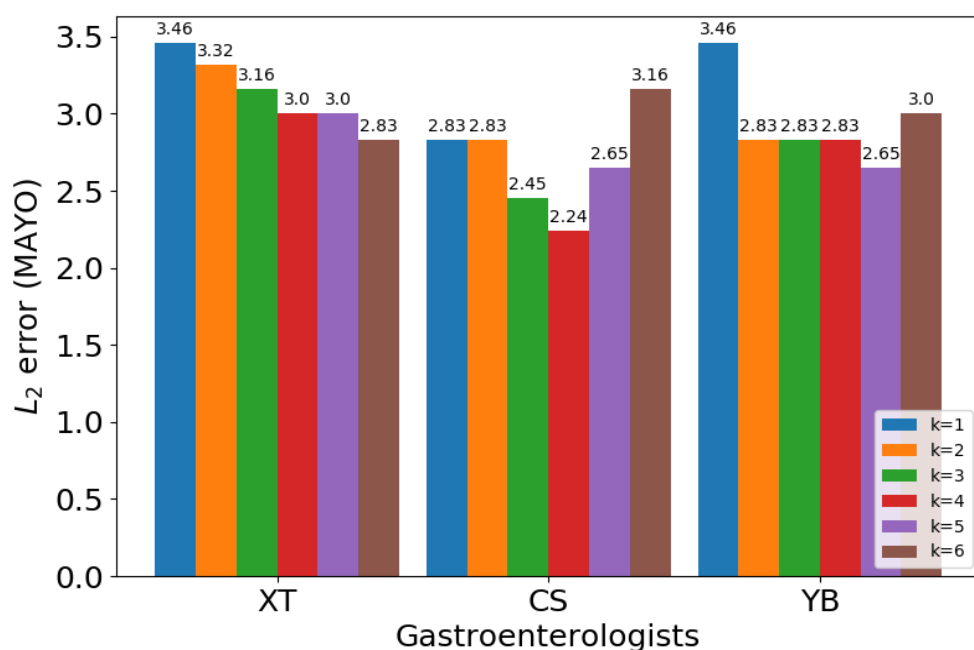
Figure 8.12: L_2 errors between the standard MAYO sub score and the estimated score using the surface of lesions.

We designed the score model by $S(B, U) = c_i P_i^b + d_i P_i^u$, and we find the best models for UCEIS are:

```
For Dr. XT, the best model with the surface of lesions is for k=6:
c_i= [12.8202, -23.0941, -22.3747, -110.295, 151.1595, -0.2719]
d_i= [-77.7351, 34.4317, 73.6002, -127.6214, 100.8813, -10.5435]
intercept= -0.6865
```

```
For Dr. CS, the best model with the surface of lesions is for k=4:
c_i= [11.4487, -16.396, 13.3557, -3.8324]
d_i= [0.2204, -17.1345, 30.0981, -10.4851]
intercept= 3.0995
```

```
For Dr. YB, the best model with the surface of lesions is for k=6:
c_i= [11.6301, -25.8716, -153.3957, 70.3061, 103.667, -0.3672]
d_i= [3.1796, 11.5913, -6.7382, 67.5971, -336.2431, 278.0887]
intercept= -1.737
```

The optimal models for the calibration with the MAYO sub-score are:

```
For Dr. CS, the best model with the surface of lesions is for k=6:
c_i= [4.4749, -12.465, 14.3398, -78.957, 80.1198, -4.8484]
d_i= [-26.6621, 8.062, 31.9028, -67.4165, 58.9363, -7.8604]
intercept= 0.4239
```

```
For Dr. CS, the best model with the surface of lesions is for k=4:
c_i= [3.8453, -6.6425, 3.6344, 1.328]
```

```
d_i= [-4.1214, -3.9306, 9.4453, -0.586]
intercept= 1.1703
```

```
For Dr. YB, the best model with the surface of lesions is for k=5:
c_i= [2.422, 0.5116, -46.7343, 38.9877, 6.4196]
d_i= [-37.4402, 22.0243, 14.6967, -0.895, -2.4345]
intercept= 0.1942
```

To summarise this part, we conclude that for Drs. XT and YB, the UCEIS computed based on the colon decomposition $k = 6$ is the best, independently of the data type (count/surface). Dr. CS shows minimum errors when considering the decomposition of the colon into $k = 5$ segments. For the MAYO sub-score, the optimal values are for $k \geq 4$, except for Dr. YB who shows the same behaviour for $k = 2, 3, 4$ when considering the count of lesions on each segment (cf Figure 8.10).

8.3.2.2   For all the gastroenterologists

In this section, we proceed to the search for the best colon decomposition for all the gastroenterologists. We used the L_2 errors computed in the previous section for all the tested values of k. We denote by S the gastroenterologist score and by $\bar{S}$ the optimal estimated score. The gastroenterologist G is an element in {XT, CS, YB}. The optimal colon decomposition is for $\hat{k}$ that we compute using the following optimization formula:

$$\hat{k} = \underset{k}{\operatorname{argmin}} \sum_{G,k} ||\bar{S}(G,k) - S(G,k)||_2^2. \tag{8.1}$$

It will be applied for UCEIS and Mayo subscore separately. The best decompositions are:

```
UCEIS-Count: the min error 28.0 is obtained for k= 6
UCEIS-Perc: the min error 24.0 is obtained for k= 6
MAYO-Count: the min error 23.0 is obtained for k= 4
MAYO-Perc: the min error 22.0 is obtained for k= 4
```

We conclude that the best colon decomposition is for $k = 6$ segments in the case of the UCEIS score and $k = 4$ segments in the case of the MAYO subscore regardless of the type of the data (count or surface).

8.4   Conclusion

In this chapter, we propose a UC severity modelling process that takes into account the space localization of the lesions in the colon. The severity of the disease is represented by the endoscopic scores applied for clinical practice, mainly the Mayo subscore and UCEIS score (cf chapter 4).

We decide to use the linear functions $\in$ {Functions: patient $\implies$ $\mathbb{R}$} and the colon parametrization of chapter 7. Instead of considering the patient with the most severe lesions like Mayo and UCEIS, we rather consider the count (or surface) of the lesions on each colon segment. We have proposed different colon decompositions to extract the local number of lesions. We do the same work by using the area of the lesions on each segment. The final score takes all segments into account through the linear model as discussed in section 8.2.

We tested the method on 13 videos from the vatic database for which three gastroenterologists have associated the severity score UCEIS and the MAYO sub-score. According to L_2 distanceS, we find that considering the colon into four segments is optimal to estimate the MAYO subscore. Whereas considering the colon into six segments is optimal to compute the UCEIS score (cf section 8.3).

This work is the first trial to have a numerical severity score taking into account the spatial extent of the lesions found in a colonoscopy video. However, the model parameters are calculated from endoscopic scores which do not take into account the spatial distribution of lesions. To be validated, the proposed numerical score must include objective markers of UC such as calprotectin and undergo clinical validation on a new database. Moreover, we want to go further in the exploration of all the decompositions of the colon and in parallel the exploration of other types of mathematical models.

In the following chapter, we will use the lesions spatial extent to bring answers to a set of medical statements like the evolution of the severity with the count of the lesions, numerical evaluation of the scoring variability between gastroenterologists and study of the abundance of the lesions regarding the colon segments.

Chapter 9

Proofs of some medical statements

Abstract

In this chapter, we investigate three medical statements related to the spatial distribution of lesions in the colon and the measurement of severity. We introduce the notion of compatible models that perform less than the error threshold α compared to the best models.

The first statement studies the lesion distribution bias. In this sense, we use solutions of linear models and ordinary differential equations. The results obtained for the compatible models suggest that the UC lesions are always concentrated near the rectum. However, compared to ulcers, bleeding lesions are more abundant between the descending segment and the rectum.

The second statement concerns the severity evolution according to the number of lesions found in colonoscopy videos. We employ linear model and severity scores for three doctors. Also based on compatible models, we find that the disease severity increases with the lesions count for all the doctors.

The third statement explores the variability of severity measurement between three gastroenterologists. For this part, we use a linear model and we find large variation between the doctors during the evaluation of bleeding lesions. However, there is an agreement for the ulcers assessment.

This chapter uses the spatial distribution of lesions along the colon and compatible models to prove some medical hypotheses.

9.1 Lesions distribution bias

In chapter 7, the maps of lesions show several profiles of the distribution of the lesions into the colon segments. For all the patients, the lesions begin by the rectum and continue propagating to the other colon segments. However, their local area measurements are different.

In this section, we decide to go in-depth into the study of the bias of the distribution of lesions in the colon. We, therefore, decide to explore the bias of the distribution of the lesions by the following statements:

> **Statement A**
>
> 1. **The** lesions are more abundant near the rectum.
> 2. **The** lesions are more concentrated between the descending colon and the rectum in comparison with the other colon parts.

The colon is parametrized by the curvilinear abscissa, i.e. by the segment $[0, 1]$ and the patient is represented by the total area of bleeding or ulcers found in the colonoscopy video.

For Statement 1, as mathematical models, we decide to introduce linear functions and solutions to an ordinary differential equation. Consequently, we seek for slopes a of the models $\{y = as + b; (a, b) \in \mathbb{R}^2; s \in [0, 1]\}$ and models $\{y' = ay, a \in \mathbb{R}\}$. This latter consists of the exponential functions $\{y = Ce^{as}, \text{ where } (C, a) \in \mathbb{R}^2; s \in [0, 1]\}$.

If only the optimal slopes are considered, the representation of the patient is therefore limited to a single number. Instead, we decide to explore models that perform close to the best with an accepted error threshold, denoted by α. Thus, a set of values will be extracted for each patient, corresponding to the slopes of the compatible models or simply called compatible slopes.

We define the $\alpha-$compatible models, the models that perform with α error in comparison with the optimal models as follows:

Definition 1 ($\alpha-$Compatible models). *Let's denote by $\hat{m}$ the optimal model, by d the distance L_1, L_2, standard deviation or any other type of discrete distance type, by D the data and by α the error threshold. The $\alpha-$compatible model $\bar{m}$ according to $\hat{m}$ satisfies $d(D, \bar{m}) \leq (1 + \alpha)d(D, \hat{m})$.*

In our work, standard deviation, denoted by `std` in `python` library, is used as a distance to search for compatible models:

Code chunk 20: bias_repartition

```python
def compatible_linmodels(x,y,alpha,candidates):
    # Return array containing alpha-compatible slopes among candidate slopes
    best_slope, best_intercept, _,_,_ = stats.linregress(x,y)
    best_dist = np.std(y - best_slope * x - best_intercept)
    return np.sort(np.append([ s for s in candidates
        if np.std(y - s*x) < (1+alpha)*best_dist], best_slope))
```

Using linear or exponential models, for each patient we seek the linear or exponential regression respectively and the set of compatible models. In our work, to prove the statement 1, we are only interested in the slopes of the compatible models.

The following code is launched to search the slopes of the compatible linear models for all the UC patients in the Vatic database:

Code chunk 21: bias_repartition (part 2)

```python
def plot_linear(figname,datap,alpha):
    plt.figure(figsize=(6,4))
    _ = plt.plot([0,0],[0,36])
    _ = plt.xlabel('Slope')
    _ = plt.ylabel('Patient number')
    for i in range(0,37):
        p = datap[i]
        x = np.arange(0,len(p),1.0)
        ac = compatible_linmodels(x,p,alpha,np.arange(-0.0005,0.001,2e-5))
        _ = plt.plot(ac,ac*0+i,'.-')

    plt.savefig(figname)
    plt.close()

# alpha is 0.1
plot_linear('biais_linearb.pdf',Data_perc_b,0.1) # Bleeding
plot_linear('biais_linearu.pdf',Data_perc_u,0.1) # Ulcers
```

Interpret with `python2`

Figure 9.1 presents the slopes of the 0.1-compatible linear models for each patient. In the case of bleeding (top), we observe that a majority of patients have a distribution bias because the compatible models have a positive slope. However, this bias is not very marked, because the value of the slopes is low and several patients have an inverse or indeterminate behaviour. The situation is clearer in the case of ulcers (bottom) since all patients have positive slopes, with a greater deviation from zero slopes.
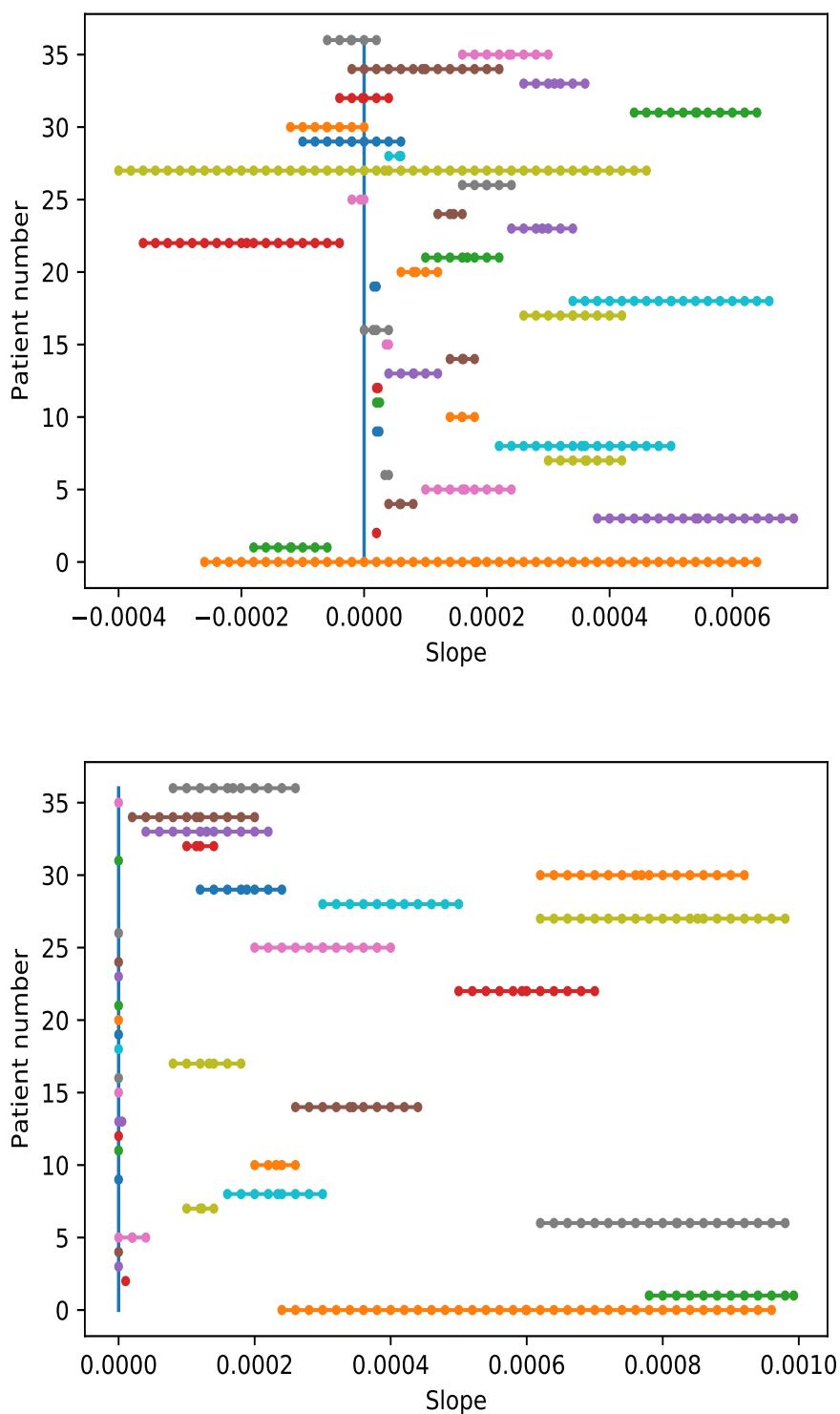
Figure 9.1: Slopes of compatible linear models with error threshold $\alpha = 0.1$. Bleeding (top) and Ulcers (bottom). There is a slight bias for the distribution of bleeding, but the bias is more significant for ulcers.

Using exponential models, we apply the following function to find the exponential regression and the set of compatible slopes:

Code chunk 22: bias_repartition (part 3)

```python
def plot_exp(figname,datap,alpha):
    plt.figure(figsize=(6,4))
    _ = plt.plot([0,0],[0,36])
    _ = plt.xlabel('a')
    _ = plt.ylabel('Patient number')
    for i in range(0,37):
        logp = np.log(datap[i]+0.0001)
        x = np.arange(0,len(logp),1.0)
        ac = compatible_linmodels(x,logp,alpha,np.arange(-0.008,0.025,4e-4))
        _ = plt.plot(ac,ac*0+i,'.-')

    plt.savefig(figname)
    plt.close()

# alpha is 0.1
plot_exp('biais_expb.pdf',Data_perc_b,0.1) # Bleeding
plot_exp('biais_expu.pdf',Data_perc_u,0.1) # Ulcers
```

Interpret with `python2`

Figure 9.2 presents the slopes of the 0.1-compatible exponential models for each patient. In the case of bleeding (top), like the linear models, we observe that almost all patients have a distribution bias because the compatible models have positive slopes. However, this bias is not very marked in comparison with the case of ulcers. For a certain number of patients, the slope is zero in the case of ulcers, which means that there is no distribution bias.

In conclusion, for most patients and for the linear and exponential regression models, statement 1 is verified because the slopes of the compatible models are positive. This means that UC lesions are abundant near the rectum.
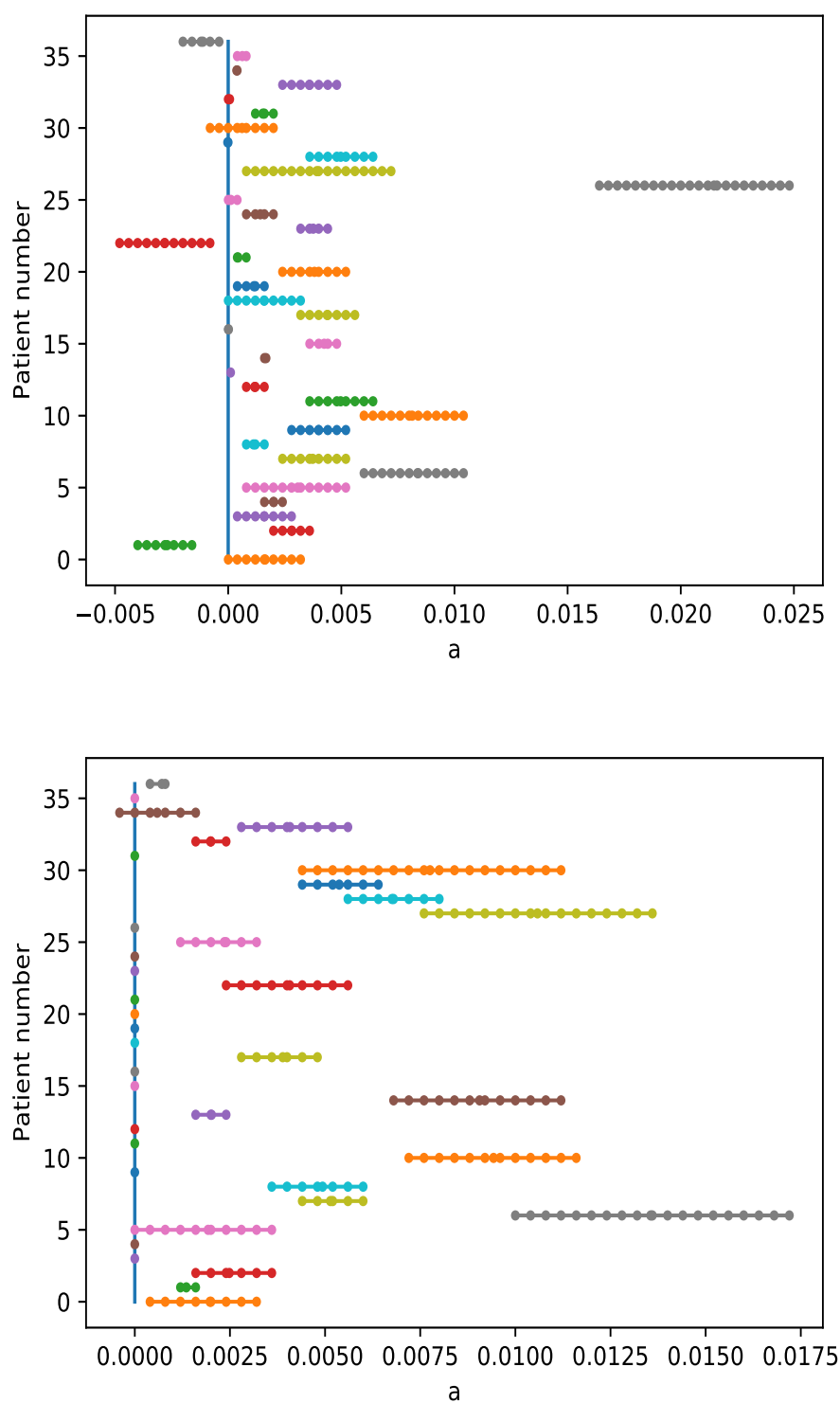
Figure 9.2: Slopes of exponential compatible models with error threshold $\alpha = 0.1$. Bleeding (top) and Ulcers (bottom). A slight bias is observed for the distribution of bleeding. In the case of ulcers, some patients have a more marked bias, while others appear unbiased.

Let's move on to the proof of the statement 2. Since the colon is parameterized by the segment $[0, 1]$, we decide to consider it in two main parts. The first part involves the cecum to the end of the transverse colon while the second part involves the descending colon to the end of the rectum. Statement 2 is verified if the lesions surface measurement at the second part is bigger than the lesions surface measurement at the first part. Consequently, an appropriate definition of statement 2 can be given as follows:

Definition 2. *Let D be the function defining the surface measurement of the lesions in the colon. If D satisfies:*

$$\int_0^{0.5} D(s)ds < \int_{0.5}^1 D(s)ds \tag{9.1}$$

where s is the curvilinear abscissa $\in [0, 1]$, then the lesions are more abundant from the descending colon to the rectum.

In the following code chunk, we perform the computation of Equation (9.1) for 37 patients of the Vatic database:

Code chunk 23: bias_repartition (part 4)

```python
bias_b, bias_u = np.full(37,True), np.full(37,True)
for i in range(0,36):
    p = Data_perc_b[i]
    L,L2 = len(p), (int) (len(p)/2)
    bias_b[i] = sum(p[0:L2])/L < sum(p[(L2+1):L])/L
    p = Data_perc_u[i]
    bias_u[i] = sum(p[0:L2])/L < sum(p[(L2+1):L])/L

print sum(bias_b), "patients out of ", len(bias_b),"verify Statement A.2 " \
"(left < right) for bleeding."

print sum(bias_u), "patients out of ", len(bias_b),"verify Statement A.2 " \
"(left < right) for ulcers."
```

Interpret with `python2`

```
28 patients out of  37 verify Statement A.2 (left < right) for bleeding.
21 patients out of  37 verify Statement A.2 (left < right) for ulcers.
```

We conclude that according to our database, 76% of patients satisfy Statement 2 for bleeding lesions while only 57% of patients satisfy it for ulcers. In summary, UC lesions are more abundant between the descending colon and the rectum in comparison with the other colon segments. Moreover, bleeding lesions are more plentiful compared to ulcers.

9.2 Evolution of the severity with the lesions

In this section, we study the relation of the disease severity with the total number of lesions through the following statement:

> **Statement B**
>
> The UC severity increases with the number of lesions in the colonoscopy video.

For this part of the work, we will use the total number of annotations instead of their surface measurements and the severity scores of 13 patients provided by our collaborators (cf chapter 5).

To model the severity scores, we decide to use linear functions i.e. $\{f(l) = al + b, (a, b) \in \mathbb{R}^2\}$, ($l = B$ for bleeding and $l = U$ for ulcers). Consequently, Statement B is verified by the patient if the corresponding model has a positive slope. As done previously, we will also explore the compatible models with error threshold α here chosen to be 0.05. The lesions are considered separately, meaning we will perform the models' search, twice, one for bleeding and one for ulcers.

We denote by `N_bleed` the number of bleeding annotations in the colonoscopy video whereas the `N_ulcer` represents the number of ulcer annotations. We study the 0.05-compatible models for bleeding by the following code chunk:

Code chunk 24: bias_repartition (part 9)

```python
x = np.array(N_bleed).transpose()
fig,ax = plt.subplots(figsize=(6,4))
for (i,uc,l) in zip(range(3),[UCEIS_XT,UCEIS_CS,UCEIS_YB],['XT','CS','YB']):
    s = compatible_linmodels(x,uc,0.05,np.arange(-0.02,0.02,3e-5))
    _ = ax.plot(s,s*0+5-i,'.-',label='UCEIS_'+l)

for (i,mayo,l) in zip(range(3),[MAYO_XT,MAYO_CS,MAYO_YB],['XT','CS','YB']):
    s = compatible_linmodels(x,mayo,0.05,np.arange(-0.02,0.02,3e-5))
    _ = ax.plot(s,s*0+2-i,'.-',label='MAYO_'+l)

_ = ax.plot([0,0],[0,5])
_ = ax.legend(loc=4); _ = ax.set_xlabel('Slope')
fig.savefig('severite-bleed-compatible.pdf')
plt.close()
```

Interpret with `python2`

In Figure 9.3 we show the compatible slopes for bleeding using the UCEIS score and Mayo subscore. One can see that the compatible slopes are almost positive, except in the case of the severity grading given by the gastroenterologist YB. We conclude that the compatible models for bleeding are increasing and consequently the severity scores are increasing with the number of bleeding lesions.
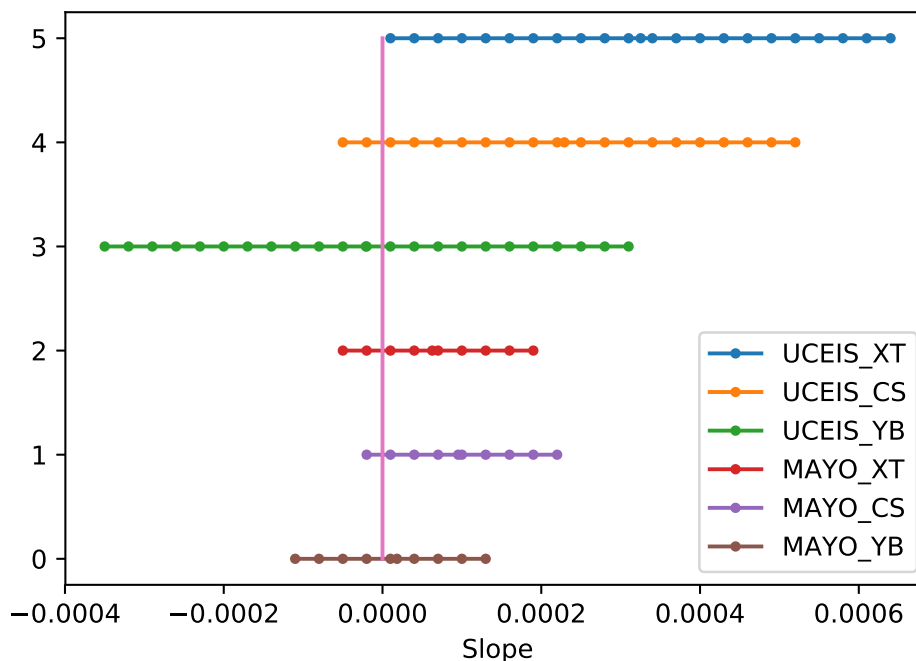
Figure 9.3: Slopes 5% compatible for the UCEIS and MAYO scores assigned by the three gastroenterologists for bleeding. Compatible models almost tend to have a positive slope, except in the case of the doctor YB.

For ulcers, we use the following code chunk to compute the compatible slopes:

Code chunk 25: bias_repartition (part 10)

```
x = np.array(N_ulcer).transpose()
fig,ax = plt.subplots(figsize=(6,4))
for (i,uc,l) in zip(range(3),[UCEIS_XT,UCEIS_CS,UCEIS_YB],['XT','CS','YB']):
    s = compatible_linmodels(x,uc,0.05,np.arange(-0.025,0.025,3e-5))
    _ = ax.plot(s,s*0+5-i,'.-',label='UCEIS_'+l)

for (i,mayo,l) in zip(range(3),[MAYO_XT,MAYO_CS,MAYO_YB],['XT','CS','YB']):
    s = compatible_linmodels(x,mayo,0.05,np.arange(-0.02,0.025,3e-5))
    _ = ax.plot(s,s*0+2-i,'.-',label='MAYO_'+l)

_ = ax.plot([0,0],[0,5])
_ = ax.legend(loc=4); _ = ax.set_xlabel('Slope')
fig.savefig('severite-ulcer-compatible.pdf')
```

Interpret with `python2`

Figure 9.4 presents the compatible slopes for ulcer lesions. We find that all the compatible models have positive slopes and thus the UC severity is increasing with the number of lesions.
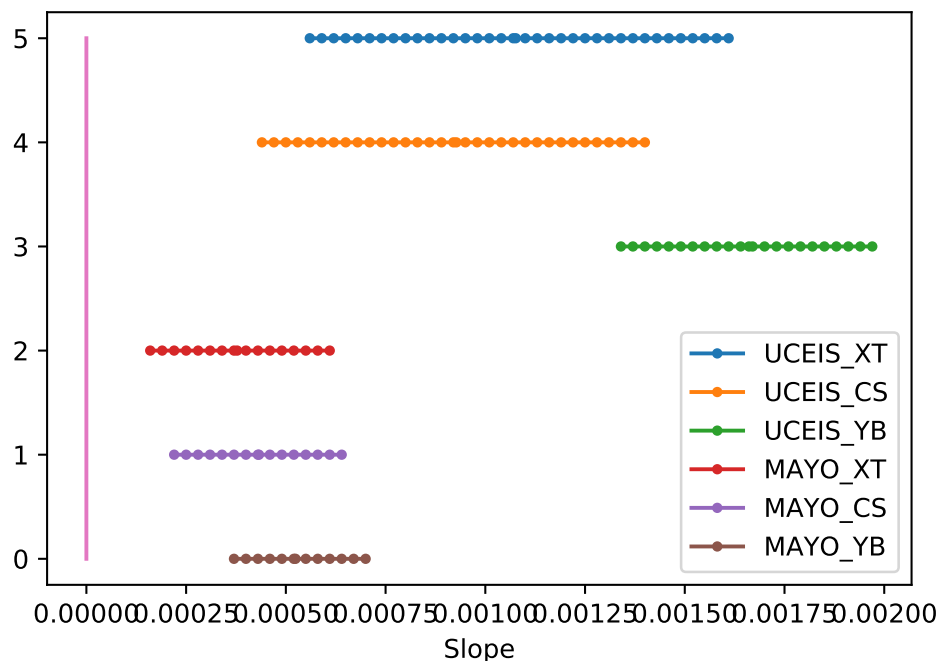
Figure 9.4: Slopes 5% compatible for the UCEIS and MAYO scores assigned by the three gastroenterologists for ulcers. All the compatible models have a positive slope.

9.3 Severity scoring variability between gastroenterologists

This section is dedicated to measuring the variability of lesions severity scoring among doctors using the UCEIS score and the MAYO subscore. More precisely, we study the following statement:

> **Statement C**
>
> The lesions severity assessment is variable between the doctors.

For this section, we decide to work also with linear functions. We use separately the surface and the count of lesions. However, we consider both the bleeding and ulcers to estimate the models' parameters. The severity score is then modeled in terms of bleeding (B) and ulcers (U) by a linear function f where $f(B, U) = aB + bU + c$, $(a, b, c) \in \mathbb{R}^3$. We thus obtain a total of six models, one linear model for each score and each gastroenterologist.

In the following code chunk we apply the function `LinearRegression` from the python library to compute the models' parameters:

Code chunk 26: bias_repartition (part 11)

```python
# UCEIS
Nb_annot = np.array([N_bleed, N_ulcer]).transpose()
models_uceis = [LinearRegression().fit(Nb_annot,g)
                for g in [UCEIS_XT, UCEIS_CS, UCEIS_YB]]
for (m,g) in zip(models_uceis,['XT','CS','YB']):
    print 'f(B,U)_',g, '=', round(m.coef_[0],6), 'B + ', \
                         round(m.coef_[1],6), 'U + ', round(m.intercept_,3)
```

Interpret with `python2`

```
f(B,U)_ XT = 0.000416 B +  0.001185 U +  3.092
f(B,U)_ CS = 0.000306 B +  0.001007 U +  3.252
f(B,U)_ YB = 0.000108 B +  0.001689 U +  1.859
```

Code chunk 27: bias_repartition (part 12)

```python
# MAYO sub-score
models_mayo = [LinearRegression().fit(Nb_annot,g)
               for g in [MAYO_XT, MAYO_CS, MAYO_YB]]
for (m,g) in zip(models_mayo,['XT','CS','YB']):
    print 'f(B,U)_',g, '=', round(m.coef_[0],6), 'B + ', \
                         round(m.coef_[1],6), 'U + ', round(m.intercept_,3)
```

Interpret with `python2`

```
f(B,U)_ XT = 9.3e-05 B +  0.000402 U +  1.916
f(B,U)_ CS = 0.000131 B +  0.000467 U +  1.728
f(B,U)_ YB = 6e-05 B +  0.00054 U +  1.32
```

Even though the coefficients for the number of ulcers are roughly the same for all the models and gastroenterologists, the obtained models present significant differences between the coefficients for bleeding for all the experts. This shows a large variation between the experts for bleeding scoring.

We also study the evolution of the severity scores with the respect to the surface of the lesions:

Code chunk 28: bias_repartition (part 17)

```python
Pr_annot = np.array([P_bleed, P_ulcer]).transpose()
models_uceis_p = [LinearRegression().fit(Pr_annot,g)
                  for g in [UCEIS_XT, UCEIS_CS, UCEIS_YB]]
for (m,g) in zip(models_uceis_p,['XT','CS','YB']):
    print 'f(B,U)_',g, '=', round(m.coef_[0],6), 'B + ', \
                         round(m.coef_[1],6), 'U + ', round(m.intercept_,3)
```

Interpret with `python2`

```
f(B,U)_ XT = 2.781648 B +  5.908825 U +  3.041
f(B,U)_ CS = 2.735894 B +  5.298106 U +  2.983
f(B,U)_ YB = 1.309063 B +  8.475124 U +  1.841
```

Code chunk 29: bias_repartition (part 18)

```
models_mayo_p = [LinearRegression().fit(Pr_annot,g)
                for g in [MAYO_XT, MAYO_CS, MAYO_YB]]
for (m,g) in zip(models_mayo_p,['XT','CS','YB']):
    print 'f(B,U)_',g, '=', round(m.coef_[0],6), 'B + ', \
                         round(m.coef_[1],6), 'U + ', round(m.intercept_,3)
```

Interpret with `python2`

```
f(B,U)_ XT = 0.569324 B +  1.67093 U +  1.985
f(B,U)_ CS = 0.924414 B +  2.147158 U +  1.734
f(B,U)_ YB = 0.301337 B +  2.534526 U +  1.412
```

We find that taking into consideration the total surface of annotated lesions in a given video, the variability of the severity measurement is remarkable in the bleeding and ulcer for all the doctors.

The linear models were useful to obtain a quantitative measurement of the variability of the grading systems among doctors. For this section, we did not employ the compatible models, only optimal models were considered.

9.4 Conclusion

This chapter attempts to prove a set of medical hypotheses or statements related to the spatial distribution of lesions found in a colonoscopy video. To do this, we studied linear models and ordinary differential equation solutions and we introduce the notion of compatible models, i.e. models that perform less than an α error threshold in comparison with the best model.

We are interested in three statements that can be listed as follows:

1. **The bias of lesion distribution in the colon** (cf section 9.1). We study models of type linear and ordinary differential equation solutions. The slopes of the compatible models are always positive, we show that the bleeding and ulcers lesions are concentrated near the rectum. On the other hand, we find that compared to ulcers, the bleeding lesions are more abundant between the descending colon and the rectum.

2. **Growth of the endoscopic severity scores according to the lesions** (cf section 9.2). We study the relation of the severity with the number of lesions using linear model. By using the UCEIS score and Mayo subscore for three gastroenterologists, we find that all compatible models' slopes are positive for bleeding and ulcers. Consequently, the endoscopic scores increase with the number of lesions found in colonoscopy videos.

3. **The variability of the severity assessment between experts** (cf sec-
   tion 9.3). According to the linear model computed for each gastroenterol-
   ogist, we find large variations between gastroenterologists while assessing
   the bleeding severity. Whereas the doctors assess almost similarly the
   severity of the ulcers.

In chapter 8, the spatial distribution of lesions along the colon segments was
employed to estimate the disease severity. In this chapter, we use it to prove
some medical hypotheses. The introduction of the compatible models' concept
was helpful to confirm some medical conclusions. According to our knowledge,
despite its medical relevance, no study has introduced the spatial distribution
of lesions. The evaluation of the severity was associated with measuring the
most severe lesions without taking into consideration the spatial extent of the
inflammation. The distribution of lesions appears to be informative for the
severity evaluation and medical hypothesis justification. A database containing
more patients with variable lesions profiles may lead to more appropriate
conclusions about the studied statements.

In the next chapter, we will propose a mathematical model of the spatial extent
of lesions along the colon. The model will be useful to study the long-time
behaviour of the disease.

Chapter 10

Reaction diffusion equations and ulcerative colitis disease

Abstract

In this chapter, we are interested in modelling the spatial distribution of ulcerative colitis lesions using the reaction-diffusion equation Fisher Kolmogorov-Petrovski-Puskinov (Fisher-KPP).

The patient is represented by the surface measure of lesions in colonoscopy frames and the colon is considered by its curvilinear abscissa like in chapter 7. For the modelling process, the patient is parametrized by two parameters: the diffusion parameter (D) and the initial condition (u_0). For the inverse modelling process, the patient is considered in an asymptotic regime and therefore, it can be considered as a travelling wave for the Fisher-KPP equation. Since the Fisher-KPP travelling wave profile is unique up to dilation that depends on the diffusion parameter, we can then compute the travelling wave profile that fits the lesions profile. Consequently, based on the colonoscopy video, we estimate the diffusion parameter of the lesions into the colon. We are then able to compute the displacement velocity as well as the lesions' invasion time to affect the entire colon.

We compute the lesions velocities and invasion times for patients having equal severity scores UCEIS. Nevertheless, the lesions move with similar velocities into the colon, they will affect the healthy parts of the colon at different times. For patients grouped into the same disease type, the bleeding lesions affect the normal colon parts faster than ulcers.

This chapter encounters the first attempt at modelling the spatial distribution of bleeding and ulcer lesions according to the colon. We show different long-term behaviour of the lesions for patients ranked similarly according to severity score.

10.1 Introduction

Inflammatory bowel diseases are known to be autoimmune disorders of the digestive tract affecting the mucosa of the gut by inflammation. Their development involves a genetic susceptibility, deregulated immune system's response and an environmental trigger. In general, bowel mucosal homeostasis includes interactions among the microbiota, the intestinal epithelium, and the gut-associated immune system. When a failure in these interactions occurs, an inflammation may precipitate.

Mathematics may help in exploring the consequence of manipulating many parameters involved in the biological phenomenon associated with particular desired scenarios. Indeed, many studies are exploring mathematical models to understand the immunopathogenesis and diseases arising from an inadequate immune system response as well.

We distinguish two levels: microscopic models that study cellular interactions and macroscopic models that consider a more general framework, namely integrating spatial distribution of studied variable cells quantities, population densities or many other examples.

10.1.1 Microscopic models

In [RBC10], the authors describe a skin disease using mathematical modelling relating the densities of some immune cells such as dendritic and T helper cells to Keratinocytes. In [ML04], the authors analyzed a mathematical model of three non-linear ordinary differential equations for chronic myelogenous leukaemia (CML), cancer affecting the blood cells. In [HJ18], the authors investigate the interaction between tumour cells, CD4$^+$ T cells, cytokines, and normal tissue cells for tumour regression.

In the case of IBDs, multiple genes play a crucial role in the immune system response such as the ones that regulate innate immunity, adaptive immunity, and epithelial barrier function. The Crohn's and ulcerative colitis diseases were identified as Th1 and Th2 mediated processes respectively [BKL11; Mat+04]. The primary function of Th1 cells is to protect the body from intracellular pathogens while the Th2 cells confer protection against extracellular pathogens.

We can also cite the work of Yates et al. [YCS04], where a mathematical model of ordinary differential equations is presented to understand the differentiation of naïve T cells following the antigen stimulation into Th1 and Th2 cells.

In 2010 [Wen+10], Wendelsdorf et al. proposed a mathematical model based on a system of 29 ordinary differential equations to understand the complex

interactions between cells and genes with bacteria in the colonic lumen involved in the IBDs's physiopathology. They found a positive inflammatory feedback loop by inflammatory M1 macrophage activation of T-cells under the immunopathology of IBD. However, due to the complexity of the proposed system, qualitative properties of cell interactions are not easy to be extracted or understood.

Later in 2013, Lo and Friedman [LAF13] extend the work of Yates et al., to a differential equations system including regulatory T cells (Treg cells), and additional cytokines that are involved in IBDs. Their objective was to study the relationships between Th1, Th2, and Treg cells in the initial phase of the inflammatory process. They show that if the inhibitions of the Treg cells are downregulated, then the Th1 or Th2 response to cytokines induced by macrophages and dendritic cells in response to commensal flora is abnormally high leading to inflammation. Otherwise, when the inhibitions rate of the Treg cells is upregulated, then the cell responses Th1 and Th2 type are abnormally low. The latter case is similar to a bacterial infection. In [Lo+16], the authors expand their previous model to include the Th17 cells pathway which plays an important role in inhibiting Treg cell differentiation that is associated with autoimmune disorders and inflammation.

In the work of Maiti et al., [Mai+15], a system of ordinary differential equations was employed to model the interaction between pro-and anti-inflammatory signalling. The model predictions present a good agreement with experimental data.

In the presented works, a diversity of parameters was considered depending on the desired biological phenomena and the addressed issues such as pro-inflammatory cytokines, anti-inflammatory mediators or density of targeted cells. Most of the obtained results in the referenced papers and the references therein are based on stability analyses of the studied system to find possible equilibrium steady states and supported by numerical simulations for some estimated parameters.

The shared property between mathematical models to IBDs is to study the microscopic level, i.e. cell levels interactions to understand the physiopathology of these diseases.

10.1.2   Macroscopic models

In this chapter, we present a different approach to deal with the spatial distribution of endoscopic lesions observed in colonoscopy videos. To the best of our knowledge, no mathematical models have been proposed to study the spatial extent of the lesions in the case of IBDs, more particularly in the case of UC disease. Due to its ability to model the spatial diffusion of a given substance in

habitat, we choose to use the reaction-diffusion equation to model the spatial distribution of UC lesions in the colon.

The mathematical models of reaction-diffusion type are widely used to describe the spatio-temporal spreading phenomenon generated by a substance or population which can be a virus, a special type of cells, inflammation, dominant genotype that spatially diffuses. The diffusion may occur through random walks, Brownian motion, hydrodynamic turbulence, or other mechanisms. The cells react to each other and their surroundings and then affect their local densities and dispersion [Kri08].

Reaction-diffusion equations are utilized in many areas of real-world application like dynamical populations, chemistry [Tur90], genetic [BT11] and combustion theory [Bar+85]. They are for instance employed to model biological invasions [AM17] or cardio-vascular diseases such as atherosclerosis [VP09]. Moreover, the reaction-diffusion equations are adapted to ecological phenomena such as the formation of a spatial pattern. In this sense, we recall the paper of Alain Turing [Tur90] who showed that any repeating phenomenon pattern in nature could be a result of the interaction between two species such as cells or molecules through specific conditions. He proposed the reaction-diffusion equations and demonstrated that the two species spread at different velocities to produce patterns. The faster one is called the inhibitor while the slower one is called an activator. Such kind of natural patterns can be seen in zebra stripes and wood spirals (cf Figure 10.1).

Figure 10.1: Examples of repeated phenomena in nature: zebra patterns (left) and woods spirals (right).

Furthermore, a special class of solutions for this type of equation, namely the travelling wavefront solutions are useful to model biological invasions [AM17] or cardio-vascular diseases such as atherosclerosis [VP09]. In this direction, many epidemiological models have been proposed to study the spreading of epidemics like the bubonic plague (or also the Black Death) in Europe. It began at the Caspian sea area in wars around 1346, then went through the mean Mediterranean routes (see map in Figure 10.2). At the end of 1347, the epidemic reached two main European ports: Marseille in France and Genoa in Italy. After

spreading widely in Europe, the epidemic comes back to its starting location, i.e. Caspian reservoir [Gau+10]. Noble [Nob74] have used reaction-diffusion equation to model the spatial spread of the epidemics. Many researchers introduce the population spatial effects for epidemiological modelling like [FK99; MY09; KLZ10].
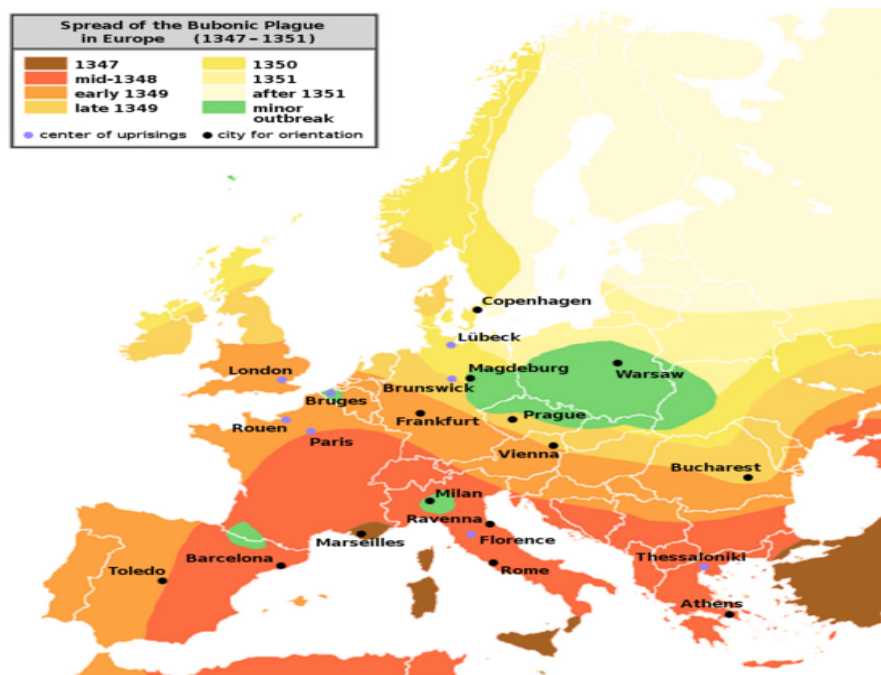
Figure 10.2: Propagation of the Bubonic plague, also known as the Black Death, in europe during the 14th century.

Concerning our work, ulcerative colitis is generally characterized by continuous inflammation affecting the innermost lining of the colon. It begins at the rectum and propagates proximally through the colon. In chapter 2, we have discussed the pathogenesis of the ulcerative colitis disease, and we have seen that the cells inflammation will continue affecting their neighbors cells. Thus the inflammation drived by UC can be seen as a spatial diffusion phenomenon. Moreover, the lesions spatial distribution can be modelled by a reaction-diffusion equation and more particularly seen as a travelling wave solution moving into the healthy parts the colon. This motivated us to choose the reaction-diffusion equation to model the spatial distribution of the bleeding and ulcers. For simplicity, we decide to use the Fisher-Kolmogorov-Petrovski-Puskinov equation from which we can extract some useful information about the disease's long-term behaviour.

The rest of the chapter is organised as follows: section 10.2 is dedicated to summarizing some theoretical properties of the reaction-diffusion equations and more particularly discussing a special type of solutions known as the travelling wave solutions. Next, in section 10.3, we present the modelling process as

well the inverse model used to estimate the model parameters. In section 10.4, we show the results for some patients from the Vatic database.

10.2 Reaction-diffusion equations

10.2.1 Some known properties

A typical form of a reaction–diffusion equation can be written as follows:

$$\partial_t u - D\Delta u = f(u,t,x), \quad t > 0,\ x \in \mathbb{R}^n, \tag{10.1}$$

with some initial condition $u_0 = u(0,x)$ in some functional space $L^\infty(\mathbb{R}^n)$, and suitable boundary conditions.

In the case of a one-dimensional space that concerns the work presented in this chapter, Equation (10.1) can be represented by a single reaction-diffusion equation of the form:

$$\partial_t u - D\Delta u = f(u,t,x), \quad t > 0,\ x \in \Omega \subset \mathbb{R}. \tag{10.2}$$

The system parameter $u(t,x)$ is a function of two real variables, the time $t > 0$ and the spatial coordinate x. The term ∂_t represents the partial derivative with respect to time t, Δ is the spatial Laplacian, D and f are the diffusion and the reaction terms respectively.

Many cases can arise depending on the nature of the reaction term f and the model parameter u. When u and f do not depend on x, and the diffusion terms (i.e. spatial effects) are ignored, we get a simple system of ordinary differential equation:

$$\partial_t u = f(u,t).$$

When u and f are time-independent, we get a so-called system of weakly coupled elliptic partial differential equations (PDEs) that is active in a spatially heterogeneous media:

$$-D\Delta u = f(u,x).$$

Several types of reaction term f were employed in the literature for reaction-diffusion systems and which can be classified into (cf Figure 10.3):

- Monostable if $f(u) > 0$ for $0 < u < 1$.
- KPP type if f is monostable and $f(u) \leqslant f'(0)u$ for $0 < u < 1$.
- Ignition type if for some $0 < \theta < 1$, the term f satisfies:

$$\begin{cases} f(u) = 0, & for \quad 0 \leqslant u \leqslant \theta, \\ f(u) > 0, & for \quad u > \theta. \end{cases}$$

- Bistable, if sor some $0 < \theta < 1$

$$\begin{cases} f(u) < 0, & for \quad 0 \leqslant u \leqslant \theta, \\ f(u) > 0, & for \quad \theta < u < 1. \end{cases}$$
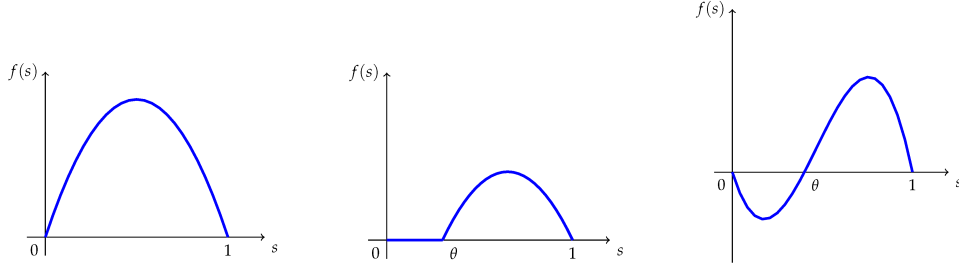
Figure 10.3: Monostable, bistable and ignition type non linearities.

For biological applications, u describes the density of a substance, population, viruses or another type of species. The diffusion term is crucial for describing the diffusion mobility of the population or the substance u at a position x and time t. Diffusion is used to represent the resulting movement from an object or body making many short movements in random directions or the same direction of movement [AM17]. For the reaction term, typical choices are $f(u) = au$ where a is the growth rate leading to an exponential growth, $f(u) = au(1 - \frac{u}{K})$, where K is the carrying capacity to model a logistic growth of the population. In addition, $f(u) = au(\frac{n}{u_0} - 1)(1 - \frac{n}{K})$, which is based on a logistic growth but if the population is too small, it will die out. Such a phenomenon may appear due to the necessity to find a mate for reproduction or to defend the group against predators. This leads to an additional term $(\frac{n}{u_0} - 1)$.

In the next section, we will present a non-linear reaction-diffusion equation known as the Fisher Kolmogorov-Petrovski-Puskinov equation.

10.2.2   Fisher Kolmogorov-Petrovski-Puskinov equation

In 1930, Fisher proposed to model the spatial diffusion of an advantageous gene such as a wave in a one-dimensional habitat [Kol37]. Kolmogorov, Petrovski, Puskinov were the first to study it mathematically. Equation (10.2) is called Fisher Kolmogorov-Petrovski-Puskinov equation, abbreviated Fisher-KPP or FKPP, if the non linearity term f is $f(u) = ru(1 - u^q)$, where r represents the growth rate of the population under study and $q > 0$.

In this work, we consider the parameters r and q are one and subsequently the one dimensional FKPP equation remains as follows:

$$\partial_t u - D\Delta u = u(1 - u), \quad t > 0,\ x \in \Omega \subset \mathbb{R}. \tag{10.3}$$

In the next section, we will explore the asymptotic behaviour of the reaction-diffusion equations, more particularly the travelling wave solutions.

10.2.3   Asymptotic behaviour

We will study the solutions of the reaction diffusion equations for a sufficiently long time with a particular attention to the case of Fisher-KPP.

10.2.3.1   Travelling Wave solutions (TW)

Travelling waves (TW) play an important role in describing the long-term behaviour of solutions to the reaction-diffusion equations. They are observed in many areas such as the result of some chemical reactions like combustion [VVV94], propagation of flames, migration of biological species, tumour growth, shock profiles in fluid dynamics[Smo12] and many other applications.

Mathematically, travelling waves are solutions moving in a particular direction with constant speed while maintaining their shape over their propagation axis. Travelling wave solutions for Equation (10.1) can be defined as follows:

Definition 3. *[Per15]   A travelling wave solution is a solution of the form $u(t,x) = w(x - vt)$ with $v \in \mathbb{R}$ is a constant called the wave speed or the travelling speed. We say it connects the states 1 and 0 if $w(-\infty) = 1, w(\infty) = 0$. The function w is the wave profile that will describe the evolution of the system between two steady states and v the wave velocity.*

There are many types of travelling waves with some of them can be given by the following definition:

Definition 4 (Types of TW)**.**
- *A travelling wave solution w is called **Wave front** if $w(-\infty) \neq w(+\infty)$.*
- *A travelling wave solution w is called **Pulse wave** if $w(-\infty) = w(+\infty)$ and $w(\xi)$ is not a constant function with $\xi \in \mathbb{R}$.*
- *A travelling wave solution w is called **Wave trains** if the wave profile is periodic.*

10.2.3.2   Travelling wave solutions for Fisher-KPP equation

In general, Fisher-KPP equation exhibits only two non negative equilibrium [Per15]: $u = 0$, unconditionnally unstable (i.e. for any small initial perturbation close to zero, the solution will grow exponentially) and $u = 1$ (i.e for any small perturbation near 1, the solution will relax exponentially to 1). Therefore, in this case, we seek travelling wave front solutions. Since the Fisher-KPP equation is invariant under change of sign of the spatial coordinate x, therefore according to definition 3 one can say:

Proposition 1. *Fisher-KPP equation admits a travelling wave front solution of the form $u(t,x) = w(x + vt)$ with $v \in \mathbb{R}$, with respect to the boundary conditions*

$w(-\infty) = 0, w(+\infty) = 1$.

In the case of the Fisher-KPP equation, there exist travelling wave solutions for which we can compute the movement's velocity. Indeed, in the first work of Kolmogorov et al. [Kol37], it has been demonstrated that all initial conditions with compact support for Equation (10.3) in the case of $D = 1$ evolve to a travelling wave solution with the minimum speed $c = 2$ [SM96].

For a general case of the diffusion parameter, we refer to [MZ05] for the existence of a travelling wave. Let us denote by $v_{min} = 2\sqrt{D}$ the minimal speed satifiying [MZ05]:

- For every $v > v_{min}$ there exists a travelling wavefront of the form $u(x,t) = w(x + vt)$ and $w(-\infty) = 0, w(+\infty) = k$.
- For $v \leq v_{min}$, there is no such monotone wavefront with speed v.
- The wavefront is unique up to translation.
- The wavefront is stable according to some class of initial functions such as compactly support functions.

Consequently, all the travelling waves for FKPP equation with compactly supported initial conditions have a unique profile. In particular, the long-term behaviour of Equation (10.3) can be then specified as follows:

Proposition 2 (Asymptotic behaviour). *Let's take Equation (10.3) with an initial condition u_0 that is compactly supported. Then, the asymptotic behaviour of u is a wavefront that we denoted by u^A. In addition, the wavefront profile is independent of u_0, and it only depends on the value of the diffusion parameter D. Moreover, u^A is moving with the velocity $v = 2\sqrt{D}$.*

Therefore, the space of travelling wave solutions for the FKPP equation with initial condition u_0 that are compactly supported is a one-dimensional space depending only on the diffusion parameter D.

The explicit expression of the travelling wave solutions for Equation (10.3) is in general not kown except for particular velocity values [MF96; BD15]. In case of Equation (10.3) with $D = 1$, Ablowitz and Zeppetella [AZ79] computed the explicit form of the solution, given by $u = [1 + c \exp\left(\frac{(x-ct)}{\sqrt{6}}\right)]^{-2}$ for the velocity value $c = \frac{5}{\sqrt{6}}$. For theorectical review, we refer the reader to the references [VP09; Per15; TV20]. In this thesis, we will not get use of the expression of the travelling wave, instead, we will be interested in its profile.

Example of generation of a Fisher-KPP travelling wave solution: In Figure 10.4, we simulate the asymptotic travelling wave solution u^A for Equation (10.3) in case of $D = 1$. We consider the space interval $[-10 : 60]$ with a discretization step $\Delta_x = 0.1$, and we consider the time interval $[0 : 150]$ with a discretization step $\Delta_t = 0.001$. The initial condition here is the one-dimensonal

heaviside function $H(x - c)$ with c is the center of the spatial interval.
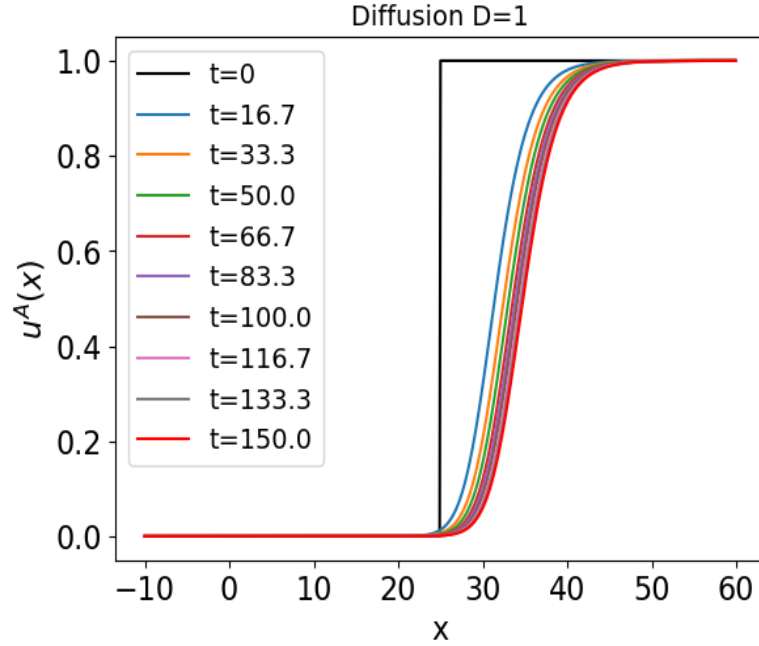
Figure 10.4: Simulation of the asymptotic travelling wave solution for Fisher-KPP equation in the case of $D = 1$. The profile of the obtained TW is the same for all the times $t > 0$ with some dilation.

10.3   Application of Fisher-KPP model to ulcerative colitis

This section is dedicated to modelling the spatial distribution of lesions found in a colonoscopy video. In the first part, we consider the patient as a solution for the Fisher-KPP equation, and we show that it evolves into a travelling wave. In the second part, we consider the patient as a travelling wave solution for the one-dimensional Fisher-KPP equation. We estimate the diffusion parameters and the velocities of the lesions' displacement into the colon. We can then compute the time at which the whole colon will be affected by the lesions which is what we call the invasion time.

10.3.1   Direct model

Let us begin by an example of bleeding spatial distribution into the colon for patient from the Vatic database. In Figure 10.5, we consider the surface of annotated bleeding in the colon represented by its curvilinear abscissa as done in the previous chapters. One can see the mucosa near the cecum is healthy (absence of lesions, $u = 0$), while the mucosa near the rectum is bleeding and shows the highest level of inflammation ($u = 1$).

$u(x)$
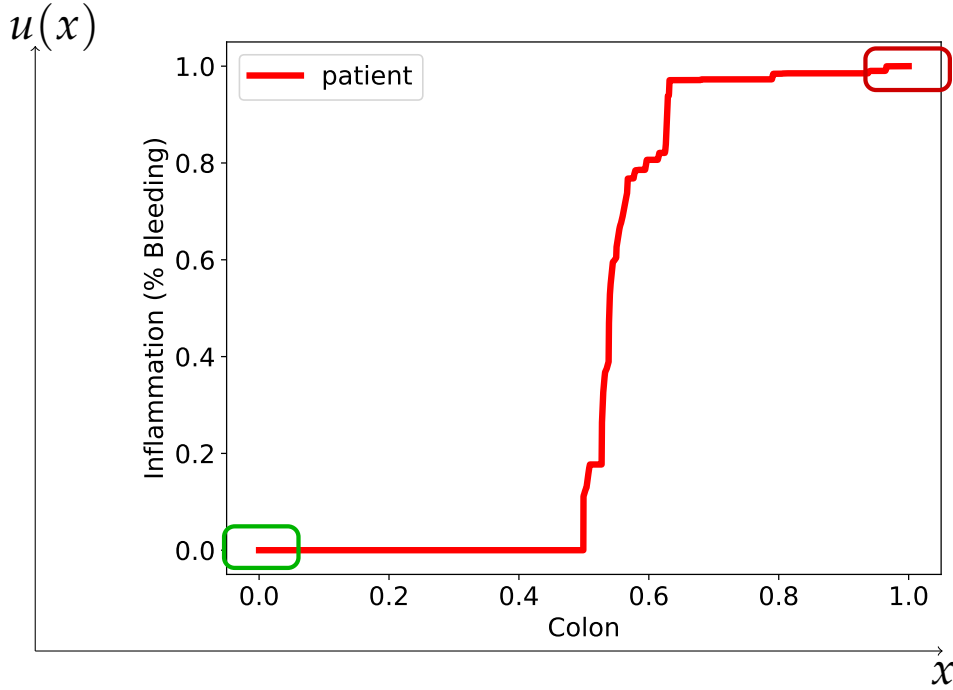
Figure 10.5: The surface of annotated bleeding denoted by u as function of the colon curvilinear abscissa denoted by x.

Towards the application of the Fisher-KPP model (cf Equation (10.3)) to UC lesions, we consider the spatial coordinate x to denote the colon's curvilinear abscissa symbolized by Ω, i.e. $\Omega = [0, 1]$. The density parameter of the model u is the surface of the lesion at a given point x. The coefficient $D > 0$ is the rate at which the lesions are supposed to diffuse into the colon. We will consider the Dirichlet boundary conditions $u(t, 0) = 0$ and $u(t, 1) = 1$. Since the patient is considered a solution for the Fisher-KPP equation, it will be represented by the couple (D, u_0).

The choice of the initial condition u_0 is not obvious. In fact, the symptoms of the UC disease appear after some time $t > 0$ following the beginning of the disease. Thus a patient $p(x)$ is in general observed at time t which is not the initial time of the disease. In other words, the colonoscopy video is in general taken after a time $t > 0$ that is not the beginning of the disease denoted by T_{initial}. The inflammation due to the disease has evolved during an unknown time t before the patient has made the clinical examinations. Due to the fact, that only one colonoscopy video is available per patient, we are conducted to consider the initial spatial distribution $u_0(x) = p(x)$ and D unknown parameter. Following the proposed modelling procedure, we are then able to compute the velocity of the lesions displacement using the relation: $v = 2\sqrt{D}$.

To simulate numerically the Fisher-KPP solution, we decide to use the finite

method, and more precisely the Forward in Time and Centered in Space numerical scheme (FTCS). The discretized form of Equation (10.3) remains as follows (for details see appendix B page 210):

$$u_i^{j+1} = u_i^j + \frac{D\Delta t}{\Delta x^2}(u_{i-1}^j - 2u_i^j + u_{i+1}^j) + \Delta t\left(u_i^j - (u_i^j)^2\right), \qquad (10.4)$$

where $i \in \{1,..,N_x\}$ is the space index with N_x is the number of points considered for the discretization of the space domain $\Omega = \{x \in \mathbb{R}, 0 \le x \le 1\}$ and $j \in \{1,..,N_t\}$ is the time index after discretization of the interval $\{0 \le t \le T, T \in \mathbb{R}^*\}$ into N_t points.

Example of direct modelling of the UC bleeding using Fisher-KPP: Let us take the example of the bleeding profile for the patient given in Figure 10.5. As we mentioned, the extracted lesions surface measures will be used as the initial condition for Equation (10.3). As a diffusion parameter, we test the value $D = 100$ using the following code chunk:

Code chunk 30: fisherkpp

```python
L=len(Data_perc_b[23])
x0, xL, delta_x = 0, L-1, 1
t0, tF, delta_t = 0, 50, 0.003
Nx, Nt = int((xL-x0)/delta_x+1), int((tF-t0)/delta_t+1)
X, T = np.linspace(x0,xL,Nx), np.linspace(t0,tF,Nt)

# initial condition
U1=np.zeros((Nx,Nt))
U1[0,:] = 0.0
# at position x=0 for all times
U1[L-1,:] = 1.0
# at position x=L-1 for all times
U1[:,0]= Data_perc_b[23] / max(Data_perc_b[23]) # at t=0

# simulation code
D=100 # Diffusion parameter
CFL=D*delta_t/delta_x**2
for t in range(Nt-1):
    U1[1:-1,t+1] = CFL*U1[2:,t] + CFL*U1[:-2,t] + \
                   (-2*CFL + 1 + delta_t)* U1[1:-1,t] - delta_t*U1[1:-1,t]**2

# figure code
_ = plt.figure()
_ = plt.xlabel('Frame number',fontsize=14)
_ = plt.ylabel('Surface of Bleeding',fontsize=14)
ts = np.floor(np.linspace(0,Nt-1,10))
for t in ts.astype(int):
    roundedt = round(T[t],1)
    _ = plt.plot(X,U1[:,t], label='t=%s'%roundedt)

_ = plt.legend()
_ = mpl.rc('xtick',labelsize=16)
_ = mpl.rc('ytick',labelsize=16)
_ = plt.rc('legend',fontsize=14)
_ = plt.tick_params(axis='both', which='minor', labelsize=14)
plt.savefig('test-patient-23.pdf',bbox_inches = 'tight')
plt.close()
```

Interpret with `python2`

We then compute the velocity at which the inflammation is moving using the code chunk:

Code chunk 31: fisherkpp (part 2)

```python
U1_trapz = np.trapz(U1,dx=delta_x,axis=0)
len(U1_trapz) # should be equal to nb of time points, here 16667

import scipy
from scipy import stats
lm = stats.linregress(T[16000:],U1_trapz[16000:])
print(lm.slope,lm.rvalue)
print 'Velocity of the propagation = '+str(lm.slope)# should be 2.sqrt D = 20
(U1_trapz[-1] - U1_trapz[-2]) / (20*delta_t) # should be 1
```

Interpret with `python2`

```
16667
(19.65732103691607, 0.9999999967132336)
Velocity of the propagation = 19.65732103691607
0.9832079143128188
```
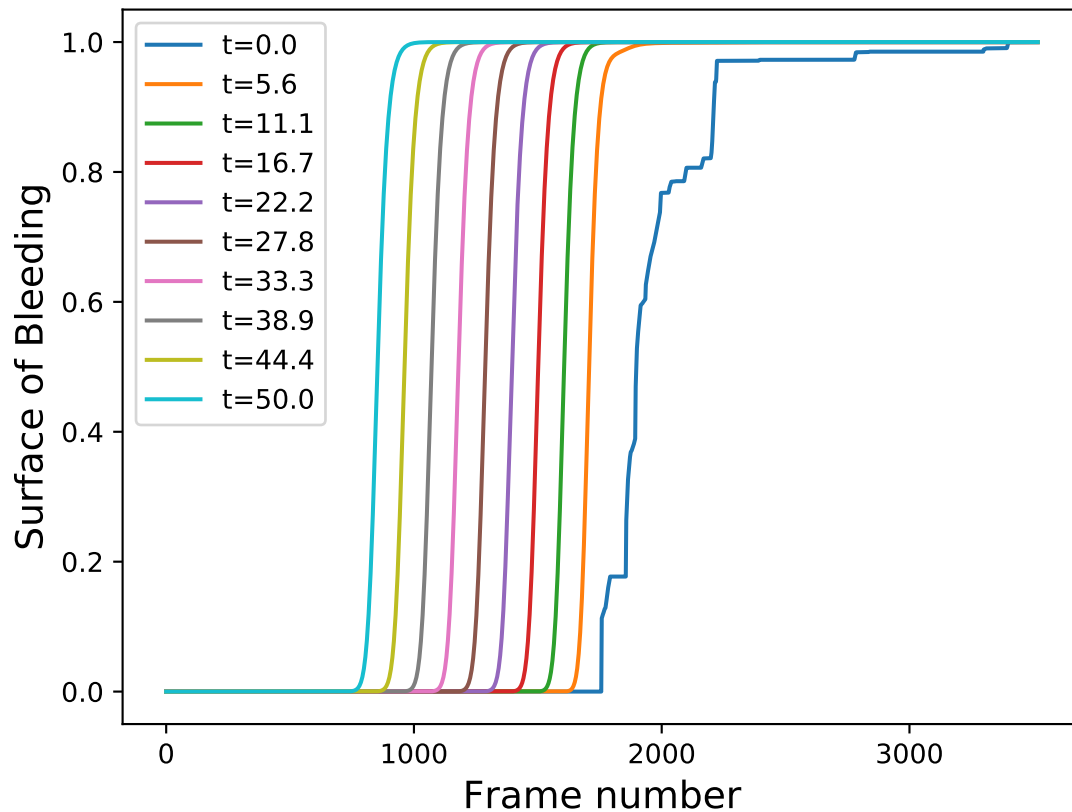

Figure 10.6: Simulation of the bleeding lesions' spatial extent as solution Fisher-KPP model with a diffusion parameter $D = 100$. A travelling wave front moving with velocity $v = 2\sqrt{100} = 20$ appears.

During the presented modelling procedure, we impose the diffusion rate D in order to generate the profile of the lesions after a chosen time T. However, in this thesis, we are interested in computing the diffusion D that corresponds to

each patient and subsequently computing the velocity at which the lesions are spreading into the colon. Therefore, a direct modelling technique cannot be useful. Instead, we propose to estimate the diffusion rate D using the colonoscopy video. This is what we call an inverse problem procedure.

10.3.2   Inverse problem

We have previously said that the colonoscopy is taken after a time $t > 0$ after the beginning of the disease. If we consider that this time is large enough, then the patient is observed in the asymptotic regime. We then decide to consider the patient as a travelling wave solution of Equation (10.3).

In Proposition 2, we have mentioned that the asymptotic behaviour of the solution for Equation (10.3) with initial compactly supported condition u_0 ($u_0(x) = 0$ when $x \to -\infty$ and $u_0(x) = 1$ when $x \to +\infty$) is a travelling wave moving with a velocity depending on the diffusion parameter D. Moreover, the profile of the travelling wave solution of Equation (10.3) being unique up to dilation, we can compute it for a general value of D by a dilation of the profile of the asymptotic travelling wave solution u^A obtained in the case of $D = 1$. The dilation can be given by the following proposition:

Proposition 3. *The Fisher-KPP travelling wave solution (D, u_0) where u_0 is an initial condition with compact support can be obtained by a spatial scale changing of the Fisher-KPP solution with diffusion parameter $D = 1$ i.e. $(1, u_0(\frac{1}{\alpha}x))$ where $\alpha = \sqrt{D}$.*

Since the temporal origin is unknown and as we move at a constant speed then the position of the travelling wave front is computable by a translation. Finally, we are able to estimate the corresponding diffusion parameters of the lesions for each patient.

We can also estimate time at which the lesions will invase all the colon. Indeed, supposing that the integral is equal one as we supposed the maximum value for u is one, then to compute the time it is sufficient to compute the difference with the surface of the actual profil to compute the displacement.

In this part of the manuscript, we decide to use the compatibility notion given by definition 1 in page 155 to find the set of compatible diffusion parameters, compatible velocities and consequently the compatible invasion times for each type of lesions.

First, we present the computation of the diffusion parameter that is compatible with the lesions:

Proposition 4. *Let S_D be the set of tested diffusion parameters D, u_p the inflammation data for a patient p. We denote by $\tilde{u}_D^A$ the asymptotic travelling wave solution of Equation (10.3) in the case of $D = 1$ i.e. u^A after a dilation with the parameter $\sqrt{D}$ and a*

convenient translation. The optimal dilation parameter D^* holds in:

$$
\begin{aligned}
D^* &= \underset{D \in S_D}{\operatorname{argmin}} J(D) \\
&= \underset{D \in S_D}{\operatorname{argmin}} \|u_p - \tilde{u}_D^A\|^2,
\end{aligned}
\tag{10.5}
$$

Second, we compute the set of compatible dilations with α error tolerance as follows:

Proposition 5. *Let α be the accepted error threshold, the set of compatible diffusion parameters, i.e. D_{comp} can be computed as follows:*

$$
D_{comp} = \{D \in S_D, \|u_p - \tilde{u}_D^A\|^2 \leq (1 + \alpha) \times \|u_p - \tilde{u}_{D^*}^A\|^2\},
$$

where S_D is the set of tested diffusion parameters D and u_p is the inflammation data vector for a patient p. $\tilde{u}_{D^*}^A$ is u^A after a dilation with the optimal parameter $\sqrt{D^*}$ and a convenient translation.

Next, we can compute the set of the compatible velocities based on Proposition 2:

Proposition 6. *We denote by D_{comp} the set of compatible dilation parameters found in Proposition 5. The set of corresponding compatible velocities, denoted by v_{comp}, can be computed using the following formula:*

$$
v_{comp} = \{2\sqrt{\mathbf{D}} \text{ for } D \in D_{comp}\}
$$

Example of inverse model for UC lesions: We also use the bleeding profile of patient given in Figure 10.5. The `fkpp_interp` function rescales the wave front solution (for Equation (10.3)) dilated with $\sqrt{D}$ by a translation.

Code chunk 32: fkpp_recalage (part 2)

```python
def fkpp_interp(p,D,figname=None):
    Xp = np.linspace(0,1,num=len(p))
    sqrtD = np.sqrt(D)
    Xi = sqrtD * X \
        + (np.trapz(U1,dx=delta_x*sqrtD) \
        - np.trapz(p,dx=Xp[1]-Xp[0]) - (xL*sqrtD-1))
    Ui = np.interp(Xp,Xi,U1)
    distD = np.trapz( (p-Ui)**2,dx=Xp[1]-Xp[0] )
    if figname != None:
        fig,ax = plt.subplots()
        ax.plot(Xp,p,'r',linewidth = 4, label ='patient')
        ax.plot(Xi,U1,"b", linewidth = 3, label='Asymptotic TW')
        plt.xticks(fontsize = 16)
        plt.yticks(fontsize = 16)
        plt.xlabel('x', fontsize=16)
        plt.ylabel('Inflammation (Bleeding)', fontsize=16)
        leg = ax.legend(prop={"size":18})
        plt.legend()
        ax.set_title("sqrtD = " + str(round(sqrtD,3)) + \
                    " distance = " + str(round(distD,3)), fontsize=20)
        fig.savefig(figname)
        plt.close()
    return distD
```

We explore the set of diffusion parameters $S_D = [0.01^2, 0.02^2]$ with the step 0.0005 as follows:

Code chunk 33: fkpp_speed

```python
D = np.arange(0.01,0.02,0.0005) ** 2
dists = [fkpp_interp(p,d) for d in D]
alpha, min_dist = 0.05, np.amin(dists)
D_comp = np.extract(dists<(1+alpha)*min_dist,D) #D compatibles
scompat = 2 * np.sqrt(np.extract(dists<(1+alpha)*min_dist,D))
print 'Vitesses compatibles', scompat
Xp = np.linspace(0,1,num=len(p))
print 'Temps d\'invasion',np.round((1-np.trapz(p,dx=Xp[1]-Xp[0]))/scompat,2)
```

Interpret with `python2`

```
Vitesses compatibles [0.026 0.027 0.028 0.029 0.03 ]
Temps d'invasion [21.53 20.73 19.99 19.3  18.66]
```

In Figure 10.7, we plot the profile of patient lesions (in red) and asymptotic travelling wave of Fisher-KPP (Equation (10.3) with $D = 1$) obtained after dilation and translation. We conclude that the optimal dilation $D^* = 0.014^2$ fits with the spatial distribution of the bleeding lesions found in the colonoscopy video.
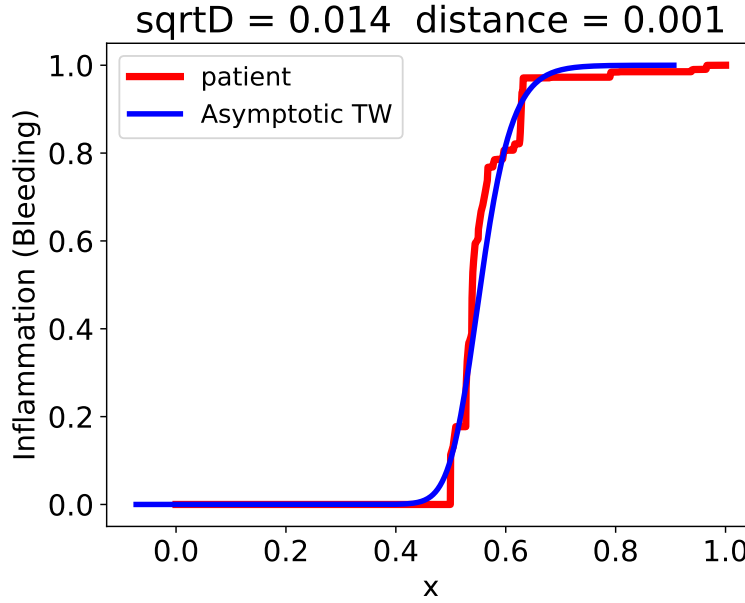
Figure 10.7: Representation of the inflammation of the patient 33 (in red) and u^A (blue) with the optimal dilation parameter $D^* = 0.014^2$.

10.4 Results: application to Vatic database

In this section, we apply the inverse modelling process proposed in subsection 10.3.2 to a set of patients from the Vatic database. The section includes four parts:

1. In subsection 10.4.1 we compare the estimated Fisher-KPP profile to the lesions profile for some patients.
2. In subsection 10.4.2, we show that the velocities are almost the same for patients having the same severity scores.
3. In subsection 10.4.3, we show that the lesions invasion times are not the same for patients having the same severity scores.
4. In subsection 10.4.4, we compute the invasion times for bleeding and ulcers for patients classified into the same type of UC. For some patients, the bleeding lesions may invade the colon more quickly than ulcer lesions.

10.4.1 Comparison of the Fisher-KPP profile with the lesions profile

We plot the asymptotic travelling wave for Fisher-KPP and the lesions surface measures for three patients having different profiles of bleeding and ulcers. In comparison with Figure 10.9 and Figure B.6, the profile in Figure 10.8 is less good because the form of the patient profile that is far from the profile of the asymptotic Fisher-KPP solution u^A.
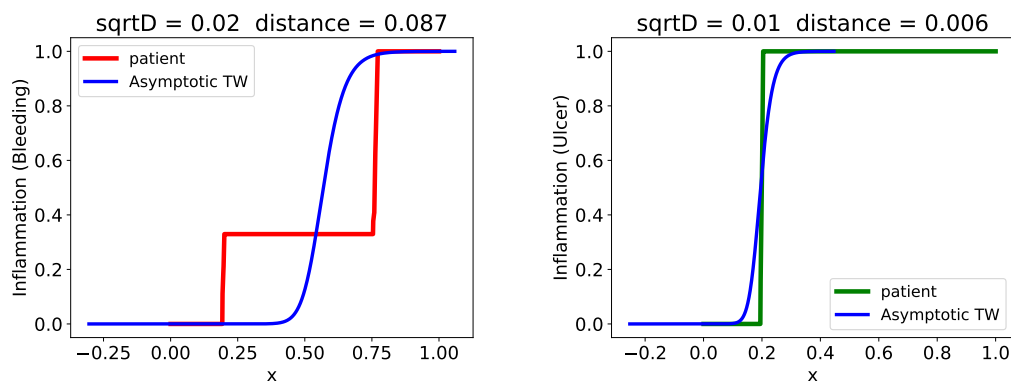
Figure 10.8: Rescaling of the travelling wavefront u^A for patient of video 3 with optimal diffusion for bleeding lesions $D_b^* = 0.02^2$ and ulcers $D_u^* = 0.01^2$.
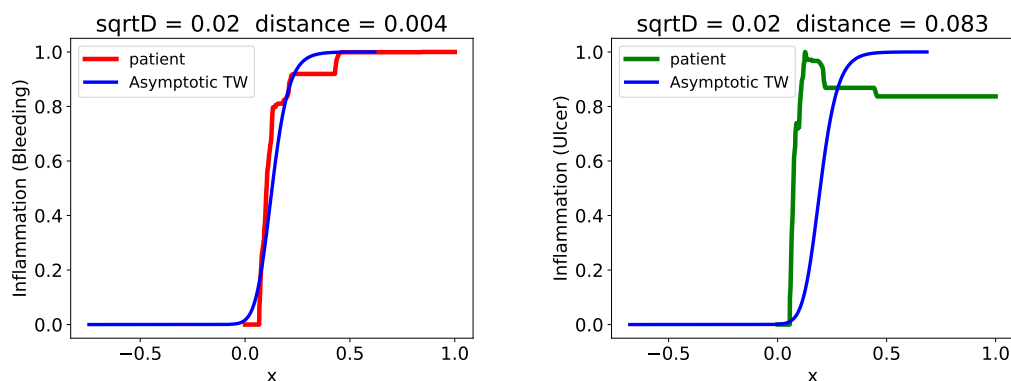
Figure 10.9: Rescaling of the travelling wavefront u^A for patient of video 7 with optimal diffusion for bleeding lesions $D_b^* = 0.02^2$ and ulcers $D_u^* = 0.02^2$.
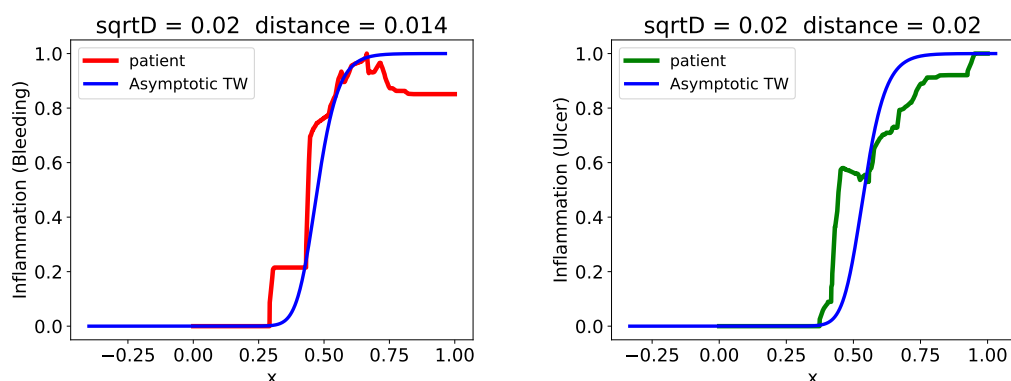
Figure 10.10: Rescaling of the travelling wavefront u^A for patient of video 13 with optimal diffusion for bleeding lesions $D_b^* = 0.02^2$ and ulcers $D_u^* = 0.02^2$.

In appendix B page 215, we show the results for more patients from Vatic database.

10.4.2 Velocities are similar for patients having same severity scores

In Table 10.1, we present the compatible velocities for bleeding (denoted by $v_{\text{comp}}^{\text{bleed}}$) and ulcers (denoted by $v_{\text{comp}}^{\text{ulcer}}$). We choose two patients for each value of score UCEIS $\in$ [2,4,6]. According to the results, the velocities for both types of lesions are very similar and varing between 0.034 and 0.039 except for the ucler velocity for patient 3.

UCEIS	Patient	$v_{\text{comp}}^{\text{bleed}}$	$v_{\text{comp}}^{\text{ulcer}}$
2	patient 3	[0.035, 0.036, 0.037, 0.038, 0.039]	[0.02]
	patient 6	[0.035, 0.036, 0.037, 0.038, 0.039]	No ulcer
4	patient 7	[0.034, 0.035, 0.036, 0.037, 0.038, 0.039]	[0.035, 0.036, 0.037, 0.038, 0.039]
	patient 17	[0.034, 0.035, 0.036, 0.037, 0.038, 0.039]	[0.038, 0.039]
6	patient 13	[0.036, 0.037, 0.038, 0.039]	[0.038, 0.039]
	patient 16	[0.038, 0.039]	[0.031, 0.032, 0.033, 0.034, 0.035, 0.036, 0.037, 0.038, 0.039]

Table 10.1: Computed velocities for bleeding and ulcer lesions for patients from Vatic database.

10.4.3 Invasion times are different among patients with the same severity scores

We also compare the time required for a lesion to diffuse in the whole colon (cf Table 10.2) for the six patients considered in subsection 10.4.2.

For each class of scores, the times' values are very dissimilar. For instance, in the case of UCEIS=2, the bleeding lesions will diffuse into the whole colon for patient 6 much more quickly than for patient 3. For UCEIS=4, the lesions show prominent dissimilarities. Bleeding for patient 7 needs less time (minimum value is 3.5) to invade the colon in comparison with patient 17 (minimum value is 14.12). Same for UCEIS=6, bleeding invasion time for patient 16 is very small in comparison with patient 13. On the other hand, ulcer lesions for patient 16 need approximately double the time of that of patient 13.

Although ranked differently, patient 3 and patient 7 show similar invasion time for bleeding since $T_{\text{comp}}^{\text{bleed}}$(patient 3) is equal to $T_{\text{comp}}^{\text{bleed}}$(patient 17).

On the other hand, for the same patient the bleeding and ulcers can affect the colon at closer times like for patient 13 or ulcers can invade the colon faster than bleeding as in the case of patient 16 where $T_{\text{comp}}^{\text{bleed}}$(patient 16) $\ll$ $T_{\text{comp}}^{\text{ulcer}}$(patient 16). However, patient 3 shows an opposing behaviour.

UCEIS	Patient	$T_{\text{comp}}^{\text{bleed}}$	$T_{\text{comp}}^{\text{ulcer}}$
2	patient 3	[16.47, 16.01, 15.58, 15.17, 14.78]	[9.96]
	patient 6	[23.91, 23.24, 22.61, 22.02, 21.45]	No ulcer
4	patient 7	[4.01, 3.9, 3.79, 3.69, 3.59, 3.5]	[5.79, 5.63, 5.48, 5.34, 5.2]
	patient 17	[16.2, 15.74, 15.3, 14.89, 14.5, 14.12]	[18.96, 18.47]
6	patient 13	[13.38, 13.02, 12.68, 12.35]	[14.41, 14.04]
	patient 16	[2.02, 1.97]	[27.74, 26.88, 26.06, 25.3, 24.57, 23.89, 23.24, 22.63, 22.05]

Table 10.2: Invasion time for bleeding and ulcer lesions for patients from Vatic database.

10.4.4   Variability of the lesions invasion times for patients having similar disease type

In Table 10.3, we show the lesions'invasion time for patients having the same class of disease: pancolitis (patients 1, 2, 37) or extensive ulcerative colitis (patients 6 and 15).

For patients classified into pancolitis, bleeding lesions have almost similar invasion times. However, there is variability in the long-term behaviour of ulcers. The invasion time in the case of patient 2 is very small in comparison with the invasion time in the case of patient 37. Ulcers will invade the colon of patient 1 more rapidly than in patients 2 and 37.

Moreover, there are dissimilarities among the invasion times of lesions for the same patient. For instance, in the case of patient 2, the bleeding lesions invade the colon much more rapidly than ulcers. The same phenomenon occurs for patient 37. Therefore, one can see that probably the bleeding will invade the colon faster than ulcers.

On the other hand, for extensive UC patients, there is a large variability between the invasion times for bleeding lesions. Bleeding lesions will invade the colon for patient 6 faster than for patient 15.

Type of UC	Patient	$T^{\text{bleed}}_{\text{comp}}$	$T^{\text{ulcer}}_{\text{comp}}$
Pancolitis	patient 1	[16.02, 15.5, 15.02, 14.56, 14.13, 13.73, 13.35, 12.99, 12.65, 12.32]	[25.87, 24.7, 23.62, 22.64, 21.73, 20.9, 20.12, 19.4, 18.74, 18.11, 17.53, 16.98, 16.46, 15.98, 15.52, 15.09, 14.68, 14.3, 13.93]
	patient 2	[17.39, 16.64, 15.94, 15.3, 14.72, 14.17, 13.66, 13.19, 12.75, 12.34, 11.96, 11.59,11.25, 10.93, 10.63, 10.34, 10.07, 9.81]	[4.25, 4.14, 4.03]
	patient 37	[22.11, 21.38, 20.69, 20.04, 19.43, 18.86, 18.32, 17.81, 17.33, 16.88, 16.44]	[10.83, 10.36, 9.92, 9.53, 9.16, 8.82, 8.51, 8.21, 7.94, 7.68]
Extensive UC	patient 6	[23.91, 23.24, 22.61, 22.02, 21.45]	No ulcer
	patient 15	[18.08, 17.55, 17.05, 16.57, 16.12, 15.7, 15.3]	No ulcer

Table 10.3: Invasion time for bleeding and ulcer lesions for patients from Vatic database.

10.5 Conclusion

In this chapter, our aim is to model the spatial distribution of ulcerative colitis lesions encountered in colonoscopy videos. We choose the non-linear reaction-diffusion equation known as the Fisher Kolmogorov-Petrovski-Puskinov equation (FKPP).

We use the lesions' local surface measurements and the colon parametrization of chapter 7. For the modelling process, the patient is considered as a solution for the Fisher-KPP. It can be then represented by two parameters, the diffusion parameter (D) and the initial condition (u_0), compactly supported. As the patient is considered in an asymptotic regime, it can be modelled as a travelling wave solution moving into the colon. As inverse modelling, we decide to estimate the model parameters, more particularly the parameter D and consequently compatible speeds of lesions progressing into the colon and the compatibles times at which they will invade the whole colon.

For patients having similar endoscopic scores UCEIS, we find that the lesions are progressing into the colon with almost the same velocities. However, the invasion times are very dissimilar. The lesions will invade the whole colon for some patients faster than others. On the other hand, we compare the lesions' invasion time for patients classified into the same UC type (pancolitis

or extensive UC). The bleeding invades the colon at a different time and faster than ulcers.

This chapter encounters the first attempt at modelling the spatial distribution of bleeding and ulcer lesions according to the colon. The Fisher-KPP equation can enable the extraction of parameters like the velocity of lesions propagation into the colon and the time at which all the colon will be affected.

We have already stated in chapter 2, the barrier point between an inflamed and healthy mucosa is not yet understood and no medical studies have explained it. Therefore, in this study, it was not taken into account. In addition, we have considered that the colonoscopy video is taken during a period of activated symptoms i.e. the disease is out of control and will continue to spread into the colon. This hypothesis suggests that the inflammation will affect healthy tissue and spread throughout the colon. Consequently, we considered the inflammation as a travelling wave propagating into the colon. In future, we want to integrate the stopping point of the disease progression to better understand the behaviour of the disease.

Chapter 11

Conclusion and future directions

11.1 Contributions of the thesis

The main goal of this thesis is to provide an objective evaluation of the ulcerative colitis disease severity. Severity scores usually consider the most severe lesions of type bleeding, ulcers and main visibility of the vascular pattern. However, the evaluation depends on the gastroenterologist's interpretation and discards the spatial extent as well as the local distribution of lesions into the colon. We, therefore, propose a set of works to measure the disease severity including the lesions' spatial distribution along with the colon.

In our first work, we propose an automatic algorithm to detect bleeding and ulcer lesions found in a colonoscopy video. The lesions are annotated by rectangles which invoked many errors in the ground truth, especially for corner pixels. In order to cope with this, we propose to modify the detector sensitivity criteria in order to take into account the detected annotations rather than detected pixels. Furthermore, we propose an efficient sampling scheme to explore the set of linear detectors. The obtained results show good agreement with the ground truth.

In the second work, we propose to visualize the lesions in the whole colon. In this sense, we use a scheme of colon anatomy and suppose that the withdrawal of the colon is taken at a constant speed during the colonoscopy examination. The proposed method brings more information about the disease severity in comparison with current endoscopic scores. In addition, it leads to fine classification between UC patients with the same severity score or same disease type.

Afterwards, for the third work, we decide to model the disease severity by considering the spatial distribution of lesions in the colon. To deal with this, we study several colon segments decompositions and we show high agreement with current severity scores.

The following work involves a new vision to deal with medical hypotheses related to lesion distribution bias and severity assessment variability between experts. We introduce the notion of compatible models that perform like the best model with some predefined error threshold. We show that the lesions are more abundant near the rectum, the UC severity increases with the number of lesions found in the colonoscopy videos, and large variability between doctors during the severity assessment of both, bleeding and ulcers.

Finally, we model the spatial distribution of lesions by the Fisher Kolmogorov-Petrovski-Puskinov (FKPP). Using the colonoscopy video of the patient, we estimate the compatible diffusion parameters and consequently the speed of lesions propagation. We also compute the time at which all the colon will be affected by the disease. The results show similar velocities of lesions propagation for patients having the same endoscopic scores. However, all the colon segments will be affected at a very dissimilar time. Furthermore, the bleeding appears to invade the colon faster than ulcers for patient having the same type of the disease.

11.2 Future directions

For most of the chapters of this manuscript, we have discussed the problems and sometimes possible improvements. Most of the explored works remain in the first essay and need further study.

The automatic algorithm presented in chapter 6 requires a comparison with the state of the art methods and an application to a public database.

To compute the geometrical maps of the lesions in chapter 7, we have made several hypotheses concerning the colonoscopy examination. On the other hand, many problems related to the choice of lesions' representation were discussed, therefore we will not rediscuss them. In that sense, it might be interesting to proceed with a protocol that can link in a better way the video frame number to the colon's spatial coordinate. Moreover, a new database is a necessity to test the performance of the method on different patient profiles and for different values of the severity scores. Furthermore, it might be interesting to investigate other forms instead of lines or maybe propose solutions for the representation at the turning angles of the colon.

The Fisher-KPP equation employed in chapter 10 to model the spatial distribution of UC lesions remains a very simplified approach to studying the long-term behaviour of the lesions. Since the UC lesions propagate until some stopping point, the modelling by travelling wave solution that will continue to move is not the best choice. An intriguing problem would be, for example, to determine

a more convenient model of type reaction-diffusion or another class of partial differential equations which can exhibit a stable travelling wave, also known as a stationary travelling wave. In this way, we might be able to estimate more accurately the behaviour of the ulcerative colitis disease and then go in-depth into the measurement of the long-term behaviour and consequently objectively study the disease severity.

Appendix A

Maps of lesions for Vatic patients

In this section, we aim to present the lesions' maps generated by the proposed technique in chapter 7 for all the patients of the Vatic database, for which we have the set of annotations for bleeding and ulcers.
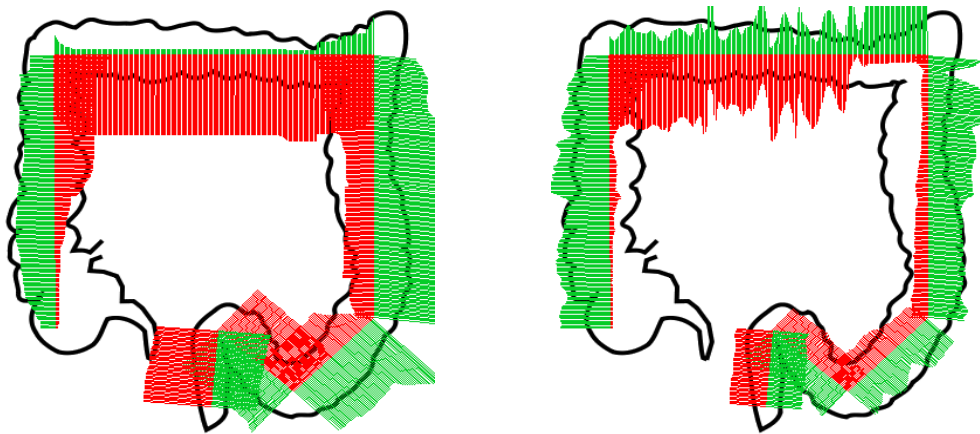
Figure A.1: Distribution of the UC lesions for the patient 1. Medical annotations on the left, and automatic detection on the right.
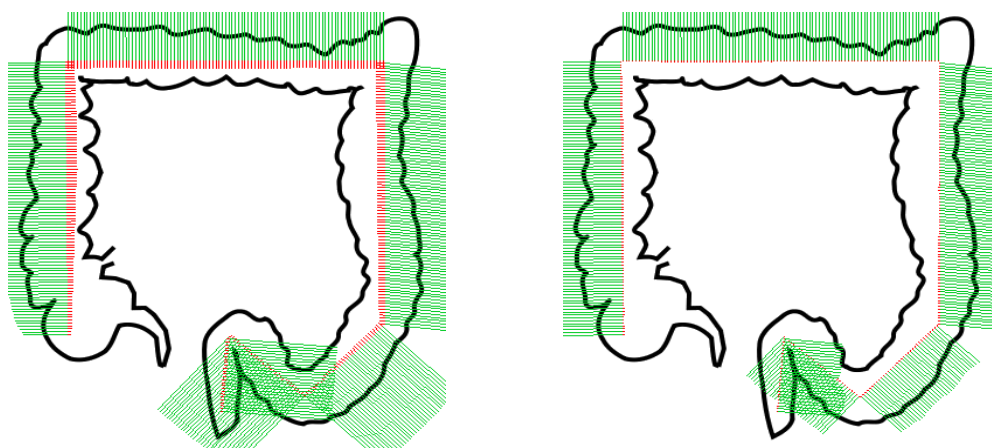
Figure A.2: Distribution of the UC lesions for the patient 2. Medical annotations on the left, and automatic detection on the right.
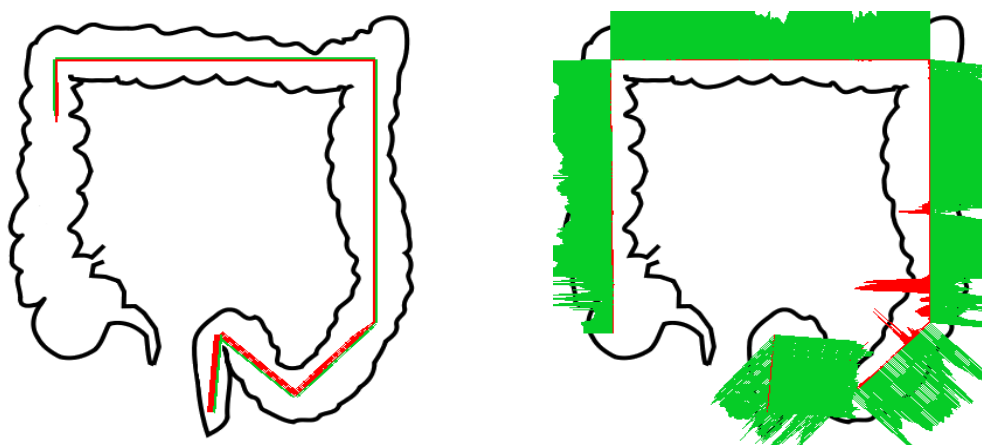
Figure A.3: Distribution of the UC lesions for the patient 3. Medical annotations on the left, and automatic detection on the right.
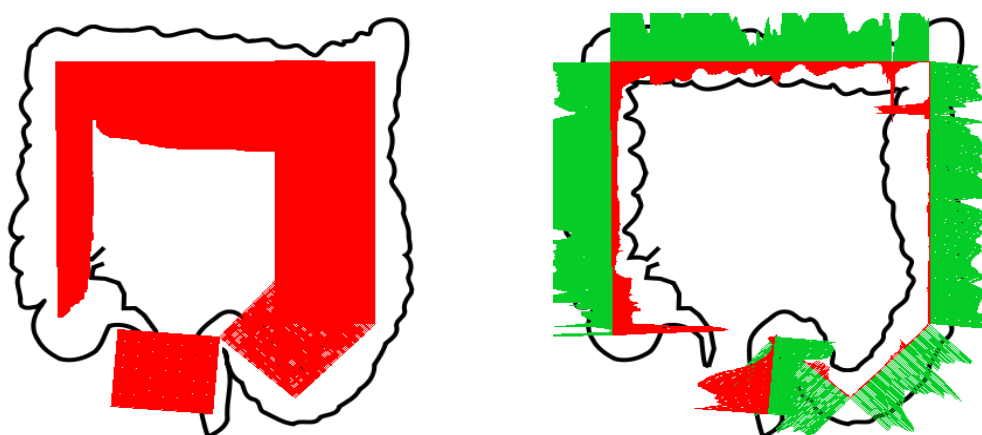
Figure A.4: Distribution of the UC lesions for the patient 5. Medical annotations on the left, and automatic detection on the right.
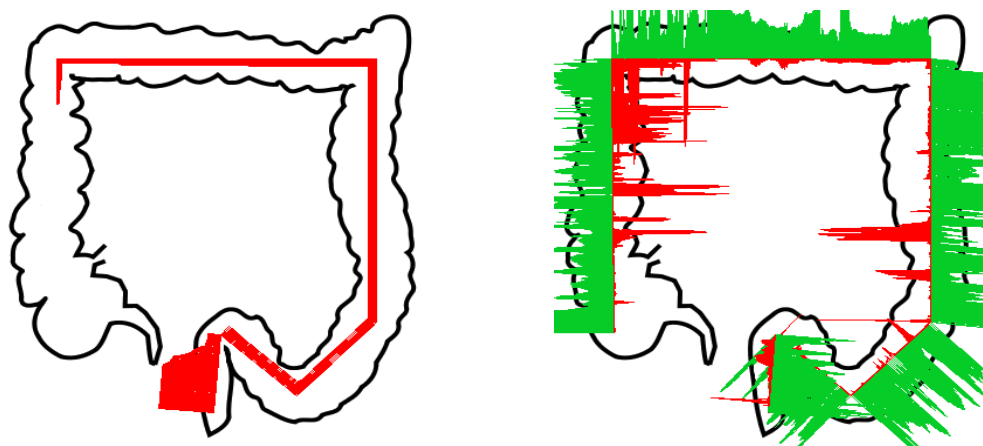
Figure A.5: Distribution of the UC lesions for the patient 6. Medical annotations on the left, and automatic detection on the right.
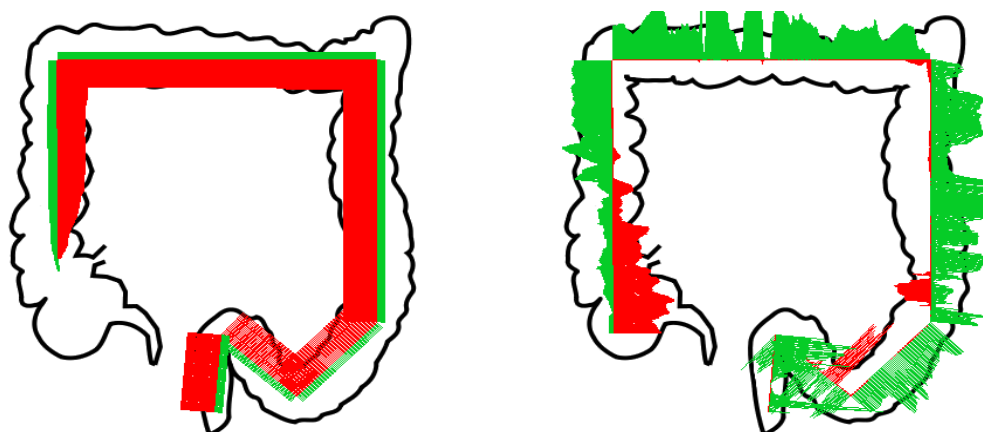
Figure A.6: Distribution of the UC lesions for the patient 7. Medical annotations on the left, and automatic detection on the right.
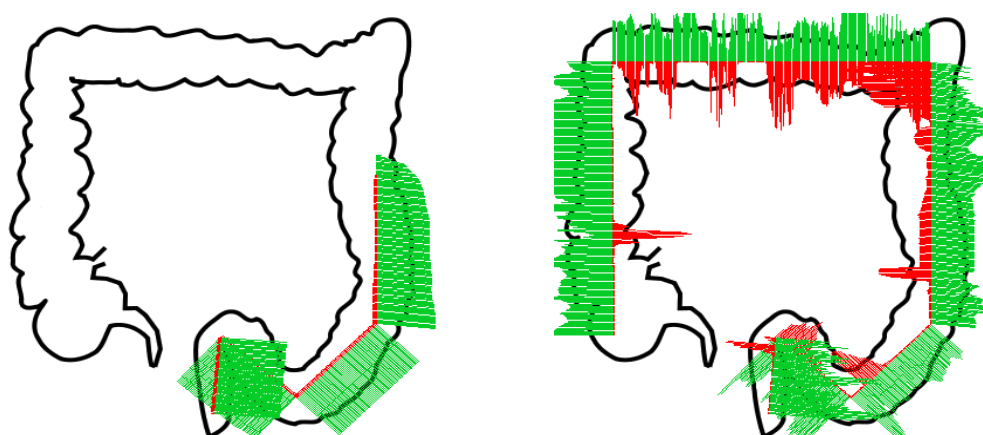
Figure A.7: Distribution of the UC lesions for the patient 9. Medical annotations on the left, and automatic detection on the right.
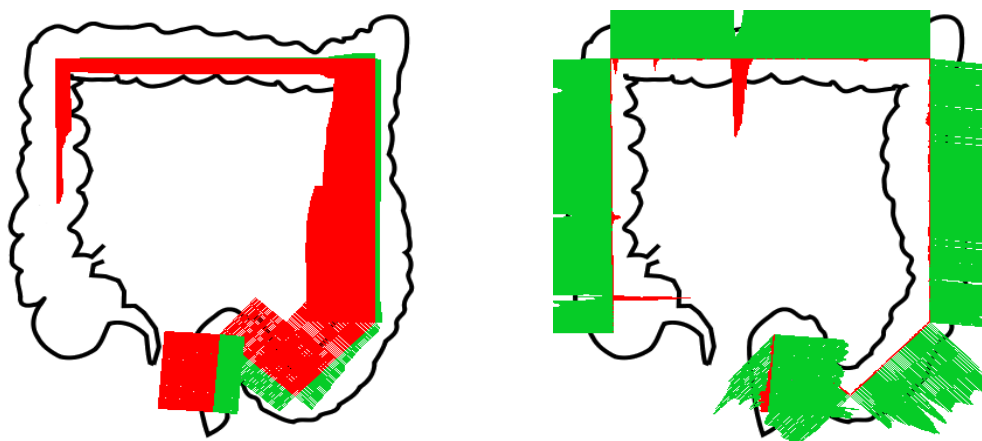
Figure A.8: Distribution of the UC lesions for the patient 10. Medical annotations on the left, and automatic detection on the right.
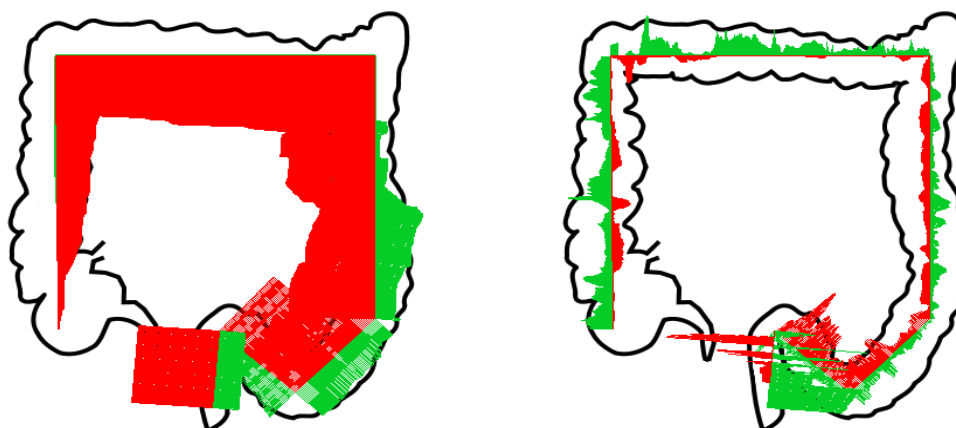
Figure A.9: Distribution of the UC lesions for the patient 11. Medical annotations on the left, and automatic detection on the right.
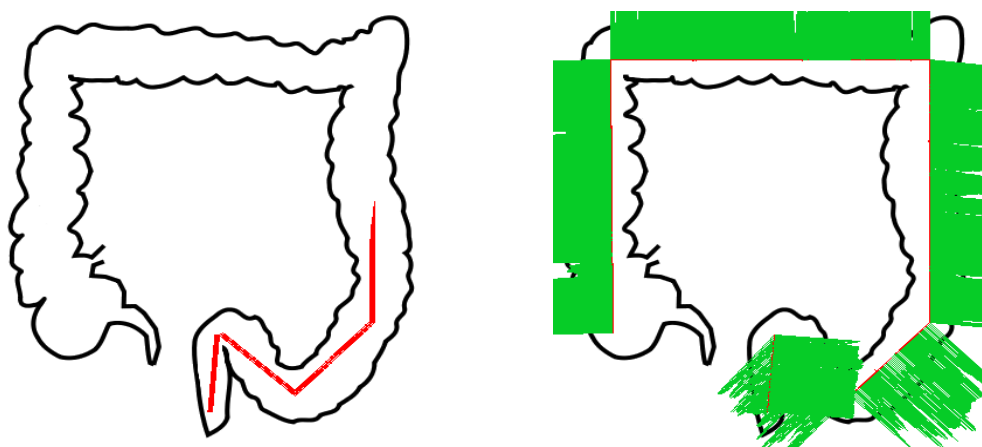
Figure A.10: Distribution of the UC lesions for the patient 12. Medical annotations on the left, and automatic detection on the right.
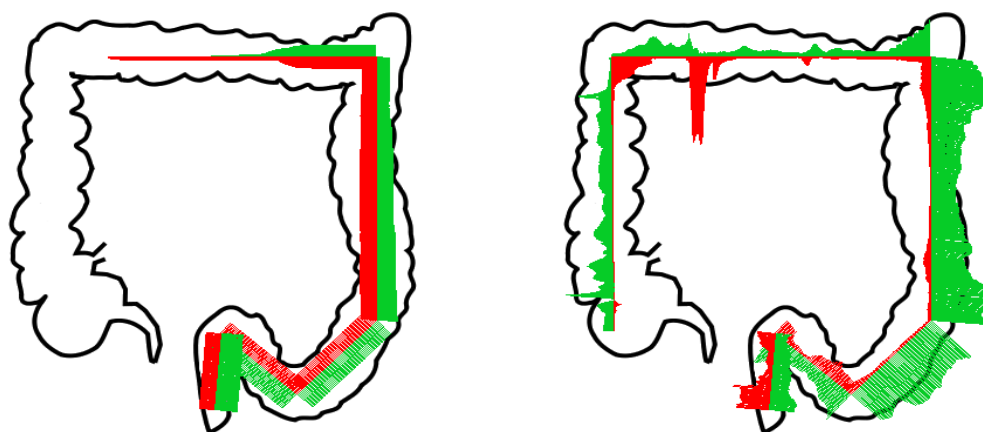
Figure A.11: Distribution of the UC lesions for the patient 13. Medical annotations on the left, and automatic detection on the right.
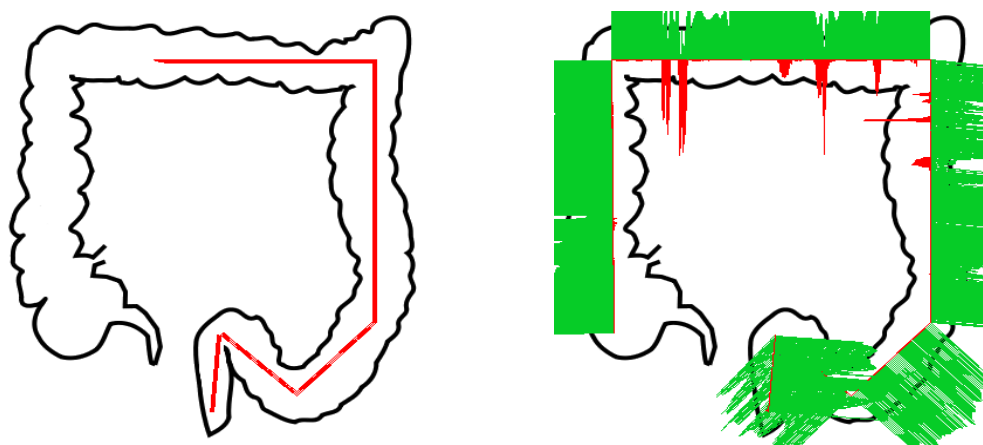
Figure A.12: Distribution of the UC lesions for the patient 14. Medical annotations on the left, and automatic detection on the right.
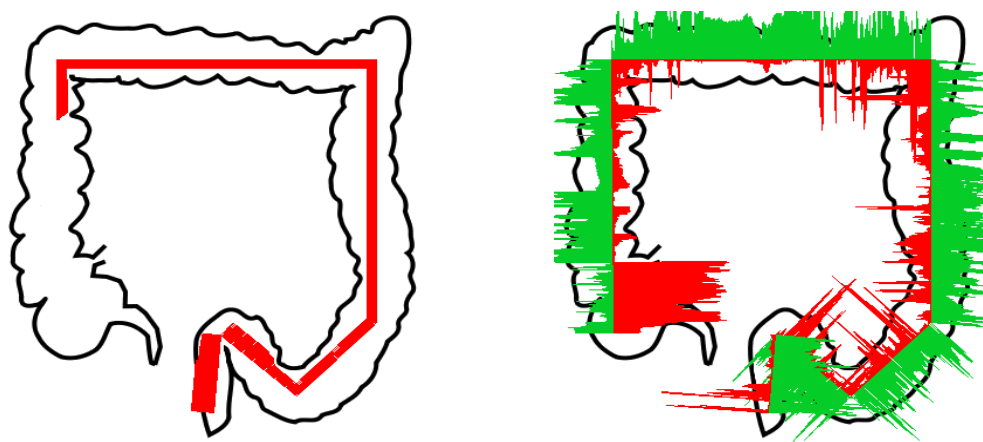
Figure A.13: Distribution of the UC lesions for the patient 15. Medical annotations on the left, and automatic detection on the right.
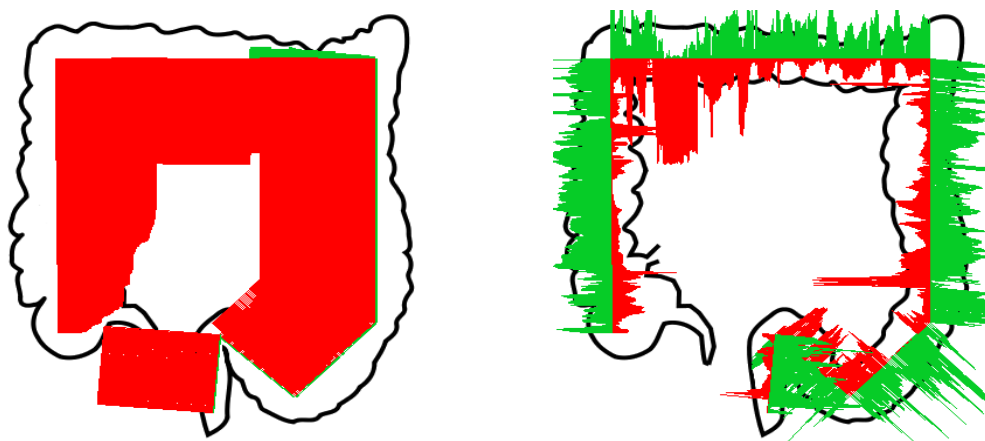
Figure A.14: Distribution of the UC lesions for the patient 16. Medical annotations on the left, and automatic detection on the right.
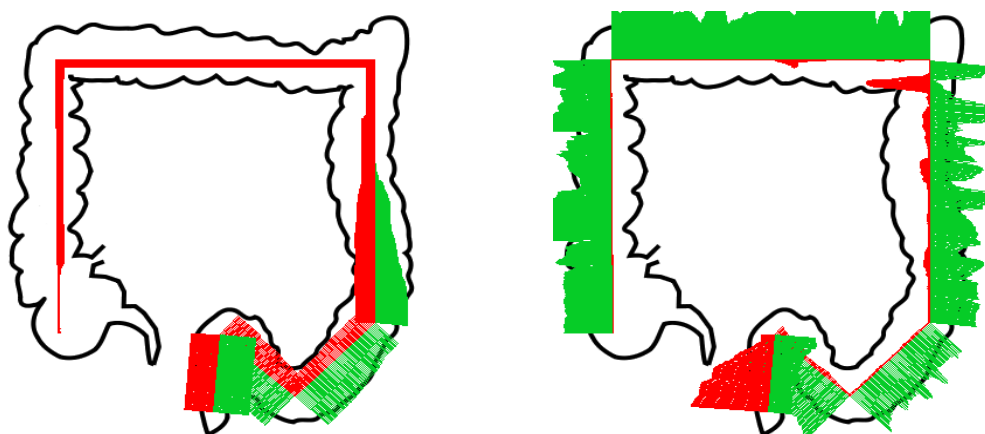
Figure A.15: Distribution of the UC lesions for the patient 17. Medical annotations on the left, and automatic detection on the right.
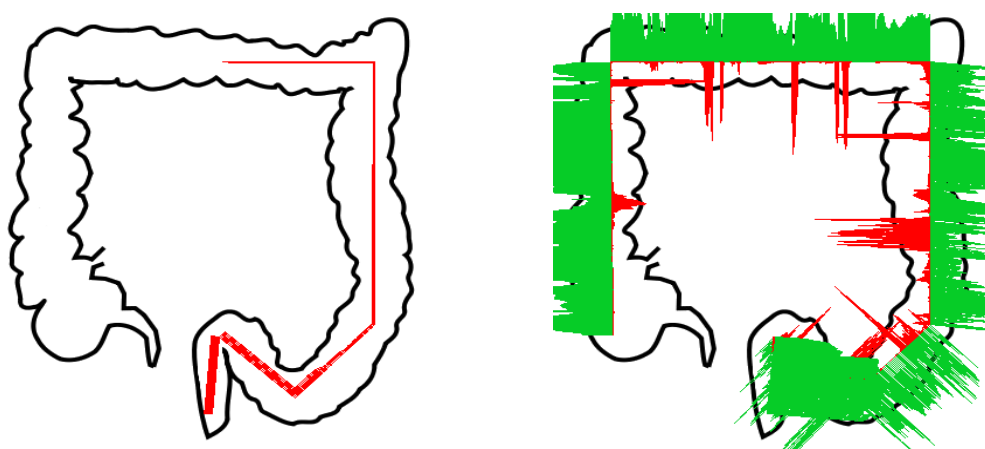
Figure A.16: Distribution of the UC lesions for the patient 19. Medical annotations on the left, and automatic detection on the right.
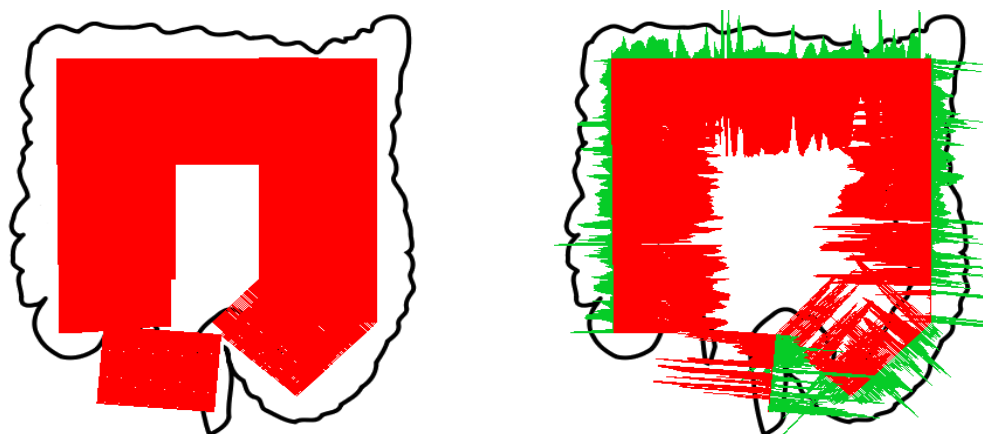
Figure A.17: Distribution of the UC lesions for the patient 21. Medical annotations on the left, and automatic detection on the right.
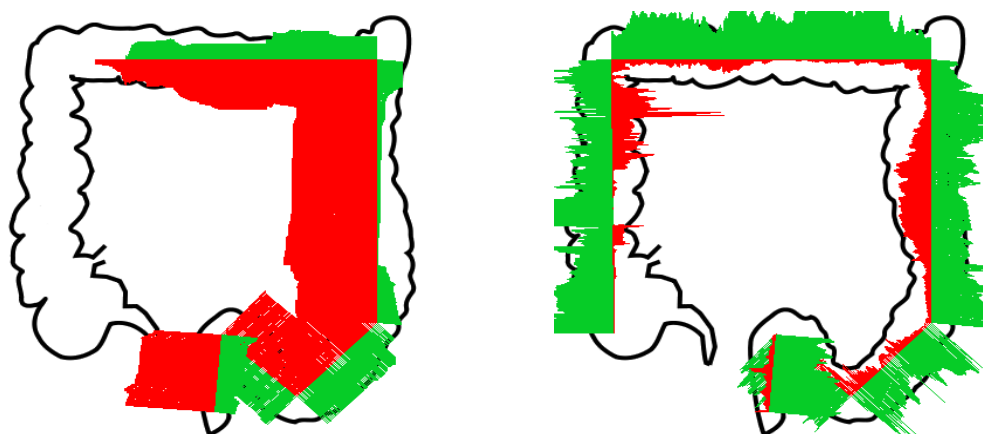
Figure A.18: Distribution of the UC lesions for the patient 23. Medical annotations on the left, and automatic detection on the right.
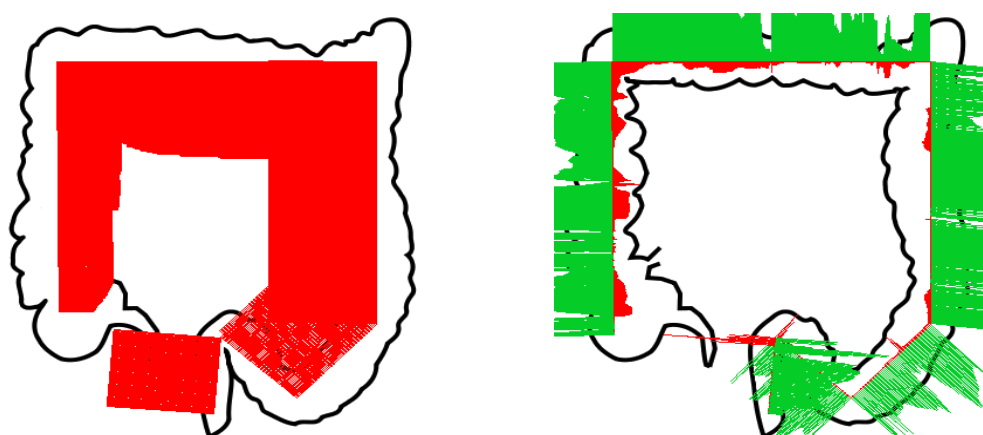
Figure A.19: Distribution of the UC lesions for the patient 24. Medical annotations on the left, and automatic detection on the right.
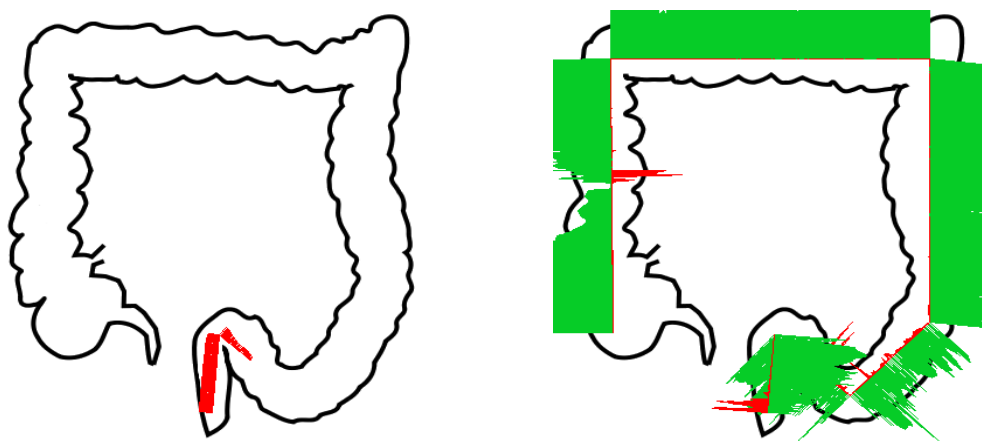
Figure A.20: Distribution of the UC lesions for the patient 27. Medical annotations on the left, and automatic detection on the right.
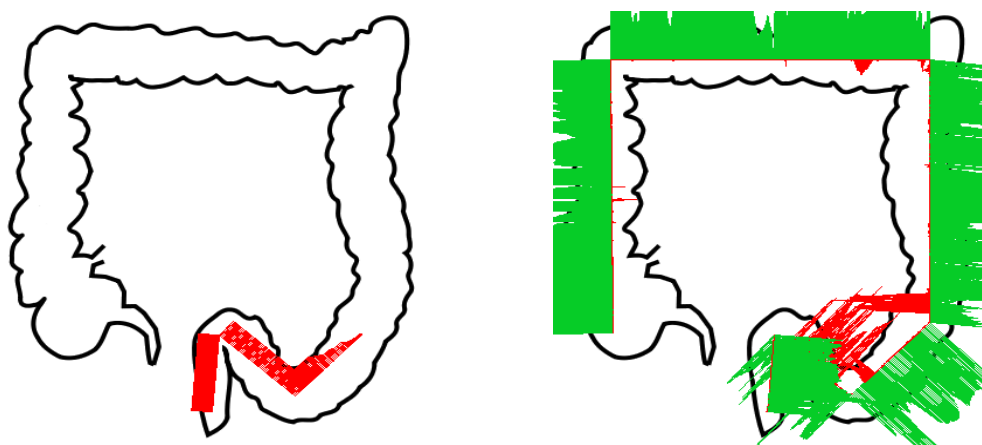
Figure A.21: Distribution of the UC lesions for the patient 29. Medical annotations on the left, and automatic detection on the right.
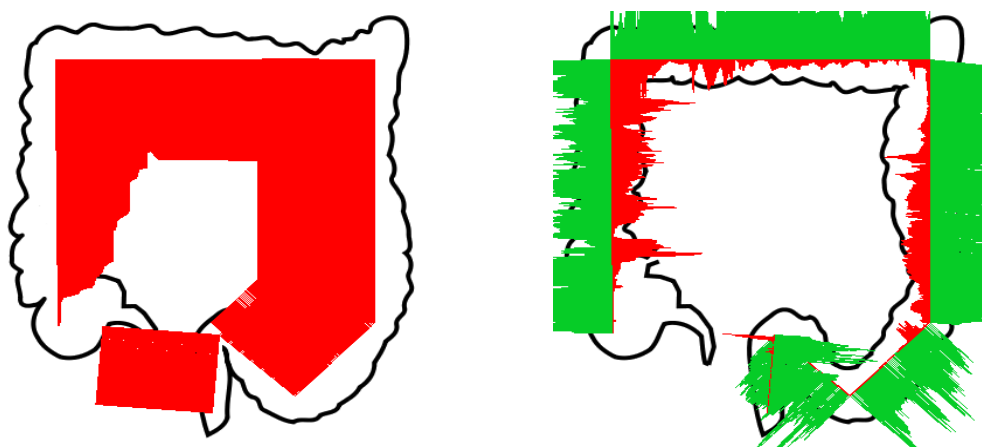
Figure A.22: Distribution of the UC lesions for the patient 31. Medical annotations on the left, and automatic detection on the right.
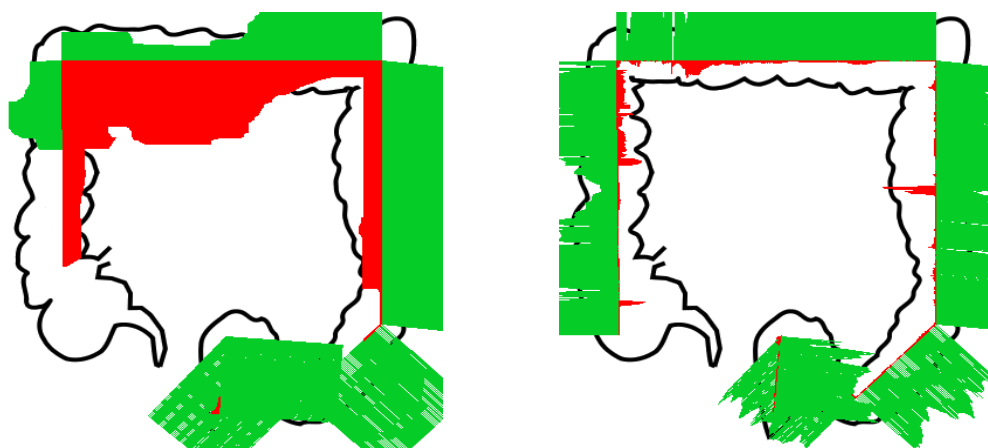
Figure A.23: Distribution of the UC lesions for the patient 32. Medical annotations on the left, and automatic detection on the right.
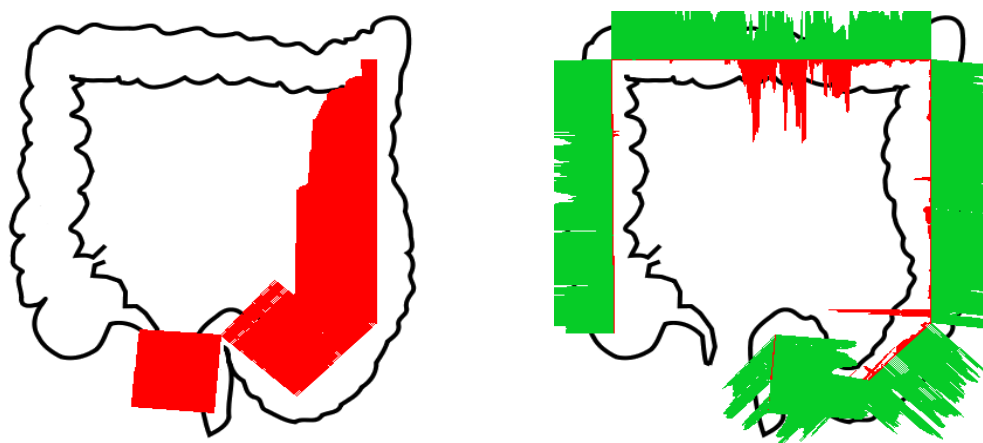
Figure A.24: Distribution of the UC lesions for the patient 33. Medical annotations on the left, and automatic detection on the right.
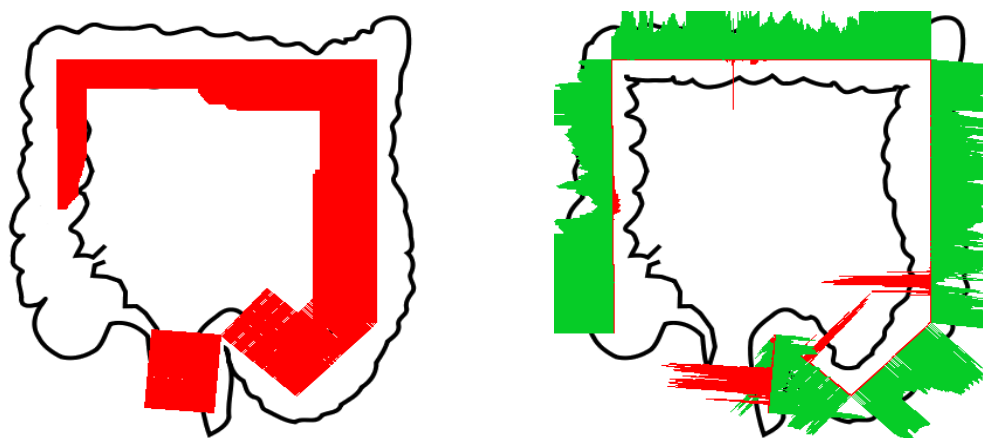
Figure A.25: Distribution of the UC lesions for the patient 34. Medical annotations on the left, and automatic detection on the right.
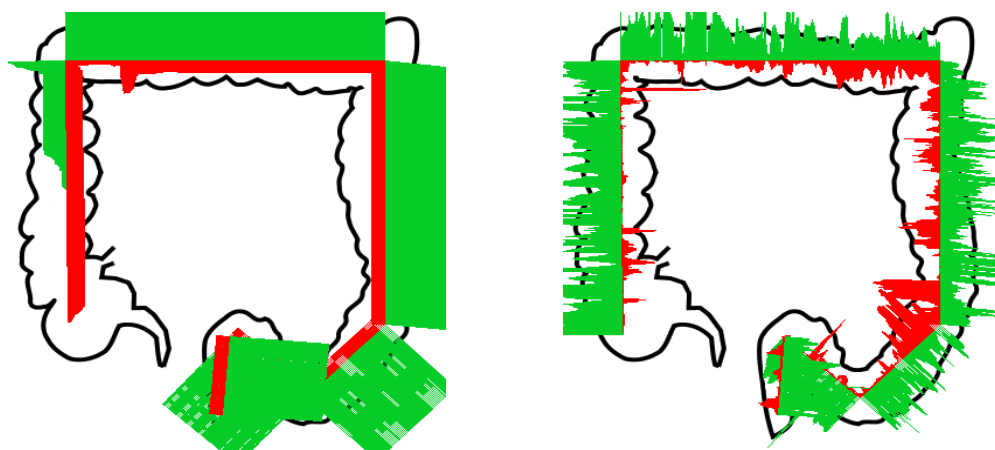
Figure A.26: Distribution of the UC lesions for the patient 37. Medical annotations on the left, and automatic detection on the right.
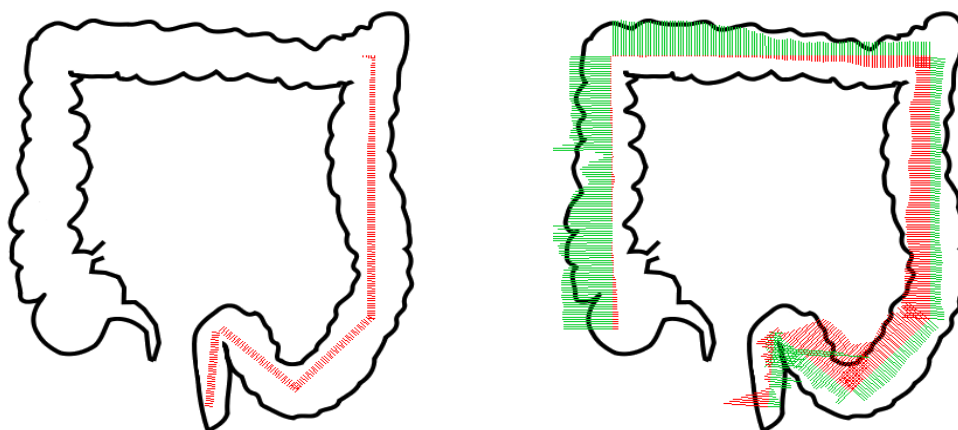
Figure A.27: Distribution of the UC lesions for the patient 38. Medical annotations on the left, and automatic detection on the right.
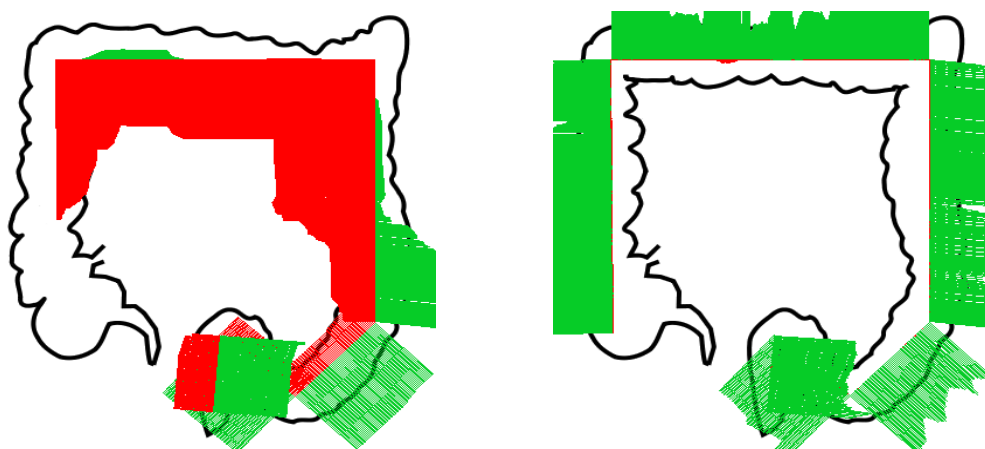
Figure A.28: Distribution of the UC lesions for the patient 39. Medical annotations on the left, and automatic detection on the right.
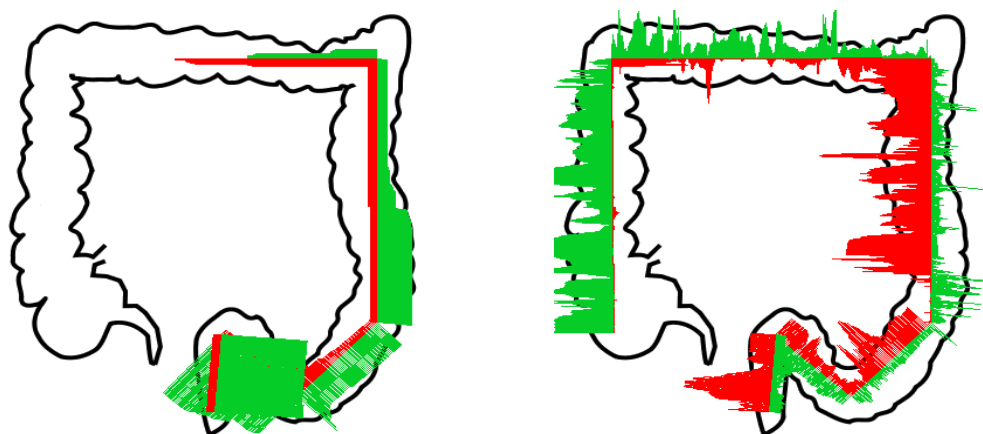
Figure A.29: Distribution of the UC lesions for the patient 40. Medical annotations on the left, and automatic detection on the right.
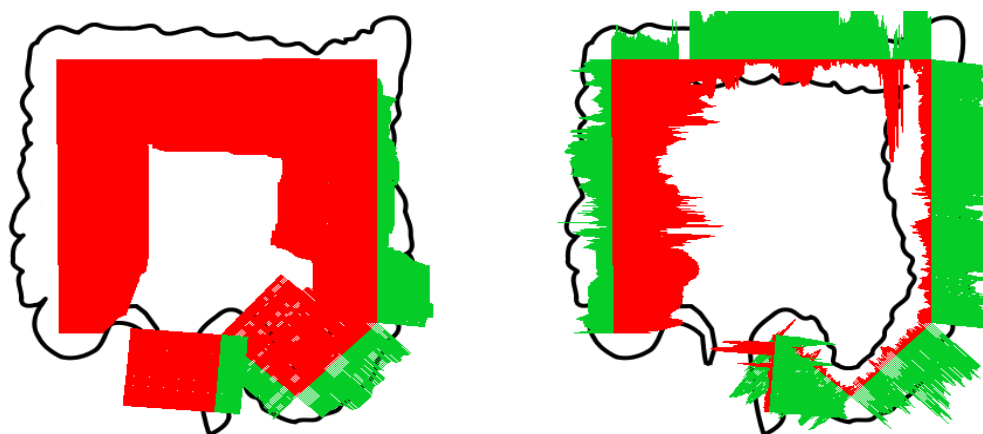
Figure A.30: Distribution of the UC lesions for the patient 41. Medical annotations on the left, and automatic detection on the right.
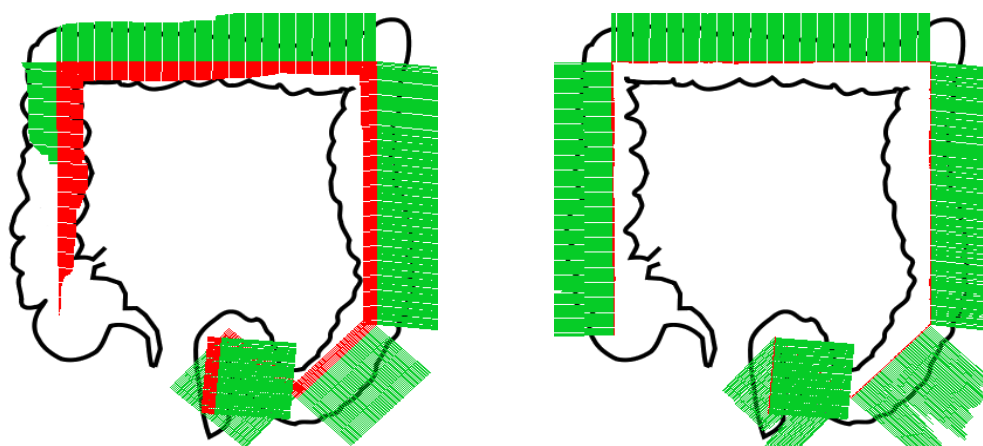
Figure A.31: Distribution of the UC lesions for the patient 42. Medical annotations on the left, and automatic detection on the right.
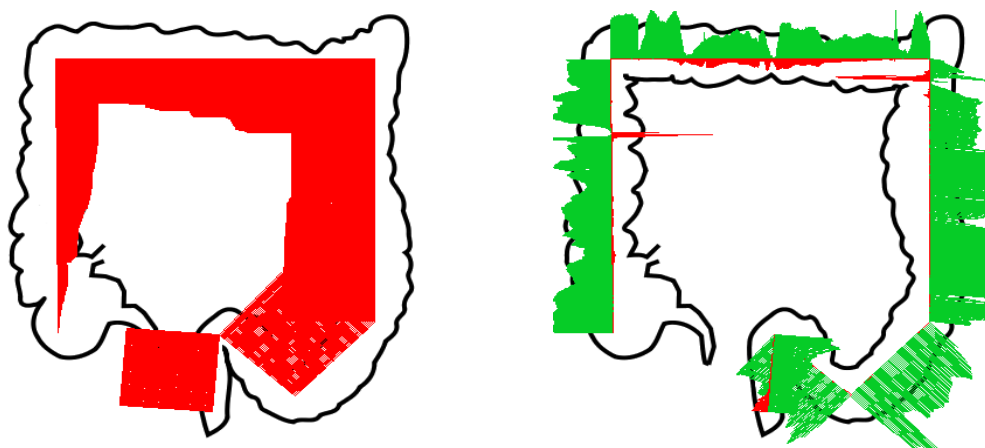
Figure A.32: Distribution of the UC lesions for the patient 43. Medical annotations on the left, and automatic detection on the right.
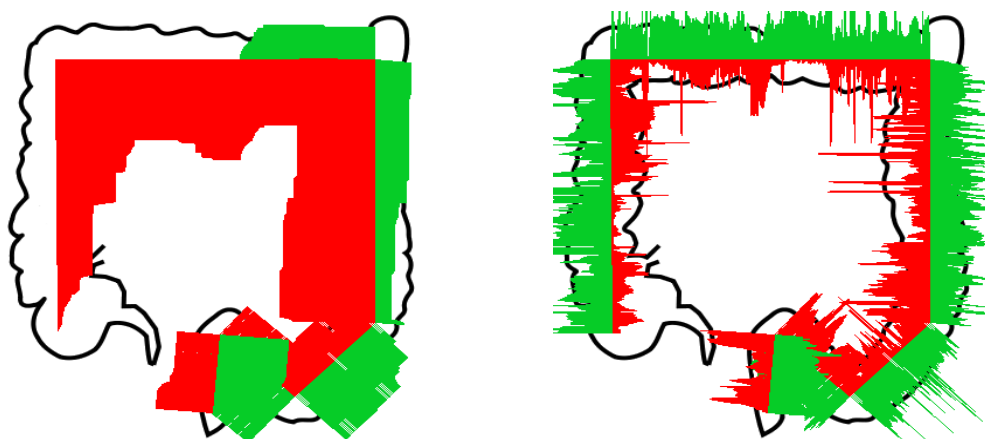
Figure A.33: Distribution of the UC lesions for the patient 44. Medical annotations on the left, and automatic detection on the right.
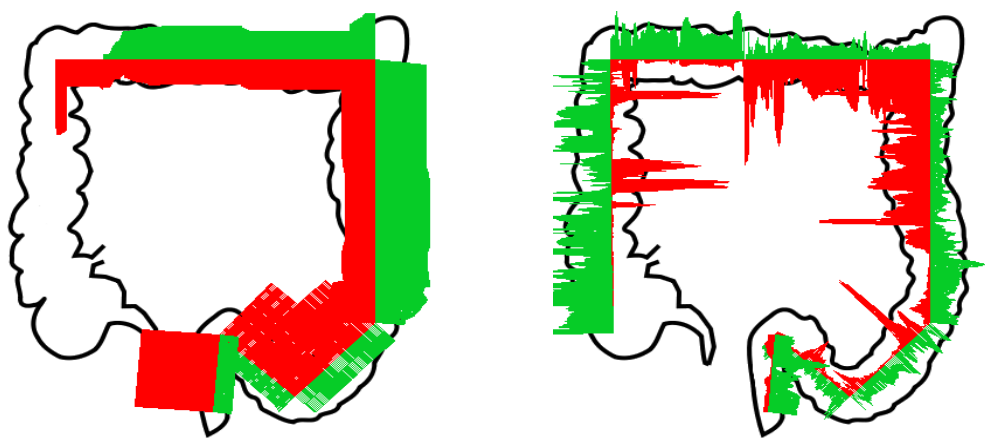
Figure A.34: Distribution of the UC lesions for the patient 46. Medical annotations on the left, and automatic detection on the right.
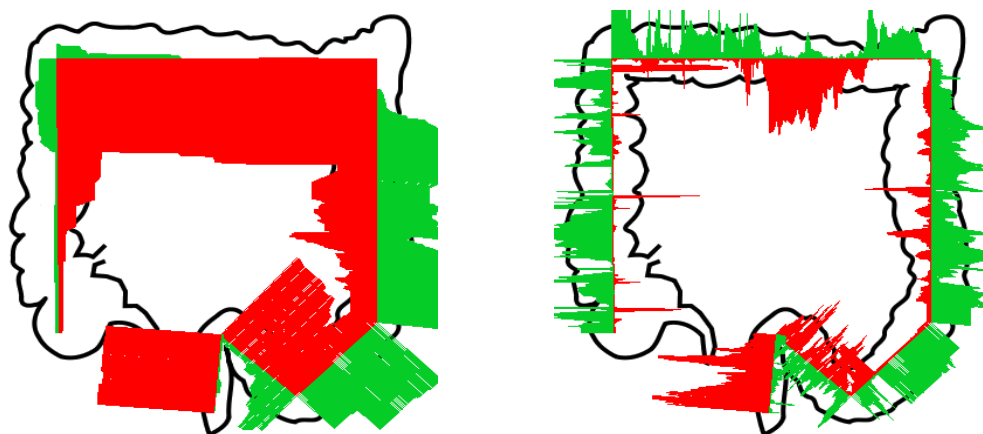
Figure A.35: Distribution of the UC lesions for the patient 47. Medical annotations on the left, and automatic detection on the right.
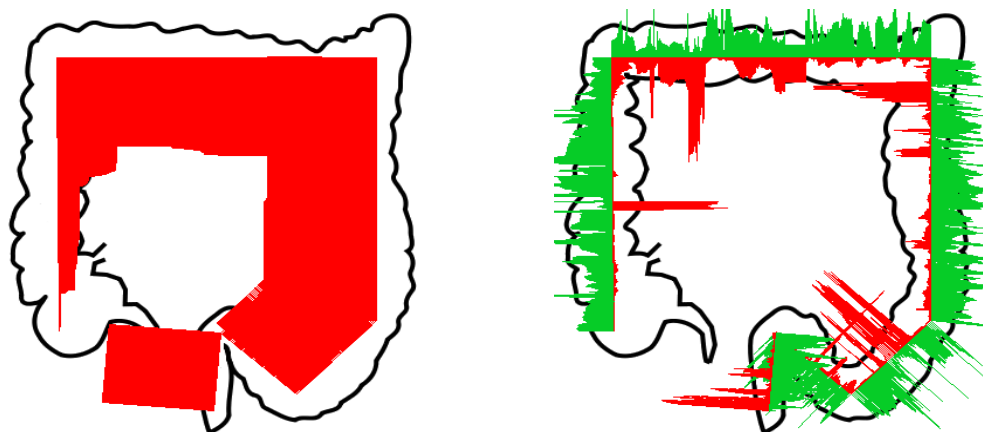
Figure A.36: Distribution of the UC lesions for the patient 48. Medical annotations on the left, and automatic detection on the right.
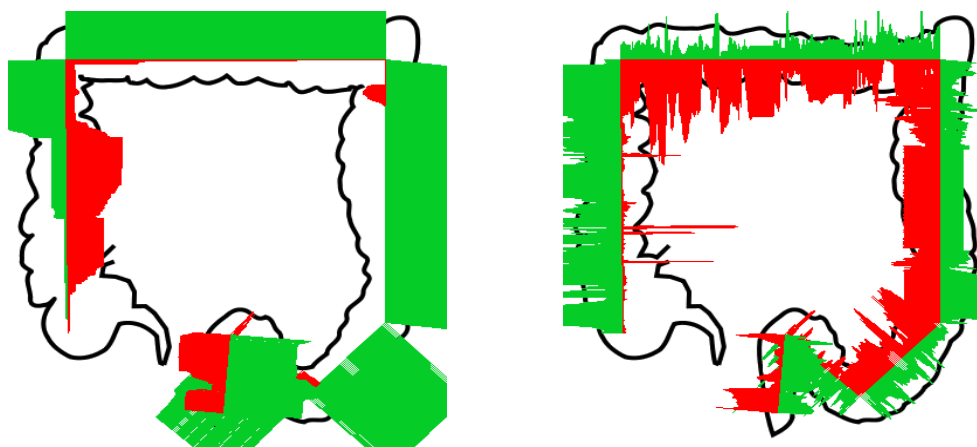
Figure A.37: Distribution of the UC lesions for the patient 49. Medical annotations on the left, and automatic detection on the right.

Appendix B

Fisher KPP simulations

This chapter encounters three parts that follow the work presented in chapter 10. First, we present the details of computation of the discretized from of the Fisher-KPP equation given by Equation (10.3). Second, we simulate it for some cases of initial conditions and diffusion terms. Third, we show the profile of generated Fisher-KPP equation in comparison with the lesions profile extracted from the colonoscopy videos.

B.1 Numerical scheme FTCS

In this section, we give some steps to obtain the discrestized form of the Fisher-KPP equation using the Forward in Time and Centered in Space numerical scheme (FTCS). In order to distinguish between space and time coordinates, superscript index j is used for time coordinate wheras subscript i is used to represent the space position i.e. the value of variable u at time $t = j$ and position $x = i$ will be written as $u_i^n = u(x = x_i, t = n)$, $x_i = i \times \Delta_x$, for $i \in \{1, .., N_x\}$, supposing that we discretise the space domain into N_x equal points and $j \in \{0, .., N_t\}$ where N_t is the number of discrestized points of the time interval.
The explicit time derivative formula:

$$u_t = \frac{u(x_i, t_{j+1}) - u(x_i, t_j)}{\Delta t} + O(\Delta t) \tag{B.1}$$

And the centered space derivative (Taylor):

$$u_{xx} = \frac{u(x_{i-1}, t_j) - 2u(x_i, t_j) + u(x_{i+1}, t_j)}{\Delta x^2} + O(\Delta x^2) \tag{B.2}$$

We suppose that we want to solve the reaction diffusion equation in a one dimensional domain i.e. $\Omega = \{x \in \mathbb{R}, 0 \leq x \leq L = 1\}$ and time interval
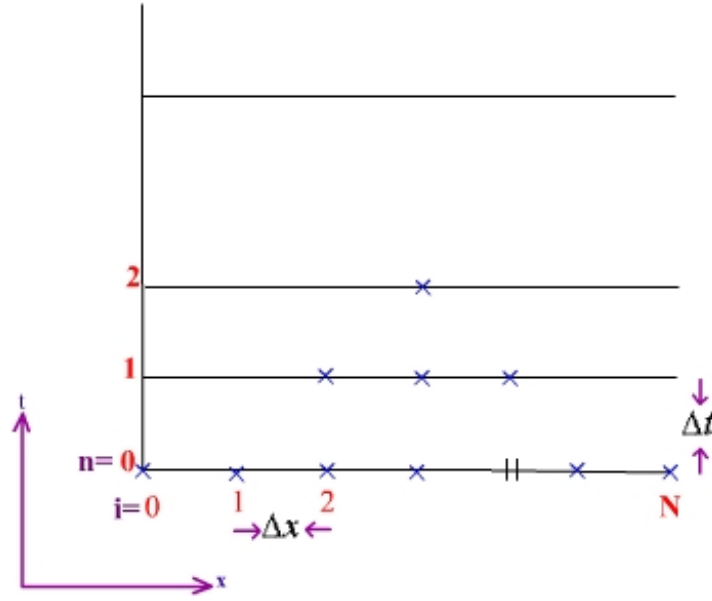
Figure B.1: Space and time discretization for the FTCS numerical scheme. Δ_x is the time step and Δ_t is the time step.

$\{0 \leq t \leq T, T \in \mathbb{R}^*\}$. The initial and boundary conditions are written as follows:

$$
\begin{aligned}
u(x,0) &= g(x), \text{ initial space distribution} \\
u(0,t) &= g_1(t) \\
u(L,t) &= g_2(t)
\end{aligned}
$$

The new discretised form of the reaction diffusion given in Equation (10.2) will remain:

$$
\frac{u(x_i, t_{j+1}) - u(x_i, t_j)}{\Delta t} = D \times \frac{u(x_{i-1}, t_j) - 2u(x_i, t_j) + u(x_{i+1}, t_j)}{\Delta x^2} \\
+ f(u(x_i, t_j)) + O(\Delta t + \Delta x^2), \tag{B.3}
$$

and, the estimated value of u at any point x_i and time step $t+1$ for Equation (10.3) will be formulated as follows:

$$
u(x_i, t_{j+1}) = u(x_i, t_j) + \frac{D\Delta t}{\Delta x^2}(u(x_{i-1}, t_j) - 2u(x_i, t_j) + u(x_{i+1}, t_j)) \\
+ \Delta t \left(u(x_i, t_j) - u(x_i, t_j)^2 \right) \tag{B.4}
$$

or also

$$
u_i^{j+1} = u_i^j + \frac{D\Delta t}{\Delta x^2}(u_{i-1}^j - 2u_i^j + u_{i+1}^j) + \Delta t \left(u_i^j - (u_i^j)^2 \right). \tag{B.5}
$$

It is well-known that proposed scheme approximates the continuous operator to order $O(\Delta_t + \Delta_x^2)$. At the space position x_n when $n = 1$, the unknown

variable u is first calculated using the initial conditions at time $t = 0$ and boundary conditions applied to values $x = 0$ and $x = L$. Once the solution at time level t_1 ($= t_0 + \Delta_t$) is obtained, the solution at level $n = 2$ is calculated in the same manner by making use of the solution at $n = 1$ and the boundary conditions at $x = 0$ and $x = L$. The same procedure is repeated until the solution reaches a steady state or until the required time maximum level is achieved.

Let denote $CFL = D\frac{\Delta_t}{\Delta_x^2}$, the Courant-Friedrichs-Levy also called CFL condition, named according to researchers who first described this requirement. *CFL* required to be bounded by a constant depending upon the particular numerical scheme. Due to the absence of a better method to get an approximate difference formula, the only requirement is that the obtained differentiate formula, must justify some tests for accuracy, consistency, stability and convergence [AM17]. By Von Neumann stability analysis, the FTCS scheme is always conditionally stable, for $0 < CFL \leq \frac{1}{2}$. During our work presented in chapter 10, we take into account the CFL condition for the chosen Δ_t and Δ_x in order to get a stable sheme.

B.2   Some examples of Fisher-KPP simulations

In this section, we give examples of simulations for the following proposition:

Proposition 7. *[BD15] For all initial conditions u_0 decreasing fast enough, there exists travelling wave fronts. If u_0 is with compact support, there exist two wave fronts: the first one comes from right and the second comes from left. If $u_0(0, t) = 0$ and $u_0(L = 1, t) = 1$, only one left moving wave front appears.*

First of all we consider different initial conditions, and then different diffusion parameters.

- **Different initial conditions but the same diffusion parameter:** We simulate the Fisher-KPP equation for $x \in X = [-20, 20]$ with space step $\Delta_x = 0.1$ and time $t \in [0, 6]$ with step $\Delta_t = 0.002$ and diffusion parameter $D = 2$. We choose two different initial conditions that are represented in black in Figure B.2. We can see that for all initial conditions u_0 decreasing fast enough, there exists travelling wavefronts. If u_0 is with compact support, then there exist two wavefronts: the first from the right and the second from the left. If $u_0(0, t) = 0$ and $u_0(L = 1, t) = 1$, only one left moving wavefront appears [BD15].

- **Same initial condition with different diffusion parameters** We also simulate the Fisher-KPP (Equation (10.3)) for $x \in X = [-20, 20]$ with space step $\Delta_x = 0.1$ and time $t \in [0, 6]$ with step $\Delta_t = 0.002$. In Figure B.3, we show that the asymptotic behaviour of the solution computed for two diffusion parameters $D_1 = 2$ and $D_2 = 4$ for the same initial condition

(represented in black). The profile of the travelling wave is the same with some dilation.
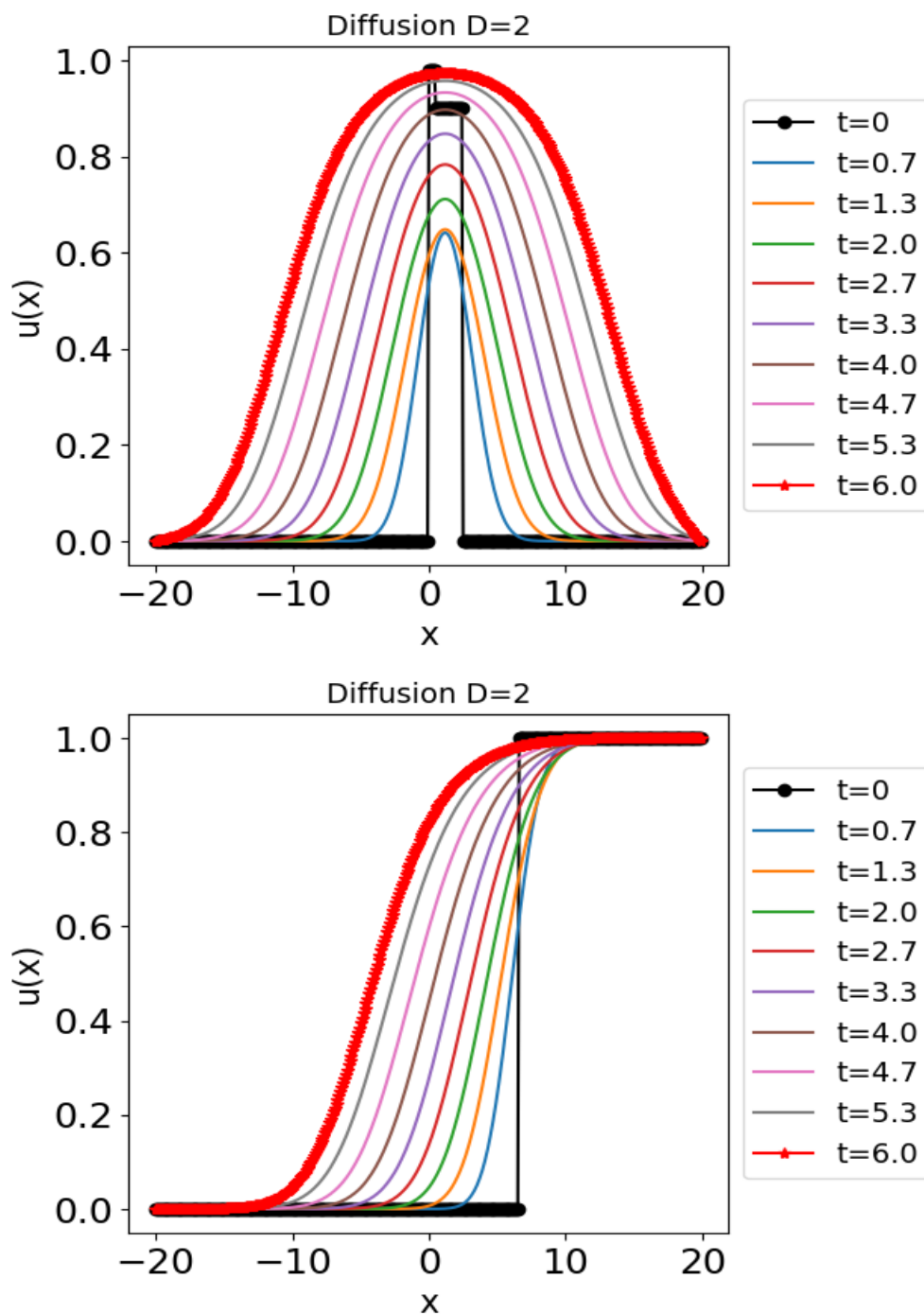
Figure B.2: Simulation of Fisher-KPP solution with two different initial conditions u_0 that are compactly supported. The same value of the diffusion parameter $D = 2$ was employed.
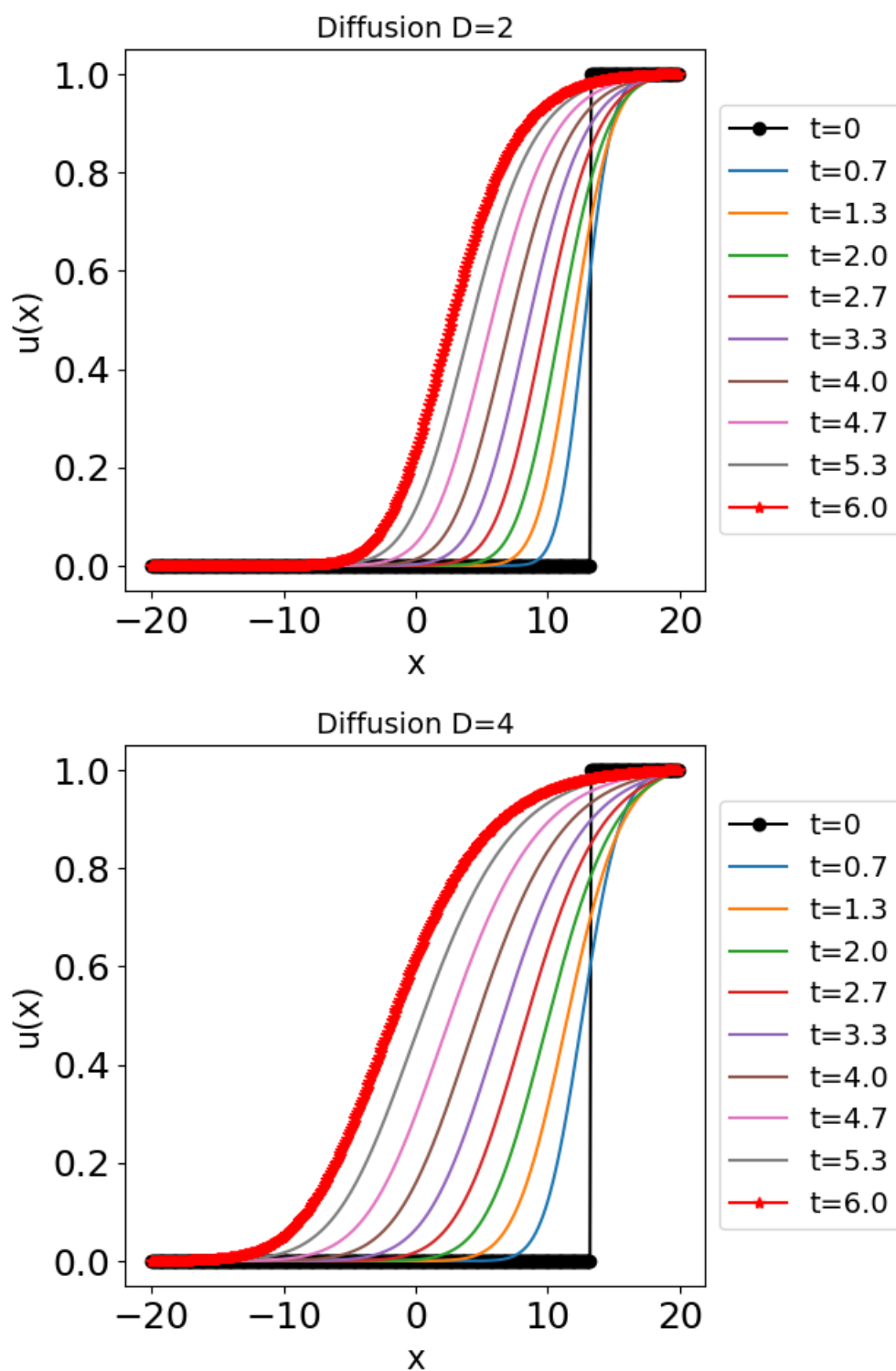
Figure B.3: Simulation of Fisher-KPP solution with initial condition u_0 compactly supported (black) with two different diffusion parameters.

B.3 Profile of patients compared to FKPP model

In this section, we plot the simulated profile by the Fisher-KPP equation for some patients from the Vatic database. As done in chapter 10, we test the same set of diffusion parameter $S_D = [0.01^2, 0.02^2]$ with step 0.0005 to find the optimal dilation in the case of bleeding and ulcers.
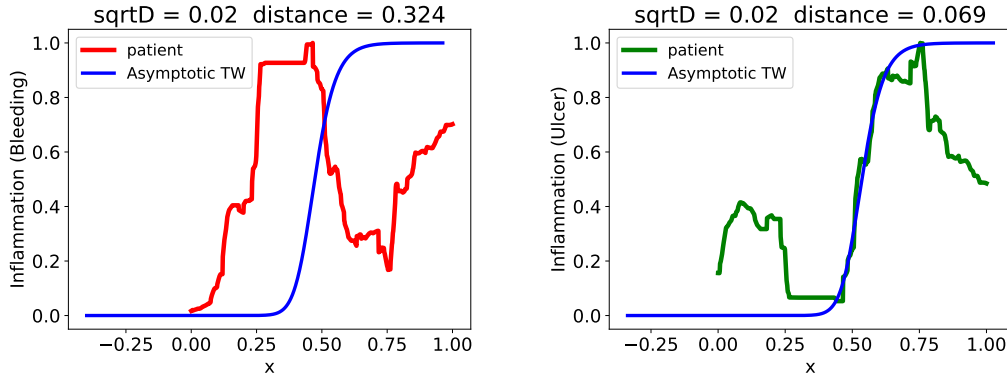
Figure B.4: Rescaling of the travelling wavefront u^A for patient of video 1 with optimal diffusion for bleeding lesions $D_b^* = 0.02^2$ and ulcers $D_u^* = 0.02^2$.
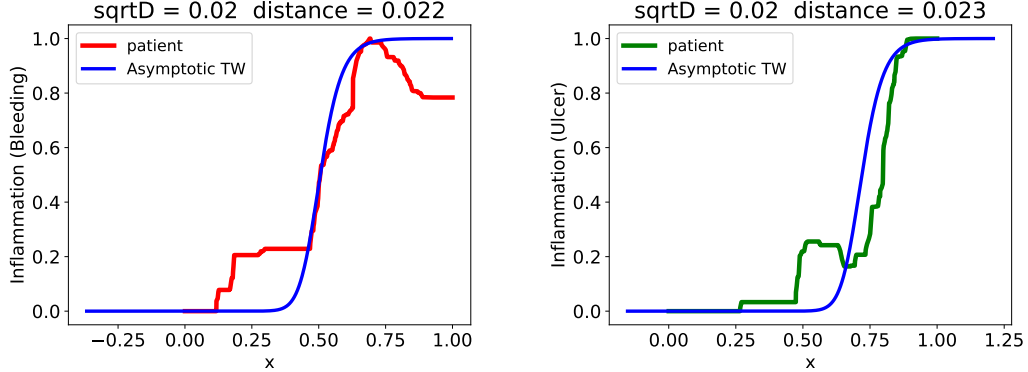
Figure B.5: Rescaling of the travelling wavefront u^A for patient of video 10 with optimal diffusion for bleeding lesions $D_b^* = 0.02^2$ and ulcers $D_u^* = 0.02^2$.
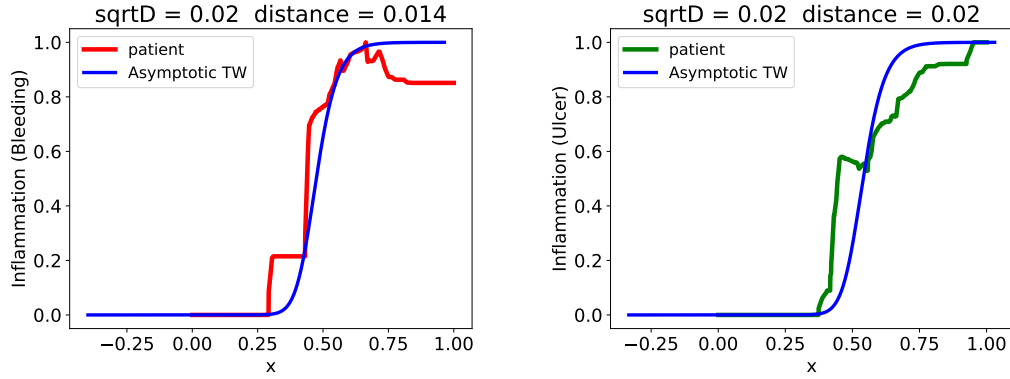
Figure B.6: Rescaling of the travelling wavefront u^A for patient of video 13 with optimal diffusion for bleeding lesions $D_b^* = 0.02^2$ and ulcers $D_u^* = 0.02^2$
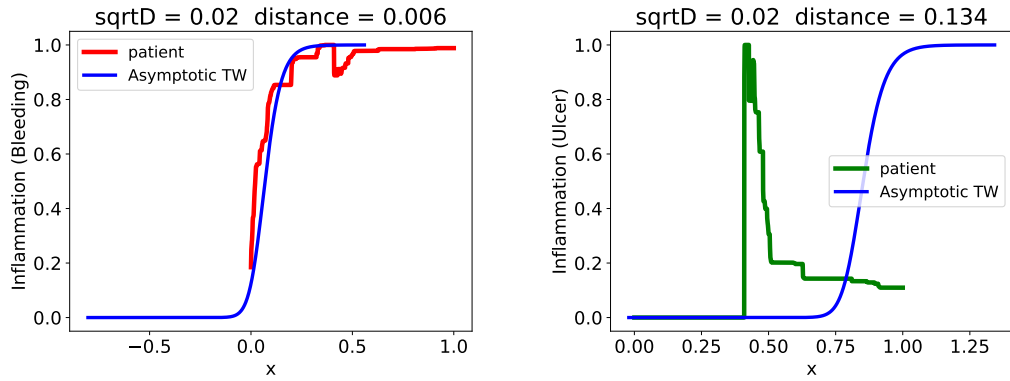
Figure B.7: Rescaling of the travelling wavefront u^A for patient of video 16 with optimal diffusion for bleeding lesions $D_b^* = 0.02^2$ and ulcers $D_u^* = 0.02^2$.

Bibliography

[AA+22]   Safaa Al-Ali et al. "AUTOMATIC BLEEDING AND ULCER DE-
            TECTION FROM LIMITED QUALITY ANNOTATIONS IN UL-
            CERATIVE COLITIS". In: *Inflammatory Bowel Diseases* 28.Supple-
            ment 1 (Jan. 2022), S19–S20. ISSN: 1078-0998. DOI: 10.1093/ibd/
            izac015.029. eprint: https://academic.oup.com/ibdjournal/
            article-pdf/28/Supplement_1/S19/42272480/izac015.029.
            pdf. URL: https://doi.org/10.1093/ibd/izac015.029.

[Ach+12a]   Radhakrishna Achanta et al. "SLIC superpixels compared to state-
            of-the-art superpixel methods". In: *IEEE transactions on pattern
            analysis and machine intelligence* 34.11 (2012), pp. 2274–2282.

[Ach+12b]   Radhakrishna Achanta et al. "SLIC superpixels compared to state-
            of-the-art superpixel methods". In: *IEEE transactions on pattern
            analysis and machine intelligence* 34.11 (2012), pp. 2274–2282.

[Ala+22]   S Alali et al. "P015 Detection of endoscopic lesions from limited
            quality annotations in colonoscopy videos". In: *Journal of Crohn's
            and Colitis* 16.Supplement 1 (Jan. 2022), pp. i142–i144. ISSN: 1873-
            9946. DOI: 10.1093/ecco-jcc/jjab232.144. eprint: https://
            academic.oup.com/ecco-jcc/article-pdf/16/Supplement_1/
            i142/42250428/jjab232.144.pdf. URL: https://doi.org/10.
            1093/ecco-jcc/jjab232.144.

[AM17]   Bader Saad Alshammari and Daoud Suleiman Mashat. "Numer-
            ical study of Fisher's equation by finite difference schemes". In:
            Applied Mathematics 8.8 (2017), pp. 1100–1116.

[AN17]   Raja Atreya and Markus F Neurath. "Current and future targets
            for mucosal healing in inflammatory bowel disease". In: *Visceral
            medicine* 33.1 (2017), pp. 82–88.

[ARG15]   Mary A Atia, Francisco C Ramirez, and Suryakanth R Gurudu.
            "Quality monitoring in colonoscopy: Time to act". In: *World journal
            of gastrointestinal endoscopy* 7.4 (2015), p. 328.

[AZ79]   Mark J Ablowitz and Anthony Zeppetella. "Explicit solutions of
            Fisher's equation for a special wave speed". In: *Bulletin of Mathe-
            matical Biology* 41.6 (1979), pp. 835–840.

[Bar+12]   Bradley A Barth et al. "Equipment for pediatric endoscopy". In: *Gastrointestinal endoscopy* 76.1 (2012), pp. 8–17.

[Bar+85]   GI Barenblatt et al. "The mathematical theory of combustion and explosions". In: *Consultants Bureau* (1985).

[Bas+12]   Md Rubel Basar et al. "Ingestible wireless capsule technology: A review of development and future indication". In: *International Journal of Antennas and Propagation* 2012 (2012).

[BCLJ64a]   JH Baron, AM Connell, and JE Lennard-Jones. "Variation between observers in describing mucosal appearances in proctocolitis". In: *British Medical Journal* 1.5375 (1964), p. 89.

[BCLJ64b]   JH Baron, AM Connell, and JE Lennard-Jones. "Variation between observers in describing mucosal appearances in proctocolitis". In: *British medical journal* 1.5375 (1964), p. 89.

[BD15]   Éric Brunet and Bernard Derrida. "An exactly solvable travelling wave equation in the Fisher–KPP class". In: *Journal of Statistical Physics* 161.4 (2015), pp. 801–820.

[BKL11]   Giorgos Bamias, Garyfallia Kaltsa, and Spiros D Ladas. "Cytokines in the pathogenesis of ulcerative colitis". In: *Discovery medicine* 11.60 (2011), pp. 459–467.

[BT11]   Nick H Barton and Michael Turelli. "Spatial waves of advance with bistable dynamics: cytoplasmic and genetic analogues of Allee effects". In: *The American Naturalist* 178.3 (2011), E48–E75.

[Buc+18]   Sarah Buckley et al. "Endoscopic Appendectomy in a Patient with Malrotation and Previous Ladd Procedure: 1703". In: *Official journal of the American College of Gastroenterology| ACG* 113 (2018), S971–S972.

[Che+21]   Tao Chen et al. "Transcolonic endoscopic appendectomy: a novel natural orifice transluminal endoscopic surgery (NOTES) technique for the sessile serrated lesions involving the appendiceal orifice". In: *Gut* (2021). ISSN: 0017-5749. DOI: 10.1136/gutjnl-2020-323018. eprint: https://gut.bmj.com/content/early/2021/01/21/gutjnl-2020-323018.full.pdf. URL: https://gut.bmj.com/content/early/2021/01/21/gutjnl-2020-323018.

[Chi+18]   Nai-Hsuan Chien et al. "Cold snare polypectomy vs cold forceps biopsy in endoscopic treatment of colonic small and diminutive polyps—Effectiveness and safety in the real world". In: *Advances in Digestive Medicine* 5.4 (2018), pp. 127–131. DOI: https://doi.org/10.1002/aid2.13093. eprint: https://onlinelibrary.wiley.com/doi/pdf/10.1002/aid2.13093. URL: https://onlinelibrary.wiley.com/doi/abs/10.1002/aid2.13093.

[CMH15]   Shannon Chang, Lisa Malter, and David Hudesman. "Disease monitoring in inflammatory bowel disease". In: *World Journal of Gastroenterology: WJG* 21.40 (2015), p. 11246.

[Cos+11]   Jacques Cosnes et al. "Epidemiology and natural history of inflammatory bowel diseases". In: *Gastroenterology* 140.6 (2011), pp. 1785–1794.

[Dav+21]   Vivek Pravin Dave et al. "Intraocular endoscopy: A review". In: *Indian Journal of Ophthalmology* 69.1 (2021), p. 14.

[Dee+18]   Farah Deeba et al. "Performance assessment of a bleeding detection algorithm for endoscopic video based on classifier fusion method and exhaustive feature selection". In: *Biomedical Signal Processing and Control* 40 (2018), pp. 415–424.

[DF11]   Silvio Danese and Claudio Fiocchi. "Ulcerative Colitis". In: *New England Journal of Medicine* 365.18 (2011). PMID: 22047562, pp. 1713–1725. DOI: 10.1056/NEJMra1102942. eprint: https://doi.org/10.1056/NEJMra1102942. URL: https://doi.org/10.1056/NEJMra1102942.

[D'h+07]   Geert D'haens et al. "A review of activity indices and efficacy end points for clinical trials of medical therapy in adults with ulcerative colitis". In: *Gastroenterology* 132.2 (2007), pp. 763–786.

[DLLA04]   Thomas De Lange, Stig Larsen, and Lars Aabakken. "Interobserver agreement in the assessment of endoscopic findings in ulcerative colitis". In: *BMC gastroenterology* 4.1 (2004), pp. 1–10.

[DXL14]   Tom C DeRoche, Shu-Yuan Xiao, and Xiuli Liu. "Histological evaluation in ulcerative colitis". In: *Gastroenterology report* 2.3 (2014), pp. 178–192.

[Fan+18]   Shanhui Fan et al. "Computer-aided detection of small intestinal ulcer and erosion in wireless capsule endoscopy images". In: *Physics in Medicine & Biology* 63.16 (2018), p. 165001.

[Fea+05]   Brian G Feagan et al. "Treatment of ulcerative colitis with a humanized antibody to the $\alpha 4\beta 7$ integrin". In: *New England Journal of Medicine* 352.24 (2005), pp. 2499–2507.

[FK99]   Miguel A Fuentes and Marcelo N Kuperman. "Cellular automata and epidemiological models with spatial dependence". In: *Physica A: Statistical Mechanics and its Applications* 267.3-4 (1999), pp. 471–486.

[FMG11]   Yanan Fu, Mrinal Mandal, and Gencheng Guo. "Bleeding region detection in WCE images based on color features and neural network". In: *2011 IEEE 54th International Midwest Symposium on Circuits and Systems (MWSCAS)*. IEEE. 2011, pp. 1–4.

[FMM80]   RICHARD G FARMER, WILLIAM M MICHENER, and EDWARD A MORTIMER. "Studies of family history among patients with inflammatory bowel disease". In: *Clinics in gastroenterology* 9.2 (1980), pp. 271–278.

[Fu+14]   Y. Fu et al. "Computer-Aided Bleeding Detection in WCE Video". In: *IEEE Journal of Biomedical and Health Informatics* 18.2 (2014), pp. 636–642.

[Gau+10]   J Gaudart et al. "Demography and diffusion in epidemics: malaria and black death spread". In: *Acta Biotheoretica* 58.2 (2010), pp. 277–305.

[Gau+19]   Anchal Gaur et al. "CHALLENGES IN DEVELOPMENT OF COLON DRUG DELIVERY SYSTEM WITH RESPECT TO DISSOLUTION STUDIES". In: *WORLD JOURNAL OF PHARMACY AND PHARMACEUTICAL SCIENCES* 8 (July 2019), pp. 1465–1491. DOI: `10.20959/wjpps20196-14051`.

[Gaw+17]   Beata Gawrońska et al. "Markers of inflammation and influence of nitric oxide on platelet activation in the course of ulcerative colitis". In: *Oncotarget* 8.40 (2017), p. 68108.

[GDS16]   Tonmoy Ghosh, Antara Das, and Rosni Sayed. "Automatic small intestinal ulcer detection in capsule endoscopy images". In: *International Journal of Scientific and Engineering Research* 7.10 (2016), pp. 737–741.

[GFW18]   Tonmoy Ghosh, Shaikh Anowarul Fattah, and Khan A Wahid. "CHOBS: color histogram of block statistics for automatic bleeding detection in wireless capsule endoscopy video". In: *IEEE journal of translational engineering in health and medicine* 6 (2018), pp. 1–12.

[Gho+14a]   Tonmoy Ghosh et al. "A statistical feature based novel method to detect bleeding in wireless capsule endoscopy images". In: *2014 International Conference on Informatics, Electronics & Vision (ICIEV)*. IEEE. 2014, pp. 1–4.

[Gho+14b]   Tonmoy Ghosh et al. "An automatic bleeding detection scheme in wireless capsule endoscopy based on histogram of an RGB-indexed image". In: *2014 36th Annual International Conference of the IEEE Engineering in Medicine and Biology Society*. IEEE. 2014, pp. 4683–4686.

[Gho+15]   Tonmoy Ghosh et al. "An automatic bleeding detection technique in wireless capsule endoscopy from region of interest". In: *2015 IEEE International Conference on Digital Signal Processing (DSP)*. IEEE. 2015, pp. 1293–1297.

[Gho+18a]   Tonmoy Ghosh et al. "Cluster based statistical feature extraction method for automatic bleeding detection in wireless capsule endoscopy video". In: *Computers in biology and medicine* 94 (2018), pp. 41–54.

[Gho+18b]   Tonmoy Ghosh et al. "Cluster based statistical feature extraction method for automatic bleeding detection in wireless capsule endoscopy video". In: *Computers in biology and medicine* 94 (2018), pp. 41–54.

[Gom+86]   P Gomes et al. "Relationship between disease activity indices and colonoscopic findings in patients with colonic inflammatory bowel disease." In: *Gut* 27.1 (1986), pp. 92–95.

[HH15]   Ahnaf Rashik Hassan and Mohammad Ariful Haque. "Computer-aided gastrointestinal hemorrhage detection in wireless capsule endoscopy videos". In: *Computer methods and programs in biomedicine* 122.3 (2015), pp. 341–353.

[HJ18]   Xiaochuan Hu and Sophia R.-J. Jang. "Dynamics of tumor–CD4+–cytokine–host cells interactions with treatments". In: *Applied Mathematics and Computation* 321 (2018), pp. 700–720. ISSN: 0096-3003. DOI: https://doi.org/10.1016/j.amc.2017.11.009. URL: https://www.sciencedirect.com/science/article/pii/S0096300317307828.

[Idd+00]   Gavriel Iddan et al. "Wireless capsule endoscopy". In: *Nature* 405.6785 (2000), pp. 417–417.

[Ike+16]   Kentaro Ikeya et al. "The ulcerative colitis endoscopic index of severity more accurately reflects clinical outcomes and long-term prognosis than the Mayo endoscopic score". In: *Journal of Crohn's and Colitis* 10.3 (2016), pp. 286–295.

[KFR18]   Amit Kumar Kundu, Shaikh Anowarul Fattah, and Mamshad Nayeem Rizve. "An automatic bleeding frame and region detection scheme for wireless capsule endoscopy videos based on interplane intensity variation profile in normalized RGB color space". In: *Journal of healthcare engineering* 2018 (2018).

[KG15]   Nimisha Elsa Koshy and Varun P Gopi. "A new method for ulcer detection in endoscopic images". In: *2015 2nd International Conference on Electronics and Communication Systems (ICECS)*. IEEE. 2015, pp. 1725–1729.

[KLZ10]   Kwang Ik Kim, Zhigui Lin, and Lai Zhang. "Avian-human influenza epidemic model with diffusion". In: *Nonlinear Analysis: Real World Applications* 11.1 (2010), pp. 313–322.

[KOKV22]   Aleksandra Kałużna, Paweł Olczyk, and Katarzyna Komosińska-Vassev. "The Role of Innate and Adaptive Immune Cells in the Pathogenesis and Development of the Inflammatory Response in Ulcerative Colitis". In: *Journal of Clinical Medicine* 11.2 (2022), p. 400.

[Kol37]   Andrei N Kolmogorov. "Étude de l'équation de la diffusion avec croissance de la quantité de matière et son application à un problème biologique". In: *Bull. Univ. Moskow, Ser. Internat., Sec. A* 1 (1937), pp. 1–25.

[Kri08]   KK Kristiansen. "Reaction Diffusion Models in Mathematical Biology Technical University of Denmark". In: *The Department of Mathematics, Lyngby, Denmark* (2008).

[Kum+]   R Vijaya Kumar et al. "Grey level to RGB using YCbCr color space Technique". In: *International Journal of Computer Applications* 975 (), p. 8887.

[LAF13]   Wing-Cheong Lo, Razvan I Arsenescu, and Avner Friedman. "Mathematical model of the roles of T cells in inflammatory bowel

disease". In: *Bulletin of mathematical biology* 75.9 (2013), pp. 1417–1433.

[Lai+09] Edwin J Lai et al. "The Boston bowel preparation scale: a valid and reliable instrument for colonoscopy-oriented research". In: *Gastrointestinal endoscopy* 69.3 (2009), pp. 620–625.

[Lan+07] Robert C Langan et al. "Ulcerative colitis: diagnosis and treatment". In: *American family physician* 76.9 (2007), pp. 1323–1330.

[Lew+08] James D Lewis et al. "Use of the noninvasive components of the Mayo score to assess clinical response in ulcerative colitis". In: *Inflammatory bowel diseases* 14.12 (2008), pp. 1660–1666.

[Liu+16] Ding-Yun Liu et al. "Identification of lesion images from gastrointestinal endoscope based on feature extraction of combinational methods with and without learning process". In: *Medical image analysis* 32 (2016), pp. 281–294.

[LKM19] Joon Seop Lee, Eun Soo Kim, and Won Moon. "Chronological review of endoscopic indices in inflammatory bowel disease". In: *Clinical endoscopy* 52.2 (2019), p. 129.

[LL08] Peter Laszlo Lakatos and Laszlo Lakatos. "Risk for colorectal cancer in ulcerative colitis: changes, causes and management strategies". In: *World journal of gastroenterology: WJG* 14.25 (2008), p. 3937.

[LL16] Ji Min Lee and Kang-Moon Lee. "Endoscopic diagnosis and differentiation of inflammatory bowel disease". In: *Clinical endoscopy* 49.4 (2016), p. 370.

[LM01] Thomas Leung and Jitendra Malik. "Representing and recognizing the visual appearance of materials using three-dimensional textons". In: *International journal of computer vision* 43.1 (2001), pp. 29–44.

[Lo+16] Wing-Cheong Lo et al. "Inflammatory bowel disease: How effective is TNF-α suppression?" In: *PloS one* 11.11 (2016), e0165782.

[LPF20] Jimmy K. Limdi, Michael Picco, and Francis A. Farraye. "A review of endoscopic scoring systems and their importance in a treat-to-target approach in inflammatory bowel disease (with videos)". In: *Gastrointestinal Endoscopy* 91.4 (2020), pp. 733–745. ISSN: 0016-5107. DOI: https://doi.org/10.1016/j.gie.2019.11.032. URL: https://www.sciencedirect.com/science/article/pii/S0016510719324824.

[Mai+15] Shreya Maiti et al. "Mathematical modeling of pro-and anti-inflammatory signaling in macrophages". In: *Processes* 3.1 (2015), pp. 1–18.

[Mar06] John K Marshall. "Reporting ileocolonoscopy in inflammatory bowel disease". In: *Canadian Journal of Gastroenterology* 20.6 (2006), pp. 399–400.

[Mat+04]   K Matsuoka et al. "T-bet upregulation and subsequent interleukin 12 stimulation are essential for induction of Th1 mediated immunopathology in Crohn's disease". In: *Gut* 53.9 (2004), pp. 1303–1308.

[Met96]   Ralph Metson. "Holmium: YAG Laser Endoscopic Sinus Surgery; A Randomized, Controlled Study". In: *The Laryngoscope* 106.S77 (1996), pp. 1–18.

[MF96]   Wen-Xiu Ma and Benno Fuchssteiner. "Explicit and exact solutions to a Kolmogorov-Petrovskii-Piskunov equation". In: *International Journal of Non-Linear Mechanics* 31.3 (1996), pp. 329–338.

[MJ+17]   Ignacio Marín-Jiménez et al. "Management of the psychological impact of inflammatory bowel disease: perspective of doctors and patients—the ENMENTE Project". In: *Inflammatory bowel diseases* 23.9 (2017), pp. 1492–1498.

[ML04]   Helen Moore and Natasha K Li. "A mathematical model for chronic myelogenous leukemia (CML) and T cell interaction". In: *Journal of theoretical biology* 227.4 (2004), pp. 513–523.

[Mon+87]   U Monsen et al. "Prevalence of inflammatory bowel disease among relatives of patients with ulcerative colitis". In: *Scandinavian journal of gastroenterology* 22.2 (1987), pp. 214–218.

[MY09]   Norberto Aníbal Maidana and Hyun Mo Yang. "Spatial spreading of West Nile Virus described by traveling waves". In: *Journal of theoretical biology* 258.3 (2009), pp. 403–417.

[MZ05]   Shiwang Ma and Xingfu Zou. "Existence, uniqueness and stability of travelling waves in a discrete reaction–diffusion monostable equation with delay". In: *Journal of Differential Equations* 217.1 (2005), pp. 54–87.

[Nag+10]   Makoto Naganuma et al. "Novel endoscopic activity index is useful for choosing treatment in severe active ulcerative colitis patients". In: *Journal of gastroenterology* 45.9 (2010), pp. 936–943.

[Naw+14]   Ruwan Nawarathna et al. "Abnormal image detection in endoscopy videos using a filter bank and local binary patterns". In: *Neurocomputing* 144 (2014), pp. 70–91.

[Nob74]   Julia V Noble. "Geographic and temporal development of plagues". In: *Nature* 250.5469 (1974), pp. 726–729.

[OEI18]   Maxwell Scale Uwadia Osagie, Osatohanmwen Enagbonma, and Amanda Iriagbonse Inyang. "Structural Dynamics and Evolution of Capsule Endoscopy (Pill Camera) Technology in Gastroenterologist Assertion". In: *arXiv preprint arXiv:1804.01171* (2018).

[Ord+12]   Ingrid Ordás et al. "Ulcerative colitis". In: *The Lancet* 380.9853 (2012), pp. 1606–1619. ISSN: 0140-6736. DOI: https://doi.org/10.1016/S0140-6736(12)60150-0. URL: https://www.sciencedirect.com/science/article/pii/S0140673612601500.

[Orl+98]   F Orlandi et al. "Observer agreement in endoscopic assessment of ulcerative colitis." In: *Italian journal of gastroenterology and hepatology* 30.5 (1998), pp. 539–541.

[Pan+11]   Guobing Pan et al. "Bleeding detection in wireless capsule endoscopy based on probabilistic neural network". In: *Journal of medical systems* 35.6 (2011), pp. 1477–1484.

[Pan+16]   Julián Panés et al. "Central endoscopy reading in inflammatory bowel diseases". In: *Journal of Crohn's and Colitis* 10.suppl_2 (2016), S542–S547.

[Per15]   Benoît Perthame. "Parabolic equations in biology". In: *Parabolic Equations in Biology*. Springer, 2015, pp. 1–21.

[Per+87]   A Pera et al. "Colonoscopy in inflammatory bowel disease: diagnostic accuracy and proposal of an endoscopic score". In: *Gastroenterology* 92.1 (1987), pp. 181–185.

[Pig+15]   Charly Pignon et al. "Flexible gastrointestinal endoscopy in ferrets (Mustela putorius furo)". In: *Veterinary Clinics: Exotic Animal Practice* 18.3 (2015), pp. 369–400.

[Pog+19]   Konstantin Pogorelov et al. "Bleeding detection in wireless capsule endoscopy videos—Color versus texture features". In: *Journal of applied clinical medical physics* 20.8 (2019), pp. 141–154.

[Pro+18]   Fay Probert et al. "Plasma nuclear magnetic resonance metabolomics discriminates between high and low endoscopic activity and predicts progression in a prospective cohort of patients with ulcerative colitis". In: *Journal of Crohn's and Colitis* 12.11 (2018), pp. 1326–1337.

[Pub]   *The capsule endoscopy website. [Online]. Available: http://www.capsuleendoscopy.org.* 2014. URL: "http : / / www . capsuleendoscopy.org.".

[RA12]   Rajaratnam Rameshshanker and Naila Arebi. "Endoscopy in inflammatory bowel disease when and why". In: *World journal of gastrointestinal endoscopy* 4.6 (2012), p. 201.

[Rac89]   Dob Rachmilewitz. "Coated mesalazine (5-aminosalicylic acid) versus sulphasalazine in the treatment of active ulcerative colitis: a randomised trial." In: *Bmj* 298.6666 (1989), pp. 82–86.

[RBC10]   Priti Kumar Roy, Jhumpa Bhadra, and Biplab Chattopadhyay. "Mathematical modeling on immunopathogenesis in chronic plaque of psoriasis: A theoretical study". In: *Proceedings of the World Congress on Engineering*. Vol. 1. 2010, pp. 550–555.

[Rex07]   Douglas K Rex. "Colonoscopy withdrawal times and adenoma detection rates". In: *Gastroenterology & hepatology* 3.8 (2007), p. 609.

[Rut+05]   Paul Rutgeerts et al. "Infliximab for induction and maintenance therapy for ulcerative colitis". In: *New England Journal of Medicine* 353.23 (2005), pp. 2462–2476.

[Sam+13]   Sunil Samuel et al. "Validation of the ulcerative colitis colonoscopic index of severity and its correlation with disease activity

measures". In: *Clinical Gastroenterology and Hepatology* 11.1 (2013), pp. 49–54.

[SBW14] Sonu Sainju, Francis M Bui, and Khan A Wahid. "Automated bleeding detection in capsule endoscopy videos using statistical features and region growing". In: *Journal of medical systems* 38.4 (2014), p. 25.

[SM96] JA Sherratt and BP Marchant. "Nonsharp travelling wave fronts in the Fisher equation with degenerate nonlinear diffusion". In: *Applied Mathematics Letters* 9.5 (1996), pp. 33–38.

[Smo12] Joel Smoller. *Shock waves and reaction—diffusion equations*. Vol. 258. Springer Science & Business Media, 2012.

[SP21] Clyde M Stauffer and Christopher Pfeifer. "Colonoscopy". In: *Stat-Pearls [Internet]* (2021).

[STI87] Kenneth W Schroeder, William J Tremaine, and Duane M Ilstrup. "Coated oral 5-aminosalicylic acid therapy for mildly to moderately active ulcerative colitis". In: *New England Journal of Medicine* 317.26 (1987), pp. 1625–1629.

[Sum+15] Shipra Suman et al. "Optimum colour space selection for ulcerated regions using statistical analysis and classification of ulcerated frames from wce video footage". In: *International Conference on Neural Information Processing*. Springer. 2015, pp. 373–381.

[Sum+17a] Shipra Suman et al. "Detection and classification of bleeding region in WCE images using color feature". In: *Proceedings of the 15th International Workshop on Content-Based Multimedia Indexing*. 2017, pp. 1–6.

[Sum+17b] Shipra Suman et al. "Feature selection and classification of ulcerated lesions using statistical analysis for WCE images". In: *Applied Sciences* 7.10 (2017), p. 1097.

[Sut+87] Lloyd R Sutherland et al. "5-Aminosalicylic acid enema in the treatment of distal ulcerative colitis, proctosigmoiditis, and proctitis". In: *Gastroenterology* 92.6 (1987), pp. 1894–1898.

[SW11] Claude Sammut and Geoffrey I Webb. *Encyclopedia of machine learning*. Springer Science & Business Media, 2011.

[TC92] D-C Tseng and C-H Chang. "Color segmentation using perceptual attributes". In: *11th IAPR International Conference on Pattern Recognition. Vol. III. Conference C: Image, Speech and Signal Analysis,* vol. 1. IEEE Computer Society. 1992, pp. 228–231.

[Tho+15] Kristian Thorlund et al. "Comparative efficacy of golimumab, infliximab, and adalimumab for moderately to severely active ulcerative colitis: a network meta-analysis accounting for differences in trial designs". In: *Expert review of gastroenterology & hepatology* 9.5 (2015), pp. 693–700.

[Tra+12] Simon PL Travis et al. "Developing an instrument to assess the endoscopic severity of ulcerative colitis: the Ulcerative Colitis Endoscopic Index of Severity (UCEIS)". In: *Gut* 61.4 (2012), pp. 535–542.

[Tra+13]   Simon PL Travis et al. "Reliability and initial validation of the ulcerative colitis endoscopic index of severity". In: *Gastroenterology* 145.5 (2013), pp. 987–995.

[Tur90]   Alan Mathison Turing. "The chemical basis of morphogenesis". In: *Bulletin of mathematical biology* 52.1-2 (1990), pp. 153–197.

[TV20]   Sergei Trofimchuk and Vitaly Volpert. "Traveling waves in delayed reaction-diffusion equations in biology [J]". In: *Mathematical Biosciences and Engineering* 17.6 (2020), pp. 6487–6514.

[TW55]   Sidney C Truelove and LJ Witts. "Cortisone in ulcerative colitis". In: *British medical journal* 2.4947 (1955), p. 1041.

[Ura+14]   Toshio Uraoka et al. "Cold polypectomy techniques for diminutive polyps in the colorectum". In: *Digestive Endoscopy* 26 (2014), pp. 98–103.

[Vas+18a]   Nadia Mohammed Vashist et al. "Endoscopic scoring indices for evaluation of disease activity in ulcerative colitis". In: *Cochrane Database of Systematic Reviews* 1 (2018).

[Vas+18b]   Michael D Vasilakakis et al. "DINOSARC: Color features based on selective aggregation of chromatic image components for wireless capsule endoscopy". In: *Computational and mathematical methods in medicine* 2018 (2018).

[VP09]   Vitaly Volpert and Sergei Petrovskii. "Reaction–diffusion waves in biology". In: *Physics of life reviews* 6.4 (2009), pp. 267–310.

[VPR13]   Carl Vondrick, Donald Patterson, and Deva Ramanan. "Efficiently scaling up crowdsourced video annotation". In: *International journal of computer vision* 101.1 (2013), pp. 184–204.

[VVV94]   AI Volpert, Vi A Volpert, and Vl A Volpert. "Traveling waves solutions of parabolic systems. Transl. Math. Mono. 140". In: *Amer. Math. Soc., Providence* (1994).

[Wal+98]   RS Walmsley et al. "A simple clinical colitis activity index". In: *Gut* 43.1 (1998), pp. 29–32.

[Wen+10]   Katherine Wendelsdorf et al. "Model of colonic inflammation: immune modulatory mechanisms in inflammatory bowel disease". In: *Journal of theoretical biology* 264.4 (2010), pp. 1225–1239.

[YCS04]   Andrew Yates, Robin Callard, and Jaroslav Stark. "Combining cytokine signalling with T-bet and GATA-3 regulation in Th1 and Th2 differentiation: a model for cellular decision-making". In: *Journal of theoretical biology* 231.2 (2004), pp. 181–196.

[Yes+20]   Karma Yeshi et al. "Revisiting inflammatory bowel disease: pathology, treatments, challenges and emerging therapeutics including drug leads from natural products". In: *Journal of clinical medicine* 9.5 (2020), p. 1273.

[You50]   William J Youden. "Index for rating diagnostic tests". In: *Cancer* 3.1 (1950), pp. 32–35.

[Yua+15] Yixuan Yuan et al. "Saliency based ulcer detection for wireless capsule endoscopy diagnosis". In: *IEEE transactions on medical imaging* 34.10 (2015), pp. 2046–2057.

[YWT+14] Jinn-Yi Yeh, Tai-Hsi Wu, Wei-Jun Tsai, et al. "Bleeding and ulcer detection using wireless capsule endoscopy images". In: *Journal of Software Engineering and Applications* 7.05 (2014), p. 422.

List of Figures

List of Tables

Lepton : List of listings